

11-7-2020

Analytical Methods and Critical Analyses Supporting Thermodynamically Consistent Characterizations of the Marine CO₂ System

Jonathan D. Sharp
University of South Florida

Follow this and additional works at: <https://digitalcommons.usf.edu/etd>



Part of the [Other Oceanography and Atmospheric Sciences and Meteorology Commons](#)

Scholar Commons Citation

Sharp, Jonathan D., "Analytical Methods and Critical Analyses Supporting Thermodynamically Consistent Characterizations of the Marine CO₂ System" (2020). *USF Tampa Graduate Theses and Dissertations*.
<https://digitalcommons.usf.edu/etd/8588>

This Dissertation is brought to you for free and open access by the USF Graduate Theses and Dissertations at Digital Commons @ University of South Florida. It has been accepted for inclusion in USF Tampa Graduate Theses and Dissertations by an authorized administrator of Digital Commons @ University of South Florida. For more information, please contact digitalcommons@usf.edu.

Analytical Methods and Critical Analyses Supporting Thermodynamically Consistent
Characterizations of the Marine CO₂ System

by

Jonathan D. Sharp

A dissertation submitted in partial fulfillment
of the requirements for the degree of
Doctor of Philosophy
College of Marine Science
University of South Florida

Major Professor: Robert H. Byrne, Ph.D.
Kristen N. Buck, Ph.D.
Richard A. Feely, Ph.D.
Brad E. Rosenheim, Ph.D.
Rik Wanninkhof, Ph.D.

Date of Approval:
October 21, 2020

Keywords: Carbonate ion, Total alkalinity, Ultraviolet spectrophotometry, Ocean carbon system consistency, Seawater titrations, Organic alkalinity

Copyright © 2020, Jonathan D. Sharp

ACKNOWLEDGEMENTS

First and foremost, I would like to thank Bob Byrne for his guidance, advice, and encouragement over the past five years. I've often stopped by Bob's office for help with a scientific question, and ended up staying for an hour or more discussing anything from college football, to U.S. politics, to the incomprehensible vastness of outer space. More often than not I'd at least hear an amusing story about one of Bob's past practical jokes or various other sorts of hijinks. Beyond these enjoyable interactions, I could always count on Bob for thoughtful critiques of my ideas and writings, and insightful conversations about chemical oceanography. It's clear to me that Bob's primary goal is to facilitate the success of his students, and I feel very lucky to have benefitted from his tireless work in support of that goal.

Thanks also to my committee members: Brad Rosenheim, Kristen Buck, Dick Feely, and Rik Wanninkhof. I'm grateful for the excellent instruction in the core principles of chemical and geological oceanography I received from Brad and Kristen. Those courses during my first year were instrumental in teaching me to think like an oceanographer, with an interdisciplinary approach to science. I've always appreciated Brad's thought-provoking scientific questions, and I've benefited greatly from Kristen's advice on professional decisions. I'm also grateful for the guidance of Dick and Rik. Dick was a chief scientist on my first research cruise; I've learned a lot from him and will continue to do so in my postdoctoral position at the University of Washington. Rik could always be counted on to inject some levity into committee meetings, and I've appreciated that he's pushed me to think about the broad implications of my dissertation work.

Thanks to each member of the Byrne Lab with whom I've spent time at CMS. I want to especially thank Katie Douglas and Erin Cuyler for teaching me about CO₂ system measurements and for being great lab mates and cruise companions. Thanks also to Katelyn Schockman and Ellie Hudson-Heck for continually being willing to assist me with my work and for being great friends. I also have to thank Kelly Diester and Sherwood Liu. Kelly was always happy to help me locate a chemical in the lab or prepare a paper or grant submission. Sherwood has been uncommonly generous with his time; he has guided me through various types of lab work and taught me a great deal about chemical oceanography. Sherwood is an exemplary mentor, and I know that many students before and after me have benefitted and will benefit from his knowledge and generosity.

I'm grateful to the scientists who participated in the 2016 West Coast Ocean Acidification cruise and the 2017 Gulf of Mexico Ecosystems and Carbon Cycling cruise, including the Chief and Co-Chief Scientists on those projects: Simone Alin, Dana Greeley, Dick Feely, Julian Herndon, Leticia Barbero, and Denis Pierrot. I learned a good deal from each of them and had great fun conducting science at sea. I also have to thank the crew of the *R.V. Ronald H. Brown* for making those trips possible, productive, and enjoyable.

I've had the opportunity to grow and learn as a scientist alongside some fantastic people during my time at CMS. I want to especially thank some members of the 2015 cohort who have been invaluable friends and colleagues: Alex Ilich, Ryan Venturelli, Dana Nieuwkerk, Nat Sawaya, Kelly Vasbinder, and Imogen Browne. Thanks also to so many others, too numerous to mention, who have filled my life in St. Petersburg with great fun in addition to great science.

A huge thanks to Carey Schafer for her constant support. Carey is brilliant, and she has been a valued critic of my written work and presentations, in addition to providing much needed emotional support.

Finally, another huge thanks to Mom and Dad and my brother, Bill, without whom I surely would not have been able to complete this Ph.D. Their love and support is, and has always been, greatly treasured.

TABLE OF CONTENTS

| | |
|---|------|
| List of Tables | v |
| List of Figures | viii |
| Abstract | xi |
| Chapter One: Introduction | 1 |
| 1.1 Inorganic Carbon in the Ocean | 1 |
| 1.2 Anthropogenic Effects | 3 |
| 1.3 CO ₂ System Equilibria | 6 |
| 1.4 Study of the Marine CO ₂ System | 9 |
| 1.5 Dissertation Overview | 11 |
| Chapter Two: Spectrophotometric Determination of Carbonate Ion Concentrations: Elimination of Instrument-Dependent Offsets and Calculation of In Situ Saturation States | 13 |
| 2.1 Abstract | 13 |
| 2.2 Introduction | 14 |
| 2.2.1 Theory | 16 |
| 2.3 Methods | 18 |
| 2.3.1 Research cruises | 18 |
| 2.3.2 [CO ₃ ²⁻] _{spec} measurement procedures | 19 |
| 2.3.3 Initial evaluation of cruise data | 19 |
| 2.3.4 Determination of spectrophotometer wavelength offsets | 20 |
| 2.3.5 Development of wavelength offset correction equation | 20 |
| 2.3.6 Refinement of [CO ₃ ²⁻] _{spec} computational algorithm | 21 |
| 2.3.7 Method to verify fitting procedure | 22 |
| 2.3.8 Development of a model to calculate in situ [CO ₃ ²⁻] _{spec} * from [CO ₃ ²⁻] _{spec} | 22 |
| 2.3.9 Calculation of spectrophotometric in situ aragonite saturation states | 23 |
| 2.4 Results and Discussion | 24 |
| 2.4.1 Initial assessment of [CO ₃ ²⁻] _{spec} cruise data, 2012 and 2016 | 24 |
| 2.4.2 Spectrophotometer wavelength offsets | 25 |
| 2.4.3 Wavelength offset correction equation | 27 |
| 2.4.4 Refined [CO ₃ ²⁻] _{spec} computational algorithm | 29 |
| 2.4.5 Verification of fitting procedure | 31 |
| 2.4.6 Model to calculate in situ [CO ₃ ²⁻] _{spec} * from [CO ₃ ²⁻] _{spec} | 32 |
| 2.4.7 Evaluation of [CO ₃ ²⁻] _{spec} -based in situ aragonite saturation states | 32 |
| 2.4.8 Implications | 35 |

| | |
|--|----|
| 2.4.9 Procedural overview | 37 |
| 2.5 Supporting Information..... | 38 |
| 2.6 Acknowledgements..... | 39 |
| Chapter Three: Development of a Model for $[\text{CO}_3^{2-}]$ Measurements at Ambient Temperature and Evaluation of Uncertainties in CO_2 System Parameters Calculated from $[\text{CO}_3^{2-}]$ | |
| 3.1 Abstract..... | 40 |
| 3.2 Introduction..... | 41 |
| 3.3 $[\text{CO}_3^{2-}]_{\text{spec}}$ Measurement Theory | 44 |
| 3.4 Methods..... | 46 |
| 3.4.1 CO_2 system measurements..... | 46 |
| 3.4.2 Parameterization procedure | 48 |
| 3.4.3 Propagation of uncertainties | 50 |
| 3.4.3.1 Standard uncertainties for input variables and constants | 52 |
| 3.4.3.2 Uncertainty propagation procedure..... | 54 |
| 3.5 Results and Discussion | 56 |
| 3.5.1 Model for calculating $[\text{CO}_3^{2-}]_{\text{spec}}$ | 56 |
| 3.5.2 Estimation of $[\text{CO}_3^{2-}]$ input uncertainty | 58 |
| 3.5.3 Uncertainty propagation under standard input conditions..... | 59 |
| 3.5.3.1 Derived A_T | 61 |
| 3.5.3.2 Derived C_T | 63 |
| 3.5.3.3 Derived pH_T | 65 |
| 3.5.3.4 Derived $p\text{CO}_2$ | 66 |
| 3.5.3.5 Derived Ω_{arag} | 68 |
| 3.5.4 Uncertainty propagation under other oceanographic conditions | 70 |
| 3.6 Conclusions..... | 72 |
| 3.7 Acknowledgements..... | 73 |
| Chapter Four: Modeling and Interpretation of Total Alkalinity Titrations in Marine and Estuarine Waters in the Presence of Proton-Binding Organic Matter | |
| 4.1 Abstract..... | 75 |
| 4.2 Introduction..... | 77 |
| 4.3 Background..... | 83 |
| 4.3.1 Quantitative description of A_T | 83 |
| 4.3.2 Measurement approaches for A_T | 87 |
| 4.3.2.1 Modified Gran function (MGF) analysis of open-cell titration data | 88 |
| 4.3.2.2 Nonlinear least squares fitting (NLSF) of closed-cell titration data | 90 |
| 4.3.2.3 Nonlinear least squares fitting (NLSF) of open-cell titration data..... | 91 |
| 4.3.2.4 Difference derivative (DD) analysis of closed-cell titration data..... | 92 |
| 4.3.2.5 Single-step titration in an open cell | 92 |
| 4.3.3 Introducing additional species to the A_T equation | 94 |

| | |
|---|-----|
| 4.5 Methods..... | 96 |
| 4.6 Results and Discussion | 99 |
| 4.6.1 Validation of ‘TITRATE.m’ model in the absence of titratable organics | 99 |
| 4.6.1.1 Comparison of model results to test dataset | 99 |
| 4.6.1.2 Comparison among measurement approaches..... | 99 |
| 4.6.2 Modeled $A_{T(\text{meas})}$ in the presence of titratable organics | 101 |
| 4.6.2.1 Effect of measurement approach | 101 |
| 4.6.2.2 Effect of dissolved organic content..... | 105 |
| 4.6.3 Implications of differing $A_{T(\text{meas})}$ results | 106 |
| 4.6.4 Calculated carbonate system parameters in the presence of titratable organics | 107 |
| 4.6.4.1 Calculated $p\text{CO}_2$ | 109 |
| 4.6.4.2 Calculated pH_T | 110 |
| 4.6.4.3 Calculated Ω_{ca} | 113 |
| 4.6.5 Practical methods of accounting for organic alkalinity | 116 |
| 4.6.5.1 Parameterization using [DOC]..... | 116 |
| 4.6.5.2 Secondary titrations | 118 |
| 4.6.5.3 Novel curve-fitting methods | 119 |
| 4.6.6 Organic alkalinity in the open ocean?..... | 119 |
| 4.7 Conclusions..... | 122 |
| 4.8 Acknowledgements..... | 124 |
| Chapter Five: Excess Alkalinity in Carbonate System Reference Materials..... | 125 |
| 5.1 Abstract..... | 125 |
| 5.2 Introduction..... | 126 |
| 5.3 Methods..... | 129 |
| 5.3.1 Pre-treatment of samples..... | 129 |
| 5.3.2 Identification of R_{pKB} | 131 |
| 5.3.3 Excess alkalinity titration..... | 133 |
| 5.3.4 Calculations of borate alkalinity and excess alkalinity..... | 134 |
| 5.3.5 C_T measurements | 136 |
| 5.3.6 Uncertainty analysis..... | 137 |
| 5.4 Results..... | 138 |
| 5.5 Discussion..... | 143 |
| 5.5.1 Excess alkalinity in CRMs..... | 143 |
| 5.5.2 Effect of A_X on CRM-based quality control of TA..... | 144 |
| 5.5.3 Effect of A_X on CRM-based derivations of CO_2 system parameters | 146 |
| 5.5.3 Excess alkalinity in the marine environment..... | 148 |
| 5.5.4 Implications for the total boron to salinity ratio (r_B) | 149 |
| 5.6 Conclusions..... | 151 |
| 5.7 Acknowledgements..... | 151 |
| Chapter Six: Discussion and Implications | 152 |
| 6.1 Future Directions in Marine CO_2 System Chemistry | 152 |
| 6.2 Direct Measurements of Seawater Carbonate Ion Concentration..... | 153 |

| | |
|---|-----|
| 6.3 Consistency in Ocean Alkalinity Measurements | 154 |
| 6.4 Thermodynamic CO ₂ System Consistency | 156 |
| 6.5 Conclusion | 157 |
| Chapter Seven: References | 159 |
| Appendix A: Copyright Permissions | 180 |
| Appendix A1. Copyright permission for chapter two..... | 180 |
| Appendix A2. Copyright permission for chapter three..... | 181 |
| Appendix A3. Copyright permission for chapter four | 182 |
| Appendix B: Supplemental Information for Chapter Two | 183 |
| Appendix B1. Supplemental figure for chapter two | 183 |
| Appendix C: Supplemental Information for Chapter Three | 184 |
| Appendix C1. Removal of Pb(II) from analytical samples..... | 184 |
| Appendix C2. Modified MATLAB routines | 185 |
| Appendix C3. Laboratory measurements used to develop the new [CO ₃ ²⁻] _{spec} model..... | 186 |
| Appendix C4. Duplicate [CO ₃ ²⁻] measurements from the GOMECC-3 cruise..... | 192 |
| Appendix C5. Supplementary error-space diagrams | 197 |
| Appendix C6. Implications for benchtop and in situ [CO ₃ ²⁻] _{spec} measurements | 201 |
| Appendix C7. References for Appendix C | 202 |
| Appendix D: Supplemental Information for Chapter Four..... | 204 |
| Appendix D1. Supplemental tables for chapter four | 204 |
| Appendix E: Supplemental Information for Chapter Five..... | 213 |
| Appendix E1. Derivations of terms | 213 |
| Appendix E2. Supplementary tables for chapter five | 217 |
| Appendix E3. References for Appendix E..... | 223 |

LIST OF TABLES

| | | |
|-----------|--|-----|
| Table 1.1 | Chemical equilibria that describe reactions of CO ₂ in seawater | 6 |
| Table 1.2 | The four “master variables” that are typically measured for studies of the marine CO ₂ system | 7 |
| Table 2.1 | Uncorrected and corrected absorbance ratios (R and R^0) for the four different seawater batches, as measured on the five spectrophotometers | 26 |
| Table 3.1 | Standard input conditions and the random and total standard uncertainties assigned to the input CO ₂ system variables and equilibrium constants for uncertainty propagation | 51 |
| Table 3.2 | Coefficients for the spectrophotometric parameters (Eq. (3.6)) that result from fitting the combined lab and field datasets, with each dataset weighted to contribute equally to the model | 56 |
| Table 3.3 | Combined standard uncertainties in CO ₂ system variables calculated using [CO ₃ ²⁻] (μmol/kg) as an input variable paired with a second (traditional) input variable | 60 |
| Table 3.4 | Combined standard uncertainties in CO ₂ system variables calculated using traditional input variable pairs | 61 |
| Table 3.5 | Combined standard uncertainties in CO ₂ system variables calculated using [CO ₃ ²⁻] (μmol/kg) as an input variable paired with a second (traditional) input variable | 71 |
| Table 4.1 | Inorganic equilibria relevant to the definition of natural-water A_T | 84 |
| Table 4.2 | A_T measurement approaches discussed in this work | 88 |
| Table 4.3 | Summary of selected studies that examined the acid–base properties of dissolved organic matter in terms of pK values | 95 |
| Table 4.4 | Adjustable input parameters for ‘TITRATE.m’ | 97 |
| Table 4.5 | Summary of methods that can be used to account for organic alkalinity..... | 116 |
| Table 5.1 | Properties of different measured seawater samples..... | 138 |

| | | |
|------------|---|-----|
| Table 5.2 | Uncertainties in input parameters for the calculation of A_X and their propagation to combined standard uncertainty in A_X in $\mu\text{mol kg}^{-1}$; calculated using Eq. (5.12)..... | 142 |
| Table 5.3 | Results of pairwise non-parametric pairwise ANOVA tests | 143 |
| Table 5.4 | Hypothetical differences (ΔpH_T) between calculated pH values ($\text{pH}_{\text{calc.}}$) and actual pH values (pH_{true}) of a CRM with a certified alkalinity of 2227.7 $\mu\text{mol kg}^{-1}$ and a certified total dissolved inorganic carbon of 2040.0 $\mu\text{mol kg}^{-1}$ | 147 |
| Table C3.1 | Data from laboratory measurements made in altered Gulf of Mexico seawater to develop the $[\text{CO}_3^{2-}]_{\text{spec}}$ model of Table 3.2 in the main text | 186 |
| Table C4.1 | Measurements of $[\text{CO}_3^{2-}]$ using ultraviolet spectrophotometry and the equation from Sharp et al. (2017) for duplicate samples collected on the GOMECC-3 cruise in 2017. | 192 |
| Table D1.1 | Definitions for notation used within chapter four | 204 |
| Table D1.2 | Differences between $A_{T(\text{meas})}$ and A_{inorg} ($\mu\text{mol kg}^{-1}$) obtained using different combinations of titration data analysis methods and organic $\text{p}K$ values: $\Delta A_T = A_{T(\text{meas})} - A_{\text{inorg}}$ | 205 |
| Table D1.3 | Differences between $A_{T(\text{meas})}$ and A_{inorg} ($\mu\text{mol kg}^{-1}$) obtained using different combinations of titration data analysis methods and initial carbonate chemistries: $\Delta A_T = A_{T(\text{meas})} - A_{\text{inorg}}$ | 206 |
| Table D1.4 | Errors in calculated carbonate system parameters that result from different combinations of measured parameters, titration and data analysis methods, and a range of organic $\text{p}K$ values..... | 207 |
| Table D1.5 | Errors in calculated carbonate system parameters that result from different combinations of measured parameters, titration and data analysis methods, and a range of initial carbonate chemistries..... | 210 |
| Table E2.1 | Sample titration data..... | 217 |
| Table E2.2 | Average titration results for each sample type | 219 |
| Table E2.3 | Total dissolved inorganic carbon ($C_{T(\text{samp.})}$) measurements of purged seawater samples..... | 219 |
| Table E2.4 | Total dissolved inorganic carbon ($C_{T(\text{NaOH})}$) measurements of Milli-Q water (230 g) spiked with NaOH titrant (150 μL)..... | 220 |

| | | |
|------------|---|-----|
| Table E2.5 | A comprehensive list of uncertainties in input parameters for the calculation of A_X and their propagation to combined standard uncertainty in A_X in $\mu\text{mol kg}^{-1}$; calculated using Eq. (5.10) in the main text..... | 221 |
|------------|---|-----|

LIST OF FIGURES

| | | |
|------------|---|----|
| Figure 1.1 | The partial pressure of atmospheric CO ₂ at Mauna Loa Observatory (red) plotted along with the partial pressure of CO ₂ (blue), pH (green), and carbonate ion concentration (purple) in surface seawater at Station ALOHA4 | 4 |
| Figure 2.1 | Initial values of $\Delta[\text{CO}_3^{2-}]$ (i.e., $[\text{CO}_3^{2-}]_{\text{pH},C_T} - [\text{CO}_3^{2-}]_{\text{spec}}$) from the two NOAA cruises, based on values of R and the algorithm of Patsavas et al. (2015a)24 | 24 |
| Figure 2.2 | Illustration of how a spectrophotometer with a wavelength offset ($\Delta\lambda_{241.1}$) of only 0.5 nm can produce a significantly different absorbance ratio than a “perfectly calibrated” spectrophotometer25 | 25 |
| Figure 2.3 | (a) Determination of R^0 (absorbance ratio when $\Delta\lambda_{241.1} = 0$) for one of the four seawater batches. (b) Determination of the wavelength offset correction equation (Eq. (2.11))28 | 28 |
| Figure 2.4 | Reprocessed values of $\Delta[\text{CO}_3^{2-}]$ (i.e., $[\text{CO}_3^{2-}]_{\text{pH},C_T} - [\text{CO}_3^{2-}]_{\text{spec}}$) from the two NOAA cruises, based on values of R^0 (obtained from Eq. (2.11)) and the refined $[\text{CO}_3^{2-}]_{\text{spec}}$ algorithm of this work (Eq. (2.8), with the parameters of Eqs. (2.12–2.14))30 | 30 |
| Figure 2.5 | Differences between the two characterizations of in situ aragonite saturation states from the two cruises33 | 33 |
| Figure 2.6 | Cross-sections of aragonite saturation state along WCOA 2016 Line 9, near the California/Oregon border (see Figure B1.1 for location)34 | 34 |
| Figure 3.1 | Values of $\Delta[\text{CO}_3^{2-}]$ ($\mu\text{mol}/\text{kg}$; $[\text{CO}_3^{2-}]_{\text{spec}} - [\text{CO}_3^{2-}]_{X,\text{pH}}$) as a function of $[\text{CO}_3^{2-}]_{X,\text{pH}}$ (where X is A_T for laboratory data and C_T for field data) for three different models for converting Pb(II) absorbance ratios to $[\text{CO}_3^{2-}]_{\text{spec}}$: (a) the model of Sharp et al. (2017), (b) the lab-based model of this work, and (c) the combined model of this work (Table 3.2)57 | 57 |
| Figure 3.2 | Relative combined standard uncertainty (%) in derived A_T as a function of the standard uncertainties in input variables shown on the x - and y -axes: (a) the best-performing $[\text{CO}_3^{2-}]$ -containing input variable pair ($[\text{CO}_3^{2-}]-C_T$) and (b) the best-performing traditional input variable pair ($p\text{CO}_2-C_T$)62 | 62 |

| | | |
|------------|--|-----|
| Figure 3.3 | Relative combined standard uncertainty (%) in derived C_T as a function of the standard uncertainties in input variables shown on the x - and y -axes: (a) the best-performing $[\text{CO}_3^{2-}]$ -containing input variable pair ($[\text{CO}_3^{2-}]$ - A_T) and (b) the best-performing traditional input variable pair ($p\text{CO}_2$ - A_T) | 64 |
| Figure 3.4 | Relative combined standard uncertainty (%) in derived $[\text{H}^+]$ as a function of the standard uncertainties in input variables shown on the x - and y -axes: (a) the best-performing $[\text{CO}_3^{2-}]$ -containing input variable pair ($p\text{CO}_2$ - $[\text{CO}_3^{2-}]$) and (b) the best-performing traditional input variable pair ($p\text{CO}_2$ - A_T)..... | 65 |
| Figure 3.5 | Relative combined standard uncertainty (%) in derived $p\text{CO}_2$ as a function of the standard uncertainties in input variables shown on the x - and y -axes: (a) the best-performing $[\text{CO}_3^{2-}]$ -containing input variable pair ($[\text{CO}_3^{2-}]$ - C_T) and (b) the best-performing traditional input variable pair (pH_T - C_T)..... | 66 |
| Figure 3.6 | Relative combined standard uncertainties (%) in aragonite saturation states derived using input $[\text{CO}_3^{2-}]$ only (leftmost set of bars) and using pairs of traditional input variables | 67 |
| Figure 4.1 | Bjerrum plots displaying concentrations $[i]$ of the major acid–base species in oxygenated seawater with $C_T = 2000 \mu\text{mol kg}^{-1}$, total phosphate (P_T) = $1.0 \mu\text{mol kg}^{-1}$, total silica (Si_T) = $15.0 \mu\text{mol kg}^{-1}$, salinity (S) = 35, temperature (t) = $25 \text{ }^\circ\text{C}$, and pressure (P) = 1 atm..... | 83 |
| Figure 4.2 | Simulated titration of a 200 g sample of oxygenated seawater with initial $\text{pH}_T = 8.1$, $C_T = 2000 \mu\text{mol kg}^{-1}$, $P_T = 1.0 \mu\text{mol kg}^{-1}$, $Si_T = 15.0 \mu\text{mol kg}^{-1}$, $S = 35$, $t = 25 \text{ }^\circ\text{C}$, and $p = 1 \text{ atm}$ | 86 |
| Figure 4.3 | Modeled differences (%) between $A_{T(\text{meas})}$ and A_{inorg} in a purely inorganic system, for the five data analysis procedures outlined in Table 4.2: $\Delta A_T = A_{T(\text{meas})} - A_{\text{inorg}}$ | 100 |
| Figure 4.4 | Modeled differences between $A_{T(\text{meas})}$ and A_{inorg} in a system that includes titratable organics, as a function of $\text{p}K_{\text{org}}$ (2.5 to 9.5): $\Delta A_T = A_{T(\text{meas})} - A_{\text{inorg}}$ | 102 |
| Figure 4.5 | Differences between ΔA_T for the closed-cell NLSF method versus ΔA_T for the other four methods, as a function of $\text{p}K_{\text{org}}$ (2.5 to 6.0) | 103 |
| Figure 4.6 | Modeled differences between $A_{T(\text{meas})}$ and A_{inorg} as a function of total organic content ($ORG_T = 0$ to $100 \mu\text{mol kg}^{-1}$) | 105 |
| Figure 4.7 | Modeled difference between $p\text{CO}_2$ calculated from $A_{T(\text{meas})}$ paired with another parameter (pH_T or C_T) versus true $p\text{CO}_{2(\text{model})}$, as a function of $\text{p}K_{\text{org}}$ (2.5 to 9.5)..... | 109 |

| | | |
|-------------|---|-----|
| Figure 4.8 | Modeled differences between pH_T calculated from $A_{T(\text{meas})}$ and another parameter (C_T or $p\text{CO}_2$) versus true $\text{pH}_{T(\text{model})}$, as a function of $\text{pH}_{T(\text{model})}$ and $C_{T(\text{model})}$ | 111 |
| Figure 4.9 | Modeled relative differences between Ω_{ca} calculated from $A_{T(\text{meas})}$ and another parameter (C_T , pH_T , or $p\text{CO}_2$) versus $\Omega_{\text{ca}(\text{model})}$, as a function of $\Omega_{\text{ca}(\text{model})}$ | 114 |
| Figure 5.1 | The two steps of the experimental procedure are detailed here | 130 |
| Figure 5.2 | Identification of a sample's absorbance ratio corresponding to its $\text{p}K_B$ value ($R_{\text{p}K_B}$)..... | 132 |
| Figure 5.3 | Dissolved inorganic carbon ($C_{T(\text{samp.})}$) in seawater samples that had been purged for ~ 1 hour with high-purity N_2 gas..... | 139 |
| Figure 5.4 | Salinity-normalized values of A_{B+X} (nA_{B+X}) for surface GoM seawater, CRM 172, CRM 176, and CRM 183..... | 140 |
| Figure 5.5 | Values of A_X determined by applying the total boron to salinity ratio of Uppström (1974) on the left and Lee et al. (2010) on the right..... | 141 |
| Figure 5.6 | Hypothetical differences between certified A_T values versus A_T values measured by closed-cell titrations (e.g., Millero et al., 1993), a fixed endpoint method (e.g., Yao and Byrne, 1998), and a difference derivative approach (e.g., Hernandez-Ayón et al., 1999)..... | 145 |
| Figure B1.1 | Left panel: Station locations for the 2016 West Coast Ocean Acidification Cruise (WCOA 2016). Right panel: Station locations for the 2012 Gulf of Mexico and East Coast Carbon Cruise (GOMECC-2) | 183 |
| Figure C5.1 | Relative combined standard uncertainty (%) in derived A_T as a function of the standard uncertainties in input variables on the x - and y -axes..... | 197 |
| Figure C5.2 | Relative combined standard uncertainty (%) in derived C_T as a function of the standard uncertainties in input variables on the x - and y -axes..... | 198 |
| Figure C5.3 | Relative combined standard uncertainty (%) in derived $[\text{H}^+]$ as a function of the standard uncertainties in input variables on the x - and y -axes..... | 199 |
| Figure C5.4 | Relative combined standard uncertainty (%) in derived $p\text{CO}_2$ as a function of the standard uncertainties in input variables on the x - and y -axes..... | 200 |

ABSTRACT

Chemical equilibria describing the unique behavior of gaseous and ionic forms of dissolved carbon dioxide (CO₂) in seawater comprise what is known as the marine CO₂ (or carbonate) system. Observations of the marine CO₂ system with high degrees of accuracy, reproducibility, spatial coverage, and temporal resolution are critical for evaluating natural cycles of carbon within the Earth system, as well as chemical and biological responses to anthropogenic CO₂ emissions.

One component of the CO₂ system is the carbonate ion (CO₃²⁻), a dissolved ion that is produced when carbonic acid (H₂CO₃⁰) dissociates both its hydrogen ions. The carbonate ion is an important buffer against seawater pH changes and is vital for marine organisms that build shells and/or skeletons out of calcium carbonate. Concentrations of carbonate, [CO₃²⁻], are typically inferred from measurements of other CO₂ system variables followed by calculations using established thermodynamic relationships.

This dissertation advances and evaluates a method for direct measurement of [CO₃²⁻]. The method is based on observations of seawater absorbance in the ultraviolet spectrum after addition of dissolved lead (Pb²⁺). The absorbance is caused by lead carbonate and lead chloride species, and its magnitude is a function of the carbonate ion concentration.

In this dissertation, an instrument-dependent artifact in [CO₃²⁻] measurements is identified and corrected, improving differences between measured and calculated [CO₃²⁻] from -2.78 ± 2.9 $\mu\text{mol kg}^{-1}$ to -0.03 ± 1.9 $\mu\text{mol kg}^{-1}$ for the datasets examined in chapter two (where $\mu \pm \sigma$ represents the mean, μ , and one standard deviation, σ). An algorithm is introduced to convert

$[\text{CO}_3^{2-}]$ measured at laboratory conditions to $[\text{CO}_3^{2-}]$ at in situ ocean conditions. Aragonite saturation states appropriate to in situ conditions are determined from laboratory-measured $[\text{CO}_3^{2-}]$ using this algorithm. The resulting saturation states show very good agreement with saturation states calculated from laboratory-measured pH and total dissolved inorganic carbon; differences are centered around zero with a standard deviation of ± 0.031 .

The $[\text{CO}_3^{2-}]$ measurement method is then extended to an extensive range of salinity (20 to 40) and temperature (3 to 40 °C). With the new, temperature-dependent algorithm, differences between measured and calculated $[\text{CO}_3^{2-}]$ for the datasets examined in chapter two are $0.02 \pm 2.0 \mu\text{mol kg}^{-1}$. This result shows almost no degradation compared to the algorithm optimized for 25 °C. Further, the extended algorithm allows for benchtop measurements of $[\text{CO}_3^{2-}]$ to be performed without temperature control, and opens up the potential for in situ measurements of $[\text{CO}_3^{2-}]$.

Estimated measurement imprecisions and systematic uncertainties are then used to evaluate combined uncertainties in CO_2 system variables that are determined via calculations involving $[\text{CO}_3^{2-}]$. An open-source code for CO_2 system error propagations was modified for this purpose and made publicly available. Notably, pairing $[\text{CO}_3^{2-}]$ with total alkalinity (A_T , or TA) or total dissolved inorganic carbon (C_T , or DIC) can lead to well-constrained characterizations of the CO_2 system.

One of the most frequently measured CO_2 system variables is A_T . The typical method for A_T measurement is titration with a strong acid of known concentration, along with measurements of initial volume or mass, amount of acid added, and pH (either by electrode or spectrophotometer). The acid amount and pH measurements are made either in a stepwise manner (typical) or after a single acid addition (less common). These measurements are followed by some form of curve fitting or the application of a single equation to determine A_T . Within this general framework,

different methods of A_T measurement are used in the marine chemistry community, and different lab groups introduce minor tweaks to a general method to arrive at their own specific protocols. Importantly, any and all proton-binding species that are active over the pH range of an A_T titration will contribute to measured A_T .

Numerical simulations detailed in this dissertation show that proton-binding organics introduce differences between A_T values determined by different commonly employed titration methods. These differences can exceed 50% of the total organic concentration. Further, proton-binding organics can cause incorrect deductions of carbonate alkalinity from A_T , which propagate to calculations of other CO₂ system variables. Each of these effects is modulated by the proton-binding affinity (or dissociation constant) of the dissolved organic matter, the method used to determine A_T , and the carbonate chemistry of the titrated sample. The demonstration of differences between A_T determined by different titration methods (given the likely omnipresence of organic proton acceptors) has implications for CO₂ system thermodynamic consistency analyses.

Experimental determinations of CO₂ system variables (especially A_T and C_T) are aided by certified reference materials (CRMs), which are used to verify numerical accuracy, temporal reproducibility, and inter-laboratory consistency of measurements. CRMs are prepared from natural seawater in large, uniform batches, and are certified for A_T and C_T . CRMs are irradiated with ultraviolet light to reduce organic contamination and are poisoned with mercuric chloride to suppress biological activity. However, CRMs are not ensured to be free of dissolved organics.

This dissertation details the results of experiments that indicate excess alkalinity in CRMs, likely due to the presence of proton-binding organic molecular structures. The experiments were initially designed to investigate the total boron to salinity ratio in seawater; however, inconsistent results between CRM batches and natural seawater from the Gulf of Mexico indicated that

isolation of the borate alkalinity component from the unexpected excess alkalinity component would be impossible. Instead, the excess alkalinity component of CRM batches is described and evaluated in the context of experimental uncertainties. Then, possible effects of the excess alkalinity on CRM-based evaluations of A_T measurement consistency and implications for seawater acid–base chemistry are discussed.

The amount of excess alkalinity detected in CRMs has the potential to bias evaluations of A_T measurement consistency by up to about $5 \mu\text{mol kg}^{-1}$, depending on a few factors including A_T measurement method and the nature of the excess alkalinity contributor. The existence of excess alkalinity in CRMs implies that, in certain ocean regions, total alkalinity is not an exclusive function of inorganic chemical species, which has implications for evaluations of thermodynamic consistency between measured and calculated CO_2 system variables. Determinations of excess alkalinity are highly influenced by the investigator’s choice of total boron to salinity ratio, the two most commonly used values of which differ by about 4%.

This dissertation significantly advances an analytical method for direct determinations of a fifth measurable CO_2 system variable. The method is uniquely suited for in situ application, which is critically important as the marine biogeochemical community looks more toward autonomous in situ sensors for ocean monitoring capabilities. This dissertation also offers a critical analysis of the effects of dissolved proton-binding organic molecules on total alkalinity measurements. “Organic alkalinity” resulting from these proton-binding molecules is one of the most likely explanations for the confounding nature of inconsistencies between CO_2 system measurements and calculations, and the work detailed here provides insight that will be helpful in solving that important issue. Finally, this dissertation describes a novel detection of excess

alkalinity in CO₂ system reference materials. The implications for quality-control efforts using those reference materials and for the acid–base chemistry of natural seawater are discussed.

CHAPTER ONE:

INTRODUCTION

1.1 Inorganic Carbon in the Ocean

The ocean carbon reservoir plays a major role in regulating the atmospheric concentration of carbon dioxide (CO_2 ; Archer et al., 1997; Sarmiento and Gruber, 2006), a steady increase in which is driving contemporary global warming and associated climatic changes (IPCC, 2013). The ocean currently holds about 45 times more carbon than the atmosphere (Friedlingstein et al., 2019) — a ratio that is progressively decreasing as the atmospheric carbon stock grows. This high degree of ocean storage is due in part to the fact that dissolved CO_2 can manifest as multiple ionic forms in addition to aqueous gas. Ocean carbon storage is also enhanced by processes that transport dissolved CO_2 against concentration gradients and away from the ocean–atmosphere interface.

In seawater, aqueous CO_2 ($\text{CO}_{2(\text{g})}$) is hydrated to form carbonic acid (H_2CO_3^0), which rapidly dissociates into both bicarbonate (HCO_3^-) and carbonate (CO_3^{2-}) ions. At typical present-day ocean-surface pH (~ 8.1), inorganic carbon is partitioned into about 0.5% aqueous CO_2 (including a small contribution from carbonic acid), 90% bicarbonate, and 9.5% carbonate. These fractions change at depth, where pressure, temperature, added CO_2 from heterotrophic respiration, and other factors shift CO_2 system equilibria (section 1.3).

Processes that transport inorganic carbon to depth in the ocean have been termed carbon pumps, because they act against the concentration gradient of dissolved CO_2 . Traditionally, three main pumps have been recognized (Volk and Hoffert, 1985; Sarmiento and Gruber, 2006): the

solubility pump is driven by the uptake of CO₂ at high latitudes, where gas solubility is enhanced, and transport to depth by ocean circulation; the soft-tissue pump is driven by uptake of dissolved CO₂ by photosynthetic organisms at the ocean surface and transport to depth by active biological processes and sinking organic particles; the hard-tissue pump is driven by uptake of dissolved CO₂ by calcifying organisms at the ocean surface and transport to depth by sinking inorganic particles. Growing evidence has indicated that the biological gravitational pumps (soft- and hard-tissue pumps) are enhanced by “particle-injection pumps” that are driven by both physical and biological processes and operate on finite spatial and temporal scales (Boyd et al., 2019).

Atmospheric CO₂ concentration responds to ocean processes that store carbon on different timescales. Surface ocean uptake is enhanced by carbonate buffering, and balanced against ocean efflux of CO₂. This balance acts over relatively short timescales (decades to centuries) to regulate atmospheric CO₂. Over longer timescales (thousands of years), buffering by calcium carbonate on the ocean floor, as well as terrestrial carbonates, is balanced against CaCO₃ formation and deposition, also contributing to the regulation of atmospheric CO₂ (Archer, 2005). Carbon can be transported to depth by ocean pumps in either dissolved or particulate form; particulate carbon re-enters the dissolved CO₂ pool via heterotrophic respiration (organic) or dissolution (inorganic). Dissolved CO₂ can be stored for more than a year below the surface mixed layer and for hundreds of years at depths greater than about 1,000 meters (Boyd et al., 2019). Particulate carbon that does not re-enter the dissolved pool within the water column can be stored for hundreds of thousands of years in ocean sediments (Broecker and Takahashi, 1978; Archer et al., 1997). Long-term burial in sediments is balanced by the gradual weathering of terrestrial rocks and transport of carbon into the ocean interior (Archer et al., 1997; Archer, 2005).

1.2 Anthropogenic Effects

For decades, human activity has been perturbing the natural cycle of carbon. Most notably, the burning of fossil fuel reserves has taken carbon that was locked away deep in the Earth and transferred it rapidly into the atmosphere, accelerating a hundred-thousand-year process to a decadal timescale. Additionally, cement production, land use changes, and agricultural processes contribute to anthropogenic carbon emissions. This “anthropogenic carbon” has been partitioned into terrestrial (~30%) and marine (~25%) reservoirs, with the surplus remaining in the atmosphere (Friedlingstein et al., 2019). Anthropogenic carbon manifests in the marine reservoir as an increase in total dissolved inorganic carbon (C_T), which has been detected by direct observations both in individual ocean basins (Sabine et al., 2008; Wanninkhof et al., 2010; Woosley et al., 2016; Carter et al., 2017, 2019) and globally (Sabine et al., 2004; Gruber et al., 2019).

This oceanic C_T increase is causing changes to the marine CO_2 system (or carbonate system), which refers to the set of chemical equilibria that describe how dissolved CO_2 behaves in seawater. A notable change is ocean acidification (OA; Broecker and Clark, 2001; Caldeira and Wickett, 2003; Feely et al., 2004; Orr et al., 2005;): an increase in the hydrogen ion concentration in seawater (Figure 1.1). Since the start of the industrial revolution (~1750), the acidity of the surface ocean (i.e., hydrogen ion concentration, $[\text{H}^+]$) has increased by over 30% (Dore et al., 2009; Lauvset et al., 2015; Jiang et al., 2019).

A consequence of OA is a decrease in seawater carbonate ion concentration ($[\text{CO}_3^{2-}]$; Figure 1.1). This decrease is easily predicted by Earth system models (Orr et al., 2005; Feely et al., 2009; Bopp et al., 2013) and has been demonstrated at ocean time-series sites (Bates et al., 2014). A decrease in the availability of dissolved CO_3^{2-} has important implications for marine calcifying organisms, which use the ion to create calcium carbonate skeletons: $\text{Ca}^{2+} + \text{CO}_3^{2-} \rightleftharpoons$

$\text{CaCO}_{3(s)}$. Specifically, OA slows CaCO_3 production in calcifying organisms (e.g., Kleypas et al., 1999; Gattuso and Buddemeier, 2000; Riebesell et al., 2000; Langdon and Atkinson, 2005; Fabry et al., 2008; Waldbusser et al., 2013; 2015) and increases dissolution rates in living organisms (e.g., Feely et al., 2004; Bednaršek et al., 2012, 2014).

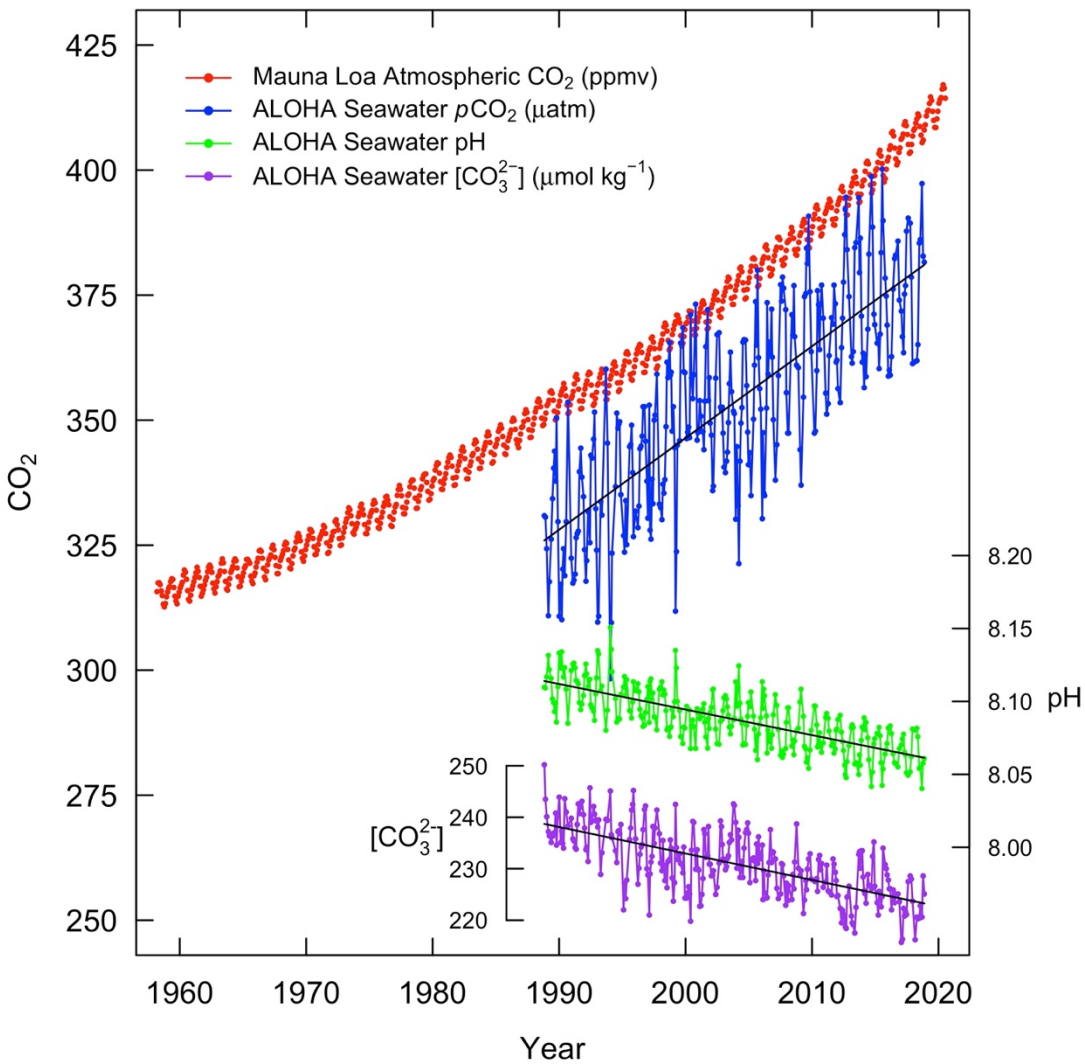


Figure 1.1. The partial pressure of atmospheric CO₂ at Mauna Loa Observatory (red) plotted along with the partial pressure of CO₂ (blue), pH (green), and carbonate ion concentration (purple) in surface seawater at Station ALOHA. Long-term trends (thin black lines) and interannual variability are apparent.

Besides its direct influence on calcifying organisms, OA has and will continue to have additional wide-ranging environmental and economic effects. OA exerts negative physiological effects on marine fishes (e.g., Munday et al., 2009; Chivers et al., 2014; Heuer and Grosell, 2014; Munday et al., 2014), directly influences the strength of the hard-tissue carbon pump (Orr et al., 2005; Berelson et al., 2007; Ridgwell et al., 2007; Dunne et al., 2012), enhances the growth of non-calcifying algae and seagrass (e.g., Diaz-Pulido et al., 2011; Fabricius et al., 2011; Porzio et al., 2011; Roleda and Hurd, 2012), and takes an economic toll on communities that depend on the ocean for ecosystem services (Cooley and Doney, 2009; Cooley et al., 2009; Ekstrom et al., 2015; Mathis et al., 2015).

In addition to anthropogenic carbon, which drives acidification across the entire ocean surface, eutrophication from the runoff of chemical fertilizers and biological waste enhances ocean acidification in subsurface coastal waters (Borges and Gypens, 2010; Sunda and Cai, 2012; Feely et al., 2018). Eutrophication fuels primary productivity at the ocean surface, which decreases dissolved inorganic carbon concentrations and increases pH. However, organic matter produced at the surface sinks to subsurface waters, fueling heterotrophic respiration. This respiration increases dissolved inorganic carbon concentrations and decreases pH. Coastal subsurface ocean acidification can be especially impactful due to the high density of fauna, especially OA-sensitive calcifiers, in coastal waters.

OA (and coastal OA) is progressing contemporaneously with other biological stressors, such as ocean warming (Wijffels et al., 2016; Cheng et al., 2019) and deoxygenation (Ito et al., 2017; Schmidtko et al., 2017). These multiple stressors can combine to have especially deleterious effects on marine organisms and the coastal communities that depend upon them (IPCC, 2014).

Table 1.1. Chemical equilibria that describe reactions of CO₂ in seawater.

| Process | Chemical Equation | Apparent Equilibrium Constant |
|--|--|---|
| Dissolution of CO ₂ into seawater | $\text{CO}_{2(\text{g})} \rightleftharpoons \text{CO}_{2(\text{aq})}$ | $K_0' = [\text{CO}_{2(\text{aq})}]/[\text{CO}_{2(\text{g})}]$ |
| Hydration of aqueous CO ₂ | $\text{CO}_{2(\text{aq})} + \text{H}_2\text{O} \rightleftharpoons \text{H}_2\text{CO}_3^0$ | $K_H' = [\text{H}_2\text{CO}_3^0]/[\text{CO}_{2(\text{aq})}]$ |
| Hydration of CO ₂ and first dissociation of carbonic acid † | $\text{CO}_2 + \text{H}_2\text{O} \rightleftharpoons \text{HCO}_3^- + \text{H}^+$ | $K_1' = [\text{HCO}_3^-][\text{H}^+]/[\text{CO}_2^*]$ |
| Second Dissociation of carbonic acid | $\text{HCO}_3^- \rightleftharpoons \text{CO}_3^{2-} + \text{H}^+$ | $K_2' = [\text{CO}_3^{2-}][\text{H}^+]/[\text{HCO}_3^-]$ |

† Because K_H' is so small (Millero, 1995), H_2CO_3 is typically grouped with $\text{CO}_{2(\text{aq})}$ in the term $[\text{CO}_2^*]$, and K_1' effectively describes both CO_2 hydration and its first dissociation.

1.3 CO₂ System Equilibria

Chemical equilibria that describe the behavior of CO₂ in seawater are given in Table 1.1. These CO₂ system equilibria are quantified by apparent thermodynamic constants, which for seawater are typically characterized by salinity, temperature, and pressure. Quantitative characterizations of seawater thermodynamic constants assume that the relative proportions of major dissolved ions are constant, and thus their concentrations can be determined exclusively from salinity.

To obtain concentrations of the chemical species listed in Table 1.1, or to perform other studies of the marine CO₂ system, at least two of four “master variables” must be determined. Those master variables are total alkalinity (A_T), total dissolved inorganic carbon (C_T), total hydrogen ion concentration expressed as a negative logarithm (pH_T), and the fugacity of CO₂ (f_{CO_2}). Table 1.2 describes each variable quantitatively and provides typical methods of measurement.

Table 1.2 The four “master variables” that are typically measured for studies of the marine CO₂ system.

| Variable | Mathematical Definition | Measurement Methods § |
|----------------|--|--|
| A_T † | $2[\text{CO}_3^{2-}]_T + [\text{HCO}_3^-]_T + [\text{B}(\text{OH})_4^-]_T$ $+ [\text{OH}^-]_T + 2[\text{PO}_4^{3-}]_T + [\text{HPO}_4^{2-}]_T$ $+ [\text{SiO}(\text{OH})_3^-]_T + [\text{NH}_3^0] + [\text{HS}^-]_T + \dots$ $- [\text{H}^+] - [\text{HSO}_4^-] - [\text{HF}^0] - [\text{H}_3\text{PO}_4^0] - \dots$ | 1) Acidimetric titration continuously monitored by an electrode 2) Acidimetric titration to a specified pH endpoint |
| C_T | $[\text{CO}_2^*] + [\text{HCO}_3^-]_T + [\text{CO}_3^{2-}]_T$ | 1) Acidification followed by manometry, coulometry, or infrared detection 2) Closed-cell acidimetric titration |
| pH ‡ | $-\log[\text{H}^+]$ | 1) Potentiometry 2) Spectrophotometry |
| $p\text{CO}_2$ | $[\text{CO}_2^*]/K_0$ | 1) Infrared determination |

† The ellipses in the A_T definition represent species that are not explicitly accounted for, such as organic acids.

‡ In seawater, pH is often defined for convenience on the total scale ($pH_T = [\text{H}^+] + [\text{HSO}_4^-]$) or the seawater scale ($pH_{SWS} = [\text{H}^+] + [\text{HSO}_4^-] + [\text{HF}^0]$).

§ These methods are detailed and references are provided in Table 1.3 of Dickson (2010b).

Relationships between these variables rely on the equilibrium constants described in Table 1.1 and, in the case of A_T , additional acid base equilibria (e.g., boric acid–borate, water–hydroxide, silicic acid–silicate, etc.). Chapter four includes more details about these additional equilibria, and the effect that organic acids can have on seawater buffering and assumed relationships between CO₂ system variables.

Another relevant equilibrium exists between solid calcium carbonate and dissolved ions of calcium and carbonate:



The dissolution of $\text{CaCO}_{3(s)}$ in seawater is quantified by a stoichiometric solubility product, K_{sp}^* (Mucci, 1983):

$$K_{sp}^* = [\text{Ca}^{2+}]_{\text{T}}[\text{CO}_3^{2-}]_{\text{T}} \quad (1.2)$$

The two most common mineral forms of $\text{CaCO}_{3(s)}$ that occur in the ocean are calcite and aragonite, each of which is assigned its own K_{sp}^* .

For a given mineral form, K_{sp}^* is the product of calcium and carbonate concentrations at equilibrium. Inorganic calcium carbonate precipitation rarely occurs in seawater, and calcium carbonate dissolution is a slow process. So, ocean waters are seldom in equilibrium with respect to $\text{CaCO}_{3(s)}$. As such, saturation state, Ω , is also defined for each mineral form of $\text{CaCO}_{3(s)}$:

$$\Omega_{\text{ca}} = [\text{Ca}^{2+}]_{\text{T}}[\text{CO}_3^{2-}]_{\text{T}}/K_{sp(\text{ca})}^* \quad (1.3)$$

and:

$$\Omega_{\text{ar}} = [\text{Ca}^{2+}]_{\text{T}}[\text{CO}_3^{2-}]_{\text{T}}/K_{sp(\text{ar})}^* \quad (1.4)$$

where subscripts “ca” and “ar” represent values that pertain to calcite and aragonite, respectively. Saturation states provide the degree to which seawater is thermodynamically over- or under-saturated with respect to dissolved calcium and carbonate ions.

Calcium carbonate saturation states in seawater are strongly controlled by pressure and dissolved carbonate concentrations (e.g., Feely et al., 2004). They play an important role in carbon cycling within the ocean interior and are useful parameters for describing physiological pressures exerted on calcifying organisms (e.g., Bednaršek et al., 2019). More information about $[\text{CO}_3^{2-}]$ and Ω is provided in chapters two and three.

1.4 Study of the Marine CO₂ System

Significant advancements in the measuring, monitoring, and modeling of the marine CO₂ system have been made over the past few decades. Measurements of C_T can be made reliably via coulometry (Johnson et al., 1985; 1987; 1993). Measurements of pH can be made with great reproducibility using purified indicator dyes (Robert-Baldo et al., 1985; Byrne et al., 1988; Byrne and Breland, 1989; Clayton and Byrne, 1993). These and other techniques have been applied to characterize the CO₂ system on cross-basin monitoring cruises that are repeated at regular intervals (e.g., Talley et al., 2016).

In addition to periodic monitoring cruises, autonomous measurements have emerged as a crucial aspect of marine CO₂ system chemistry (Bushinsky et al., 2019). Profiling floats (e.g., Johnson and Claustre, 2016; Claustre et al., 2019; Roemmich et al., 2019), moorings (e.g., Sutton et al., 2017), and autonomous vehicles (e.g., Meinig et al., 2019) have been outfitted with biogeochemical sensors to monitor the CO₂ system with high spatial and temporal resolution. Ships of opportunity have also been employed to obtain high quality datasets of $p\text{CO}_2$ in the global ocean (Pfeil et al., 2013; Bakker et al., 2016; Wanninkhof et al., 2020).

Carefully prepared standards of CO₂ in seawater (Dickson et al., 2003; Dickson, 2010a) can verify the accuracy of field measurements and the performance of in situ sensors. Algorithms to estimate A_T and other variables (e.g., Millero et al., 1998; Lee et al., 2006; Carter et al., 2016; Sauzède et al., 2017; Bittig et al., 2018; Carter et al., 2018) allow for full characterizations of the CO₂ system where they would otherwise not be possible. Global syntheses of CO₂ system data for the ocean interior (Key et al., 2004; Sabine et al., 2005; Key et al., 2010; Suzuki et al., 2013; Olsen et al., 2020) have allowed for large-scale estimates of anthropogenic carbon storage in the ocean (Sabine et al., 2004; Gruber et al., 2019) and projections of future ocean conditions (e.g., Gruber

et al., 2012; Bopp et al., 2013; Dunne et al., 2013; Kwiatkowski and Orr, 2018; Jiang et al., 2019) to be made with ever increasing confidence.

As measurement technologies and implementations have progressed, evaluations of consistency between CO₂ system measurements and calculations have been made (e.g., Chen et al., 2015; Salt et al., 2016; Fong and Dickson, 2019; Raimondi et al., 2019). Though certain variables compare more favorably than others, CO₂ system calculations never perfectly align with measurements. This can result from random imprecisions in measurements, uncertainties in characterizations of equilibrium constants, or systematic errors in measurements.

Recommendations have been made as to the “optimal” pairings of CO₂ system variables that should be used to calculate the remainder of the system. The A_T - C_T pair has been supported, because samples can be preserved and measurements of both variables have low associated uncertainties (Dickson, 2010b). Also, the C_T -pH pair has been supported, because of potential difficulties in interpreting A_T values when organic alkalinity is present (Dickson, 2010b).

To that end, an often ignored uncertainty in A_T measurements is one associated with organic alkalinity. Dissolved organic molecules in seawater can bind with protons during titration, contributing to A_T measurements in uncertain ways (Kim and Lee, 2009; Kuliński et al., 2014). This problem can be especially insidious in coastal environments that, as discussed in Section 1.2, experience nutrient runoff and high degrees of surface productivity (Hernandez-Ayón et al., 2007; Patsavas et al., 2015b). This dissertation explores in detail uncertainties in A_T associated with organic contributions.

Coherence between measurements and calculations is critically important for demonstrating our understanding of how the seawater CO₂ system functions, and how it affects the health of marine species, the dynamics of Earth’s climate, and the speciation of trace metals in

seawater. As such, a major goal in marine CO₂ system chemistry today is to address repeatedly observed thermodynamic inconsistency issues — such as differences between measured and calculated pH values — and to seek explanations and remedies for these issues (Ocean Carbonate System Intercomparison Forum, <https://www.us-ocb.org/ocean-carbonate-system-intercomparison-forum/>).

1.5 Dissertation Overview

This dissertation describes advancements in measurement capabilities and interpretations of measured quantities related to the marine CO₂ system. The results and discussions presented herein will support future studies of marine CO₂ system chemistry and promote enhanced thermodynamic consistency between measured and calculated variables.

Chapters two and three detail major improvements to a method for directly measuring [CO₃²⁻] in seawater. The method is refined for consistency between measurements made using different instruments (chapter 2), extended for measurements made at temperatures other than 25 °C (chapter 3), and evaluated in terms of the propagation of random and systematic uncertainties to calculated variables (chapter 3). Direct measurements of [CO₃²⁻] allow for obviation of certain uncertainties that can be introduced by calculating [CO₃²⁻] from other measurable variables.

Chapter four delves into errors in measured A_T that can be caused by the presence of proton-binding organic matter in a seawater sample. The chapter concludes that different methods of obtaining A_T from titration data can yield different measured values if proton-binding organics exert significant influence, which may even occur in the open ocean (where organics are typically considered negligible).

Finally, chapter five presents results that suggest a hitherto undescribed excess component of total alkalinity in reference materials for oceanic CO₂ system measurements. The chapter considers the implications of excess alkalinity for CO₂ system studies, proposes a small but significant effect that excess alkalinity may have on quality control for A_T measurements, and discusses uncertainties that factor into excess alkalinity determinations. Chapter six summarizes the findings of this dissertation and speculates about future directions of research that can build upon this work.

CHAPTER TWO:
SPECTROPHOTOMETRIC DETERMINATION OF CARBONATE ION
CONCENTRATIONS: ELIMINATION OF INSTRUMENT-DEPENDENT OFFSETS
AND CALCULATION OF IN SITU SATURATION STATES

Note: This chapter has been reprinted (adapted) with permission from:

Sharp, J.D., Byrne, R.H., Liu, X., Feely, R.A., Cuyler, E.E., Wanninkhof, R., Alin, S.R., 2017. Spectrophotometric Determination of Carbonate Ion Concentrations: Elimination of Instrument-Dependent Offsets and Calculation of In Situ Saturation States. *Environmental Science and Technology* 51, 9127–9136.

Copyright 2017 American Chemical Society.

2.1 Abstract

This work describes an improved algorithm for spectrophotometric determinations of seawater carbonate ion concentrations ($[\text{CO}_3^{2-}]_{\text{spec}}$) derived from observations of ultraviolet absorbance spectra in lead-enriched seawater. Quality-control assessments of $[\text{CO}_3^{2-}]_{\text{spec}}$ data obtained on two NOAA research cruises (2012 and 2016) revealed a substantial inter-cruise difference in average $\Delta[\text{CO}_3^{2-}]$ (the difference between a sample's $[\text{CO}_3^{2-}]_{\text{spec}}$ value and the corresponding $[\text{CO}_3^{2-}]$ value calculated from paired measurements of pH and dissolved inorganic carbon). Follow-up investigation determined that this discordance was due to the use of two different spectrophotometers, even though both had been properly calibrated. Here we present an essential methodological refinement to correct $[\text{CO}_3^{2-}]_{\text{spec}}$ absorbance data for small but significant

instrumental differences. After applying the correction (which, notably, is not necessary for pH determinations from sulfonephthalein dye absorbances) to the shipboard absorbance data, we fit the combined-cruise dataset to produce empirically updated parameters for use in processing future (and historical) $[\text{CO}_3^{2-}]_{\text{spec}}$ absorbance measurements. With the new procedure, the average $\Delta[\text{CO}_3^{2-}]$ offset between the two aforementioned cruises was reduced from $3.7 \mu\text{mol kg}^{-1}$ to $0.7 \mu\text{mol kg}^{-1}$, which is well within the standard deviation of the measurements ($1.9 \mu\text{mol kg}^{-1}$). We also introduce an empirical model to calculate in situ carbonate ion concentrations from $[\text{CO}_3^{2-}]_{\text{spec}}$. We demonstrate that these in situ values can be used to determine calcium carbonate saturation states that are in good agreement with those determined by more laborious and expensive conventional methods.

2.2 Introduction

The current trend of increasing atmospheric carbon dioxide (CO_2) concentration and the dissolution of some of that CO_2 into the ocean is significantly altering seawater chemistry (Doney et al., 2009; Feely et al., 2004; Sabine et al., 2004). Anthropogenic CO_2 is decreasing both seawater pH and the concentration ratio of $[\text{CO}_3^{2-}]/[\text{HCO}_3^-]$ in the ocean (Byrne, 2014). Recognition of this phenomenon has motivated global carbon monitoring studies (Talley et al., 2016) and numerous regional efforts (Barton et al., 2012; Feely et al., 2008; 2016; Gruber et al., 2012; Wanninkhof et al., 2015; Wei et al., 2009) intended to enhance our understanding of the marine CO_2 system.

The marine CO_2 system is commonly examined by directly determining two or more of the four primary CO_2 system measurement parameters: pH, total dissolved inorganic carbon (C_T), total alkalinity (A_T), and CO_2 fugacity (f_{CO_2}). Any two of these parameters can be used with

thermodynamic CO₂ system models to calculate all remaining system parameters, including carbonate ion concentrations ($[\text{CO}_3^{2-}]$) (Dickson et al., 2007).

Of the four dissolved CO₂ species in seawater (CO_{2(aq)}, H₂CO₃, HCO₃⁻, and CO₃²⁻), carbonate ions are of particular importance due to their control over calcium carbonate (CaCO₃) saturation states (Ω). Saturation states regulate calcification rates of marine calcifying organisms (Bednaršek et al., 2014; 2016; Langdon et al., 2000; 2005; Waldbusser et al., 2015; 2016), water column dissolution rates of solid CaCO₃ (e.g., calcite, aragonite; Keir, 1980; Subhas et al., 2015), and preservation of solid CaCO₃ in sediments (Morse, 1978; Morse and Arvidson, 2002). All of these processes are critical components of both local and global carbon budgets.

Recent development of a method to determine total carbonate ion concentrations in seawater ($[\text{CO}_3^{2-}]_{\text{spec}}$) through spectrophotometric observations of lead equilibria has added carbonate as a fifth measurable CO₂ system parameter (Byrne and Yao, 2008). Several studies have demonstrated the efficacy of this method (Easley et al., 2013; Fajar et al., 2015; Patsavas et al., 2015a). Determinations of $[\text{CO}_3^{2-}]_{\text{spec}}$ are advantageous because they are rapid, simple, and inexpensive; they are also amenable to adaption for in situ analyses.

In this paper, we identify a methodological artifact that creates incongruent $[\text{CO}_3^{2-}]_{\text{spec}}$ values for absorbance measurements made with different spectrophotometers. We describe this artifact and its consequences, as well as an essential methodological refinement to avoid such problems in the future (and to correct past occurrences). The refined protocol includes instrument-specific assessments of wavelength calibration offsets and a new computational algorithm for calculating $[\text{CO}_3^{2-}]_{\text{spec}}$ from offset-corrected absorbance measurements. Additionally, we present a model for calculating in situ CaCO₃ saturation states directly from shipboard measurements of $[\text{CO}_3^{2-}]_{\text{spec}}$. The datasets used in this study include 2,681 corresponding observations of Pb(II)

absorbance spectra, salinity, C_T , and pH obtained on two NOAA research cruises in 2012 and 2016.

2.2.1 Theory

The absorbance (λA) of Pb(II) in seawater at a given wavelength (λ) is described by the following equation (Byrne, 1981; Soli et al., 2008):

$$\frac{\lambda A}{l \cdot [\text{Pb}]_T} = \frac{\lambda \varepsilon_{\text{Pb}} + \lambda \varepsilon_{\text{PbCO}_3} \cdot c_{\text{CO}_3} \beta_1 \cdot [\text{CO}_3^{2-}]}{1 + c_{\text{CO}_3} \beta_1 \cdot [\text{CO}_3^{2-}]} \quad (2.1)$$

where l is the pathlength of the spectrophotometer cell and $[\text{Pb}]_T$ is the total lead concentration. The term $\lambda \varepsilon_{\text{PbCO}_3}$ represents the molar absorptivity of PbCO_3^0 , $\lambda \varepsilon_{\text{Pb}}$ represents the absorbance per mole of Pb(II) at low pH (attributable to Pb^{2+} and lead chloride complexes), and $c_{\text{CO}_3} \beta_1$ is the formation constant for PbCO_3^0 expressed in terms of the total (free plus ion-paired) carbonate ion concentration ($[\text{CO}_3^{2-}]$). All carbonate ion concentrations in this paper are expressed as total concentrations.

The complexation of lead and carbonate is represented by



and the formation constant for PbCO_3^0 is defined as

$$c_{\text{CO}_3} \beta_1 = \frac{[\text{PbCO}_3^0]}{[\text{Pb}^{2+}]_T [\text{CO}_3^{2-}]} \quad (2.3)$$

where $[\text{PbCO}_3^0]$ is the concentration of dissolved PbCO_3^0 (including minor contributions from PbCO_3Cl^-) and $[\text{Pb}^{2+}]_T$ is the sum concentration of free lead and lead chloride complexes.

Using Eq. (2.1), the absorbance ratio of Pb(II) in seawater measured at wavelengths of 234 and 250 nanometers (nm) is given as (Byrne and Yao, 2008)

$$R = \frac{250A}{234A} = \frac{250\varepsilon_{\text{Pb}} + 250\varepsilon_{\text{PbCO}_3} \cdot c_{\text{CO}_3} \beta_1 \cdot [\text{CO}_3^{2-}]}{234\varepsilon_{\text{Pb}} + 234\varepsilon_{\text{PbCO}_3} \cdot c_{\text{CO}_3} \beta_1 \cdot [\text{CO}_3^{2-}]} \quad (2.4)$$

Eq. (2.4) can be rearranged to provide an equation that allows for determination of $[\text{CO}_3^{2-}]$ (i.e., $[\text{CO}_3^{2-}]_{\text{spec}}$) in terms of the ratio (R) of Pb(II) absorbances at 234 and 250 nm in lead-enriched seawater (Byrne and Yao, 2008):

$$-\log[\text{CO}_3^{2-}]_{\text{spec}} = \log\{\text{CO}_3\beta_1/e_2\} + \log\{(R - e_1)/(1 - R \cdot e_3/e_2)\} \quad (2.5)$$

where e_1 , e_2 , and e_3/e_2 are salinity-dependent molar absorbance ratios defined as

$$e_1 = \frac{250\epsilon_{\text{PbCO}_3}}{234\epsilon_{\text{PbCO}_3}}, e_2 = \frac{250\epsilon_{\text{Pb}}}{234\epsilon_{\text{PbCO}_3}}, e_3/e_2 = \frac{234\epsilon_{\text{Pb}}}{250\epsilon_{\text{Pb}}} \quad (2.6)$$

Absorbances at 350 nm, a non-absorbing wavelength, are also recorded for correction of baseline absorbance changes caused by variations in cell positioning, lamp intensity, etc. Baseline-corrected absorbance ratios are calculated as

$$R = \frac{250A_{-350A}}{234A_{-350A}} \quad (2.7)$$

where $_{350}A$ is the absorbance measurement at 350 nm relative to the original baseline (seawater-only) measurement at the same wavelength.

Eq. (2.5), which is parallel in form to the equation used to determine seawater pH on the total scale (pH_T) from sulfonephthalein absorbance ratios (Clayton and Byrne, 1993; Liu et al., 2011), allows for convenient calculation of $[\text{CO}_3^{2-}]_{\text{spec}}$ with a minimal number of parameters. The $\log\{\text{CO}_3\beta_1/e_2\}$, e_1 , and e_3/e_2 terms have been previously determined through laboratory experiments and empirical fitting of field data (Byrne and Yao, 2008; Easley et al., 2013; Patsavas et al., 2015a). The most recent characterization of these terms as quadratic functions of salinity at 25 °C is presented in Patsavas et al. (2015a).

2.3 Methods

2.3.1 Research cruises

The 2012 NOAA Gulf of Mexico and East Coast Carbon Cruise (GOMECC-2) was carried out between July 21 and August 13 on the NOAA Ship *Ronald H. Brown* (Wanninkhof et al., 2012). A total of 93 stations across 8 transects in the Gulf of Mexico and off the East Coast of the United States were sampled from surface to seafloor (Figure B1.1). Hydrographic data (salinity, temperature, and depth) were measured with a rosette-mounted CTD (SBE *9plus*, Sea-Bird Scientific). Measured chemical parameters included pH_T , $[\text{CO}_3^{2-}]_{\text{spec}}$, C_T , A_T , f_{CO_2} , dissolved oxygen, and nutrients. All CO_2 system parameters except $[\text{CO}_3^{2-}]_{\text{spec}}$ were determined using the standard operating protocols detailed in Dickson et al. (2007). Purified *m*-cresol purple was used for spectrophotometric pH_T measurements (Liu et al., 2011). Coulometry was used to measure C_T (Johnson et al., 1985). A total of 1,216 $[\text{CO}_3^{2-}]_{\text{spec}}$ measurements were made, and a total of 1,077 conjugate measurements of $[\text{CO}_3^{2-}]_{\text{spec}}$, pH_T , and C_T were available for comparison.

The 2016 NOAA West Coast Ocean Acidification Cruise (WCOA 2016) was carried out between May 5 and June 7 on the NOAA Ship *Ronald H. Brown*. A total of 135 stations across 16 transects between central Baja California ($\sim 25^\circ\text{N}$) and waters north of Vancouver Island ($\sim 52^\circ\text{N}$) were sampled from surface to seafloor (Figure B1.1). Procedures to collect hydrographic and chemical data were identical to those used on the GOMECC-2 cruise. A total of 1,761 $[\text{CO}_3^{2-}]_{\text{spec}}$ measurements were made, and a total of 1,604 conjugate measurements of $[\text{CO}_3^{2-}]_{\text{spec}}$, pH_T , and C_T were available for comparison.

2.3.2 $[\text{CO}_3^{2-}]_{\text{spec}}$ measurement procedures

On both cruises, carbonate ion concentrations were measured according to the procedures outlined in Patsavas et al. (2015a). Seawater samples were collected directly from Niskin bottles into quartz optical cells, which were immediately sealed with TeflonTM caps, then thermostatted to 25 °C (± 0.01 °C). For each cell, a baseline (seawater-only) measurement was followed by a 20 μL addition of 22 mM lead perchlorate ($\text{Pb}(\text{ClO}_4)_2$) solution. Five spectra were recorded for each sample of lead-enriched seawater, and absorbance values at 234, 250, and 350 nm were recorded and averaged. An absorbance ratio (Eq. (2.7)) was calculated for each sample. Absorbance measurements were made using Agilent 8453 UV-visible spectrophotometers (Agilent Technologies) — the same model but different instruments on the two cruises.

2.3.3 Initial evaluation of cruise data

Measured $[\text{CO}_3^{2-}]_{\text{spec}}$ values were determined using Eq. (2.5) with measured absorbance ratios (R) and the perturbation correction and salinity-dependent parameters from Eqs. (2.12–2.15) in Patsavas et al. (2015a).

For comparison to these shipboard $[\text{CO}_3^{2-}]_{\text{spec}}$ measurements, paired measurements of pH_T and C_T were used to calculate $[\text{CO}_3^{2-}]_{\text{pH},C_T}$ values for the same samples. Version 2.1 of the CO2SYS Microsoft Excel program (Pierrot et al., 2006) was used for all CO_2 system calculations in this paper, with the dissociation constants of Lueker et al. (2000), the K_{HSO_4} formulation of Dickson (1990b), and the total boron to salinity ratio of Lee et al. (2010). Uncertainty in the resulting $[\text{CO}_3^{2-}]_{\text{pH},C_T}$ dataset was approximately 2 $\mu\text{mol kg}^{-1}$.

For our analyses, archived data that were flagged 4 (bad) according to WOCE quality control standards (Swift, 2008) were excluded. Data flagged 2 (acceptable), 3 (questionable), or 6

(duplicate) were included. While the distinction between “acceptable” and “questionable” measurements is largely at the discretion of the investigator (Swift, 2008), this practice ensured that all measurements explicitly flagged as “bad” were excluded from our analyses.

Residual (Δ) values were determined for each sample: $\Delta[\text{CO}_3^{2-}] = [\text{CO}_3^{2-}]_{\text{pH,C}_T} - [\text{CO}_3^{2-}]_{\text{spec}}$. For each dataset, outliers were eliminated by deleting $\Delta[\text{CO}_3^{2-}]$ values that were more than three standard deviations from the mean $\Delta[\text{CO}_3^{2-}]$ value (1.4% of the data points were eliminated).

2.3.4 Determination of spectrophotometer wavelength offsets

The wavelength calibrations of five Agilent 8453 UV-visible spectrophotometers — all of which had been previously calibrated according to manufacturer’s instructions and some of which had been used on recent research cruises — were assessed using SRM 2034 (Travis et al., 2005), a National Institute of Standards and Technology (NIST) holmium oxide wavelength standard. Dilute holmium oxide solution exhibits several distinct absorbance peaks between 240 and 650 nm. Using signal averaging, Agilent 8453 spectrophotometers can locate the positions of these peaks to the hundredth of a nanometer. The instrument-specific wavelength offset ($\Delta\lambda_{241.1}$) is defined as the difference between the standard wavelength of one absorbance peak of SRM 2034 ($\lambda_{\text{NIST}} = 241.10$ nm) and the wavelength at which the spectrophotometer reports that peak (λ_{spec}):

$$\Delta\lambda_{241.1} = \lambda_{\text{NIST}} - \lambda_{\text{spec}}.$$

2.3.5 Development of wavelength offset correction equation

The measured wavelength offsets of the five spectrophotometers were used to develop an equation to correct measured absorbance ratios (R) for instrument-specific wavelength offsets.

Four seawater batches with distinct carbonate ion concentrations (~ 130 to $250 \mu\text{mol kg}^{-1}$) were examined. Triplicate samples from each batch were analyzed on each spectrophotometer, according to the procedure detailed in Section 2.3.2, and the average R of each triplicate set was calculated.

This R dataset was then used to determine, for each seawater batch, the theoretical absorbance ratio, R^0 , that would have been observed on a “perfectly calibrated” instrument (i.e., one with a wavelength offset of 0 nm). For each batch, a linear least squares regression was performed using the five R values (one from each spectrophotometer) and the five values of $\Delta\lambda_{241.1}$. The y -intercepts of the resulting regression equations yielded four batch-specific values of R^0 .

Finally, differences between the 20 values of R and R^0 (ΔR) were computed and plotted against $\Delta\lambda_{241.1}$. A linear regression through the data yielded an equation for absorbance ratio corrections as a function of wavelength offset.

2.3.6 Refinement of $[\text{CO}_3^{2-}]_{\text{spec}}$ computational algorithm

After characterizing the GOMECC-2 and WCOA 2016 spectrophotometers (Section 2.3.4) and using the wavelength correction equation (Section 2.3.5) to obtain offset-corrected absorbance ratios (R^0) from the 2,681 shipboard absorbance measurements, we used the offset-corrected dataset to generate a revised set of parameters for the $[\text{CO}_3^{2-}]_{\text{spec}}$ computational algorithm. Eq. (2.5) was fitted to $[\text{CO}_3^{2-}]_{\text{pH,C}_T}$ values, using R^0 values in place of R and second-order salinity-dependent polynomials for $\log\{\text{CO}_3\beta_1/e_2\}$, e_1 , and e_3/e_2 (SigmaPlot software). The fitting procedure, which was similar to that of Easley et al. (2013), yielded a set of empirically defined

parameters that can be used with a modification of Eq. (2.5) in order to determine $[\text{CO}_3^{2-}]_{\text{spec}}$ from offset-corrected ultraviolet absorbance ratios (R^0):

$$-\log[\text{CO}_3^{2-}]_{\text{spec}} = \log\{\text{CO}_3\beta_1/e_2\} + \log\{(R^0 - e_1)/(1 - R^0 \cdot e_3/e_2)\} \quad (2.8)$$

2.3.7 Method to verify fitting procedure

To verify that this fitting procedure generated parameters that can adequately describe an independent dataset, the combined GOMECC-2 and WCOA 2016 dataset was randomly divided into two groups. One group of R^0 values was used to obtain provisional characterizations of the $\log\{\text{CO}_3\beta_1/e_2\}$, e_1 , and e_3/e_2 parameters, according to the empirical fitting procedure described above. The other group of R^0 values was then processed with Eq. (2.8), using these provisional parameters, to obtain $[\text{CO}_3^{2-}]_{\text{spec}}$ values. The resulting $[\text{CO}_3^{2-}]_{\text{spec}}$ values were compared with $[\text{CO}_3^{2-}]_{\text{pH,C}_T}$ values for the same samples.

2.3.8 Development of a model to calculate in situ $[\text{CO}_3^{2-}]_{\text{spec}}^*$ from $[\text{CO}_3^{2-}]_{\text{spec}}$

An empirical model was developed to calculate values of $[\text{CO}_3^{2-}]_{\text{spec}}^*$ (carbonate ion concentrations at in situ temperature, t , and pressure, P) from values of $[\text{CO}_3^{2-}]_{\text{spec}}$ (determined at laboratory conditions of 25 °C and 1 atm total pressure). The resulting $[\text{CO}_3^{2-}]_{\text{spec}}^*$ values allow for the calculation of in situ CaCO_3 saturation states and thus, if the available data cover an adequate geographic extent, the mapping of saturation horizons. The form of the model is based on similar empirical models that have been presented for in situ pH calculations (Millero, 1979; 1995):

$$[\text{CO}_3^{2-}]_{\text{spec}}^* = [\text{CO}_3^{2-}]_{\text{spec}} + A + Bt + Ct^2 \quad (2.9)$$

where t is temperature (°C) and A , B , and C are functions of S , P , and $[\text{CO}_3^{2-}]_{\text{spec}}$.

To generate a synthetic dataset to determine the empirical parameters A , B , and C , 462 pairs of fixed A_T (2088 to 2564 $\mu\text{mol kg}^{-1}$) and C_T (1740 to 2564 $\mu\text{mol kg}^{-1}$) values spanning a range of A_T/C_T ratios (1.0 to 1.2) were input to CO2SYS Version 2.1 (Pierrot et al., 2006) over specified ranges of temperature, salinity, and pressure ($t = 0$ to 40 $^{\circ}\text{C}$, $S = 20$ to 40, and $P = 0$ to 2500 dbars). For each input condition, a value of $[\text{CO}_3^{2-}]$ at 25 $^{\circ}\text{C}$ and 0 dbars (analogous to $[\text{CO}_3^{2-}]_{\text{spec}}$) was calculated, along with a corresponding value of $[\text{CO}_3^{2-}]$ at in situ t and P (analogous to $[\text{CO}_3^{2-}]_{\text{spec}}^*$). Silicate and phosphate concentrations were omitted as the effect they have on the difference between in situ and ex situ $[\text{CO}_3^{2-}]$ is negligible. The resulting synthetic dataset contained a total of 492,492 unique conditions. Using a least-squares fitting routine (SigmaPlot software), the calculated values of in situ $[\text{CO}_3^{2-}]_{\text{spec}}^*$ were modeled (Eq. (2.9)) as a function of t , S , P , and $[\text{CO}_3^{2-}]_{\text{spec}}$.

2.3.9 Calculation of spectrophotometric in situ aragonite saturation states

The resulting $[\text{CO}_3^{2-}]_{\text{spec}}^*$ model was applied to the 2012 and 2016 field measurements of $[\text{CO}_3^{2-}]_{\text{spec}}$ to calculate in situ aragonite saturation states (Ω_A), here termed $\Omega_{A(\text{spec})}$:

$$\Omega_{A(\text{spec})} = \frac{[\text{Ca}^{2+}]_T [\text{CO}_3^{2-}]_{\text{spec}}^*}{K'_{\text{spA}}} \quad (2.10)$$

where $[\text{Ca}^{2+}]_T$ is the total calcium ion concentration, $[\text{CO}_3^{2-}]_{\text{spec}}^*$ is the in situ total carbonate ion concentration (free plus ion-paired), and K'_{spA} is the apparent thermodynamic solubility product for aragonite ($K'_{\text{spA}} = [\text{Ca}^{2+}]_T [\text{CO}_3^{2-}]_{\text{sat}}^*$, where $[\text{CO}_3^{2-}]_{\text{sat}}^*$ is carbonate concentration at saturation). $[\text{Ca}^{2+}]_T$ was estimated from salinity measurements ($[\text{Ca}^{2+}]_T = 0.0102821 \cdot S/35$; Millero et al., 2008), and K'_{spA} was determined using the equations of Mucci (1983) with the pressure correction of Millero (1979).

The resulting spectrophotometric in situ aragonite saturation states were compared to in situ saturation states calculated from paired shipboard measurements of pH_T and C_T , here termed $\Omega_{A(\text{pH}, C_T)}$.

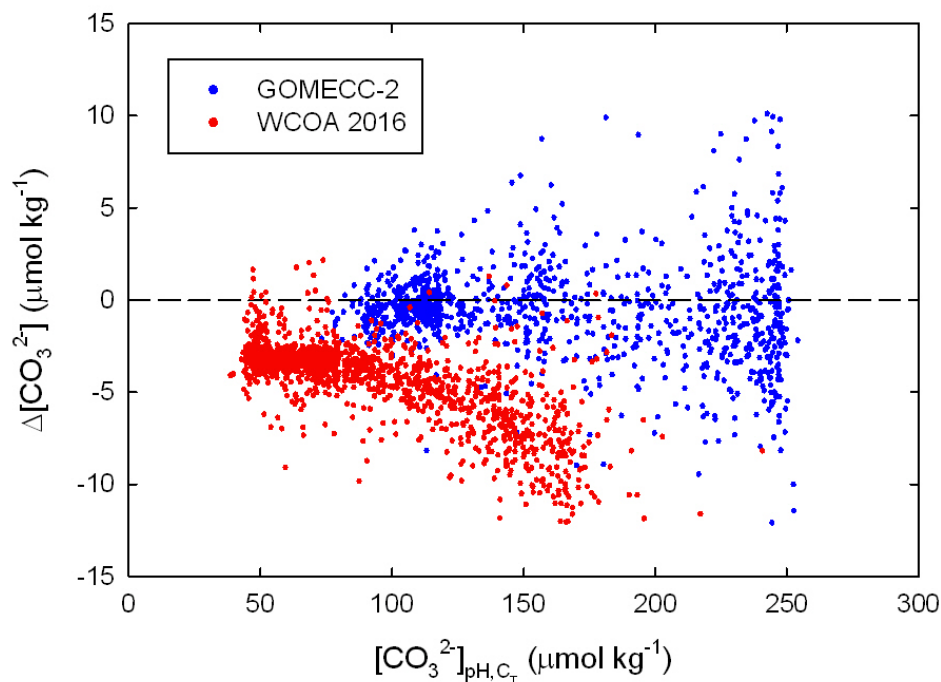


Figure 2.1. Initial values of $\Delta[\text{CO}_3^{2-}]$ (i.e., $[\text{CO}_3^{2-}]_{\text{pH}, C_T} - [\text{CO}_3^{2-}]_{\text{spec}}$) from the two NOAA cruises, based on values of R and the algorithm of Patsavas et al. (2015a). Values of $[\text{CO}_3^{2-}]_{\text{spec}}$ were determined from shipboard absorbance measurements, and values of $[\text{CO}_3^{2-}]_{\text{pH}, C_T}$ were calculated from paired shipboard measurements of pH_T and C_T .

2.4 Results and Discussion

2.4.1 Initial assessment of $[\text{CO}_3^{2-}]_{\text{spec}}$ cruise data, 2012 and 2016

Systematic differences in $\Delta[\text{CO}_3^{2-}]$ values (on average, $3.7 \mu\text{mol kg}^{-1}$) between the GOMECC-2 and WCOA 2016 cruises (Figure 2.1) are apparent when absorbance measurements are processed using the algorithm from Patsavas et al. (2015a). The overall average $\Delta[\text{CO}_3^{2-}]$ of the combined-cruise dataset is $-2.78 \pm 2.9 \mu\text{mol kg}^{-1}$. The $\Delta[\text{CO}_3^{2-}]$ values for the GOMECC-2 dataset

are reasonably scattered about zero because the Patsavas et al. (2015a) algorithm was empirically optimized using the (uncorrected) GOMECC-2 data. Results described in the following sections demonstrate that the $\Delta[\text{CO}_3^{2-}]$ differences shown in Figure 2.1 are due to the use of different spectrophotometers (with different wavelength offsets) on the two cruises.

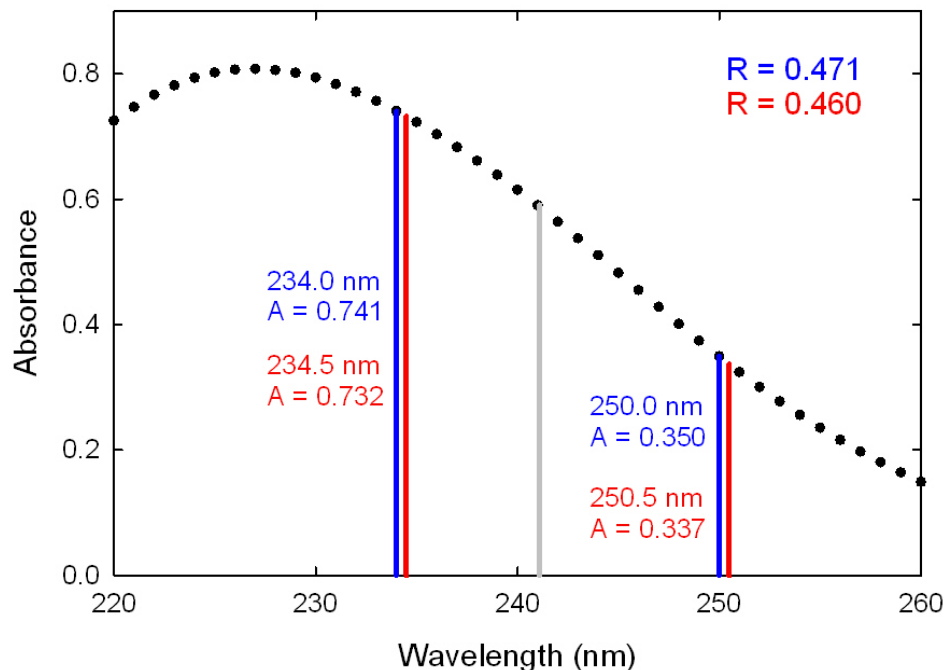


Figure 2.2. Illustration of how a spectrophotometer with a wavelength offset ($\Delta\lambda_{241.1}$) of only 0.5 nm can produce a significantly different absorbance ratio than a “perfectly calibrated” spectrophotometer. The black dots represent a typical absorbance spectrum observed in seawater enriched with $\text{Pb}(\text{ClO}_4)_2$. The blue lines represent absorbances measured at 234.0 and 250.0 nanometers (by the “perfectly calibrated” spectrophotometer), and the red lines represent absorbances ostensibly measured at the same wavelengths but actually measured at 234.5 and 250.5 nanometers (by the spectrophotometer with the wavelength offset). The gray line represents the location at which the wavelength offset is assessed according to the NIST standard (241.10 nm). The absorbance ratios calculated using each pair of absorbance measurements are shown.

2.4.2 Spectrophotometer wavelength offsets

For the spectrophotometer characterizations, 241.10 nm was chosen to be the wavelength of focus because (a) it lies between the $[\text{CO}_3^{2-}]_{\text{spec}}$ measurement wavelengths of 234 and 250 nm

and (b) SRM 2034 shows an especially sharp absorbance peak at 241.10 nm (Travis et al., 2005).

Figure 2.2 describes conceptually how sub-nanometer wavelength offsets lead to errors in measured Pb(II) absorbance ratios.

Table 2.1. Uncorrected and corrected absorbance ratios (R and R^0) for the four different seawater batches, as measured on the five spectrophotometers. The corresponding values of $[\text{CO}_3^{2-}]_{\text{spec}}$ and $[\text{CO}_3^{2-}]_{\text{spec}}$ residuals (i.e., measured $[\text{CO}_3^{2-}]_{\text{spec}}$ minus the $[\text{CO}_3^{2-}]_{\text{spec}}$ mean for the batch) are also shown. SS_{total} is the total sum of squared residuals. These data were all processed using the algorithm of Patsavas et al. (2015a).

| Seawater Batch # | Uncorrected Data | | | Corrected Data | | |
|------------------|------------------|--|---|----------------|--|---|
| | R | $[\text{CO}_3^{2-}]_{\text{spec}}$ ($\mu\text{mol kg}^{-1}$) | $[\text{CO}_3^{2-}]_{\text{spec}}$ Residual ($\mu\text{mol kg}^{-1}$) | R^0 | $[\text{CO}_3^{2-}]_{\text{spec}}$ ($\mu\text{mol kg}^{-1}$) | $[\text{CO}_3^{2-}]_{\text{spec}}$ Residual ($\mu\text{mol kg}^{-1}$) |
| 1 | 0.452 | 245.59 | 0.13 | 0.452 | 246.27 | 2.58 |
| | 0.452 | 245.20 | -0.27 | 0.454 | 241.86 | -1.84 |
| | 0.447 | 259.16 | 13.69 | 0.454 | 241.07 | -2.62 |
| | 0.459 | 228.72 | -16.75 | 0.453 | 242.65 | -1.04 |
| | 0.451 | 248.67 | 3.21 | 0.452 | 246.62 | 2.92 |
| 2 | 0.483 | 181.29 | 0.27 | 0.483 | 181.71 | 1.78 |
| | 0.484 | 180.33 | -0.68 | 0.485 | 178.65 | -1.29 |
| | 0.478 | 189.26 | 8.25 | 0.485 | 177.95 | -1.99 |
| | 0.491 | 170.14 | -10.87 | 0.485 | 178.62 | -1.31 |
| | 0.482 | 184.05 | 3.04 | 0.482 | 182.75 | 2.81 |
| 3 | 0.495 | 164.12 | 0.04 | 0.495 | 164.49 | 1.36 |
| | 0.496 | 162.80 | -1.27 | 0.498 | 160.98 | -2.15 |
| | 0.490 | 171.96 | 7.89 | 0.497 | 162.10 | -1.03 |
| | 0.503 | 154.25 | -9.83 | 0.497 | 161.98 | -1.15 |
| | 0.493 | 167.25 | 3.17 | 0.494 | 166.11 | 2.98 |
| 4 | 0.520 | 132.90 | -0.18 | 0.520 | 133.18 | 0.81 |
| | 0.521 | 132.28 | -0.80 | 0.522 | 131.17 | -1.19 |
| | 0.514 | 139.80 | 6.73 | 0.521 | 132.32 | -0.05 |
| | 0.528 | 125.54 | -7.54 | 0.522 | 131.15 | -1.22 |
| | 0.519 | 134.87 | 1.79 | 0.519 | 134.02 | 1.65 |
| | | $SS_{\text{total}} =$ | 951.0 | | $SS_{\text{total}} =$ | 68.9 |

The wavelength offsets ($\Delta\lambda_{241.1}$) of the five wavelength-calibrated spectrophotometers examined in this work were 0.01 nm, -0.04 nm, -0.26 nm, 0.21 nm, and -0.03 nm. The specified wavelength accuracy limit for Agilent 8453 spectrophotometers is ± 0.5 nm. All of the spectrophotometers were well within this limit.

The three “Uncorrected Data” columns of Table 2.1 show absorbance ratios (R) measured for the four different seawater batches on the five different spectrophotometers; the resulting values of $[\text{CO}_3^{2-}]_{\text{spec}}$, calculated using Eq. (2.5) and the parameters of Patsavas et al. (2015a); and the resulting residuals (i.e., $[\text{CO}_3^{2-}]_{\text{spec}}$ minus the mean $[\text{CO}_3^{2-}]_{\text{spec}}$ value for the given seawater batch). The $[\text{CO}_3^{2-}]_{\text{spec}}$ residuals, which range from -16.75 to $13.69 \mu\text{mol kg}^{-1}$, are consistently largest in magnitude for the spectrophotometers with the largest wavelength offsets.

2.4.3 Wavelength offset correction equation

Figure 2.3a illustrates how the R data of Table 2.1 were used to obtain, for each seawater batch, the absorbance ratio that would have been measured by a “perfectly calibrated” spectrophotometer, as defined in Section 2.3.5 (i.e., R^0). This example, from seawater batch #2, is representative of the other three batches as well.

Figure 2.3b shows ΔR values ($R - R^0$) plotted as a function of wavelength offset ($\Delta\lambda_{241.1}$). Linear regression of these data yielded an empirical relationship that can be used to convert R values determined on any wavelength-calibrated spectrophotometer to offset-corrected values of R^0 :

$$R^0 = R - 0.0265 \cdot \Delta\lambda_{241.1} \quad (2.11)$$

The three “Corrected Data” columns of Table 2.1 show the corrected absorbance ratios thus obtained (R^0); the resulting values of $[\text{CO}_3^{2-}]_{\text{spec}}$, calculated using Eq. (2.8) and the parameters of Patsavas et al. (2015a); and the resulting $[\text{CO}_3^{2-}]_{\text{spec}}$ residuals.

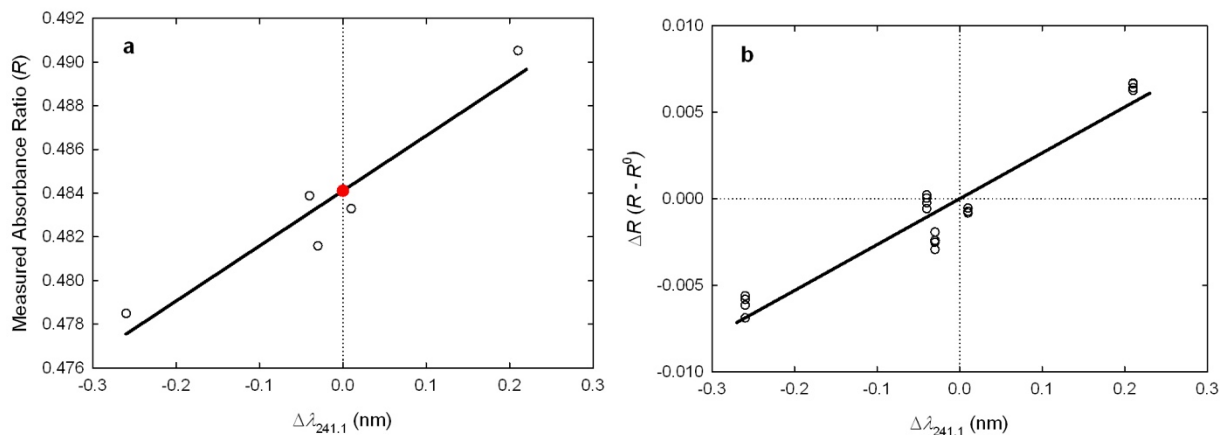


Figure 2.3. (a) Determination of R^0 (absorbance ratio when $\Delta\lambda_{241.1} = 0$) for one of the four seawater batches. R values determined on the five different spectrophotometers are plotted against each instrument’s wavelength offset ($\Delta\lambda_{241.1}$). The y-intercept (denoted by the red dot) is the batch-specific R^0 — the absorbance ratio that would have been reported by a “perfectly calibrated” spectrophotometer. (b) Determination of the wavelength offset correction equation (Eq. (2.11)). Values of ΔR were plotted against the wavelength offset of the measuring spectrophotometer. The linear regression yields a correction equation that can be used to convert measured R values to offset-corrected values of R^0 .

Comparison of the corrected and uncorrected data shows that the R^0 values exhibit far less variation among instruments than do the original R values. Similarly, the $[\text{CO}_3^{2-}]_{\text{spec}}$ residuals for the corrected data show no anomalously large values such as those seen in the residuals of the uncorrected data. Indeed, in terms of carbonate ion concentrations, the corrected data show an average (per batch) standard deviation of $2.01 \mu\text{mol kg}^{-1}$ compared to $7.40 \mu\text{mol kg}^{-1}$ for the uncorrected data.

These observations demonstrate that for the types of UV-visible spectrophotometers often used for shipboard and laboratory work (Agilent 8453 instruments, in this case), the accuracy

necessary for $[\text{CO}_3^{2-}]_{\text{spec}}$ measurements is not achieved using the wavelength recalibration procedure (Venable and Eckerle, 1979) recommended by the manufacturer. Offsets well within the specified wavelength accuracy limit (± 0.5 nm, in this case) can lead to considerable inconsistencies in measured $[\text{CO}_3^{2-}]_{\text{spec}}$. For example, the 0.5 nm offset shown in Figure 2.2 corresponds to a 10% difference in $[\text{CO}_3^{2-}]_{\text{spec}}$. Wavelength offsets for instruments provided by other manufacturers likely have similar implications.

The proposed wavelength offset correction (Eq. (2.11)), which is based on the NIST standard SRM 2034, is an effective way to remedy the problem. Repeated evaluations with SRM 2034 have indicated that the wavelength offset for a given instrument remains quite constant over time (provided the instrument is not recalibrated in the interim).

It is important to note that the sub-nanometer wavelength offsets described in this paper are not detrimental to spectrophotometric pH_T measurements obtained from sulfonephthalein absorbance ratios. The wavelengths used for pH_T measurements are located at the crests of absorbance peaks (Byrne and Breland, 1989; Clayton and Byrne, 1993; Liu et al., 2011), where small discrepancies in wavelength calibration have no observable effect on measured absorbance ratios.

2.4.4 Refined $[\text{CO}_3^{2-}]_{\text{spec}}$ computational algorithm

The salinity-dependent parameters obtained through the empirical fitting procedure described in Section 2.3.6 are:

$$\log\{\text{CO}_3\beta_1/e_2\} = 6.87057 - 0.142142 \cdot S + 0.00190892 \cdot S^2 \quad (2.12)$$

$$e_1 = 0.787458 - 0.0339648 \cdot S + 0.000583574 \cdot S^2 \quad (2.13)$$

$$e_3/e_2 = 2.52288 - 0.0383205 \cdot S \quad (2.14)$$

A quadratic term in the e_3/e_2 parameter, which was reported in previous publications (Byrne and Yao, 2008; Easley et al., 2013; Patsavas et al., 2015a), proved to be insignificant in this context and was therefore dropped. To obtain a spectrophotometric carbonate ion concentration for a seawater sample, these parameters are to be used in Eq. (2.8), which relates $[\text{CO}_3^{2-}]_{\text{spec}}$ to offset-corrected absorbance ratios (R^0).

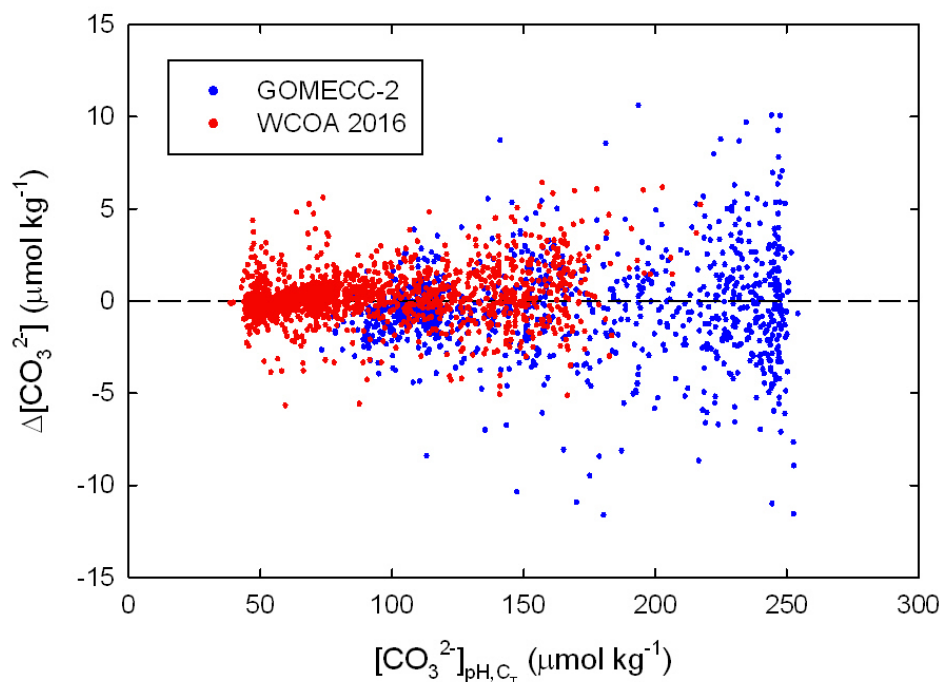


Figure 2.4. Reprocessed values of $\Delta[\text{CO}_3^{2-}]$ (i.e., $[\text{CO}_3^{2-}]_{\text{pH},\text{C}_T} - [\text{CO}_3^{2-}]_{\text{spec}}$) from the two NOAA cruises, based on values of R^0 (obtained from Eq. (2.11)) and the refined $[\text{CO}_3^{2-}]_{\text{spec}}$ algorithm of this work (Eq. (2.8), with the parameters of Eqs. (2.12–2.14)). Values of $[\text{CO}_3^{2-}]_{\text{spec}}$ were determined from shipboard absorbance measurements, and values of $[\text{CO}_3^{2-}]_{\text{pH},\text{C}_T}$ were calculated from paired shipboard measurements of pH_T and C_T .

Values of $\Delta[\text{CO}_3^{2-}]$ for the GOMECC-2 and WCOA 2016 cruises, determined using Eqs. (2.11) and (2.8) (with the parameters of Eqs. (2.12–2.14)), are displayed in Figure 2.4. Outliers were again eliminated by deleting $\Delta[\text{CO}_3^{2-}]$ values that were more than three standard deviations

from the mean $\Delta[\text{CO}_3^{2-}]$ of each dataset (1.3% of the data points were eliminated). The combined correction procedure and new computational algorithm produce concordant $[\text{CO}_3^{2-}]_{\text{spec}}$ results obtained using different instruments on different cruises. The average value of $\Delta[\text{CO}_3^{2-}]$ was $-0.03 \pm 1.9 \mu\text{mol kg}^{-1}$, and the average difference in $\Delta[\text{CO}_3^{2-}]$ between the two cruises was $0.7 \mu\text{mol kg}^{-1}$. This comparison represents a substantial improvement over the results obtained using the Patsavas et al. (2015a) algorithm with uncorrected R values (Figure 2.1).

The relative standard uncertainty of the $[\text{CO}_3^{2-}]_{\text{spec}}$ measurements was 1.5%. In the context of the measurement quality goals of the Global Ocean Acidification Observing Network (GOA-ON), this result is well within the weather objective, which “requires the carbonate ion concentration...to have a relative standard uncertainty of 10%” (Newton et al., 2014). It also very nearly meets the climate objective, which “requires that a change in the carbonate ion concentration be estimated at a particular site with a relative standard uncertainty of 1%” (Newton et al., 2014). It is encouraging that, at present, spectrophotometric measurements of carbonate ion concentrations can nearly achieve GOA-ON’s climate objective, even when the data used to assess concentration changes are collected using different instruments and with different operators.

2.4.5 Verification of fitting procedure

The parameters described in Eqs. (2.12–2.14) (obtained by fitting the entire combined-cruise dataset) can be considered as optimal for computation of $[\text{CO}_3^{2-}]_{\text{spec}}$ from corrected absorbance measurements. As a demonstration of the efficacy of this fitting procedure, an additional assessment (Section 2.3.7) was undertaken by processing one half of the cruise data using $\log\{\text{CO}_3\beta_1/e_2\}$, e_1 , and e_3/e_2 parameters that were generated by fitting the other half of the data. The resulting average $\Delta[\text{CO}_3^{2-}]$ was $-0.10 \pm 2.1 \mu\text{mol kg}^{-1}$. This result compares favorably

with the average $\Delta[\text{CO}_3^{2-}]$ obtained by parameterizing the entire combined-cruise dataset to obtain Eqs. (2.12–2.14) ($-0.03 \pm 1.9 \mu\text{mol kg}^{-1}$).

2.4.6 Model to calculate in situ $[\text{CO}_3^{2-}]_{\text{spec}}^*$ from $[\text{CO}_3^{2-}]_{\text{spec}}$

The fitting procedure described in Section 2.3.8 provided an empirical relationship between in situ carbonate ion concentrations ($[\text{CO}_3^{2-}]_{\text{spec}}^*$) and carbonate ion concentrations measured under laboratory conditions ($[\text{CO}_3^{2-}]_{\text{spec}}$). The parameters A , B , and C in Eq. (2.9) have the following dependencies on S , P (dbars), and $[\text{CO}_3^{2-}]_{\text{spec}}$ (here expressed in $\mu\text{mol kg}^{-1}$):

$$10^2 \cdot A = 296.280 - 28.6065 \cdot S - 23.2553 \cdot (P/100) - 2.81230 \cdot [\text{CO}_3^{2-}]_{\text{spec}} \quad (2.15)$$

$$10^3 \cdot B = -54.2813 + 6.50835 \cdot S + 3.68097 \cdot (P/100) + 1.94542 \cdot [\text{CO}_3^{2-}]_{\text{spec}} \quad (2.16)$$

$$10^4 \cdot C = 8.20538 + 1.63374 \cdot S - 0.375824 \cdot (P/100) - 0.504280 \cdot [\text{CO}_3^{2-}]_{\text{spec}} \quad (2.17)$$

According to Eq. (2.9), carbonate ion concentration increases with increasing temperature by somewhat more than $0.4 \mu\text{mol kg}^{-1}$ per $^\circ\text{C}$. With increasing pressure, carbonate ion concentration decreases by somewhat less than $0.2 \mu\text{mol kg}^{-1}$ per 100 dbars. For the range of data considered in the model, the differences between in situ carbonate concentrations calculated using (a) coupled values of A_T and C_T versus (b) Eq. (2.9) and Eqs. (2.15–2.17) with a theoretical $[\text{CO}_3^{2-}]_{\text{spec}}$ value showed a standard deviation of $\pm 0.51 \mu\text{mol kg}^{-1}$.

2.4.7 Evaluation of $[\text{CO}_3^{2-}]_{\text{spec}}$ -based in situ aragonite saturation states

Using the field data, it was possible to compare two independent characterizations of aragonite saturation state: $\Omega_{A(\text{pH}, C_T)}$ versus $\Omega_{A(\text{spec})}$. Differences between the two are shown as a

function of measured $[\text{CO}_3^{2-}]_{\text{spec}}^*$ in Figure 2.5. The average difference was -0.0007 ± 0.022 for the WCOA 2016 cruise and 0.0011 ± 0.041 for the GOMECC-2 cruise.

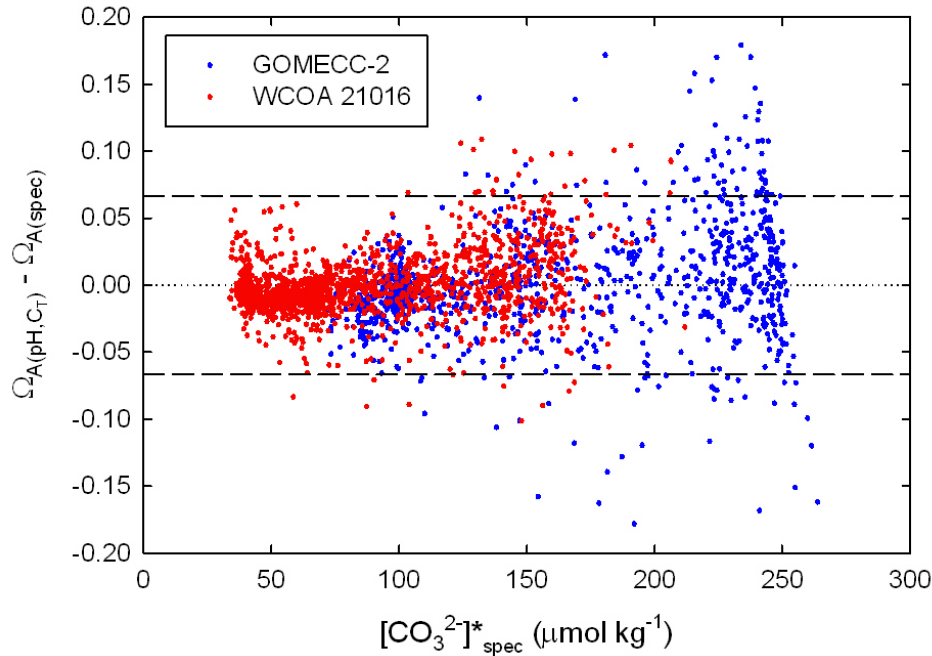


Figure 2.5. Differences between the two characterizations of in situ aragonite saturation states from the two cruises. Values of $\Omega_{A(\text{pH},\text{C}_T)}$ were calculated using paired shipboard measurements of pH_T and C_T , and values of $\Omega_{A(\text{spec})}$ were calculated using shipboard measurements of $[\text{CO}_3^{2-}]_{\text{spec}}^*$. The interval constrained by the dashed lines contains 95% of all observations.

Representative cross sections of $\Omega_{A(\text{pH},\text{C}_T)}$ and $\Omega_{A(\text{spec})}$ are shown in the top two panels of Figure 2.6, and a cross-section of their differences is shown in the bottom panel. Saturation states computed using the new model agree well with those calculated from paired measurements of C_T and pH_T , especially in surface waters where saturation states can significantly alter the life cycles of calcareous organisms.

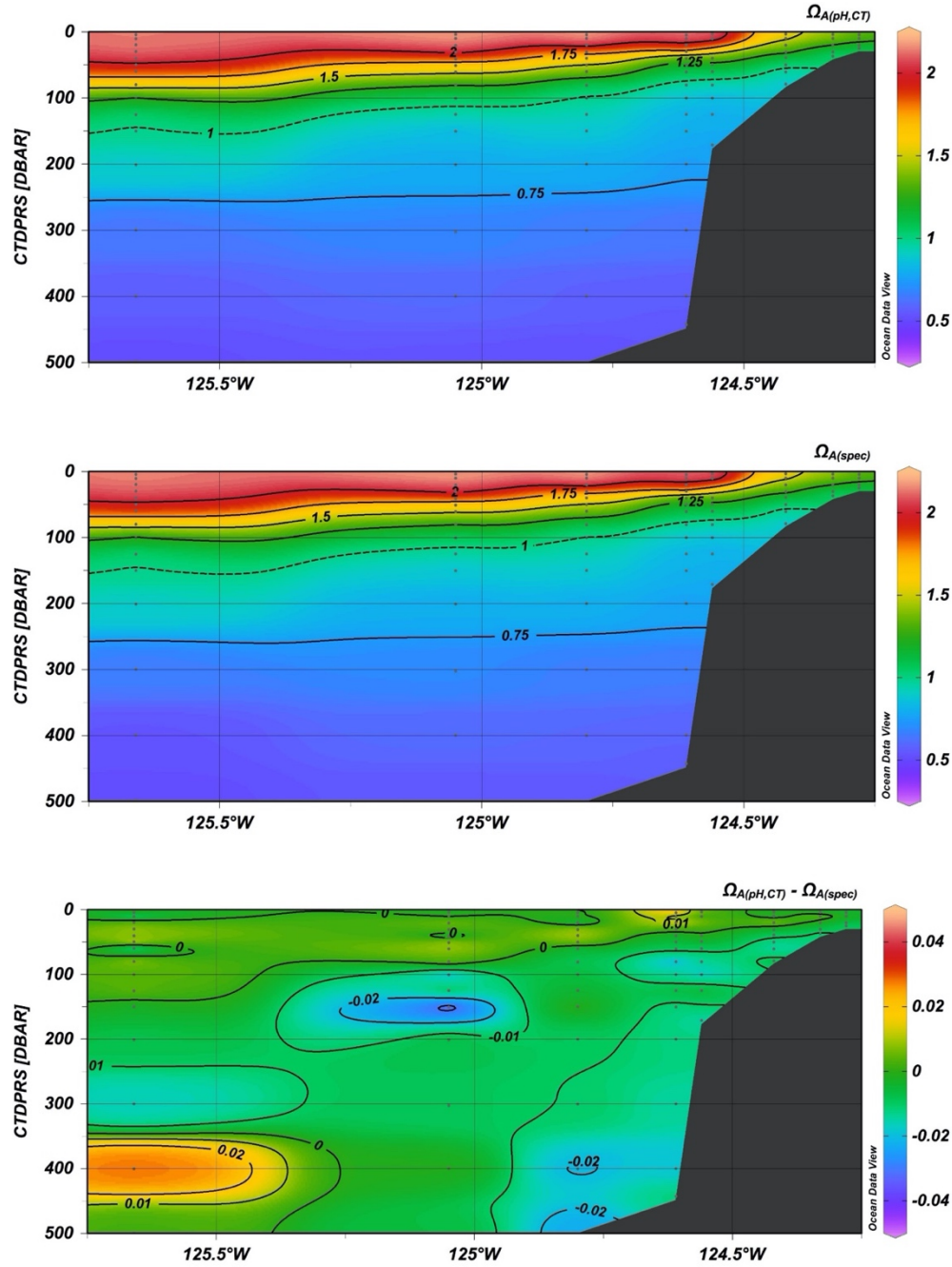


Figure 2.6. Cross-sections of aragonite saturation state along WCOA 2016 Line 9, near the California/Oregon border (see Figure B1.1 for location). The top panel shows $\Omega_{A(pH,CT)}$, determined by calculation from shipboard measurements of pH_T (spectrophotometric) and C_T (coulometric). The middle panel shows $\Omega_{A(spec)}$, determined by calculation from shipboard measurements of $[CO_3^{2-}]_{spec}$, Eq. (2.9), Eqs. (2.15–2.17), and Eq. (2.10). The dashed lines indicate the aragonite saturation horizon (i.e., where $\Omega_A = 1$). The bottom panel shows the difference between $\Omega_{A(pH,CT)}$ and $\Omega_{A(spec)}$. On the y-axes, CTDPRS is pressure in decibars (DBAR), as measured by the CTD.

Overall, the relative standard uncertainty of the $\Omega_{A(\text{spec})}$ calculations is less than 2%. Again, this result can be viewed in the context of GOA-ON's measurement quality goals (Newton et al., 2014). GOA-ON presents relative standard uncertainty goals for $[\text{CO}_3^{2-}]$ (10% for the weather objective, 1% for the climate objective), which closely correspond to relative standard uncertainties in Ω . Similar to the $[\text{CO}_3^{2-}]_{\text{spec}}$ result, the relative standard uncertainty of the $\Omega_{A(\text{spec})}$ calculations is well within GOA-ON's weather objective and nearly meets the climate objective.

The closely similar saturation state depictions of Figure 2.6 can also be viewed in context of the cost, time, and manpower required to produce those data. Determinations of in situ $\Omega_{A(\text{pH}, \text{C}_T)}$ (top panel) require a spectrophotometer and a coulometer, with a combined per-sample analysis time of ~13 minutes (~3 minutes for pH_T and ~10 minutes for C_T), and two teams of analysts to sustain 24-hour operations at an acceptable pace. Determinations of in situ $\Omega_{A(\text{spec})}$ (middle panel) require only a spectrophotometer, with a per-sample analysis time of ~3 minutes, and a single team of analysts to sustain 24-hour operations at an acceptable pace.

2.4.8 Implications

Previous publications (Byrne and Yao, 2008; Easley et al., 2013; Fajar et al., 2015; Patsavas et al., 2015a) have discussed the advantages of spectrophotometric determinations of seawater carbonate ion concentrations. This work builds on that earlier body of work by (a) identifying and eliminating a significant instrumental artifact and (b) extending the utility of $[\text{CO}_3^{2-}]_{\text{spec}}$ measurements to provide in situ carbonate ion concentrations and in situ CaCO_3 saturation states.

The laboratory spectrophotometers required to measure $[\text{CO}_3^{2-}]_{\text{spec}}$ are widely available and relatively inexpensive, unlike the specialized equipment required to measure C_T and A_T . This work, moreover, improves the quality of the data that such spectrophotometers can deliver. In addition, measurements of $[\text{CO}_3^{2-}]_{\text{spec}}$ are, like spectrophotometric pH_T measurements, far more rapid than measurements of C_T and A_T .

A critical advantage of $[\text{CO}_3^{2-}]_{\text{spec}}$ is that it can be used as a fifth measurable CO_2 system parameter; this addition has implications for examinations of internal consistency. Measurements of $[\text{CO}_3^{2-}]_{\text{spec}}$ (like pH_T and C_T) are not biased by organic alkalinity, which can influence internal consistency when A_T is used as an input parameter (Patsavas et al., 2015b). Similarly, $[\text{CO}_3^{2-}]_{\text{spec}}$ can provide insight into known problems, such as the observed bias in calculated f_{CO_2} that is evident at high f_{CO_2} when A_T and C_T are used as input parameters (Hoppe et al., 2012). The use of carbonate as a fifth reliable measurement parameter is also beneficial because of its methodological similarity to spectrophotometric pH_T measurements. No other two CO_2 system parameters have this similarity, whereby a single type of instrumentation can be used for determinations of two parameters via measurements of absorbance ratios. This has implications for CO_2 system characterizations that are both accurate and methodologically simple.

Our model for calculating in situ $[\text{CO}_3^{2-}]_{\text{spec}}^*$ values and CaCO_3 saturation states from shipboard $[\text{CO}_3^{2-}]_{\text{spec}}$ measurements bypasses the need for labor-intensive, conjugate measurements of multiple (i.e., two or more) CO_2 system measurement variables (C_T , A_T , pH , or f_{CO_2}) to determine Ω . As saturation states in the world's oceans continue to decline (Feely et al., 2004; 2012) and as shoaling saturation horizons more regularly bring corrosive water ($\Omega_A < 1$) onto continental shelves (Feely et al., 2008), simple, labor-saving methods to evaluate saturation

states are increasingly valuable to researchers and to natural resource and business (e.g., aquaculture) managers.

An important implication of this work is that previously collected datasets of absorbance ratios for $[\text{CO}_3^{2-}]_{\text{spec}}$ determinations can be reprocessed. If the spectrophotometer used to collect those data is still available (and has not been re-calibrated), its wavelength offset can be determined and the archived absorbance ratios can be corrected with Eq. (2.11) to yield R^0 values for use in Eq. (2.8) (with the parameters of Eqs. (2.12–2.14)). The result is a $[\text{CO}_3^{2-}]_{\text{spec}}$ dataset with improved precision and an accuracy that is linked to a NIST standard.

Spectrophotometric carbonate measurements are also amenable to use in situ (Byrne and Yao, 2008). Realization of in situ measurement capabilities will require direct, physical chemical characterization of the temperature and pressure dependencies of the $[\text{CO}_3^{2-}]_{\text{spec}}$ computational algorithm, including equilibrium constants and molar absorptivities. This capability is especially important because in situ spectrophotometric measurements can be obtained essentially continuously (>1 measurement per second), thus allowing for observations of $[\text{CO}_3^{2-}]_{\text{spec}}$ and saturation state with very high spatial and temporal resolution on moorings, profiling floats, gliders, Niskin rosette frames, seawater flow-through systems, and other platforms.

2.4.9 Procedural overview

The general procedure to spectrophotometrically measure seawater carbonate ion concentrations is as follows:

First, for a given spectrophotometer, the wavelength offset ($\Delta\lambda_{241.1} = \lambda_{\text{NIST}} - \lambda_{\text{spec}}$) is determined using SRM 2034 (Travis et al., 2005) from NIST. It is important that this $\Delta\lambda_{241.1}$ value

be thereafter associated with all $[\text{CO}_3^{2-}]_{\text{spec}}$ absorbance data collected with this instrument. If the instrument is recalibrated, the wavelength offset must be redetermined.

Next, $[\text{CO}_3^{2-}]_{\text{spec}}$ of seawater samples can be determined via the following steps: (1) for each sample, measure an absorbance ratio (R) using absorbances measured at 234, 250, and 350 nm according to the $\text{Pb}(\text{ClO}_4)_2$ procedure outlined in Section 2.3.2 and in Patsavas et al. (2015a); (2) calculate corrected absorbance ratios (R^0) with Eq. (2.11), using the instrument-specific $\Delta\lambda_{241.1}$; and (3) calculate $[\text{CO}_3^{2-}]_{\text{spec}}$ with Eq. (2.8), using R^0 and the salinity-dependent parameters given in Eqs. (2.12–2.14). It is important to note that the titrant-induced perturbation equation presented in Patsavas et al. (2015a) is not utilized in this updated method.

Additionally, because of the possible use of multi-wavelength measurement techniques (Byrne and Kester, 1978; 1981; Byrne et al., 1981) in the future, we recommend also recording Pb(II) absorbances at wavelengths surrounding the primary target wavelengths (e.g., 233, 234, and 235 nm).

Before being discarded, lead-enriched seawater should be passed through an ion exchange resin (e.g., Chelex® 100 Resin from Bio-Rad) or treated by other means to remove Pb(II), which is toxic to aquatic life (Fernández and Beiras, 2000; Nadella et al., 2013; Warnau et al., 1994).

2.5 Supporting Information

Figure included in Appendix B1 to show station locations for the GOMECC-2 and WCOA 2016 cruises. The transect featured in Figure 2.6 is designated.

2.6 Acknowledgements

This material is based on work supported by the National Science Foundation, Award No. OCE-1220110. Support for J.D. Sharp was provided by the NSF Graduate Research Fellowship Program, Award No. 1144244, and by the Anne and Werner Von Rosenstiel Fellowship in Marine Science from the University of South Florida College of Marine Science. Drs. Rik Wanninkhof, Richard Feely, Simone Alin, and their staff, as well as the GOMECC-2 and WCOA 2016 cruises, were supported by NOAA's Ocean Acidification Program, Atlantic Oceanographic and Meteorological Laboratory, and Pacific Marine Environmental Laboratory. This is PMEL contribution number 4644. We would like to thank Dr. Nora Katie Douglas, Dr. Regina Easley, Dr. Mark Patsavas, Dr. Bo Yang, and Dr. Yong-Rae Kim for their assistance in collecting and analyzing field samples. We thank Dana Greeley and Julian Herndon, along with the captain, officers, and crew of the NOAA Ship *Ronald H. Brown*, for support with planning and execution of the fieldwork. Special thanks are given to Dr. Tonya Clayton for her insightful comments and editorial assistance. The authors are grateful for the constructive comments of three anonymous reviewers.

CHAPTER THREE:
**DEVELOPMENT OF A MODEL FOR [CO₃²⁻] MEASUREMENTS AT AMBIENT
TEMPERATURE AND EVALUATION OF UNCERTAINTIES IN CO₂ SYSTEM
PARAMETERS CALCULATED FROM [CO₃²⁻]**

Note: This chapter has been reprinted (adapted) with permission from:

Sharp, J.D., Byrne, R.H., 2019. Carbonate ion concentrations in seawater: Spectrophotometric determination at ambient temperatures and evaluation of propagated calculation uncertainties. *Marine Chemistry* 209, 70–80.

Copyright 2018 Elsevier.

3.1 Abstract

In ocean waters, the carbonate ion is of crucial importance to benthic and pelagic organisms that build their physical support structures out of calcium carbonate (CaCO₃). Marine carbonate ion concentrations ([CO₃²⁻]) are measurable through spectrophotometric observations of the ultraviolet (UV) light absorbed by lead carbonate in Pb-enriched seawater, but previous characterizations of the Pb UV-absorption model have been applicable only at a fixed temperature of 25 °C. In this paper, the model is extended to a temperature range of 3 to 40 °C and a salinity range of 20 to 40. This advancement allows for determinations of [CO₃²⁻] with temperature measurement rather than temperature control, thus decreasing the required financial investment and instrumental complexity. The extended model also represents a significant step toward the

development of automated inline or in situ $[\text{CO}_3^{2-}]$ sensors and promotes the utility of $[\text{CO}_3^{2-}]$ as a fifth measured variable for inclusion in studies of the marine carbon dioxide (CO_2) system. Therefore, a quantitative evaluation of propagated uncertainties in CO_2 system calculations based on $[\text{CO}_3^{2-}]$ as an input variable was also performed. The results show that total dissolved inorganic carbon (C_T) and total alkalinity (A_T) are the most suitable measured variables to pair with measured $[\text{CO}_3^{2-}]$ as input to such calculations. Pairing $[\text{CO}_3^{2-}]$ with the partial pressure of CO_2 yields relatively low uncertainty in calculated pH — comparable to that resulting from conventional input pairs — but relatively high uncertainties in calculated A_T and C_T . Pairing $[\text{CO}_3^{2-}]$ with pH results in relatively high uncertainties in all calculated variables. CaCO_3 saturation states (Ω) determined from measured $[\text{CO}_3^{2-}]$ (alone) can circumvent some sources of uncertainty inherent to conventional (two-variable) calculations. Simpler, more direct ways of measuring $[\text{CO}_3^{2-}]$ open up new opportunities for marine researchers and others interested in monitoring CaCO_3 saturation states in seawater.

3.2 Introduction

Over the course of industrialized history, anthropogenic processes such as fossil fuel combustion, cement production, and land use change have released an estimated 645 ± 80 petagrams of carbon into Earth's atmosphere (1750–2016) (Le Quéré et al., 2018). This large, rapid release of carbon — primarily in the form of carbon dioxide (CO_2) — has resulted in measurable impacts on not only climate (Matthews et al., 2009; Ramanathan, 1988; Solomon et al., 2009) but also seawater chemistry. Oceanic uptake of CO_2 (Humphreys et al., 2018; Takahashi et al., 2002, 2009; Wanninkhof, 1992; Weiss et al., 1982) results in the formation of carbonic acid (H_2CO_3), which rapidly dissociates to cause a decrease in seawater pH (i.e., an increase in

hydrogen ion concentration, $[H^+]$) in a process known as ocean acidification (Bates et al., 2014; Doney et al., 2009; Feely et al., 2009; Orr et al., 2005; Zeebe et al., 2008).

The marine CO_2 system — involving a series of interconnected equilibria that constitute the dominant buffering system in the ocean — somewhat resists anthropogenically induced acidification. Some of the hydrogen ions released by the dissociation of carbonic acid ($H_2CO_3 \rightleftharpoons H^+ + HCO_3^-$) complex with carbonate ions ($H^+ + CO_3^{2-} \rightleftharpoons HCO_3^-$) to mitigate the potential pH drop. Consequently, ocean acidification results in not only increased $[H^+]$ but also decreased carbonate ion concentration ($[CO_3^{2-}]$) (Feely et al., 2004, 2012; Orr et al., 2005). Considering the direct and indirect sensitivities of certain marine biota (and the industries that rely upon them) to seawater $[CO_3^{2-}]$, the repercussions of this worldwide $[CO_3^{2-}]$ decline are especially serious in coastal regions, where human communities will feel the impacts (Ekstrom et al., 2015; Mathis et al., 2015).

Historically, due to the unavailability of suitable analytical methods, $[CO_3^{2-}]$ has not been directly measured in seawater chemical analyses. Instead $[CO_3^{2-}]$ is usually calculated from two of the four CO_2 system variables that are more typically measured (Park, 1969): total alkalinity (A_T), total dissolved inorganic carbon (C_T), pH, and partial pressure of CO_2 (pCO_2). Recently though, a novel application of the speciation behavior of Pb(II) in seawater (Byrne, 1981) has allowed for spectrophotometric measurements of total carbonate ion concentrations ($[CO_3^{2-}]_{spec}$) by quantifying the ultraviolet (UV) light absorbed by lead carbonate ($PbCO_3^0$) and lead chloride complexes in Pb(II)-enriched seawater (Byrne and Yao, 2008). This method has been iteratively refined through both laboratory investigations and field measurements and has been employed successfully on oceanographic research cruises in the Pacific, Atlantic, Arctic, and Mediterranean oceans (Easley et al., 2013; Fajar et al., 2015; Patsavas et al., 2015a; Sharp et al., 2017).

Compared to the common practice of deriving seawater carbonate ion concentrations from measurements of other CO₂ system variables, measuring [CO₃²⁻]_{spec} provides a more direct assessment of this oceanographically important quantity. These spectrophotometric measurements therefore also provide more direct evaluations of calcium carbonate (CaCO₃) saturation states (Ω), for both aragonite (Ω_{arag}) and calcite (Ω_{cal}). Spectrophotometric measurements of carbonate ion concentrations are advantageous (especially at sea) due to their speed, affordability, and simplicity (Byrne and Yao, 2008).

With this study, we seek to improve the efficiency and simplicity of [CO₃²⁻]_{spec} measurements by eliminating the requirement for meticulous temperature control. Previous descriptions of the UV-absorption behavior of Pb(II) in seawater have limited the [CO₃²⁻]_{spec} method to a fixed temperature of 25 °C and a salinity range of ~20 to ~37. Here, we present a model that extends this description across a range of temperature (T) from 3 to 40 °C and a range of salinity (S) from 20 to 40. This advancement allows for benchtop measurements of seawater [CO₃²⁻]_{spec} without the use of expensive and cumbersome temperature control devices, thus making the procedure more accessible to investigators limited by space or cost. This work may motivate the development and deployment of instruments for inline or in situ determinations of seawater [CO₃²⁻]_{spec}.

We also explore combined standard uncertainties in marine CO₂ system variables that have been calculated using [CO₃²⁻]_{spec} as one member of a pair of input variables. Uncertainties in CO₂ system calculations have been critically evaluated before (Dickson, 2010b; Dickson and Riley, 1978; Millero, 1995; Orr et al., 2018), and combined standard uncertainties in derived variables are now more routinely reported (e.g., Fassbender et al., 2017; Lauvset and Gruber, 2014; Sutton et al., 2016; Williams et al., 2017). However, no study has yet considered [CO₃²⁻] as an input

variable for uncertainty propagations. We therefore utilize a newly available software package for routine uncertainty propagation (Orr et al., 2018) to explore the uncertainties that can result from using $[\text{CO}_3^{2-}]_{\text{spec}}$ to calculate other CO_2 system variables. This analysis elucidates the best variables to pair with measured $[\text{CO}_3^{2-}]_{\text{spec}}$ for reliable characterizations of the marine CO_2 system.

3.3 $[\text{CO}_3^{2-}]_{\text{spec}}$ Measurement Theory

The intricacies of the theory governing determinations of $[\text{CO}_3^{2-}]_{\text{spec}}$ from ultraviolet observations of Pb(II) absorbance spectra are detailed elsewhere (Byrne, 1981; Byrne and Yao, 2008; Easley et al., 2013; Patsavas et al., 2015a; Sharp et al., 2017; Soli et al., 2008). Major points relevant to this paper are highlighted in the following paragraphs.

Complexation of Pb^{2+} and CO_3^{2-} is represented by:



The associated equilibrium constant, ${}_{\text{CO}_3}\beta_1$, is given by:

$${}_{\text{CO}_3}\beta_1 = \frac{[\text{PbCO}_3^0]}{[\text{Pb}^{2+}]_{\text{T}}[\text{CO}_3^{2-}]} \quad (3.2)$$

where $[\text{PbCO}_3^0]$ is the sum concentration of Pb(II) complexed with carbonate, including minor contributions from mixed-ligand species (e.g., PbCO_3Cl^-); $[\text{Pb}^{2+}]_{\text{T}}$ is the sum concentration of free Pb^{2+} , Pb(II)-chloride species, and some minor Pb(II)-sulfate species; and $[\text{CO}_3^{2-}]$ is the total concentration of free and ion-paired carbonate. All carbonate ion concentrations presented in this paper are total concentrations. All ion concentrations are given in terms of moles or micromoles per kilogram of solution (not per kilogram of solute).

The absorbance of Pb(II) in seawater at a particular wavelength λ is described by:

$$\frac{\lambda A}{l \cdot [\text{Pb}]_{\text{T}}} = \frac{\lambda \varepsilon_{\text{Pb}^{2+}} + \lambda \varepsilon_{\text{PbCO}_3^0} \cdot {}_{\text{CO}_3}\beta_1 \cdot [\text{CO}_3^{2-}]}{1 + {}_{\text{CO}_3}\beta_1 \cdot [\text{CO}_3^{2-}]} \quad (3.3)$$

where ${}_{\lambda}A$ is absorbance at wavelength λ , l is the pathlength of the spectrophotometer cell, $[\text{Pb}]_{\text{T}}$ is the total concentration of Pb(II) in the sample, and ${}_{\lambda}\epsilon_j$ is the molar absorptivity of species j at wavelength λ . The ratio (R) of absorbance measurements taken at 250 and 234 nanometers (nm) is given by:

$$R = \frac{{}_{250}A}{{}_{234}A} = \frac{{}_{250}\epsilon_{\text{Pb}} + {}_{250}\epsilon_{\text{PbCO}_3} \cdot \text{CO}_3\beta_1 \cdot [\text{CO}_3^{2-}]}{{}_{234}\epsilon_{\text{Pb}} + {}_{234}\epsilon_{\text{PbCO}_3} \cdot \text{CO}_3\beta_1 \cdot [\text{CO}_3^{2-}]} \quad (3.4)$$

In practice, the non-absorbing wavelength of 350 nm is also used to correct for background absorbance changes:

$$R = \frac{{}_{250}A - {}_{350}A}{{}_{234}A - {}_{350}A} \quad (3.5)$$

Eq. (3.4) is algebraically rearranged to yield:

$$-\log[\text{CO}_3^{2-}]_{\text{spec}} = \log\{\text{CO}_3\beta_1/e_2\} + \log\{(R^0 - e_1)/(1 - R^0 \cdot e_3/e_2)\} \quad (3.6)$$

where e_1 , e_2 , and e_3/e_2 are molar absorptivity ratios defined as

$$e_1 = \frac{{}_{250}\epsilon_{\text{PbCO}_3}}{{}_{234}\epsilon_{\text{PbCO}_3}}, e_2 = \frac{{}_{250}\epsilon_{\text{Pb}}}{{}_{234}\epsilon_{\text{PbCO}_3}}, e_3/e_2 = \frac{{}_{234}\epsilon_{\text{Pb}}}{{}_{250}\epsilon_{\text{Pb}}} \quad (3.7)$$

In Eq. (3.6), $[\text{CO}_3^{2-}]_{\text{spec}}$ is the spectrophotometrically determined total carbonate ion concentration and the absorbance ratio originally denoted by R has been replaced with an absorbance ratio (R^0) that has been corrected for non-resolvable wavelength scale inaccuracies, as described by Sharp et al. (2017):

$$R^0 = R - 0.0265 \cdot \Delta\lambda_{241.1} \quad (3.8)$$

where $\Delta\lambda_{241.1}$ is the difference between 241.10 nm (λ_{NIST} ; the standard location of one absorbance peak of a NIST holmium oxide standard, SRM 2034) and the wavelength at which the spectrophotometer in use reports that peak (λ_{spec}): $\Delta\lambda_{241.1} = \lambda_{\text{NIST}} - \lambda_{\text{spec}}$.

The three Eq. (3.6) parameters ($\log\{\text{CO}_3\beta_1/e_2\}$, e_1 , and e_3/e_2) are influenced by S , T , and pressure (P). In previous work (Byrne and Yao, 2008; Easley et al., 2013; Patsavas et al., 2015a;

Sharp et al., 2017), these parameters have been described as functions of S at a T of 25 °C and a P of 1 atm.

3.4 Methods

3.4.1 CO₂ system measurements

Natural seawater ($S \approx 37$) was collected from surface waters of the northeastern Gulf of Mexico off the West Florida Shelf. For laboratory analyses, this seawater was diluted with Milli-Q water to obtain salinities <37 or slowly evaporated at laboratory conditions to obtain salinities >37 . Salinity was measured with a Portasal 8410A salinometer (Guideline Instruments). To alter seawater carbonate composition, small amounts of HCl or NaOH (1 M, Fisher Scientific) were added to several batches of seawater at a variety of salinities from 20 to 40.

The A_T of each seawater batch was measured using the spectrophotometric single-step titration procedure of Liu et al. (2015). A tungsten FO-6000 fiber optic light source (World Precision Instruments) was used along with a USB4000 spectrophotometer (Ocean Optics). For acidimetric titration, HCl (0.25 M) in NaCl solution (0.45 M, MP Biomedicals) was delivered to samples with a Metrohm 665 Dosimat (Brinkmann). Due to the small volume of titrant (<2 mL, $I = 0.7$ m) relative to sample (>200 mL, $I = 0.4$ to 0.8 m), any change in ionic strength during the titration had a negligible effect on measured A_T . Throughout the titrations, seawater pH on the total scale (pH_T) was monitored with bromocresol purple (Sigma, Lot #104H3625). Duplicate A_T measurements were performed to evaluate analytical precision, and accuracy was verified with Certified Reference Materials (CRMs) from the Scripps Institution of Oceanography (Dickson et al., 2003).

From each seawater batch with an established (i.e., measured) A_T , samples were collected into glass optical cells (~30 mL) and analyzed promptly for pH_T over a range of T from 3 to 40 °C. The procedure of Liu et al. (2011) was used with purified *m*-cresol purple (Aldrich, Lot #7005HH). The temperature range of this work (3 to 40 °C) extends slightly beyond that used to develop the Liu et al. (2011) model (5 to 35 °C), but a theoretical extrapolation of the model showed no significant deviations in calculated pH_T values from those that would be expected at slightly higher and lower temperatures.

When the pH_T samples were collected, complementary samples were collected into quartz optical cells (~30 mL) for measurements of Pb(II) absorbance ratios. These measurements were conducted at temperatures as close as possible to those of the pH_T measurements. Mirroring the procedures of Patsavas et al. (2015a) and Sharp et al. (2017), a seawater blank measurement was first recorded. Then, 20 μL of 22 mM lead perchlorate ($\text{Pb}(\text{ClO}_4)_2$; Acros Organics) solution was added to the cell. Next, five sample absorbances were promptly recorded at each of three wavelengths: 234, 250, and 350 nm. It is important that absorbance values be recorded promptly after addition of the $\text{Pb}(\text{ClO}_4)_2$ in order to limit the potential formation of trace amounts of $\text{PbCO}_{3(s)}$ in low-salinity samples. Absorbances were averaged and used with Eq. (3.5) to calculate an absorbance ratio, which was corrected with Eq. (3.8) for wavelength calibration inaccuracies (Sharp et al., 2017).

The absorbance measurements were obtained using three different Agilent 8453 diode array UV–visible spectrophotometers. Gilmont micrometer syringes (model GS-1200) were used to deliver the liquid reagents. Temperature was adjusted and maintained with an Ecoline RE 120 water bath (Lauda). Immediately after each set of absorbance measurements was obtained, the temperature of the seawater within each optical cell was measured using a high-accuracy digital

thermometer (Eutechnics), which was calibrated against a 2804A quartz thermometer (Hewlett-Packard). The total number of sample measurements, N , was 182.

After measurements of Pb(II) absorbance ratios were complete, measured samples were passed through a column of Chelex® 100 resin (Bio-Rad Laboratories) to prevent any unnecessary release of Pb(II) to the environment. ICP-MS analyses (Appendix C1) confirmed that the resin effectively removes Pb(II) from a seawater matrix that has been spiked with Pb(ClO₄)₂.

To supplement the laboratory measurements, datasets from the 2012 Gulf of Mexico and East Coast Carbon Cruise (GOMECC-2; Wanninkhof et al., 2016; $N = 1061$) and the 2016 West Coast Ocean Acidification Cruise (WCOA 2016; Alin et al., 2017; $N = 1585$) were also utilized. GOMECC-2 was carried out between 21 July and 13 August, 2012, aboard the NOAA ship *Ronald H. Brown*, and WCOA 2016 was carried out between 5 May and 7 June, 2016, also aboard the *Ronald H. Brown*. All four CO₂ system variables were measured on both cruises, along with standard hydrographic data (S , T , and P). Pb(II) absorbance ratios were also measured for determinations of [CO₃²⁻]_{spec}. A_T was measured by open cell titration, with a stated uncertainty of 0.1%; C_T was measured by coulometry, with a stated uncertainty of 0.1%; pH_T was measured at 25 °C by spectrophotometry, with an accuracy tied to Tris seawater buffer calibration and a stated precision of ± 0.001 units; and surface pCO_2 was measured by continuous equilibration, with a stated accuracy of ± 2 μatm and a stated precision of ± 0.01 μatm .

3.4.2 Parameterization procedure

All routine CO₂ system calculations were performed using the CO2SYS MATLAB program (van Heuven et al., 2011), which is based on the original CO2SYS program of Lewis and Wallace (1998) and on the work of Pierrot et al. (2006). The equilibrium constant formulations

given in Table 3.1 were used, along with the K_{HSO_4} formulation from Dickson (1990b) and the K_{HF} formulation from Dickson and Riley (1979).

The laboratory measurements of A_T and pH_T , along with estimated concentrations of total phosphate (P_T) and silicate (Si_T), were used to calculate total carbonate ion concentrations ($[\text{CO}_3^{2-}]_{\text{AT,pH}}$) for each temperature at which a Pb(II) absorbance ratio was measured. The phosphate and silicate concentrations were estimated using the average values of surface samples at offshore stations of the GOMECC-2 cruise (Wanninkhof et al., 2016): $P_T = 0.02 \mu\text{mol/kg}$ and $Si_T = 0.76 \mu\text{mol/kg}$. These concentrations were low enough that their cumulative effect on calculated $[\text{CO}_3^{2-}]_{\text{AT,pH}}$ was well within the uncertainty limits for carbonate measurements.

Eq. (3.6) was fit to the calculated $[\text{CO}_3^{2-}]_{\text{AT,pH}}$ values using SigmaPlot (Systat Software). Wavelength-corrected Pb(II) absorbance ratios (R^0 , Eq. (3.8)) were used, and the polynomial equations used to parameterize $\log\{\text{CO}_3\beta_1/e_2\}$, e_1 , and e_3/e_2 were of the form

$$Z = a_0 + b_0S + b_1S^2 + c_0T + c_1T^2 + d_0ST \quad (3.9)$$

where Z represents one of the parameters (i.e., $\log\{\text{CO}_3\beta_1/e_2\}$, e_1 , or e_3/e_2). Insignificant terms were dropped until a t -test indicated that each coefficient was significant at a 95% confidence level.

The resulting model (based on laboratory measurements over a wide range of T) was used to determine $[\text{CO}_3^{2-}]_{\text{spec}}$ values for the GOMECC-2 and WCOA 2016 datasets at 25 °C (the T at which the shipboard pH_T and Pb(II) absorbance ratios were measured). To assess the goodness of fit of the laboratory-based model, these shipboard $[\text{CO}_3^{2-}]_{\text{spec}}$ values were compared to their corresponding $[\text{CO}_3^{2-}]_{\text{CT,pH}}$ values (i.e., the $[\text{CO}_3^{2-}]$ values derived from field measurements of C_T and pH_T).

Subsequently, in order to maximize the reliability and scope of the model, Eq. (3.6) was fit to the laboratory $[\text{CO}_3^{2-}]_{\text{AT,pH}}$ and field-based $[\text{CO}_3^{2-}]_{\text{CT,pH}}$ values simultaneously, using the polynomial structure of Eq. (3.9) for $\log\{\text{CO}_3\beta_1/e_2\}$, e_1 , and e_3/e_2 . Weighting factors inversely proportional to the size of each dataset (laboratory vs. cruise) were applied so that each set contributed equally to the model. This procedure yielded a set of empirically defined parameters that can be used with Eq. (3.6) to calculate $[\text{CO}_3^{2-}]_{\text{spec}}$ from Pb(II) absorbance ratios in tandem with measured temperature and salinity over the ranges $3\text{ }^\circ\text{C} < T < 40\text{ }^\circ\text{C}$ and $20 < S < 40$.

3.4.3 Propagation of uncertainties

The routine uncertainty propagation software packages of Orr et al. (2018) expand upon four commonly used software packages that compute marine CO_2 system chemistry: CO2SYS for Microsoft Excel, CO2SYS for MATLAB, seacarb for R, and mocsy for Fortran. Much like the original CO2SYS program itself (Lewis and Wallace, 1998), the uncertainty propagation software that has been developed by Orr et al. (2018) should prove to be quite valuable in the study of marine CO_2 system chemistry. The routines can be easily understood and utilized by virtually all marine chemists, and the ability to constrain calculated variables within an uncertainty envelope without considerable extra work will be beneficial for interpretations of experimental results. Furthermore, the option to delineate between uncertainty contributions from individual input parameters (both variables and constants) can provide important information about the aspects of marine CO_2 system chemistry (e.g., measurement methods, equilibrium constant determinations, etc.) that require more detailed research in order to further improve the reliability of system characterizations.

Table 3.1. Standard input conditions and the random and total standard uncertainties assigned to the input CO₂ system variables and equilibrium constants for uncertainty propagation. Peripheral variables ($T = 18$ °C, $S = 35$, $P = 1$ atm) are assumed to have been perfectly measured (i.e., are assigned standard uncertainty values of zero), and nutrients are ignored (i.e., are assigned concentrations and standard uncertainty values of zero).

| Variable or Equilibrium Constant | Input Value or Equilibrium Constant Reference | Random Uncertainty | Total Uncertainty (Random + Systematic) |
|---|---|--------------------|---|
| A_T ($\mu\text{mol/kg}$) | 2300.0 † | 2 † | 2 † |
| C_T ($\mu\text{mol/kg}$) | 2000.0 † | 2 † | 2 † |
| pH_T | 8.139 § | 0.003 † | 0.01 † |
| pCO_2 (μatm) | 308.4 § | 2 † | 2 † |
| $[\text{CO}_3^{2-}]$ ($\mu\text{mol/kg}$) | 204.8 § | 0.7% ‡ | 2.0% ‡ |
| $\text{p}K_0$ | Weiss (1974) | 0.002 † | 0.002 † |
| $\text{p}K_1$ | Lueker et al. (2000) | 0.0055 † | 0.0075 † |
| $\text{p}K_2$ | Lueker et al. (2000) | 0.010 † | 0.015 † |
| $\text{p}K_B$ | Dickson (1990a) | 0.01 † | 0.01 † |
| $\text{p}K_W$ | Millero (1995) | 0.01 † | 0.01 † |
| $\text{p}K_{\text{sp(arag)}}$ | Mucci (1983) | 0.020 † | 0.020 † |
| $\text{p}K_{\text{sp(cal)}}$ | Mucci (1983) | 0.020 † | 0.020 † |
| B_T/S | Lee et al. (2010) | 0.4% ¥ | 2.0% † |

† Taken from Orr et al. (2018)

§ Calculated using the specified temperature (18 °C), salinity (35), pressure (1 atm), A_T (2300.0 $\mu\text{mol/kg}$), and C_T (2000.0 $\mu\text{mol/kg}$)

‡ Discussed in Section 3.5.2

¥ Fractional uncertainty equal to one standard deviation of the measurements from Lee et al. (2010)

For this work, the MATLAB CO2SYS routine (slightly modified from van Heuven et al., 2011) and the MATLAB uncertainty propagation routines of Orr et al. (2018) were modified to accept $[\text{CO}_3^{2-}]$ and standard uncertainty in $[\text{CO}_3^{2-}]$ as input variables. These modifications allow for rapid CO₂ system calculations that include inputs of $[\text{CO}_3^{2-}]$, and also for examination of the sensitivities of output variables to uncertainties in input $[\text{CO}_3^{2-}]$. The modified routines are available for download (see Appendix C2).

The uncertainty propagation routines employ the method of moments to estimate the combined standard uncertainties of calculated variables from standard uncertainties of input variables and equilibrium constants (e.g., Ellison and Williams, 1992):

$$u_c^2(y) = \left(\frac{\delta y}{\delta x_1}\right)^2 u^2(x_1) + \left(\frac{\delta y}{\delta x_2}\right)^2 u^2(x_2) + 2 \left(\frac{\delta y}{\delta x_1}\right) \left(\frac{\delta y}{\delta x_2}\right) u(x_1) u(x_2) r(x_1, x_2) \quad (3.10)$$

In this case, standard uncertainties of just two input variables are considered. In Eq. (3.10), $u_c(y)$ is the combined standard uncertainty of calculated variable y , $u(x_n)$ is the standard uncertainty of input variable x_n , $r(x_1, x_2)$ is the correlation coefficient between the standard uncertainties of x_1 and x_2 , and $\left(\frac{\delta y}{\delta x_n}\right)$ is the calculated change in y associated with a given change in x_n .

Eq. (3.10), which represents the method of moments, can be expanded to include many input variable uncertainties; it can also be simplified to the Gaussian approach by neglecting covariance terms (i.e., the terms that include correlation coefficients). With the Orr et al. (2018) uncertainty propagation routines and our modified MATLAB routine, the magnitudes of the input-associated standard uncertainties can be freely adjusted (i.e., specified) by the user.

3.4.3.1 Standard uncertainties for input variables and constants

Orr et al. (2018) emphasize the distinction between the *random* and *systematic* components of standard uncertainties. For measured variables, random components of standard uncertainties are evaluated in terms of the consistency between repeated measurements. Systematic components are corrected for, whenever possible, using standard reference materials; however, systematic components must still be considered for certain measured variables (e.g., pH) for which reference materials are not available. For equilibrium constants, random components of standard uncertainties are evaluated in terms of the goodness of fit of a model expression to the data on which the model is based; systematic components, though more difficult to identify, can be

coarsely evaluated by comparing different model expressions obtained for a given constant by independent research groups. For each measured variable or equilibrium constant, random and systematic components of standard uncertainty are combined in quadrature to obtain total standard uncertainties.

The standard uncertainties and combined standard uncertainties given in this paper are always expressed in the context of one standard deviation (1σ), as is the convention in Orr et al. (2018). These 1σ uncertainties, which represent 68% confidence intervals, can easily be expanded to 2σ (~95% confidence), 3σ (99.7% confidence), and so on.

The physical–chemical conditions specified for our CO₂ system calculations (termed “standard input conditions”) and the random and total (i.e., random plus systematic) components of standard uncertainties are summarized in Table 3.1. Typical standard uncertainties in T and S measurements contribute negligibly to combined standard uncertainties (Orr et al., 2018), so those input uncertainties are not considered in this analysis.

In high-nutrient regions, standard uncertainties in nutrient concentrations can contribute somewhat to propagated uncertainties if A_T is used as an input variable. Even then, though, their uncertainty contribution rarely exceeds 0.1% (Orr et al., 2018). Therefore, nutrient concentrations (and uncertainties) are not considered in this analysis.

The contribution of dissolved or particulate organic molecules to titration alkalinity can be a source of A_T uncertainty, particularly in rivers and nearshore environments (Cai et al., 1998; Kim and Lee, 2009; Ko et al., 2016; Yang et al., 2015). The magnitude of this uncertainty contribution, however, can be difficult to estimate, and it is likely not significant in all marine environments. Therefore, uncertainty associated with organic alkalinity is not considered in this analysis. For

cases where such uncertainty may be significant, it can be accounted for manually and included in the user-specified standard uncertainty in input A_T (Orr et al., 2018).

To illustrate combined standard uncertainties resulting from CO₂ system calculations within different marine settings, four sets of physical–chemical input conditions (in addition to the standard input conditions) were defined. These case studies were formulated to represent surface waters of a United States (US) West Coast upwelling event (cool temperatures, high C_T , low pH_T), nearshore areas in the Gulf of Maine (moderate temperatures, low C_T , high pH_T), the Southern Ocean (cold temperatures, high C_T , high pH_T), and the tropical ocean (warm temperatures, low C_T , high pH_T).

3.4.3.2 Uncertainty propagation procedure

The MATLAB routines modified from those of Orr et al. (2018) were used to calculate combined standard uncertainties in derived CO₂ system variables, neglecting covariances between the standard uncertainties of input variables (i.e., the Gaussian approach). The combined standard uncertainties were calculated by using $[CO_3^{2-}]$ paired, in turn, with every other input variable (A_T , C_T , pH_T , and pCO_2) to calculate all other CO₂ system variables. For comparison, combined standard uncertainties were also calculated using “traditional” input variable pairs: A_T - C_T , A_T - pH_T , A_T - pCO_2 , C_T - pH_T , C_T - pCO_2 , and pH_T - pCO_2 .

Combined standard uncertainties in derived Ω values were determined using the following equation to calculate Ω :

$$\Omega_i = ([Ca^{2+}][CO_3^{2-}])/K_{sp(i)}^* \quad (3.11)$$

where i represents either aragonite (_{arag}) or calcite (_{cal}), $[Ca^{2+}]$ is the total calcium ion concentration estimated from S (Riley and Tongudai, 1967), and $K_{sp(i)}^*$ is the corresponding (aragonite or calcite)

stoichiometric solubility product. To calculate Ω from input $[\text{CO}_3^{2-}]$, no second CO_2 system variable is required. To calculate Ω from a traditional input variable pair, $[\text{CO}_3^{2-}]$ is first calculated from that pair and then entered into Eq. (3.11).

Standard uncertainty for the total calcium to S ratio (Ca_T/S) was not considered in this analysis because (1) uncertainty in this ratio would contribute similarly to combined standard uncertainties in derived Ω values regardless of the input; (2) independent estimates of Ca_T/S (Carpenter, 1957; Cox and Culkin, 1966; Riley and Tongudai, 1967) differ only slightly ($\sim 0.2\%$) compared to independent estimates of B_T/S (Lee et al., 2010; Uppström, 1974; $\sim 4.0\%$), a parameter for which input uncertainty is considered; and (3) because the Ca_T/S ratio varies with depth (Cox and Culkin, 1966), its uncertainty is challenging to estimate and is not constant between different ocean regimes. So, while individual studies should consider standard uncertainties in $[\text{Ca}^{2+}]$ estimates from salinity when looking at surface waters, it is not a worthwhile consideration when comparing combined standard uncertainties in Ω calculated from different input variables.

Following the lead of Orr et al. (2018), error-space diagrams were created. Each diagram displays contours of relative combined standard uncertainty in a derived variable as a function of the standard uncertainties of two input variables. (For the equilibrium constants and B_T/S , total standard uncertainties (Table 3.1) were used.) Each diagram represents a specified set of physical–chemical conditions — in this case, the standard input conditions given in Table 3.1.

3.5 Results and Discussion

3.5.1 Model for calculating $[\text{CO}_3^{2-}]_{\text{spec}}$

The laboratory data used for the model fits are shown in Appendix C3. The analytical precision of the A_T measurements, assessed as the average standard deviation between repeated measurements of duplicate samples ($N = 32$), was $\pm 1.2 \mu\text{mol/kg}$.

Table 3.2. Coefficients for the spectrophotometric parameters (Eq. (3.6)) that result from fitting the combined lab and field datasets, with each dataset weighted to contribute equally to the model. Each parameter Z takes the form of Eq. (3.9). We recommend using these parameter values in Eq. (3.6) to calculate $[\text{CO}_3^{2-}]_{\text{spec}}$ from measurements of Pb(II) absorbance ratios in seawater at 25 °C, ambient temperatures, or in situ temperatures

$$\text{Eq. (3.9): } Z = a_0 + b_0S + b_1S^2 + c_0T + c_1T^2 + d_0ST$$

| Z | $a_0 \cdot 10$ | $b_0 \cdot 10^3$ | $b_1 \cdot 10^4$ | $c_0 \cdot 10^3$ | $c_1 \cdot 10^5$ | $d_0 \cdot 10^5$ |
|----------------------------------|----------------|------------------|------------------|------------------|------------------|------------------|
| $\log\{\text{CO}_3\beta_1/e_2\}$ | 55.6674 | -51.0194 | 4.61423 | - | - | -13.6998 |
| $e1$ | 1.09519 | 4.49666 | - | 1.95519 | 2.44460 | -2.01796 |
| $e3/e2$ | 32.4812 | -79.7676 | 6.28521 | -11.8691 | -3.58709 | 32.5849 |

To evaluate the various models that calculate $[\text{CO}_3^{2-}]_{\text{spec}}$ from Pb(II) absorbances, we define $\Delta[\text{CO}_3^{2-}]$ as the difference between a calculated value of $[\text{CO}_3^{2-}]_{X,\text{pH}}$ (where X is A_T for the laboratory data and C_T for the cruise data) and its corresponding value of $[\text{CO}_3^{2-}]_{\text{spec}}$. The three panels of Fig. 3.1 show absolute $\Delta[\text{CO}_3^{2-}]$ as a function of $[\text{CO}_3^{2-}]_{X,\text{pH}}$ for three different models. Fig. 3.1 demonstrates that absolute $\Delta[\text{CO}_3^{2-}]$ increases proportionally with $[\text{CO}_3^{2-}]$ itself; therefore, relative standard deviation (RSD) is used to assess the goodness of fit of each model to a given dataset.

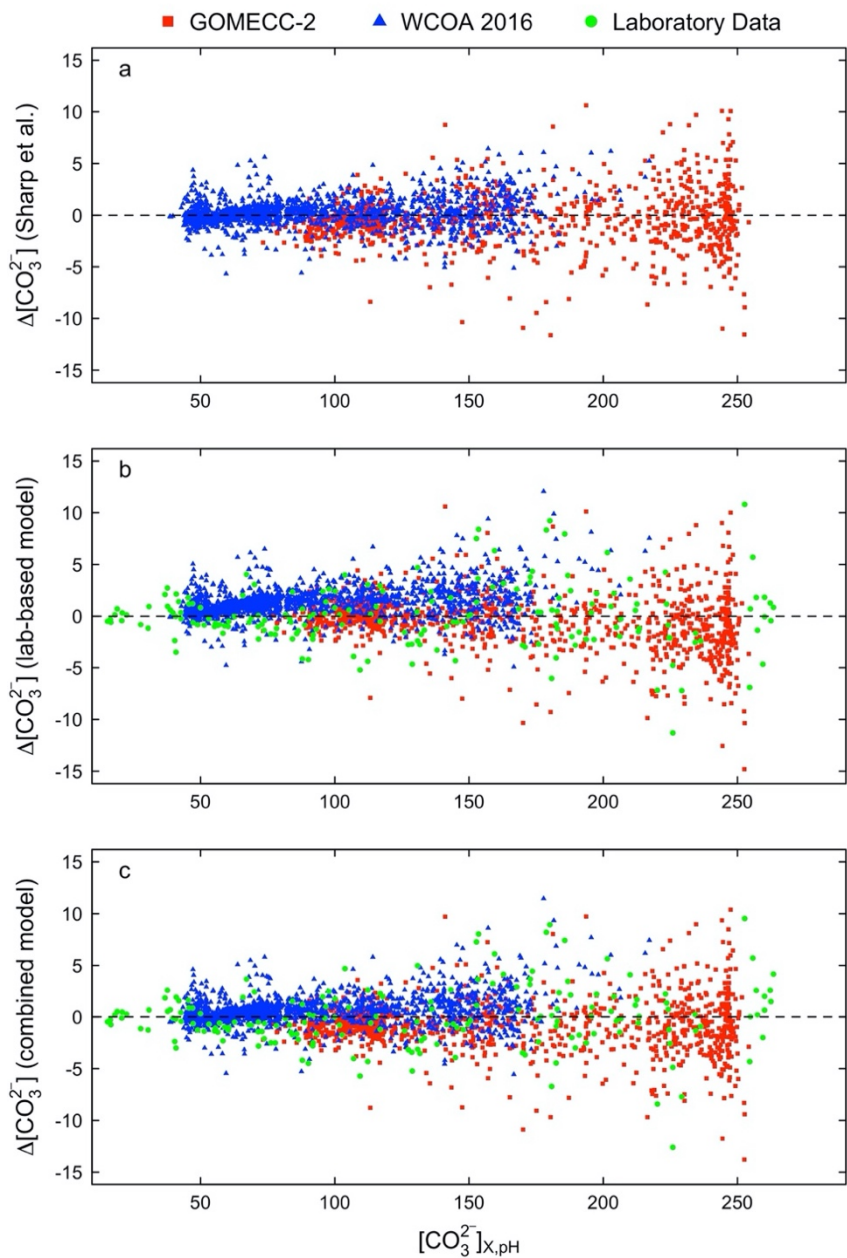


Figure 3.1. Values of $\Delta[\text{CO}_3^{2-}]$ ($\mu\text{mol/kg}$; $[\text{CO}_3^{2-}]_{\text{spec}} - [\text{CO}_3^{2-}]_{X,\text{pH}}$) as a function of $[\text{CO}_3^{2-}]_{X,\text{pH}}$ (where X is A_T for laboratory data and C_T for field data) for three different models for converting Pb(II) absorbance ratios to $[\text{CO}_3^{2-}]_{\text{spec}}$: (a) the model of Sharp et al. (2017), (b) the lab-based model of this work, and (c) the combined model of this work (Table 3.2).

Fig. 3.1a shows $\Delta[\text{CO}_3^{2-}]$ values calculated from the cruise measurements and the model of Sharp et al. (2017). This model is applicable only at $T = 25$ °C. (No laboratory data were available at this temperature.) The RSD is $\pm 1.5\%$.

Fig. 3.1b shows $\Delta[\text{CO}_3^{2-}]$ values calculated from the cruise and laboratory measurements and the lab-based model of this work. The RSD for the cruise dataset is $\pm 1.7\%$, and the RSD for the laboratory dataset is $\pm 2.1\%$. The reasonable scatter of the cruise data about zero (average $\Delta[\text{CO}_3^{2-}]$ of $0.6 \mu\text{mol/kg}$) and the similarity of this cruise-data RSD and the Sharp et al. (Fig 3.1a) cruise-data RSD (i.e., $\pm 1.7\%$ versus $\pm 1.5\%$) effectively serve to validate the data obtained in the laboratory.

Fig. 3.1c shows $\Delta[\text{CO}_3^{2-}]$ values calculated from the cruise and laboratory measurements and the combined model of this work (i.e., fitting Eq. (3.6) to both the laboratory and cruise datasets). The resulting model coefficients are given in Table 3.2. The RSD for the cruise dataset is $\pm 1.6\%$, and the RSD for the laboratory dataset is $\pm 2.2\%$.

To calculate $[\text{CO}_3^{2-}]_{\text{spec}}$ from UV absorbances measured at any T (3 to 40 °C) and S (20 to 40), the coefficients given in Table 3.2 can be used in Eq. (3.9) to determine the three parameters needed in Eq. (3.6) (i.e., $\log\{\text{CO}_3\beta_1/e_2\}$, e_1 , and e_3/e_2). We recommend the use of this model for $[\text{CO}_3^{2-}]_{\text{spec}}$ determinations at 25 °C, at ambient laboratory temperatures, and at in situ temperatures.

3.5.2 Estimation of $[\text{CO}_3^{2-}]$ input uncertainty

Realistic estimates of the random and systematic components of $[\text{CO}_3^{2-}]$ uncertainty are critical to the proper evaluation of combined standard uncertainties in derived CO_2 system variables. For this analysis, we estimate the random and systematic components of standard uncertainty in $[\text{CO}_3^{2-}]$ in the context of $[\text{CO}_3^{2-}]_{\text{spec}}$ measurements. For the random component, a value of 0.7% was assigned based on the relative repeatability of duplicate $[\text{CO}_3^{2-}]_{\text{spec}}$ samples ($N = 148$) collected on a 2017 research cruise in the Gulf of Mexico (Appendix C4). To estimate the systematic component, the RSD of the new $[\text{CO}_3^{2-}]_{\text{spec}}$ model fit was considered (Section 3.5.1).

The RSDs for the cruise ($\pm 1.6\%$) and laboratory ($\pm 2.2\%$) datasets were average to obtain 1.9% as an estimate of the systematic component of standard uncertainty in $[\text{CO}_3^{2-}]$.

Using Eq. (3.10), estimates for the random (0.7%) and systematic (1.9%) uncertainty components were combined in quadrature to obtain an estimate of 2.0% for total standard uncertainty in $[\text{CO}_3^{2-}]$. In theory, this estimated total standard uncertainty in $[\text{CO}_3^{2-}]$ takes into account both $[\text{CO}_3^{2-}]_{\text{spec}}$ measurement imprecision and uncertainty inherent in the $[\text{CO}_3^{2-}]_{\text{spec}}$ calculation model, which itself is defined according to calculations that depend on other measured CO_2 system variables and equilibrium constants.

3.5.3 Uncertainty propagation under standard input conditions

Table 3.3 shows the combined standard uncertainties (Eq. (3.10)) in CO_2 system variables calculated using $[\text{CO}_3^{2-}]$ as one of two input variables under standard input conditions (Table 3.1). For comparison, Table 3.4 shows the combined standard uncertainties calculated using traditional input variable pairs under the same conditions. Accompanying error-space diagrams (Orr et al., 2018) are shown in Figs. 3.2–3.5 and Appendix C5. Each diagram is discussed in detail in Sections 3.5.3.1–3.5.3.4, but here we briefly introduce the concept of these diagrams, their general components, and the interpretations of these components.

Error-space diagrams allow for semi-quantitative assessments of relative combined standard uncertainties in derived variables across a range of input uncertainties (Orr et al., 2018). For each derived variable, two error-space diagrams are presented (Figs. 3.2–3.5): one (on the left) for the best-performing $[\text{CO}_3^{2-}]$ -containing input pair (i.e., the pair that delivers the lowest combined standard uncertainty under standard input conditions), and another (on the right) for the

best-performing traditional input pair. Error-space diagrams for the remaining $[\text{CO}_3^{2-}]$ -containing input pairs are shown in Appendix C5.

Table 3.3. Combined standard uncertainties in CO_2 system variables calculated using $[\text{CO}_3^{2-}]$ ($\mu\text{mol/kg}$) as an input variable paired with a second (traditional) input variable. The specified physical–chemical conditions and standard input uncertainties for this analysis are given in Table 3.1.

| Uncertainties Propagated | Input Vars. | | $u_c(A_T)$ ($\mu\text{mol/kg}$) | $u_c(C_T)$ ($\mu\text{mol/kg}$) | $u_c(\text{pH}_T)$ | $u_c(p\text{CO}_2)$ (μatm) | $u_c(\Omega_{\text{arag}})^*$ |
|--------------------------|----------------------|----------------|--------------------------------------|--------------------------------------|--------------------|--|-------------------------------|
| | Var. 1 | Var. 2 | | | | | |
| Random | $[\text{CO}_3^{2-}]$ | A_T | - | 4.23 | 0.0112 | 9.54 | 0.147 |
| | $[\text{CO}_3^{2-}]$ | C_T | 3.94 | - | 0.0105 | 8.57 | 0.147 |
| | $[\text{CO}_3^{2-}]$ | pH_T | 45.47 | 45.40 | - | 9.52 | 0.147 |
| | $[\text{CO}_3^{2-}]$ | $p\text{CO}_2$ | 26.73 | 25.70 | 0.0062 | - | 0.147 |
| Total | $[\text{CO}_3^{2-}]$ | A_T | - | 8.03 | 0.0193 | 16.25 | 0.159 |
| | $[\text{CO}_3^{2-}]$ | C_T | 7.56 | - | 0.0178 | 14.04 | 0.159 |
| | $[\text{CO}_3^{2-}]$ | pH_T | 85.30 | 84.71 | - | 19.59 | 0.159 |
| | $[\text{CO}_3^{2-}]$ | $p\text{CO}_2$ | 45.01 | 41.48 | 0.0096 | - | 0.159 |

* For a given error scenario (random or total), $u_c(\Omega_{\text{arag}})$ is calculated directly from $[\text{CO}_3^{2-}]$, rather than from the pair of variables, so it is equivalent for all four rows.

In each diagram, the solid black dot shows the relative combined standard uncertainty ($u_c(y)$ as a percentage of y) obtained under standard input conditions with total standard uncertainties in input variables; the numerical value of relative $u_c(y)$ is given at the top of the diagram. On some diagrams, an open (white) dot also shows the relative combined standard uncertainty obtained using only the random standard uncertainties in input variables; this distinction is applicable only for input pairs that include input $[\text{CO}_3^{2-}]$ or pH_T . The thick black contour is the pair–constants curve, along which the uncertainty contribution from the equilibrium constants is equal to the contribution from the input variable pair. The thin black line is the pair line, along which the uncertainty contributions from the two input variables are equal. These

reference points can be used to rapidly identify dominant contributors to combined standard uncertainty under the specified set of conditions across ranges of standard uncertainties in input variables.

Table 3.4. Combined standard uncertainties in CO₂ system variables calculated using traditional input variable pairs. The specified physical–chemical conditions and standard input uncertainties for this analysis are given in Table 3.1.

| Uncertainties Propagated | Input Vars. | | $u_c(A_T)$ ($\mu\text{mol/kg}$) | $u_c(C_T)$ ($\mu\text{mol/kg}$) | $u_c(\text{pH}_T)$ | $u_c(p\text{CO}_2)$ (μatm) | $u_c([\text{CO}_3^{2-}])$ ($\mu\text{mol/kg}$) | $u_c(\Omega_{\text{arag}})$ |
|--------------------------|---------------|----------------|--------------------------------------|--------------------------------------|--------------------|--|---|-----------------------------|
| | Var. 1 | Var. 2 | | | | | | |
| Random | A_T | C_T | - | - | 0.0086 | 7.32 | 2.61 | 0.153 |
| | A_T | pH_T | - | 4.91 | - | 5.11 | 4.01 | 0.159 |
| | A_T | $p\text{CO}_2$ | - | 4.76 | 0.0055 | - | 3.84 | 0.158 |
| | C_T | pH_T | 5.45 | - | - | 4.82 | 4.43 | 0.161 |
| | C_T | $p\text{CO}_2$ | 5.97 | - | 0.0060 | - | 4.59 | 0.162 |
| | pH_T | $p\text{CO}_2$ | 38.88 | 33.75 | - | - | 6.29 | 0.175 |
| Total | A_T | C_T | - | - | 0.0118 | 9.73 | 3.30 | 0.156 |
| | A_T | pH_T | - | 8.75 | - | 10.51 | 6.84 | 0.180 |
| | A_T | $p\text{CO}_2$ | - | 6.45 | 0.0071 | - | 5.54 | 0.169 |
| | C_T | pH_T | 9.63 | - | - | 9.60 | 7.65 | 0.187 |
| | C_T | $p\text{CO}_2$ | 7.99 | - | 0.0076 | - | 6.58 | 0.178 |
| | pH_T | $p\text{CO}_2$ | 75.91 | 63.52 | - | - | 12.41 | 0.241 |

3.5.3.1 Derived A_T

For A_T calculated from an input pair that includes $[\text{CO}_3^{2-}]$, $u_c(A_T)$ is lowest when $[\text{CO}_3^{2-}]$ is paired with C_T (Table 3.3). The $[\text{CO}_3^{2-}]-\text{pH}_T$ and $[\text{CO}_3^{2-}]-p\text{CO}_2$ pairs are far less reliable (see Table 3.3 and also Fig. C5.1 in Appendix C5).

The error-space diagram for the $[\text{CO}_3^{2-}]-C_T$ pair is shown in Fig. 3.2a. As indicated by the solid black dot, relative $u_c(A_T)$ under standard input conditions with total input uncertainties (Table 3.1) is 0.33%. The position of the solid dot above the pair line (thin black line) suggests that

$u([\text{CO}_3^{2-}])$ contributes more strongly to $u_c(A_T)$ than does $u(C_T)$. The pair-constants curve (thick black contour) is located at a relative uncertainty of about 0.25%. This curve indicates where standard uncertainties in the equilibrium constants contribute the greater proportion of $u_c(A_T)$ (i.e., within the curve) and where standard uncertainties in the input variable pair contribute the greater proportion of $u_c(A_T)$ (i.e., outside the curve).

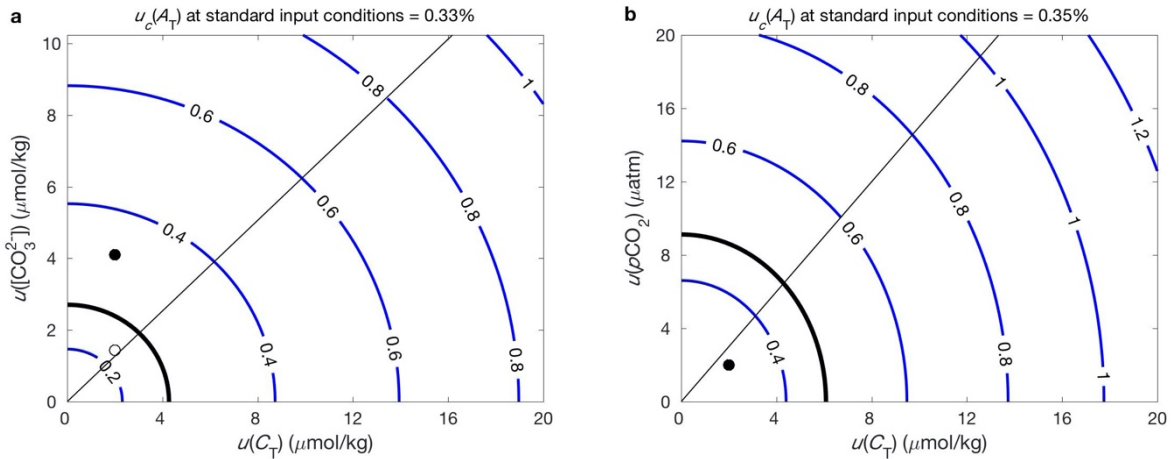


Figure 3.2. Relative combined standard uncertainty (%) in derived A_T as a function of the standard uncertainties in input variables shown on the x - and y -axes: (a) the best-performing $[\text{CO}_3^{2-}]$ -containing input variable pair ($[\text{CO}_3^{2-}]$ - C_T) and (b) the best-performing traditional input variable pair ($p\text{CO}_2$ - C_T). Each error-space diagram shows relative combined standard uncertainty contours obtained under standard input conditions, with total input uncertainties in equilibrium constants and total input uncertainties in measured variables (black dot). In some cases, the result obtained using only random input uncertainties in measured variables is also shown (white dot). The thick black contour denotes where the uncertainty contribution from the equilibrium constants is equal to the contribution from the input pair. The thin black line denotes where the uncertainty contributions from the two input variables are equal.

When total input uncertainties are propagated for traditional variable pairs (Table 3.4), $u_c(A_T)$ is lowest with the C_T - $p\text{CO}_2$ pair. The accompanying error-space diagram (Fig. 3.2b) shows that the contributions of $u(C_T)$ and $u(p\text{CO}_2)$ to $u_c(A_T)$ are roughly similar, and that $u_c(A_T)$ under standard input conditions with total input uncertainties lies within the pair-constants curve (i.e.,

the uncertainty contribution from the equilibrium constants is greater than that from the input variables).

A notable result is that relative $u_c(A_T)$ from the $[\text{CO}_3^{2-}]-C_T$ pair (0.33%) lies outside the pair-constants curve. This finding suggests that standard uncertainties in the input variables (primarily $[\text{CO}_3^{2-}]$) contribute more to $u_c(A_T)$ than do standard uncertainties in the equilibrium constants. It follows then that a reduction in $[\text{CO}_3^{2-}]$ measurement uncertainty could markedly reduce $u_c(A_T)$ calculated from this pair. For example, the open dot in Fig. 3.2a represents relative $u_c(A_T)$ after the elimination of the systematic component of $[\text{CO}_3^{2-}]$ uncertainty. Under these conditions, the uncertainty contribution of the input pair is less than that of the equilibrium constants. The relative $u_c(A_T)$ value represented by this open dot is actually lower than relative $u_c(A_T)$ calculated from a C_T - $p\text{CO}_2$ pair with input variable uncertainties equal to zero (i.e., the origin of Fig. 3.2b).

Tables 3.3 and 3.4 show how, under standard input conditions with total input uncertainties, $u_c(A_T)$ from the $[\text{CO}_3^{2-}]-C_T$ pair (7.56 $\mu\text{mol/kg}$) compares with $u_c(A_T)$ from the more traditional C_T - $p\text{CO}_2$ pair (7.99 $\mu\text{mol/kg}$).

3.5.3.2 Derived C_T

For C_T calculated from an input pair that includes $[\text{CO}_3^{2-}]$, $u_c(C_T)$ is lowest when $[\text{CO}_3^{2-}]$ is paired with A_T (Table 3.3). As in the case of derived A_T , the $[\text{CO}_3^{2-}]-\text{pH}_T$ and $[\text{CO}_3^{2-}]-p\text{CO}_2$ pairs are far less reliable (see Table 3.3 and also Fig. C5.2 in Appendix C5). The error-space diagram for the $[\text{CO}_3^{2-}]-A_T$ pair is displayed in Fig. 3.3a. Under standard input conditions with total input uncertainties (Table 3.1), relative $u_c(C_T)$ is 0.40%. In this case, $u([\text{CO}_3^{2-}])$ contributes more to $u_c(C_T)$ than does $u(A_T)$, and the uncertainty contribution from the input variables is greater

than that from the equilibrium constants. So, as in the case of derived A_T , a reduction in $[\text{CO}_3^{2-}]$ measurement uncertainty could markedly reduce $u_c(C_T)$ calculated from the $[\text{CO}_3^{2-}]$ - A_T pair.

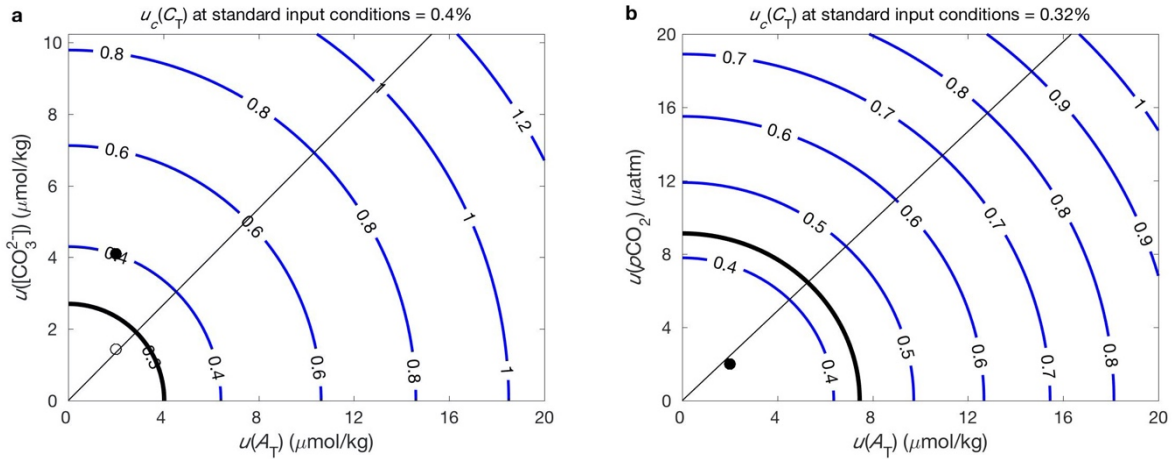


Figure 3.3. Relative combined standard uncertainty (%) in derived C_T as a function of the standard uncertainties in input variables shown on the x - and y -axes: (a) the best-performing $[\text{CO}_3^{2-}]$ -containing input variable pair ($[\text{CO}_3^{2-}]$ - A_T) and (b) the best-performing traditional input variable pair ($p\text{CO}_2$ - A_T). For more information, see Section 3.5.3 and the Fig. 3.2 caption.

For the traditional input variable pairs (Table 3.4), $u_c(C_T)$ is lowest when A_T is paired with $p\text{CO}_2$. The error-space diagram for this pair (Fig. 3.3b) shows that combined standard uncertainty contributions from $u(A_T)$ and $u(p\text{CO}_2)$ are roughly equivalent and that their cumulative uncertainty contribution is smaller than the contribution from the equilibrium constants.

Tables 3.3 and 3.4 show how, under standard input conditions with total input uncertainties, $u_c(C_T)$ from the $[\text{CO}_3^{2-}]$ - A_T pair (8.03 $\mu\text{mol/kg}$) compares with $u_c(C_T)$ from the more traditional A_T - $p\text{CO}_2$ pair (6.45 $\mu\text{mol/kg}$).

3.5.3.3 Derived pH_T

For pH_T calculated from an input pair that includes $[CO_3^{2-}]$, $u_c(pH_T)$ is lowest when $[CO_3^{2-}]$ is paired with pCO_2 (Table 3.3). The $[CO_3^{2-}]-A_T$ and $[CO_3^{2-}]-C_T$ pairs generate greater combined standard uncertainty (see Table 3.3 and also Fig. C5.3 in Appendix C5). Because pH_T is expressed on a logarithmic scale, the error-space diagrams for calculated pH_T (Fig. 3.4) are displayed in terms of relative $[H^+]$ uncertainty. The error-space diagram for the $[CO_3^{2-}]-pCO_2$ pair (Fig. 3.4a) shows a relative $u_c([H^+])$ of 2.21% under standard input conditions with total input uncertainties (Table 3.1). In this case, $u([CO_3^{2-}])$ contributes more to $u_c([H^+])$ than does $u(pCO_2)$ and a greater proportion of $u_c([H^+])$ is associated with the equilibrium constant uncertainties than with the input variable uncertainties.

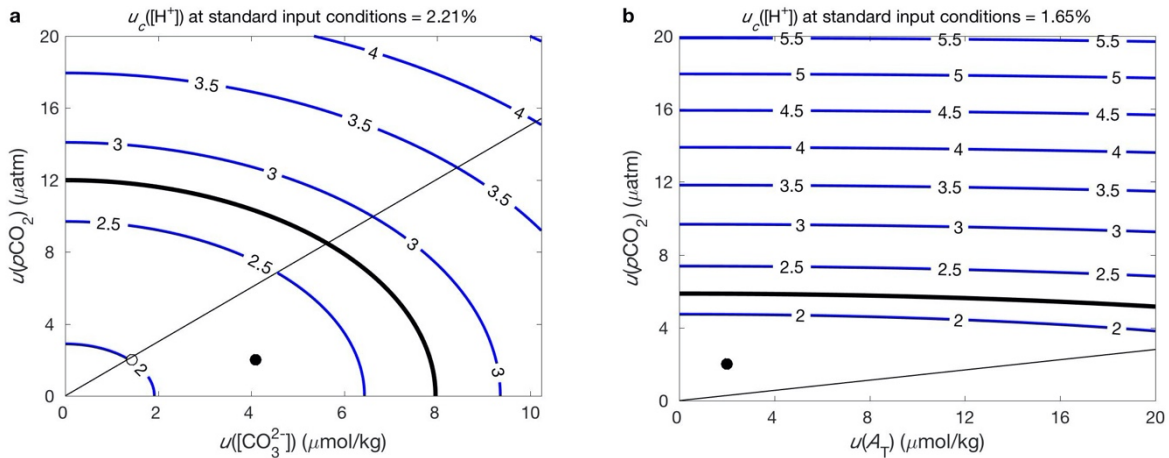


Figure 3.4. Relative combined standard uncertainty (%) in derived $[H^+]$ as a function of the standard uncertainties in input variables shown on the x - and y -axes: (a) the best-performing $[CO_3^{2-}]$ -containing input variable pair (pCO_2 - $[CO_3^{2-}]$) and (b) the best-performing traditional input variable pair (pCO_2 - A_T). For more information, see Section 3.5.3 and the Fig. 3.2 caption.

For the traditional variable pairs (Table 3.4), $u_c(pH_T)$ is lowest when A_T is paired with pCO_2 . The error-space diagram for this pair (Fig. 3.4b) indicates that $u_c([H^+])$ is disproportionately

influenced by $u(p\text{CO}_2)$ compared to $u(A_T)$. This result suggests that accuracy in A_T measurements is not exceedingly critical when calculating pH_T from the A_T - $p\text{CO}_2$ pair.

Tables 3.3 and 3.4 show how, under standard input conditions with total input uncertainties, $u_c(\text{pH}_T)$ from the $[\text{CO}_3^{2-}]$ - $p\text{CO}_2$ pair (0.0096 units) compares with $u_c(\text{pH}_T)$ from the more traditional A_T - $p\text{CO}_2$ pair (0.0071 units).

3.5.3.4 Derived $p\text{CO}_2$

For $p\text{CO}_2$ calculated from an input pair that includes $[\text{CO}_3^{2-}]$, $u_c(p\text{CO}_2)$ is lowest when $[\text{CO}_3^{2-}]$ is paired with C_T (Table 3.3). The error-space diagram for this pair (Fig. 3.5a) shows a relative $u_c(p\text{CO}_2)$ of 4.55% under standard input conditions with total input uncertainties (Table 3.1). The diagram also shows that combined standard uncertainty in $p\text{CO}_2$ is influenced disproportionately by $u([\text{CO}_3^{2-}])$ when the $[\text{CO}_3^{2-}]$ - C_T pair is used. Error-space diagrams for $p\text{CO}_2$ derived using the other $[\text{CO}_3^{2-}]$ -containing pairs are shown in Fig. C5.4 in Appendix C5.

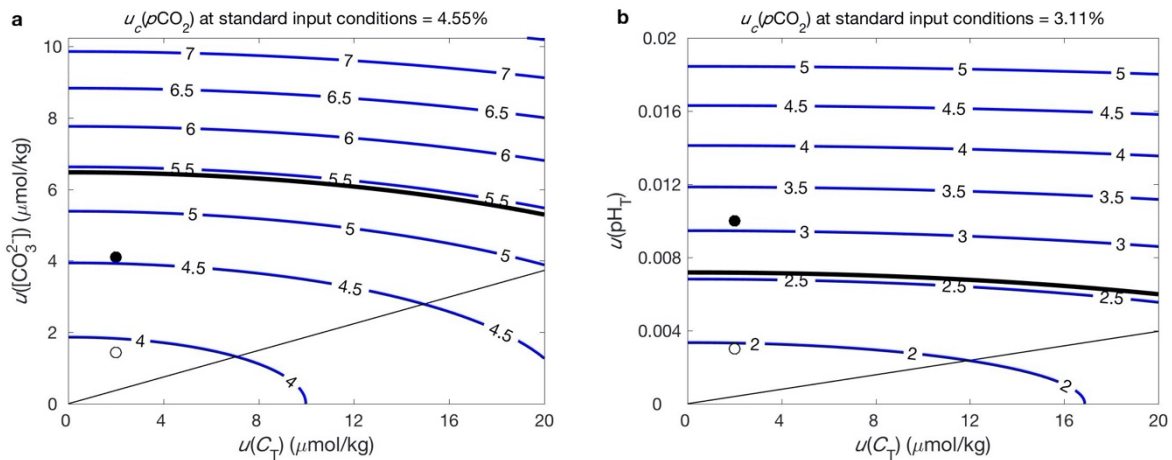


Figure 3.5. Relative combined standard uncertainty (%) in derived $p\text{CO}_2$ as a function of the standard uncertainties in input variables shown on the x- and y-axes: (a) the best-performing $[\text{CO}_3^{2-}]$ -containing input variable pair ($[\text{CO}_3^{2-}]$ - C_T) and (b) the best-performing traditional input variable pair (pH_T - C_T). For more information, see Section 3.5.3 and the Fig. 3.2 caption.

For the traditional variable pairs (Table 3.4), $u_c(p\text{CO}_2)$ is lowest when C_T is paired with pH_T . The error-space diagram for this pair (Fig. 3.5b) indicates that $u_c(p\text{CO}_2)$ is disproportionately influenced by $u(\text{pH}_T)$. This pattern bears a resemblance to that of $u_c(\text{pH}_T)$ calculated from the A_T - $p\text{CO}_2$ pair (Fig. 3.4b).

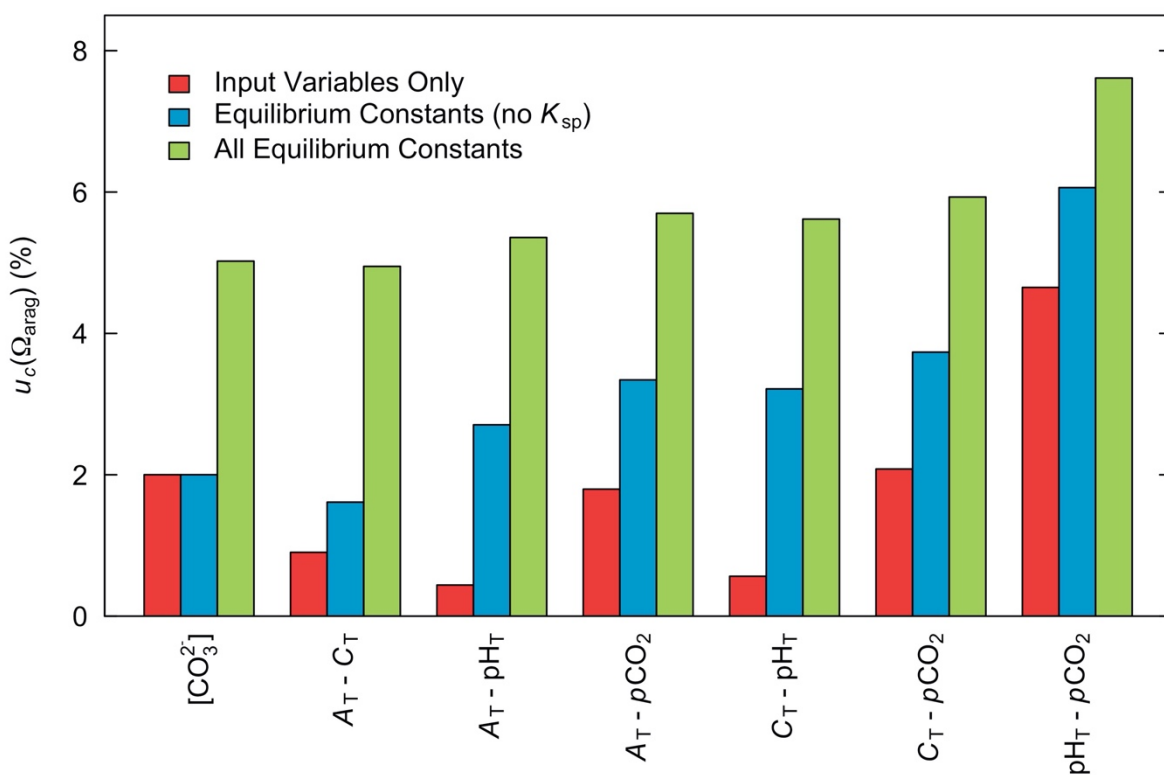


Figure 3.6. Relative combined standard uncertainties (%) in aragonite saturation states derived using input $[\text{CO}_3^{2-}]$ only (leftmost set of bars) and using pairs of traditional input variables. Uncertainties were propagated for standard uncertainties in input variables only (red bars); standard uncertainties in input variables and equilibrium constants, excluding $u(K_{sp})$ (blue bars); and standard uncertainties in all input variables and equilibrium constants, including $u(K_{sp})$ (green bars). In each case, total standard uncertainties (Table 3.1) are used.

In almost all cases, $u_c(p\text{CO}_2)$ derived from a $[\text{CO}_3^{2-}]$ -containing variable pair (Table 3.3) is greater than that resulting from traditional input pairs (Table 3.4). Under standard input

conditions with total input uncertainties, $u_c(p\text{CO}_2)$ derived from the $[\text{CO}_3^{2-}]-C_T$ pair (14.04 μatm) is nearly 1.5 times that derived from the more traditional $C_T\text{-pH}_T$ input pair (9.60 μatm).

3.5.3.5 Derived Ω_{arag}

Comparisons between the final columns of Table 3.3 and Table 4.4 indicate that, in both the random uncertainty scenario and total (random + systematic) uncertainty scenario, $u_c(\Omega_{\text{arag}})$ determined from input of $[\text{CO}_3^{2-}]$ is relatively low and is comparable to the best performing traditional variable pair ($A_T\text{-}C_T$). Similar results are obtained for Ω_{cal} , but we focus here on Ω_{arag} due to aragonite's higher solubility and greater oceanographic significance in the context of ocean acidification.

This result must be viewed in the context of the hydrographic input and output conditions, chemical input conditions, and input uncertainties (Table 3.1). That is to say, under different conditions, other input pairs may produce Ω_{arag} values with lower uncertainties than are produced by input $[\text{CO}_3^{2-}]$ and input $A_T\text{-}C_T$. It should be noted that conversion of $[\text{CO}_3^{2-}]$ to in situ conditions using a second carbonate system variable (for example, to determine an in situ saturation state from $[\text{CO}_3^{2-}]$ measured at laboratory conditions) introduces a small amount of additional uncertainty, but not nearly enough to change the interpretations presented here.

Fig. 3.6 offers a more detailed presentation of combined standard uncertainties in Ω_{arag} . Fig. 3.6 displays relative (%) $u_c(\Omega_{\text{arag}})$ values calculated using (1) standard uncertainties of input CO_2 system variables only; (2) standard uncertainties of input CO_2 system variables and equilibrium constants, excluding $u(K_{\text{sp}})$; and (3) standard uncertainties of input CO_2 system variables and equilibrium constants, including $u(K_{\text{sp}})$.

When standard uncertainties in input variables and equilibrium constants are propagated (green bars), the lowest $u_c(\Omega_{\text{arag}})$ values arise from the input of $[\text{CO}_3^{2-}]$ (alone) and of the $A_{\text{T}}-C_{\text{T}}$ pair (Fig. 3.6). These relative $u_c(\Omega_{\text{arag}})$ values are nearly equivalent — about 5.0%. For $u_c(\Omega_{\text{arag}})$ resulting from the input of $[\text{CO}_3^{2-}]$, this good reliability stems from the fact that the combined standard uncertainty depends only on $[\text{CO}_3^{2-}]$ measurement uncertainty (discussed in Section 3.5.2) and standard uncertainty in the CaCO_3 solubility product (which equally influences Ω_{arag} derived from any variable or variable pair). For $u_c(\Omega_{\text{arag}})$ resulting from the input of $A_{\text{T}}-C_{\text{T}}$, the good reliability results from the small influence of equilibrium constant uncertainties on calculated $[\text{CO}_3^{2-}]$ (see the second column from the right of Table 3.4).

The effectiveness of the $A_{\text{T}}-C_{\text{T}}$ pair is highly dependent on low input uncertainties ($\pm 2 \mu\text{mol kg}^{-1}$) in A_{T} and C_{T} measurements (Table 3.1). With greater input uncertainties, $u_c(\Omega_{\text{arag}})$ values would rapidly increase. This is due to the outsized sensitivity of Ω_{arag} to uncertainty in A_{T} and C_{T} when the $A_{\text{T}}-C_{\text{T}}$ pair is used for calculations (see Table 5d of Orr et al., 2018). For this reason, we do not recommend the $A_{\text{T}}-C_{\text{T}}$ pair for calculations of Ω_{arag} in environments that may promote large uncertainties in either A_{T} or C_{T} measurements (e.g., environments expected to be influenced by organic alkalinity).

In each case, the difference between the blue (middle) and red (leftmost) bars represents primarily the influence that $u(K_1)$ and $u(K_2)$ exert over $u_c(\Omega_{\text{arag}})$. Uncertainties in K_1 and K_2 do not influence $u_c(\Omega_{\text{arag}})$ in the case of $[\text{CO}_3^{2-}]$ input. Similarly, the difference between the green (rightmost) and blue bars represents the influence that $u(K_{\text{sp}})$ exerts over $u_c(\Omega_{\text{arag}})$. A major takeaway is that standard uncertainty in K_{sp} — estimated at 5% by Mucci (1983) — has a strong influence on the combined standard uncertainty in Ω_{arag} (discussed in Orr et al., 2018).

Overall, $u_c(\Omega_{\text{arag}})$ is relatively low when calculated from $[\text{CO}_3^{2-}]$ (given our estimated level of measurement uncertainty). In other words, the Pb(II) absorbance method of measuring $[\text{CO}_3^{2-}]_{\text{spec}}$ offers a simple and reliable technique for evaluating Ω_{arag} .

3.5.4 Uncertainty propagation under other oceanographic conditions

All of the preceding results were obtained using the physical–chemical input conditions specified in Table 3.1. Examining the propagation of standard uncertainties under a wider range of marine conditions can provide insight into how environmental conditions might influence the selection of CO₂ system variables to measure, as well as how to interpret or weight derived variables.

Table 3.5 details the results obtained by pairing $[\text{CO}_3^{2-}]$ with other input variables at conditions that might be observed in surface waters of (1) a US West Coast upwelling event, (2) nearshore areas of the Gulf of Maine, (3) the Southern Ocean, and (4) the tropical ocean. Patterns in the combined standard uncertainties are largely consistent across these settings, though subtle differences do occur. In every case, C_T is the measured variable that is best suited to pair with $[\text{CO}_3^{2-}]$ for determining the entire system.

Combined standard uncertainties in A_T and C_T derived from the $[\text{CO}_3^{2-}]$ - C_T and $[\text{CO}_3^{2-}]$ - A_T pairs are highest in the warm, relatively CO₂-poor waters of the tropical ocean. Combined standard uncertainties in $p\text{CO}_2$ derived from all pairs are highest in the highly acidic US West Coast upwelling waters — more than twice the corresponding uncertainties in the other ocean regimes. Combined standard uncertainties in derived pH_T are consistently similar for each input pair across all ocean regimes, and are lowest using the $[\text{CO}_3^{2-}]$ - $p\text{CO}_2$ pair. These examples illustrate that, when propagating standard uncertainties and evaluating the reliabilities of derived

variables, it is always important to consider the specific physical–chemical conditions pertinent to the system under investigation.

Table 3.5. Combined standard uncertainties in CO₂ system variables calculated using [CO₃²⁻] (μmol/kg) as an input variable paired with a second (traditional) input variable. All calculations use total standard uncertainties in the input variables and equilibrium constants (Table 3.1). In each of these four cases, nutrients are ignored and $P = 1$ atm.

| Ocean Regime | Second Input Variable | $u_c(A_T)$ (μmol/kg) | $u_c(C_T)$ (μmol/kg) | $u_c(\text{pH}_T)$ | $u_c(\text{pCO}_2)$ (μatm) |
|--|-----------------------------|-------------------------|-------------------------|--------------------|-------------------------------|
| US West Coast Upwelling, May † $T = 9.55$ °C $S = 33.75$ [CO ₃ ²⁻] = 60.8 | A_T (2250 μmol/kg) | - | 4.51 | 0.0178 | 43.69 |
| | C_T (2200 μmol/kg) | 4.22 | - | 0.0171 | 40.51 |
| | pH_T (7.696) | 97.38 | 99.61 | - | 60.41 |
| | pCO_2 (950.5 μatm) | 47.49 | 46.48 | 0.0095 | - |
| Gulf of Maine, Aug. § $T = 18.00$ °C $S = 31.50$ [CO ₃ ²⁻] = 149.1 | A_T (2120 μmol/kg) | - | 6.27 | 0.0188 | 18.98 |
| | C_T (1910 μmol/kg) | 5.93 | - | 0.0176 | 16.94 |
| | pH_T (8.047) | 82.56 | 82.54 | - | 23.97 |
| | pCO_2 (378.3 μatm) | 42.49 | 39.95 | 0.0096 | - |
| Southern Ocean Surface ‡ $T = -0.49$ °C $S = 33.96$ [CO ₃ ²⁻] = 103.8 | A_T (2295 μmol/kg) | - | 5.23 | 0.0183 | 15.41 |
| | C_T (2155 μmol/kg) | 4.96 | - | 0.0174 | 14.17 |
| | pH_T (8.116) | 94.95 | 95.72 | - | 20.54 |
| | pCO_2 (323.1 μatm) | 47.61 | 45.85 | 0.0096 | - |
| Tropical Ocean Surface ‡ $T = 27.01$ °C, $S = 34.92$ [CO ₃ ²⁻] = 237.2 | A_T (2300 μmol/kg) | - | 9.00 | 0.0197 | 19.61 |
| | C_T (1960 μmol/kg) | 8.42 | - | 0.0179 | 16.65 |
| | pH_T (8.076) | 82.64 | 81.70 | - | 22.97 |
| | pCO_2 (361.4 μatm) | 44.29 | 40.14 | 0.0096 | - |

† Approximate T , S , A_T , and C_T (with calculated pH_T , pCO_2 , and [CO₃²⁻]) from a coastal upwelling event captured on WCOA 2016 (Alin et al., 2017)

§ Approximate T , S , A_T , and C_T (with calculated pH_T , pCO_2 , and [CO₃²⁻]) from coastal stations of the New Hampshire transect of GOMECC-2 (Wanninkhof et al., 2016)

‡ Conditions taken from Orr et al. (2018)

3.6 Conclusions

We present here a new model (Table 3.2 and Eq. (3.6)) for determining $[\text{CO}_3^{2-}]_{\text{spec}}$ from Pb(II) absorbance ratios measured with UV-visible spectrophotometers across ranges of T (3 to 40 °C) and S (20 to 40). The effectiveness of this model compares well with previously proposed fixed-temperature models, with an RSD of approximately 1.5% in an over-determined system. With this UV-absorption model, absolute uncertainties in $[\text{CO}_3^{2-}]_{\text{spec}}$ increase proportionally with $[\text{CO}_3^{2-}]$ itself. However, at concentrations that might require the most precise measurements (i.e., $[\text{CO}_3^{2-}] < 100 \mu\text{mol/kg}$, where Ω_{arag} and Ω_{cal} are typically near 1), absolute uncertainties are relatively low ($\sim 1 \mu\text{mol/kg}$).

The new model allows for benchtop measurements of $[\text{CO}_3^{2-}]_{\text{spec}}$ without the requirement of temperature control — only temperature measurement is required. This relaxation of analytical requirements is highly advantageous in terms of speed, cost, and simplicity of instrumental setup. The model also makes feasible the prospect of autonomous inline and in situ $[\text{CO}_3^{2-}]_{\text{spec}}$ measurements. Additional implications of the new model are detailed in Appendix C6. All in all, the model presented here should prove especially useful to shellfish hatchery managers, marine resource managers, environmental researchers, and others who wish to accurately determine carbonate ion concentrations and CaCO_3 saturation states, particularly in the context of limited space or financial resources.

We also estimate the standard uncertainty in measured $[\text{CO}_3^{2-}]_{\text{spec}}$, and we assess combined standard uncertainties that result from using $[\text{CO}_3^{2-}]$ to calculate other variables of the CO_2 system. When seeking to characterize the entire CO_2 system, C_T is the most effective variable to pair with $[\text{CO}_3^{2-}]_{\text{spec}}$, though A_T can also serve as a suitable partner. Pairing $[\text{CO}_3^{2-}]_{\text{spec}}$ with $p\text{CO}_2$ can lead

to relatively low uncertainties in calculated pH_T . Pairing $[\text{CO}_3^{2-}]_{\text{spec}}$ exclusively with pH_T is not advisable.

Measurements of $[\text{CO}_3^{2-}]_{\text{spec}}$ make it possible to reliably calculate Ω_{arag} from just a single chemical measurement. This is advantageous as extensive research has demonstrated that Ω_{arag} is a significant variable in governing the health of marine bivalves (Waldbusser et al., 2013, 2015) and calcifying plankton (Bednaršek et al., 2014, 2017; Fabry et al., 2008). Accurate and convenient determinations of Ω_{arag} will become increasingly important as ocean acidification continues to cause rapid decline of Ω_{arag} in surface waters across the global ocean (Feely et al., 2004, 2008, 2012).

The critical examination of propagated uncertainties presented here highlights the potential value of $[\text{CO}_3^{2-}]_{\text{spec}}$ measurements for CO_2 system characterizations (when appropriately paired with another measured variable) and for efficient evaluations of CaCO_3 saturation states in field and laboratory settings. The speed and simplicity of $[\text{CO}_3^{2-}]_{\text{spec}}$ measurements also make them ideal for inclusion in internal consistency analyses of analytically over-determined systems (e.g., Alin et al., 2017). Given the new model presented here, $[\text{CO}_3^{2-}]_{\text{spec}}$ measurements can be considered a convenient and affordable tool available to marine chemists and any others interested in monitoring calcium carbonate saturation states in seawater.

3.7 Acknowledgements

Support for J.D. Sharp was provided by the NSF Graduate Research Fellowship Program, Award No. 1144244, and by the William and Elsie Knight Endowed Fellowship for Marine Science from the University of South Florida College of Marine Science. R.H. Byrne was supported by NSF Award OCE-1220110. We thank the scientists, officers, and crew aboard the

NOAA Ship *Ronald H. Brown* during the GOMECC-2 and WCOA 2016 cruises. Special thanks are given to Dr. Tonya Clayton for her insightful comments and editorial assistance. Thanks are also given to Dr. Kelly Deister for running the ICP-MS samples. This work has benefited greatly from the comments of Dr. Alfonso Mucci and two anonymous reviewers.

CHAPTER FOUR:
MODELING AND INTERPRETATION OF TOTAL ALKALINITY TITRATIONS IN
MARINE AND ESTUARINE WATERS IN THE PRESENCE OF PROTON-BINDING
ORGANIC MATTER

Note: This chapter has been reprinted (adapted) with permission from:

Sharp, J.D., Byrne, R.H., 2020. Interpreting measurements of total alkalinity in marine and estuarine waters in the presence of proton-binding organic matter. *Deep Sea Research Part I: Oceanographic Research Papers*, 103338.

Copyright 2020 Elsevier.

4.1 Abstract

Total alkalinity (A_T) is one of four measurable cornerstone parameters for characterizing the marine carbonate system, yet its measurement by standard titration methods is subject to systematic misinterpretations in the presence of uncharacterized dissolved organic molecules in ocean and estuarine waters. A consequence of these misinterpretations may be the lack of thermodynamic consistency that is routinely observed among measured and calculated parameters of the carbonate system. In this work, a numerical model is used to illustrate (a) how proton-binding dissolved organic molecules influence the reported results of total alkalinity titrations in marine and estuarine settings and (b) how errors in interpretations of reported A_T values can then propagate through carbonate system calculations, thus distorting biogeochemical interpretations

of calculated parameters. We examine five distinct approaches for alkalinity measurement by titration. Ideally, the difference between the measured (reported) A_T and the conventional (thermodynamic) definition of inorganic alkalinity (A_{inorg}) would be zero. However, in the presence of titratable organic matter, our model results show consistent non-zero differences that vary with the chemical properties of the organic matter. For all five titration approaches, the differences between reported A_T and A_{inorg} are greatest when the negative logarithm of the organic acid dissociation constant ($\text{p}K_{\text{org}}$) is between approximately 5 and 7. The differences between reported A_T and A_{inorg} also display previously undescribed variation among measurement approaches, most significantly when $\text{p}K_{\text{org}}$ is between approximately 3 and 6 (typical of carboxylic acid groups). The measurement approaches that are most effective at limiting the unfavorable influence of these relatively low- $\text{p}K$ organic acids on A_T are closed-cell titrations and single-step titrations that are terminated at a relatively high pH. For calculated carbonate system parameters relevant to in situ conditions (e.g., pH, pCO_2 , calcium carbonate mineral saturation states), errors resulting from the presence of proton-binding organics are largest when calculations are based on the input pair of directly measured dissolved inorganic carbon (C_T) and directly measured A_T , and can vary in magnitude depending on the titration approach that is used to obtain A_T . The modeling results presented in this work emphasize the importance of (a) determining A_T in a manner that accounts for the ubiquity of organic alkalinity in marine and estuarine waters and (b) working toward a clearer understanding of the phenomena underlying the routine lack of internal consistency between measured versus calculated carbonate system parameters. Total alkalinity measurements should begin to incorporate either implicit or explicit evaluations of the titration characteristics of the natural organic carbon present in each sample. To that end, we recommend use of secondary titrations to directly measure organic alkalinity (sample-by-sample), characterization of

relationships between total dissolved organic carbon concentrations and organic alkalinity (on local to regional scales), and/or exploration of novel curve-fitting procedures to infer the behavior of organic functional groups from titration data.

4.2 Introduction

Total alkalinity (A_T) is one of the most important measured parameters pertaining to the chemistry of natural waters. When defined in terms of moles or charge equivalents per kilogram of solution, A_T is not influenced by changes in temperature or pressure, nor is it altered by the exchange of carbon dioxide (CO_2) gas with the atmosphere. As a result, A_T is a carbonate system parameter that mixes conservatively and is relatively well-correlated with salinity in marine waters (Broecker and Peng, 1982; Millero et al., 1998). A_T does exhibit minor variations associated with biogeochemical processes such as primary production, organic matter respiration, and the formation or dissolution of calcium carbonate (Brewer et al., 1975; Brewer and Goldman, 1976; Goldman and Brewer, 1980; Sarmiento and Gruber, 2006; Zeebe and Wolf-Gladrow, 2001).

Due to its stable and conservative nature, A_T is useful in estimating other (unmeasured) carbonate system parameters and in characterizing complex biogeochemical processes. In natural waters, measured A_T can be paired with another measured carbonate system parameter — total dissolved inorganic carbon (C_T), pH, or the partial pressure of CO_2 ($p\text{CO}_2$) — to estimate unmeasured parameters. For example, A_T has been used with C_T (Bates, 2007) and pH (Williams et al., 2017) to calculate $p\text{CO}_2$ for quantifications of CO_2 exchange across the air–sea interface. Oceanic distributions of A_T can also be used directly to detect changes in biological calcification or the export of calcium carbonate (CaCO_3) from the surface ocean (Carter et al., 2016; Ilyina et al., 2009). Study of these processes is important for determining how carbon is transformed and

transported between various global reservoirs. This information is especially critical now, as anthropogenic CO₂ is being continuously released to the Earth system in large quantities (Friedlingstein et al., 2019), fueling global warming (IPCC, 2013) and ocean acidification (Caldeira and Wickett, 2003; Feely et al., 2004; Orr et al., 2005).

In natural waters, A_T is defined by Dickson (1981) as the number of moles of protons equivalent to the excess of proton acceptors over proton donors in one kilogram of solution. Proton acceptors are bases formed from weak acids with dissociation constants (K_A) less than or equal to $10^{-4.5}$ at zero ionic strength, 25 °C, and atmospheric pressure; proton donors are acids with dissociation constants greater than $10^{-4.5}$ under those same conditions. These environmental conditions are indicated by the superscript naught on the dissociation constant: K_A^0 . The specification of $K_A^0 = 10^{-4.5}$ as the cutoff between proton acceptors and donors designates the set of chemical species that represent the “zero level of protons” (*ZLP*) (Dickson, 1981; Wolf-Gladrow et al., 2007).

By treating the main inorganic chemical constituents found in natural waters according to Dickson’s (1981) definition, an expression is obtained that represents the inorganic alkalinity (A_{inorg}) of natural waters:

$$A_{\text{inorg}} = [\text{HCO}_3^-] + 2[\text{CO}_3^{2-}] + [\text{B}(\text{OH})_4^-] + [\text{OH}^-] + [\text{HPO}_4^{2-}] + 2[\text{PO}_4^{3-}] + [\text{SiO}(\text{OH})_3^-] + [\text{HS}^-] + 2[\text{S}^{2-}] + [\text{NH}_3^0] - [\text{H}^+]_f - [\text{HSO}_4^-] - [\text{HF}^0] - [\text{H}_3\text{PO}_4^0] \quad (4.1)$$

Each term in Eq. (4.1) is a total ionic concentration that encompasses both free and complexed ions, except for $[\text{H}^+]_f$, which represents only the free proton concentration. The expression for A_{inorg} given by Eq. (4.1) is especially robust for practical purposes due to the specification of the *ZLP* at $K_A^0 = 10^{-4.5}$, which separates proton donors and acceptors by more than three orders of magnitude in terms of their K_A^0 values (Wolf-Gladrow et al., 2007). When defined using this *ZLP*, Eq. (4.1)

can be expressed simply as an excess of inorganic proton acceptors ($A_{A,inorg}$) over inorganic proton donors ($A_{D,inorg}$):

$$A_{inorg} = A_{A,inorg} - A_{D,inorg} \quad (4.2)$$

In natural waters with acid–base systems that are exclusively controlled by well-characterized inorganic species, the mathematical definition of A_{inorg} given in Eq. (4.1) exactly describes A_T (i.e., $A_T = A_{inorg}$). In this scenario, proper techniques for measuring alkalinity by titration are unambiguous and robust (e.g., Dickson, 1981; Hansson and Jagner, 1973; Millero et al., 1993). In most natural environments, however, dissolved organic molecules with poorly defined proton-exchange properties are present at some concentration, thus complicating interpretations of alkalinity titrations (Bradshaw and Brewer, 1988; Brewer et al., 1986; Cantrell et al., 1990).

Alkalinity is typically determined by titrating a sample with a strong acid of known concentration. Titration proceeds from the sample’s initial pH (e.g., approximately 8.1 for surface seawater) to a pH lower than the sample’s second equivalence point (e.g., approximately 3.0). Thus, not all organics present in a sample are significant in the context of an alkalinity titration; only those organics with pK_A values within or near to the pH range of the titration will affect the alkalinity determination. In this paper, “titratable organics” refers to those organic chemical species that exchange protons in a quantitatively significant way during an alkalinity titration. Significant concentrations of titratable organics can make the concept of A_T quantitatively ambiguous, because chemical species that are not included in the rigorously defined A_{inorg} of Eq. (4.1) can contribute to measured A_T . Quantitative ambiguity in A_T can affect not only qualitative interpretations of alkalinity measurements but also calculations of carbonate system parameters.

To account explicitly for the influence of titratable organics, A_T could ideally be written as the sum of inorganic alkalinity (A_{inorg}) plus organic alkalinity (A_{org}). This sum represents the excess of both inorganic proton acceptors (positive terms in Eq. (4.1)) and organic proton acceptors ($A_{A,\text{org}}$) over both inorganic proton donors (negative terms in Eq. (4.1)) and organic proton donors ($A_{D,\text{org}}$):

$$A_T = A_{\text{inorg}} + A_{\text{org}} = (A_{A,\text{inorg}} - A_{D,\text{inorg}}) + (A_{A,\text{org}} - A_{D,\text{org}}) \quad (4.3)$$

Direct measurements to quantitatively characterize the proton-exchange properties of all organic molecules in a sample would be highly desirable and would allow for the separation of organic proton acceptors and donors using a strict *ZLP* cutoff of $K_A^0 = 10^{-4.5}$ (Dickson, 1981). However, current analytical constraints make this kind of precise characterization impractical (Byrne, 2014; Kuliński et al., 2014).

Assemblages of organic molecules commonly found in natural waters are heterogenous in terms of their chemical composition (Carlson and Hansell, 2015; Repeta, 2015) and their proton-exchange properties (Altmann and Buffle, 1988; Perdue et al., 1984; Perdue and Lytle, 1983; Tipping and Hurley, 1992). An additional complication is that some of the more common functional groups of dissolved organic molecules are carboxyl groups, which exhibit acid dissociation behavior very near to the *ZLP* (Oliver et al., 1983; Ritchie and Perdue, 2003). Therefore, even if the proton-exchange properties of these organic molecules were to be estimated, their role as proton acceptors or donors in the context of an A_T titration would remain ambiguous. Consequently, due to the impracticality of quantifying the A_{org} term in Eq. (4.3), A_T in systems with titratable organics cannot be rigorously defined.

Measurements of A_T rely on (a) operationally well-defined acidimetric titrations and (b) careful analysis of titration data. Over time, a number of approaches for this two-step process have

been developed (see section 4.3.2). Each approach produces a distinct measured titration alkalinity ($A_{T(\text{meas})}$), which is in actuality an A_T “best estimate” that is linked implicitly to the measurement approach (i.e., the titration technique in combination with the method of data analysis). With this important subtlety in mind, Eq. (4.3) can be recast in the framework of $A_{T(\text{meas})}$:

$$A_{T(\text{meas})} = A_{\text{inorg}} + A_{\text{org}(\text{meas})} \quad (4.4)$$

Here, $A_{T(\text{meas})}$ is the quantity reported as the outcome of an alkalinity titration, A_{inorg} is as defined in Eq. (4.1), and $A_{\text{org}(\text{meas})}$ represents the concentration of all protons that bind to organic molecules during the titration. This $A_{\text{org}(\text{meas})}$ term is not defined explicitly as an excess of proton acceptors over donors because, due to the structural heterogeneity and behavioral ambiguity of naturally occurring organic molecules, standard models for acid–base behavior in natural waters do not contain explicit terms for organics. Any organic species that binds protons during an alkalinity titration, no matter the K_A^0 value of the species, will contribute positively to $A_{\text{org}(\text{meas})}$ and therefore to $A_{T(\text{meas})}$.

Typically, $A_{\text{org}(\text{meas})}$ is assumed to be negligible. In other words, $A_{T(\text{meas})}$ (or A_T estimated from regression equations fitted to a dataset of $A_{T(\text{meas})}$ values (e.g., Carter et al., 2018)) is implicitly equated with A_{inorg} . The quantity $A_{T(\text{meas})}$ is often then used as if it were A_{inorg} — e.g., to perform calculations of C_T , pH, $p\text{CO}_2$, and other carbonate system parameters. The result can be a set of calculated parameters that are poorly defined.

Significant differences between $A_{T(\text{meas})}$ and A_{inorg} have been demonstrated in certain natural environments (rivers, estuaries, and coastal oceans) and in phytoplankton cultures — all systems reasonably expected to be influenced by titratable organics (Cai et al., 1998; Hernández-Ayón et al., 2007; Hu et al., 2015; Kim and Lee, 2009; Tishchenko et al., 2006). These differences can be practically represented at ΔA_T ($A_{T(\text{meas})} - A_{\text{inorg}}$), and have often been attributed to non-negligible

$A_{\text{org(meas)}}$ (see Eq. (4.4)). ΔA_{T} values appear to increase in magnitude with increasing concentrations of dissolved organics (Kim and Lee, 2009; Kuliński et al., 2014) and can cause significant errors in calculated carbonate system parameters (Abril et al., 2015; Hoppe et al., 2012; Ko et al., 2016; Koeve and Oeschies, 2012; Tishchenko et al., 2006).

Less obvious, but perhaps more troubling than the expected issues in high-organic environments, is the fact that internal consistency analyses in environments thought to be negligibly influenced by titratable organics (e.g., oligotrophic open-ocean systems) have also proven to be problematic. Studies of over-determined carbonate system datasets have consistently failed to resolve differences between certain measured and calculated carbonate system parameters. A notable example is the repeatedly observed difference between pH measured spectrophotometrically versus pH calculated from paired measurements of $A_{\text{T(meas)}}$ and C_{T} (Carter et al., 2013, 2018; McElligott et al., 1998; Williams et al., 2017). This and other internal consistency issues have led some investigators to propose that, even in the open ocean, $A_{\text{org(meas)}}$ may represent a non-negligible component of $A_{\text{T(meas)}}$ (Fong and Dickson, 2019; Patsavas et al., 2015b; Salt et al., 2016; Yang et al., 2015).

The aim of the work reported in this paper is to illustrate, through numerical modeling, the quantitative consequences that titratable organics have on $A_{\text{T(meas)}}$ determined by titration. The consequences are represented as ΔA_{T} , or the difference between $A_{\text{T(meas)}}$ and the well-defined A_{inorg} . This work examines (1) the implications of choosing one titration technique (and associated data analysis method) over another, (2) the importance of the protonation behavior (i.e., pK) of the organic matter itself, and (3) the propagation of errors in interpretations of $A_{\text{T(meas)}}$ to calculations of other carbonate system parameters. The overarching goal is to help inform the choices of investigators working on carbonate system dynamics in potentially high-organic environments and

to stimulate discussions within the marine chemistry community regarding how to manage uncertainties associated with the influence of organic matter on alkalinity titrations.

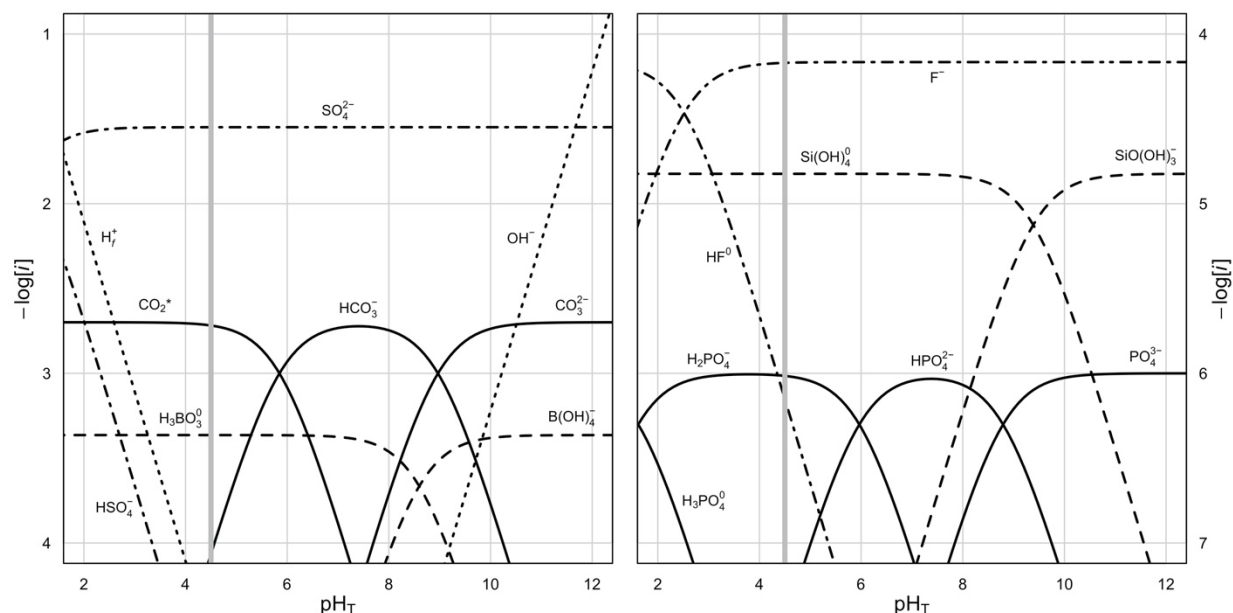


Figure 4.1. Bjerrum plots displaying concentrations $[i]$ of the major acid–base species in oxygenated seawater with $C_T = 2000 \mu\text{mol kg}^{-1}$, total phosphate (P_T) = $1.0 \mu\text{mol kg}^{-1}$, total silica (Si_T) = $15.0 \mu\text{mol kg}^{-1}$, salinity (S) = 35, temperature (t) = $25 \text{ }^\circ\text{C}$, and pressure (P) = 1 atm. The K_A^0 cutoff of Dickson (1981) that defines the zero level of protons is shown by the thick vertical grey line. The left panel displays species formed from chemical constituents with total concentrations greater than $10^{-4} \text{ mol kg}^{-1}$, whereas the right panel displays species formed from chemical constituents with total concentrations less than $10^{-4} \text{ mol kg}^{-1}$.

4.3 Background

4.3.1 Quantitative description of A_T

Dickson’s (1981) definition of total alkalinity (see section 4.2) is based on a “proton condition” rather than a purely empirical titration endpoint (see also Johansson and Wedborg, 1982). A proton condition is defined by the group of chemical species that dominate at the *ZLP*. To quantitatively assess any natural-water alkalinity titration according to a proton condition, an accurate model for the acid–base reactions that occur in the sample is critical. As an example, the

proton condition relevant to inorganic species in oxygenated seawater (Fig. 4.1) can be easily surmised from the quantitative information in Table 4.1 and Dickson's designation of $K_A^0 = 10^{-4.5}$ as the defining value of the *ZLP*:

$$[\text{H}^+]_f + [\text{HSO}_4^-] + [\text{HF}^0] + [\text{H}_3\text{PO}_4^0] = [\text{HCO}_3^-] + 2[\text{CO}_3^{2-}] + [\text{B}(\text{OH})_4^-] + [\text{OH}^-] + [\text{SiO}(\text{OH})_3^-] + [\text{HPO}_4^{2-}] + 2[\text{PO}_4^{3-}] \quad (4.5)$$

All symbols included in Eq. (4.5) and the following discussion are defined in detail in Table D1.1 in Appendix D1.

Table 4.1. Inorganic equilibria relevant to the definition of natural-water A_T . Values of $\text{p}K_A^0$ are used to define proton acceptors versus donors, with acceptors having $\text{p}K_A^0 \geq 4.5$ and donors having $\text{p}K_A^0 < 4.5$ (Dickson, 1981). The values of $\text{p}K_A$ and the constituent concentrations ($[i]$) are for oxygenated seawater with $\text{pH}_T = 8.1$, $C_T = 2000 \mu\text{mol kg}^{-1}$, $P_T = 1.0 \mu\text{mol kg}^{-1}$, $S_{iT} = 15.0 \mu\text{mol kg}^{-1}$, $S = 35$, $t = 25 \text{ }^\circ\text{C}$, and $P = 1 \text{ atm}$.

| Equilibrium (bold species contributes to A_T) | Equilibrium Constant | $\text{p}K_A^0$ | $\text{p}K_A$ | $[i]$ (bold species, $\mu\text{mol kg}^{-1}$) | Reference |
|---|----------------------|-----------------|---------------|---|--------------------------|
| $\text{H}_2\text{O} \rightarrow \text{OH}^- + \text{H}^+$ | K_W | 13.995 | 13.220 | 7.58 | Millero (1995) |
| $\text{Si}(\text{OH})_4^0 \rightarrow \text{SiO}(\text{OH})_3^- + \text{H}^+$ | K_{Si} | 9.825 | 9.387 | 0.74 | Yao and Millero (1995) |
| $\text{NH}_4^+ \rightarrow \text{NH}_3^0 + \text{H}^+$ (anoxic) | K_{NH_4} | 9.245 | 9.266 | 0.00 | Yao and Millero (1995) |
| $\text{HCO}_3^- \rightarrow \text{CO}_3^{2-} + \text{H}^+$ | K_2 | 10.330* | 8.966 | 238.51 | Lueker et al. (2000) |
| $\text{HPO}_4^{2-} \rightarrow \text{PO}_4^{3-} + \text{H}^+$ | K_{P_3} | 12.345 | 8.792 | 0.17 | Yao and Millero (1995) |
| $\text{B}(\text{OH})_3 + \text{H}_2\text{O} \rightarrow \text{B}(\text{OH})_4^- + \text{H}^+$ | K_B | 9.236 | 8.597 | 104.39 [†] | Dickson (1990a) |
| $\text{H}_2\text{S}^0 \rightarrow \text{HS}^- + \text{H}^+$ (anoxic) | K_{S_1} | 6.980 | 6.520 | 0.00 | Millero et al. (1988) |
| $\text{H}_2\text{PO}_4^- \rightarrow \text{HPO}_4^{2-} + \text{H}^+$ | K_{P_2} | 7.200 | 5.965 | 0.83 | Yao and Millero (1995) |
| $\text{CO}_{2(\text{aq})} + \text{H}_2\text{O} \rightarrow \text{HCO}_3^- + \text{H}^+$ | K_1 | 6.351* | 5.847 | 1751.70 | Lueker et al. (2000) |
| $\text{HF}^0 \rightarrow \text{F}^- + \text{H}^+$ | K_F | 3.174 | 2.626 | 0.00 [†] | Dickson and Riley (1979) |
| $\text{H}_3\text{PO}_4^0 \rightarrow \text{H}_2\text{PO}_4^- + \text{H}^+$ | K_{P_1} | 2.149 | 1.615 | 0.00 | Yao and Millero (1995) |
| $\text{HSO}_4^- \rightarrow \text{SO}_4^{2-} + \text{H}^+$ | K_{HSO_4} | 1.993 | 0.999 | 0.00 [†] | Dickson (1990b) |

* Values of $\text{p}K_1^0$ and $\text{p}K_2^0$ are from Millero (1979) because the salinity range given by Lueker et al. (2000) is 19–43.

[†] Conservative constituent ratios with respect to salinity for total boron, fluoride, and sulfate are given by Lee et al. (2010), Riley (1965), and Morris and Riley (1966), respectively.

Eq. (4.5) excludes some terms included in the full definition of A_{inorg} (Eq. (4.1)) because this discussion focuses on simple, oxygenated seawater. However, additional species formed from inorganic acids (e.g., ammonium and hydrogen sulfide) or organic acids (e.g., carboxyl and phenol groups) could in concept be included as well.

Because A_T represents the excess of proton acceptors over donors, it can be described in the context of this discussion by rearranging Eq. (4.5) to yield:

$$A_T = [\text{HCO}_3^-] + 2[\text{CO}_3^{2-}] + [\text{B}(\text{OH})_4^-] + [\text{OH}^-] + [\text{SiO}(\text{OH})_3^-] + [\text{HPO}_4^{2-}] + 2[\text{PO}_4^{3-}] - [\text{H}^+]_f - [\text{HSO}_4^-] - [\text{HF}^0] - [\text{H}_3\text{PO}_4^0] \quad (4.6)$$

Defining A_T in this way (i.e., according to a proton condition) allows for expression of an acidimetric titration of M_0 kilograms of natural water with M_A kilograms of acid of concentration C_A as

$$M_0 A_T = M_A C_A + M_T \{ [\text{HCO}_3^-] + 2[\text{CO}_3^{2-}] + [\text{B}(\text{OH})_4^-] + [\text{OH}^-] + [\text{SiO}(\text{OH})_3^-] + [\text{HPO}_4^{2-}] + 2[\text{PO}_4^{3-}] - [\text{H}^+]_f - [\text{HSO}_4^-] - [\text{HF}^0] - [\text{H}_3\text{PO}_4^0] \} \quad (4.7)$$

where M_T is the sum of M_0 and M_A . Using dissociation constant relationships and dilution corrections, Eq. (4.7) can alternatively be expressed as

$$M_0 A_T = M_A C_A + M_0 \left\{ \frac{C_T}{1 + \frac{[\text{H}^+]_T + K_2}{[\text{H}^+]_T}} + \frac{2 \cdot C_T}{1 + \frac{[\text{H}^+]_T + [\text{H}^+]_T^2}{K_2 K_1}} + \frac{B_T}{1 + \frac{[\text{H}^+]_T}{K_B}} + \frac{S_{\text{Si}}}{1 + \frac{[\text{H}^+]_T}{K_{\text{Si}}}} + \frac{P_T}{1 + \frac{[\text{H}^+]_T + [\text{H}^+]_T^2 + K_{\text{P3}}}{K_{\text{P2}} + K_{\text{P1}} K_{\text{P2}} + [\text{H}^+]_T}} + \frac{2 \cdot P_T}{1 + \frac{[\text{H}^+]_T + [\text{H}^+]_T^2 + [\text{H}^+]_T^3}{K_{\text{P3}} + K_{\text{P2}} K_{\text{P3}} + K_{\text{P1}} K_{\text{P2}} K_{\text{P3}}} - \frac{S_T}{1 + \frac{K_S}{[\text{H}^+]_f}} - \frac{F_T}{1 + \frac{K_F}{[\text{H}^+]_T}} - \frac{P_T}{1 + \frac{K_{\text{P1}}}{[\text{H}^+]_T} + \frac{K_{\text{P1}} K_{\text{P2}}}{[\text{H}^+]_T^2} + \frac{K_{\text{P1}} K_{\text{P2}} K_{\text{P3}}}{[\text{H}^+]_T^3}} \right\} - M_T \left\{ [\text{H}^+]_f - \frac{K_W}{[\text{H}^+]_T} \right\} \quad (4.8)$$

Dissociation constant relationships (Table D1.1) are mostly defined in terms of hydrogen ion concentrations on the total scale ($[\text{H}^+]_T$):

$$[\text{H}^+]_T = [\text{H}^+]_f + [\text{HSO}_4^-] = [\text{H}^+]_f + \frac{S_T}{1 + \frac{K_S}{[\text{H}^+]_f}} \quad (4.9)$$

Common terms in Eq. (4.8) (e.g., phosphate terms with P_T in the numerator) could be combined for mathematical simplicity but here are kept separate to emphasize the individual chemical species described by each term. Eqs. (4.5–4.8) are the basis for the discussions of alkalinity measurement approaches presented in section 4.3.2.

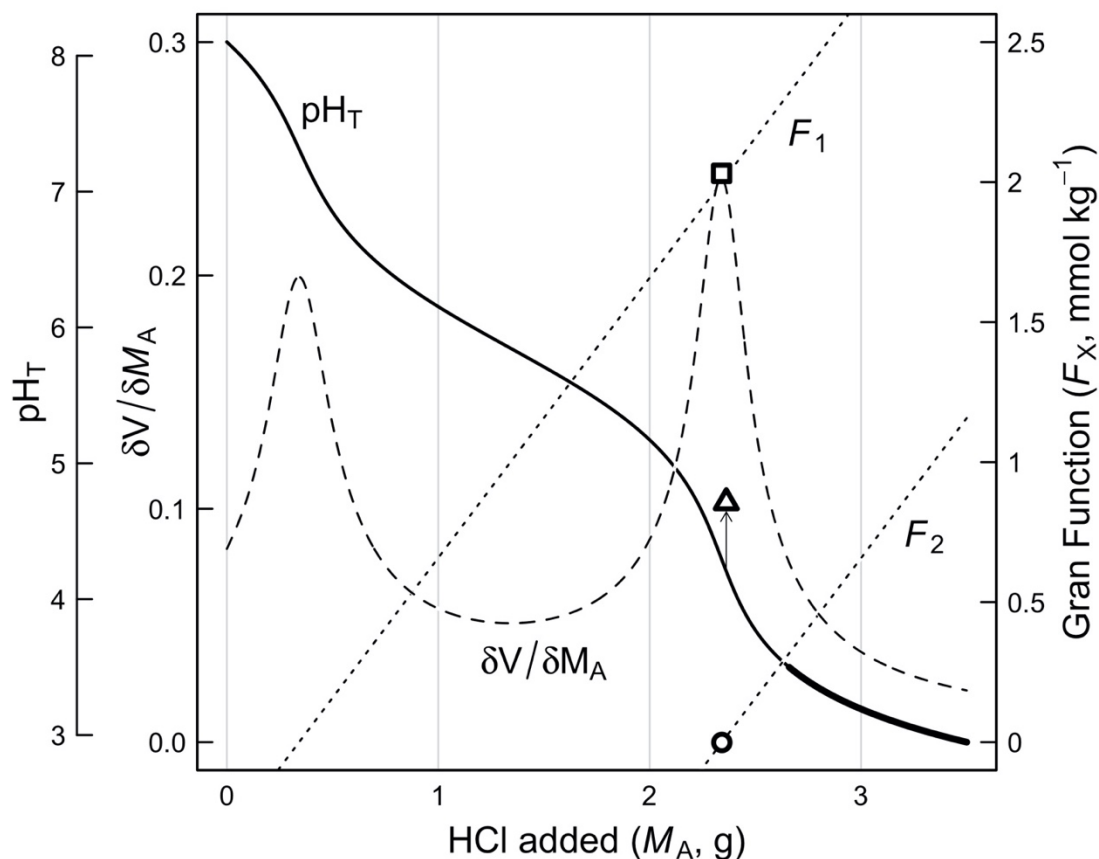


Fig. 4.2. Simulated titration of a 200 g sample of oxygenated seawater with initial $\text{pH}_T = 8.1$, $C_T = 2000 \mu\text{mol kg}^{-1}$, $P_T = 1.0 \mu\text{mol kg}^{-1}$, $S_{i,T} = 15.0 \mu\text{mol kg}^{-1}$, $S = 35$, $t = 25 \text{ }^\circ\text{C}$, and $p = 1 \text{ atm}$. The titrant is 0.2 M HCl. The solid black line is the simulated titration curve — i.e., the pH_T over the course of a typical multi-step titration. The other lines and symbols illustrate the various methods by which $A_{T(\text{meas})}$ can be determined from the titration curve. The dotted lines display the first and second Gran functions, F_1 and F_2 (Eq. (4.11)), and the circle shows the point at which the second Gran function is equal to zero. The dashed line displays the difference derivative of electrical potential in volts (V), and the square shows the second peak of the difference derivative function. The triangle shows the solution pH_T obtained after terminating a single-step titration at a pH_T of 4.20 and then purging CO_2 (arrow) from the sample solution. The thicker portion of the titration curve shows the pH_T range over which multi-step open-cell titrations are evaluated ($3.5 > \text{pH}_T > 3.0$).

4.3.2 Measurement approaches for A_T

As stated in section 4.2, A_T is generally evaluated by titrating a sample solution with a strong acid of known concentration. A simulated titration curve is shown in Fig. 4.2. One of two acidimetric titration approaches is typically employed: (1) titration in a stepwise manner, with measurements of electrical potential at each step (a “multi-step titration”) or (2) titration to a pre-determined endpoint, followed by CO_2 purging and a measurement of pH (a “single-step titration”).

Multi-step titration, the traditional method for measuring A_T in natural waters, is recognized explicitly as the best-practice method for measurements in seawater (Dickson et al., 2007). A multi-step titration is typically monitored by a glass electrode/reference electrode pH cell. Electrical potential is recorded manually or automatically at each titration step. Electrical potential values are related to hydrogen ion concentrations by the Nernst equation:

$$E = E^0 + \left(\frac{RT}{F}\right)\ln[\text{H}^+]_f \quad (4.10)$$

where E is the electrical potential developed by the pH cell, E^0 is the standard electrode potential, R is the ideal gas constant, T is the absolute temperature in K, and F is the Faraday constant. The Nernst equation can be applied to any pH scale, so long as the electrodes in use are properly calibrated on that scale.

Single-step A_T titration (Breland and Byrne, 1993; Liu et al., 2015; Yao and Byrne, 1998) has become more widely used in recent years due to the precision in total scale pH (pH_T) measurements offered by sulfonephthalein indicators (Byrne and Breland, 1989; Clayton and Byrne, 1993). Single-step titrations are appealing because of their speed (one addition of acid rather than a series of incremental additions) and simplicity.

This work focuses on five A_T measurement approaches that are widely used today: four involve analysis of multi-step titration data (subsections 4.3.2.1–4.3.2.4) and one involves analysis of single-step titration data (subsection 4.3.2.5). Each approach is summarized in Table 4.2. Fig. 4.2 illustrates the corresponding mathematical functions used to determine $A_{T(\text{meas})}$ from the titration curve.

Table 4.2. A_T measurement approaches discussed in this work. The descriptions in column two represent how data analysis is performed by the 'TITRATE.m' model, discussed later in this work.

| Measurement approach | Description |
|---|---|
| Modified Gran function (MGF), open-cell titration data | Standard electrode potential, E^0 , is iteratively refined using data from a multi-step titration of a CO ₂ -purged sample (see Dickson et al., 2003) to calculate values of the second Gran function (F_2 ; Eq. (4.12)). F_2 values are fit against M_A by linear least squares analysis from $\text{pH}_T = 3.5$ to 3.0 (Hansson and Jagner, 1973) to determine A_T . |
| Nonlinear least squares fit (NLSF), closed-cell titration data | The full titration curve (Eq. (4.13)) for a multi-step closed-cell titration is fit using nonlinear least squares analysis. A multiplier f is used with hydrogen ion concentration estimates calculated from measured E values and estimated E^0 . Adjustable parameters in the fit are f , A_T , and C_T (Dickson, 1981; Johansson and Wedborg, 1982). |
| Nonlinear least squares fit (NLSF), open-cell titration data | The titration curve from $\text{pH}_T = 3.5$ to 3.0 (Eq. (4.14)) for a multi-step open-cell titration is fit using nonlinear least squares analysis. A multiplier f is used with hydrogen ion concentration estimates calculated from measured E values and estimated E^0 . Adjustable parameters in the fit are f and A_T (Dickson et al., 2003). |
| Difference derivative (DD) analysis, closed-cell titration data | Difference derivatives (DDs, calculated using Eq. (4.15)) at each step of a multi-step closed-cell titration are fit against M_A to a cubic spline interpolation. The second peak of the cubic function is located by taking the derivative of the cubic function (Hernández-Ayón et al., 1999). |
| Single-step titration, open-cell | The final pH_T of the purged solution (after termination of a single-step titration at $\text{pH}_T \approx 4.20$) is used with M_A to determine A_T (calculated using Eq. (4.16)) (Liu et al., 2015; Yao and Byrne, 1998). |

4.3.2.1 Modified Gran function (MGF) analysis of open-cell titration data

Dyrssen (1965) was the first to use the mathematical method of Gran (1950, 1952) to estimate the A_T of natural waters from multi-step titration data. Gran's method transforms

nonlinear plots of the electrical potential of a solution versus the amount of added acid into plots (“Gran plots”) of linear functions that converge at the titration equivalence point. Dyrssen’s (1965) method was further described by Dyrssen and Sillén (1967). Advancements in theory and methodology by Hansson and Jagner (1973) led to the use of modified Gran functions (MGFs), which account for minor acid–base species (i.e., those other than bicarbonate, carbonate, and borate) in A_T determinations. Much subsequent work in the field has been based on the use of MGFs to analyze alkalinity titrations (Almgren et al., 1977; Bradshaw et al., 1981; Bradshaw and Brewer, 1980; Gieskes, 1973).

The MGF pertaining to the second equivalence point of a natural water sample (F_2) describes chiefly the titration of bicarbonate to carbonic acid (Dickson, 1981; Hansson and Jagner, 1973):

$$F_2 = M_T\{[H^+]_f + [HSO_4^-] + [HF^0] + [H_3PO_4^0] - [HCO_3^-]\} \quad (4.11)$$

Chemical species that are negligible in concentration across the pH range near the second equivalence point have been dropped from Eq. (4.11).

MGFs are used most commonly today to evaluate data from open-cell titrations (e.g., Winn et al., 1998), during which CO_2 is allowed to outgas after an initial acid addition before the titration is continued to low pH (as in Dickson et al., 2003). To determine A_T from open-cell titration data using an MGF approach, Eq. (4.11) is first adjusted to define species concentrations using dissociation constant relationships and to reflect the outgassing of CO_2 :

$$F_2 = M_T[H^+]_f + M_0 \left\{ \frac{S_T}{1 + \frac{K_S}{[H^+]_f}} + \frac{F_T}{1 + \frac{K_F}{[H^+]_T}} + \frac{P_T}{1 + \frac{K_{P1}}{[H^+]_T} + \frac{K_{P1}K_{P2}}{[H^+]_T^2} + \frac{K_{P1}K_{P2}K_{P3}}{[H^+]_T^3}} \right\} \quad (4.12)$$

After an initial guess is made for E^0 , $[H^+]$ values ($[H^+]_f$ and $[H^+]_T$) at each titration step are calculated using Eqs. (4.9) and (4.10). An estimate for F_2 is calculated using these $[H^+]$ values and

Eq. (4.12). Then, a linear least squares regression is performed for the F_2 vs. M_A data across the specified pH range to obtain an estimate for A_T . An adjustment is made to E^0 , and the process is repeated iteratively until the change in A_T is below a specified threshold.

The open-cell MGF method is used to determine A_T at Station ALOHA in the Pacific Ocean, as part of the Hawaii Ocean Time-series program (Winn et al., 1991).

4.3.2.2 Nonlinear least squares fitting (NLSF) of closed-cell titration data

In the 1980s, nonlinear least squares fitting of the titration curve itself emerged as a method estimating A_T and C_T from a multi-step titration in a closed cell (Dickson, 1981; Johansson and Wedborg, 1982; Millero et al., 1993). For the nonlinear least squares fit (NLSF) approach, all the terms in Eq. (4.8) are set to zero (Dickson, 1981; Johansson and Wedborg, 1982):

$$M_0 A_T - M_A C_A - M_0 \left\{ \frac{C_T}{1 + \frac{[H^+]_T}{K_1} + \frac{K_2}{[H^+]_T}} + \frac{2 \cdot C_T}{1 + \frac{[H^+]_T}{K_2} + \frac{[H^+]_T^2}{K_1 K_2}} + \frac{B_T}{1 + \frac{[H^+]_T}{K_B}} + \frac{Si_T}{1 + \frac{[H^+]_T}{K_{Si}}} + \frac{P_T}{1 + \frac{[H^+]_T}{K_{P2}} + \frac{[H^+]_T^2}{K_{P1} K_{P2}} + \frac{K_{P3}}{[H^+]_T}} + \frac{2 \cdot P_T}{1 + \frac{[H^+]_T}{K_{P3}} + \frac{[H^+]_T^2}{K_{P2} K_{P3}} + \frac{[H^+]_T^3}{K_{P1} K_{P2} K_{P3}}} - \frac{S_T}{1 + \frac{K_S}{[H^+]_f}} - \frac{F_T}{1 + \frac{K_F}{[H^+]_T}} - \frac{P_T}{1 + \frac{K_{P1}}{[H^+]_T} + \frac{K_{P1} K_{P2}}{[H^+]_T^2} + \frac{K_{P1} K_{P2} K_{P3}}{[H^+]_T^3}} \right\} + M_T \left\{ [H^+]_f - \frac{K_W}{[H^+]_T} \right\} = 0 \quad (4.13)$$

Using a Gran-type approximation, initial estimates for E^0 , A_T , and C_T are obtained. The estimated E^0 is used with measured E values to calculate estimated hydrogen ion concentrations ($[H^+]'$) at each titration step. A multiplier f is defined to calculate $[H^+]_T$ values at each step (Dickson et al., 2007): $[H^+]_T = f[H^+]'$. Then, values of M_A and $[H^+]'$ are used with a least squares routine (typically a Levenberg–Marquardt algorithm) and Eqs. (4.10) and (4.13) to simultaneously compute f , A_T , and C_T . The multiplier f is used to calculate $[H^+]_T$ values and E^0 .

Barron et al. (1983) demonstrated that there is little difference between A_T determined from closed-cell titration data using the MGF approach versus the NLSF approach. The closed-cell NLSF approach has been used on recent repeat hydrography cruises across the globe as part of the US GO-SHIP program (e.g., Baringer et al., 2016; Volkov et al., 2019). Overall, however, the closed-cell titration technique has become somewhat less prevalent in recent years due to the development (Johnson et al., 1985) and refinement of the more reliable coulometric technique for determining C_T and also difficulties associated with calibrating the volume of closed-cell systems (Dickson et al., 2003).

4.3.2.3 Nonlinear least squares fitting (NLSF) of open-cell titration data

A method for analyzing A_T titrations in open cells (after allowing CO_2 to escape) by least squares fitting of a lower portion of the titration curve (e.g., $3.5 > \text{pH} > 3.0$) was described by Dickson et al. (2003). For this method, inorganic carbon terms and terms that are negligible across a low pH range are dropped from Eq. (4.13):

$$M_0 A_T - M_A C_A + M_0 \left\{ \frac{S_T}{1 + \frac{K_S}{[\text{H}^+]_f}} + \frac{F_T}{1 + \frac{K_F}{[\text{H}^+]_T}} + \frac{P_T}{1 + \frac{K_{P1}}{[\text{H}^+]_T} + \frac{K_{P1}K_{P2}}{[\text{H}^+]_T^2} + \frac{K_{P1}K_{P2}K_{P3}}{[\text{H}^+]_T^3}} \right\} + M_T [\text{H}^+]_f = 0 \quad (4.14)$$

Using a Gran-type approximation, initial estimates are obtained for E^0 and A_T . The estimated E^0 is used with measured E values to calculate $[\text{H}^+]'$ at each titration step and a multiplier f is again defined: $[\text{H}^+]_T = f[\text{H}^+]'$. Then, values of M_A and $[\text{H}^+]'$ are used with a NLSF routine and Eqs. (4.10) and (4.14) to simultaneously compute f and A_T .

The open-cell NLSF method is used to determine the A_T of Certified Reference Material (CRM) from Scripps Institution of Oceanography (Dickson et al., 2003). This method, like the closed-cell NLSF method, has also been used on recent repeat hydrography cruises across the globe as part of the US GO-SHIP program (e.g., Cross et al., 2017; Speer et al., 2018).

4.3.2.4 Difference derivative (DD) analysis of closed-cell titration data

Hernández-Ayón et al. (1999) described a method involving the use of difference derivatives (DDs) to directly determine A_T from closed-cell multi-step titration data. This approach, which does not depend on a pre-defined acid–base model (e.g., Eq. (4.1)), allows for the detection of dissolved titratable organics by also providing measurements of initial pH and C_T . In this approach, DDs of electrical potential measurements in volts (V) with respect to added acid mass (M_A) are computed at each step (n) during a titration:

$$\delta V / \delta M_A = (V_{n+1} - V_n) / (M_{A(n+1)} - M_{A(n)}) \quad (4.15)$$

The DDs are plotted as a function of M_A and then fit to a cubic spline interpolation. The second peak of the spline function corresponds to the second equivalence point, which is used to determine A_T . Hernández-Ayón et al. (1999) demonstrated that this technique is independent of any errors in dissociation constants or conservative constituent ratios.

The DD analysis method has been used for studies of organic alkalinity (Hernández-Ayón et al., 2007; Muller and Bleie, 2008), biological calcification (Steller et al., 2007), and general carbonate system studies (Álvarez et al., 2014; Cantoni et al., 2012).

4.3.2.5 Single-step titration in an open cell

A fundamentally different approach was advanced by Breland and Byrne (1993) with their description of a method for determining A_T by using a single addition of HCl (rather than incremental stepwise additions) and spectrophotometric measurement of excess acid after complete purging of CO_2 from the sample solution. This method was based somewhat on the work of Culberson et al. (1970), who described a single-step approach that used electrometric

measurement of excess acid. Yao and Byrne (1998) introduced continuous pH monitoring to the Breland and Byrne (1993) approach to minimize the excess acid term, and Liu et al. (2015) automated the process.

In this method, an indicator dye (bromocresol purple or bromocresol green) is added to the sample, which allows the titration to be monitored continuously by a spectrophotometer. This approach permits titrant acid to be added quickly at first, then slowly until the sample reaches a pre-determined endpoint (e.g., $\text{pH}_T = 4.20$) at which (1) the excess acid exceeds the residual bicarbonate and (2) only free H^+ , HSO_4^- , HF^0 , and HCO_3^- contribute appreciably to the proton balance.

After CO_2 is purged from the sample using a dry gas stream (e.g., high-purity N_2), HCO_3^- no longer contributes to the proton balance and A_T can be calculated using a modified version of Eq. (4.8):

$$A_T = (M_A C_A - M_T [\text{H}^+]_T - M_0 (F_T / (1 + \frac{K_F}{[\text{H}^+]_T}))) / M_0 \quad (4.16)$$

Notice that hydrogen ion concentration here is expressed on the total scale (Eq. (4.9)), accounting for both $[\text{H}^+]_f$ and $[\text{HSO}_4^-]$; a term (with F_T in the numerator) is therefore included in Eq. (4.16) to account for HF^0 . Alternatively, hydrogen ion concentration could be expressed on the seawater scale (Breland and Byrne, 1993; Yao and Byrne, 1998):

$$[\text{H}^+]_{\text{sws}} = [\text{H}^+]_f + [\text{HSO}_4^-] + [\text{HF}^0] \quad (4.17)$$

and the HF^0 term omitted. The single-step method is appealing because the amount of excess acid remaining after the purging of CO_2 can be kept relatively low ($<30 \mu\text{mol kg}^{-1}$), meaning that any error in the final pH_T measurement contributes minimally to measured A_T (± 0.01 in pH_T translates to about $\pm 0.5 \mu\text{mol kg}^{-1}$ in $A_{T(\text{meas})}$).

The single-step method has been used to measure alkalinity for studies of CaCO_3 dissolution (Naviaux et al., 2019a; 2019b), organic alkalinity (Yang et al., 2015), and cephalopod metabolism (Birk et al., 2018).

4.3.3 Introducing additional species to the A_T equation

In section 4.3.1, it was indicated that additional chemical species (e.g., organic acids) can be added to the proton condition given in Eq. (4.5), and therefore to the A_T definition given in Eq. (4.6). To rigorously account for these species, their total concentrations and dissociation behaviors (K_A values) would have to be known. In a system with a non-negligible concentration of total ammonia (NH_3_T), for example, the influence of ammonia (NH_3^0 , defined as a proton acceptor) would be accounted for in Eq. (4.8) by adding a positive term of the form $M_0(\text{NH}_3_T/(1 + [\text{H}^+]_T/K_{\text{NH}_4}))$, where K_{NH_4} is the dissociation constant of the ammonium ion.

Similarly, a titratable organic base (X^-) formed from a weak acid (HX^0) with a total concentration X_T and a pure water dissociation constant $\text{p}K_{\text{X}}^0 \geq 4.5$ at 25 °C would be included in Eq. (4.8) by adding a positive term of the form $M_0(X_T/(1 + [\text{H}^+]_T/K_{\text{X}}))$. A titratable organic acid (HY^0) with a total concentration of Y_T and a pure water dissociation constant $\text{p}K_{\text{Y}}^0 < 4.5$ at 25 °C would be included by adding a negative term of the form $-M_0(Y_T/(1 + K_{\text{Y}}/[\text{H}^+]_T))$.

Much recent work has focused on qualitatively characterizing organic molecules in natural waters (e.g., Arakawa et al., 2017; Ben Ali Daoud and Tremblay, 2019; Broek et al., 2020; Hertkorn et al., 2006, 2013; Longnecker and Kujawinski, 2017). These studies and others have identified a wide variety of organic molecular functional groups and structures. The continuous spectrum on which these molecular properties occur results in a continuous distribution of proton-exchange behavior (Fukushima et al., 1995; Perdue et al., 1984).

Table 4.3 displays the results of several studies that have examined the proton-exchange properties of organics found in natural waters or culture experiments. These studies identified approximate centers of distribution for organic acid pK values. Some of these studies also reported effective concentrations for each functional group, but those values are not displayed in Table 4.3 because they are highly variable and hold little value when obtained from phytoplankton cultures or pre-concentrated natural organic matter.

Table 4.3. Summary of selected studies that examined the acid–base properties of dissolved organic matter in terms of pK values. The numbered pK values (pK_1 , pK_2 , and pK_3) correspond to explicit fits of titration curves, whereas the “bulk” pK values correspond to fits obtained using dissolved organic carbon concentrations and organic alkalinity estimates according to Eq. (4) in Kuliński et al. (2014).

| Reference | Location | pK_1 | pK_2 | pK_3 |
|-------------------------------|-----------------------------|-----------|-----------|--------|
| Paxeus and Wedborg (1985)* | Göta River, Sweden | 2.66 | 4.21 | 5.35 |
| | Göta River, Sweden | 6.65 | 8.11 | 9.54 |
| Cai et al. (1998) | Satilla River, GA, USA | 4.46 | 6.64 | 8.94 |
| De Souza Sierra et al. (2001) | Santa Catarina Is., Brazil | 5.51–5.99 | 9.09–9.85 | |
| Hruška et al. (2003) | Czech Republic stream | 2.50 | 4.42 | 6.70 |
| | Sweden stream | 3.04 | 4.51 | 6.46 |
| Muller and Bleie (2008) | Norwegian fjord | 4.10 | 9.16 | |
| Yang et al. (2015) | Coquina Key, FL, USA | 5.31 | 7.05 | |
| | Bayboro Harbor, FL, USA | 5.45 | 7.32 | |
| Ko et al. (2016) | Coastal Korea | 4.4 | 6.1 | |
| | Culture species | pK_1 | pK_2 | pK_3 |
| Fein et al. (1997) | <i>Bacillus subtilis</i> | 4.82 | 6.9 | 9.4 |
| Ko et al. (2016) | <i>Prorocentrum minimum</i> | 4.9 | 6.9 | |
| | <i>Emiliana huxleyi</i> | 4.8 | 6.9 | |
| | <i>Skeletonema costatum</i> | 4.9 | 6.8 | |
| | Location | Bulk pK | | |
| Kuliński et al. (2014) | Baltic Sea | 7.53 | | |
| Ulfso et al. (2015) | Baltic Sea | 7.34 | | |

* Paxeus and Wedborg (1985) described six separate groups of charge sites for a single sample, displayed here across two lines of the table.

Table 4.3 illustrates that estimates of organic acid pK values can be quite heterogenous; in other words, there is not a clear “typical” set of organic pK values that can be applied to natural organic matter. The bulk pK values do show some promise for practical application, but more work is needed to determine whether the Baltic Sea material is universally representative of marine and estuarine dissolved organic matter. Due to the pervasive lack of essential pK information, organic acids are almost always excluded from the chemical models used to evaluate A_T .

As noted in section 4.2, any chemical species that binds protons during the course of an acidimetric titration will contribute quantitatively to $A_{T(\text{meas})}$ in the form of $A_{\text{org}(\text{meas})}$. These species can certainly include those that are not explicitly accounted for in the acid–base models that defines A_{inorg} (e.g., Eq. (4.1); Dickson, 1981). The extent to which $A_{T(\text{meas})}$ deviates from A_{inorg} (i.e., ΔA_T) in the presence of unidentified titratable organics is a function of the concentrations and proton-exchange properties of the organic molecules, the inorganic chemistry of the natural water sample, the pH range over which titration data are analyzed, and the method of that data analysis. The effects of these different factors on the results of total alkalinity titrations will be discussed in this paper.

4.5 Methods

To model A_T measurements in the presence of dissolved organic matter, a program (‘TITRATE.m’, hereafter referred to as “the model”) was written for MATLAB (MathWorks®); this code is available on GitHub at <https://github.com/jonathansharp/AlkTitrationModel>. The model generates simulated titration data, then analyzes those data using the five independent A_T measurement approaches described in section 4.3.2, and provides an $A_{T(\text{meas})}$ value that would be

obtained by each method. The adjustable input parameters for the model are listed in Table 4.4, along with the default values for surface seawater without organics.

Table 4.4. Adjustable input parameters for ‘TITRATE.m’.

| Parameter | Default value | Unit |
|--|---------------|-------------------------|
| Salinity (S) | 35 | none |
| Temperature (T) | 25 | °C |
| Total dissolved inorganic carbon (C_T) | 2000 | $\mu\text{mol kg}^{-1}$ |
| pH _T | 8.1 | none |
| Total phosphate concentration (P_T) | 1 | $\mu\text{mol kg}^{-1}$ |
| Total silicate concentration (Si_T) | 15 | $\mu\text{mol kg}^{-1}$ |
| Total ammonium concentration (NH_4^+) | 0 | $\mu\text{mol kg}^{-1}$ |
| Total hydrogen sulfide concentration (H_2S) | 0 | $\mu\text{mol kg}^{-1}$ |
| Sample mass (M_0) | 200 | g |
| Titrant molality (C_A) | 0.2 | mol kg^{-1} |
| Total organic acid concentration (ORG_T) | 0 | $\mu\text{mol kg}^{-1}$ |
| Dissociation constant of organic acid ($\text{p}K_{\text{org}}$) | 0 | mol kg^{-1} |

Conservative constituent ratios and dissociation constants in the model are determined according to the references given in Table 4.1. At $0 < S < 20$, K_1 and K_2 are determined using the formulation of Waters et al. (2014), which essentially corrects pH scale inconsistencies associated with the K_1 and K_2 formulations given by Millero (2010).

The model simulates an alkalinity titration by first calculating the concentrations of all acid–base species at the initial conditions specified by the input parameters. Then, HCl is incrementally added in a step-wise manner. The total mass of HCl used for the simulated titration ($M_{A(\text{tot})}$) is calculated by the equation given in Dickson et al. (2007): $M_{A(\text{tot})} = 0.0035 \cdot M_0 / C_A$. The mass of HCl added at each titration step is $M_{A(\text{tot})}/1000$, meaning the model simulates 1000 steps.

At each step, hydrogen ion concentration is determined using an iterative procedure, both using the initial C_T value (to simulate retention of inorganic carbon for closed-cell titrations) and

using $C_T = 0$ (to simulate purging of inorganic carbon for open-cell titrations). Eq. (4.10) is used to convert hydrogen ion concentrations to E values.

Once the simulated titration is complete, data analysis is performed in five different ways according to the summary of measurement approaches provided in Table 4.2. For the single-step titration, the closed-cell titration curve is fit to a spline function. The M_A value at which the pH_T estimated from the closed-cell spline function is equal to 4.2 (before purging of inorganic carbon) is used to determine the corresponding open-cell $[\text{H}^+]_T$ value (to simulate CO_2 purging). These M_A and $[\text{H}^+]_T$ values are used as inputs to Eq. (4.16). Reported $A_{T(\text{meas})}$ values obtained by each of the five measurement approaches can be compared for a range of assumed organic molecular characteristics.

The model was first used to simulate alkalinity titrations of solutions without any organics (section 4.6.1); this provided a baseline to assess consistency in $A_{T(\text{meas})}$ among the five measurement approaches. Then, a simple organic acid was added to the model to determine how its presence influenced $A_{T(\text{meas})}$ (and ΔA_T) determined by each approach (sections 4.6.2 and 4.6.3). Carbonate system parameters were calculated by treating $A_{T(\text{meas})}$ values as A_{inorg} (section 4.6.4). Calculations were performed using CO2SYS (Lewis and Wallace, 1998) for MATLAB (Van Heuven et al., 2011), with all other input parameters (besides alkalinity) as defined precisely by the ‘TITRATE.m’ model inputs. Finally, practical methods for measuring or estimating organic alkalinity are discussed (section 4.6.5) and the possibility of organic alkalinity in the open ocean is explored (section 4.6.6).

4.6 Results and Discussion

4.6.1 Validation of ‘TITRATE.m’ model in the absence of titratable organics

4.6.1.1 Comparison of model results to test dataset

To validate that the data analysis routines embedded in the model provide accurate calculations of $A_{T(\text{meas})}$, two steps were taken. First, open-cell titration data from the example calculation given in section 7.4 of SOP 3b in Dickson et al. (2007) were analyzed using the model’s open-cell NLSF routine. This routine gave an $A_{T(\text{meas})}$ of 2260.09 $\mu\text{mol kg}^{-1}$ and an E^0 of 0.394395 V, nearly identical to the $A_{T(\text{meas})}$ of 2260.06 $\mu\text{mol kg}^{-1}$ and E^0 of 0.394401 V given by the NLSF performed by Dickson et al. (2007). This close agreement confirms that the open-cell NLSF routine embedded in the model is performing as it should.

4.6.1.2 Comparison among measurement approaches

Next, to validate the other data analysis routines, data generated by the model from simulated titrations of natural water with no organic acids (default conditions given in Table 4.4) were analyzed by each routine. The resulting $A_{T(\text{meas})}$ values were compared to A_{inorg} as defined precisely by the model inputs according to Eq. (4.1). Fig. 4.3 shows relative values of ΔA_T (i.e., $A_{T(\text{meas})} - A_{\text{inorg}}$) for these simulated titrations as a function of salinity and corresponding C_T . As detailed in section 4.2, ΔA_T is conceptually analogous to the $A_{\text{org}(\text{meas})}$ quantity presented in Eq. (4.4); however the two are not identical, as misestimates of A_{inorg} that are unrelated to dissolved organics will also manifest in ΔA_T . The C_T range in Fig. 4.3 was determined by assuming a functional relationship with salinity: $C_T = S \cdot 50 + 300$. Because no organics were included, $A_{\text{inorg}} = A_T$ by definition. So, in a perfectly characterized system, $A_{T(\text{meas})}$ and A_{inorg} will be exactly equal and ΔA_T will be zero.

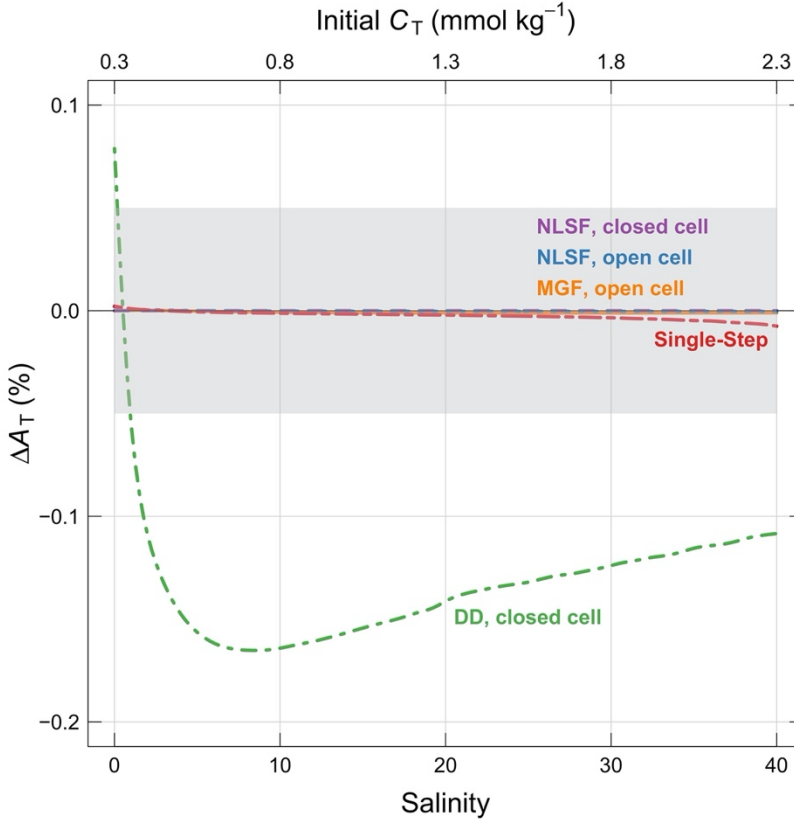


Fig. 4.3. Modeled differences (%) between $A_{T(\text{meas})}$ and A_{inorg} in a purely inorganic system, for the five data analysis procedures outlined in Table 4.2: $\Delta A_T = A_{T(\text{meas})} - A_{\text{inorg}}$. The shaded region represents a typically estimated measurement precision for A_T ($\pm 0.05\%$). The sample solution is oxygenated natural water with $\text{pH}_T = 8.1$, $P_T = 1.0 \mu\text{mol kg}^{-1}$, $S_{i_T} = 15.0 \mu\text{mol kg}^{-1}$, $t = 25 \text{ }^\circ\text{C}$, $p = 1 \text{ atm}$, and $ORG_T = 0 \mu\text{mol kg}^{-1}$. Results are shown as functions of S and C_T . Values of C_T were determined by assuming a functional relationship with S : $C_T = 50 \cdot S + 300$.

Fig. 4.3 shows that most measurement approaches provide $A_{T(\text{meas})}$ values that are virtually identical to A_{inorg} . One noticeable deviation is the single-step method's slight overestimate of A_T at very low salinities (at most by 0.002%) and underestimate at most other salinities (at most by 0.008%). These minor errors can be explained by small contributions from borate and phosphate species at the final pH, which are not explicitly accounted for by Eq. (4.16). These errors could be eliminated by the addition of small corrective terms to that equation. However, these corrections are not made here because the errors are well within state-of-the-art measurement precision for

total alkalinity, which is typically reported as $\pm 0.05\%$ at best (the shaded region of the Fig. 4.3), and often higher.

The most conspicuous result displayed in Fig. 4.3, though, is the difference between ΔA_T determined by the DD method versus ΔA_T determined by the other four methods. This result is not entirely surprising (c.f. Rigobello-Masini and Masini, 2001) because the DD method is the only one of the five that is not explicitly based on a proton condition defined rigorously by a thermodynamic acid–base model. So, unlike the methods that rely on a proton condition, the DD method provides a value for $A_{T(\text{meas})}$ that is not necessarily exactly consistent with A_T as defined by Dickson (1981). Still, $A_{T(\text{meas})}$ determined by the DD method remains within 0.2% (less than 3 $\mu\text{mol kg}^{-1}$) of A_T across the range of salinities and C_T values in Fig. 4.3, and any inconsistencies can be assessed by comparing measurements of CRMs (Dickson et al., 2003).

The analysis described here validates that (1) the ‘TITRATE.m’ model successfully simulates and analyzes alkalinity titrations and (2) despite the caveat associated with the DD method, the five independent data analysis methods produce $A_{T(\text{meas})}$ values that sufficiently estimate A_T under “normal” conditions (i.e., no organic species).

4.6.2 Modeled $A_{T(\text{meas})}$ in the presence of titratable organics

4.6.2.1 Effect of measurement approach

To highlight the effect that titratable organics have on $A_{T(\text{meas})}$, an organic acid with a total concentration equal to 20 $\mu\text{mol kg}^{-1}$ (ORG_T) was added to the model at the inorganic conditions given in Table 4.4. The value of $ORG_T = 20 \mu\text{mol kg}^{-1}$ was chosen because coastal and estuarine waters often have titratable organic concentrations that are near or well above this level (e.g., Cai et al., 1998; Kuliński et al., 2014; Yang et al., 2015), whereas observations in open ocean surface

waters suggest that it may be logical to expect concentrations of titratable organic acids of as much as $10 \mu\text{mol kg}^{-1}$, even in areas where organic alkalinity is traditionally neglected (see section 4.6.6). So, $ORG_T = 20 \mu\text{mol kg}^{-1}$ is an intermediate value to these two extremes, and is convenient for illustrative purposes.

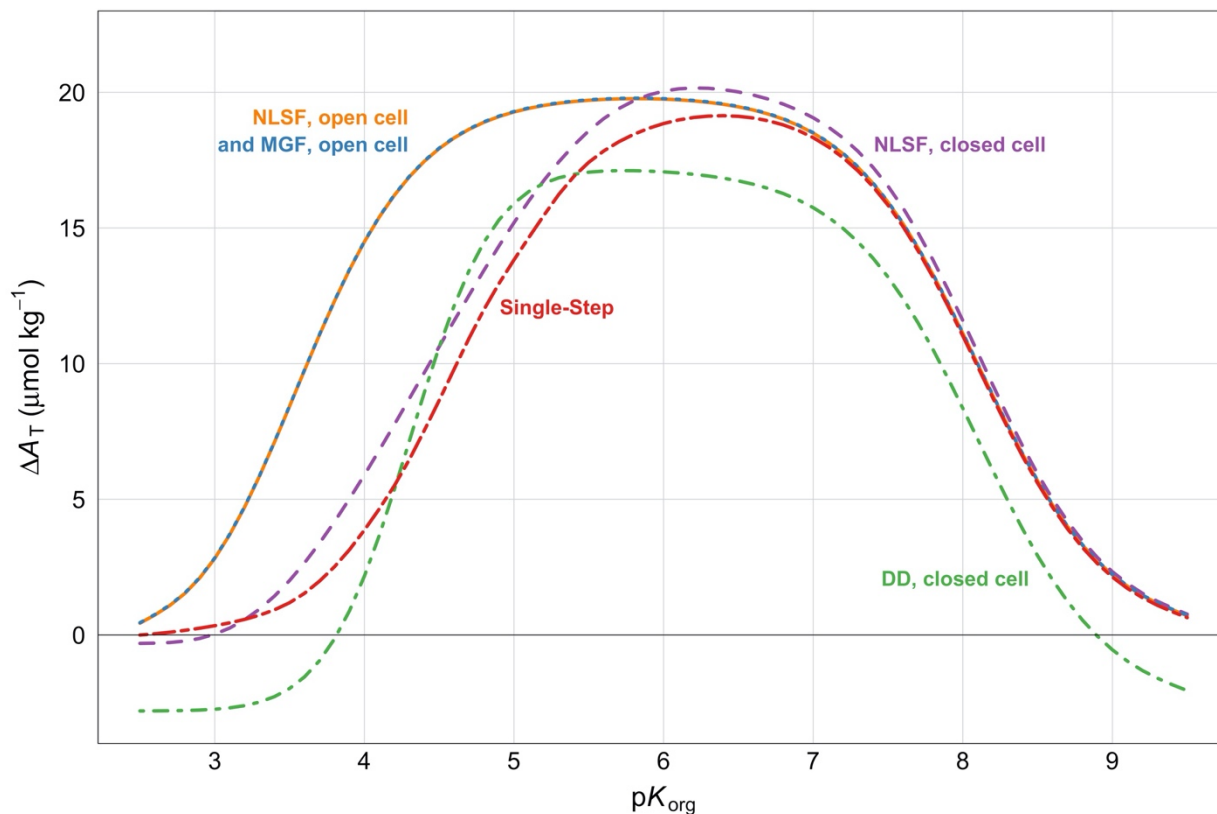


Fig. 4.4. Modeled differences between $A_{T(\text{meas})}$ and A_{inorg} in a system that includes titratable organics, as a function of pK_{org} (2.5 to 9.5): $\Delta A_T = A_{T(\text{meas})} - A_{\text{inorg}}$. The sample solution is oxygenated seawater with $\text{pH}_T = 8.1$, $C_T = 2000 \mu\text{mol kg}^{-1}$, $P_T = 1.0 \mu\text{mol kg}^{-1}$, $Si_T = 15.0 \mu\text{mol kg}^{-1}$, $t = 25 \text{ }^\circ\text{C}$, $S = 35$, $p = 1 \text{ atm}$, and $ORG_T = 20 \mu\text{mol kg}^{-1}$.

Across a range of pK_{org} (2.5 to 9.5), values of ΔA_T were computed for each measurement approach (Fig. 4.4; Table D1.2). These ΔA_T values represent the difference between measured total alkalinity ($A_{T(\text{meas})}$, determined using the five discrete data analysis methods) and inorganic alkalinity (A_{inorg} , defined precisely by the model inputs according to Eq. (4.1)). Again, any

difference will be mainly due to the effect of $A_{\text{org(meas)}}$ (Eq. (4.4)). Table D1.3 similarly contains ΔA_T values across a range of initial sample pH_T and C_T with fixed $\text{p}K_{\text{org}}$ values.

Fig. 4.4 shows that the largest ΔA_T values (up to 100% of ORG_T) are seen in the $\text{p}K_{\text{org}}$ range of about 5.0–7.0. This result is reasonable because, given this $\text{p}K_{\text{org}}$ range, the organic acid is almost fully dissociated at the initial sample pH and the conjugate base becomes almost fully protonated during the course of each titration.

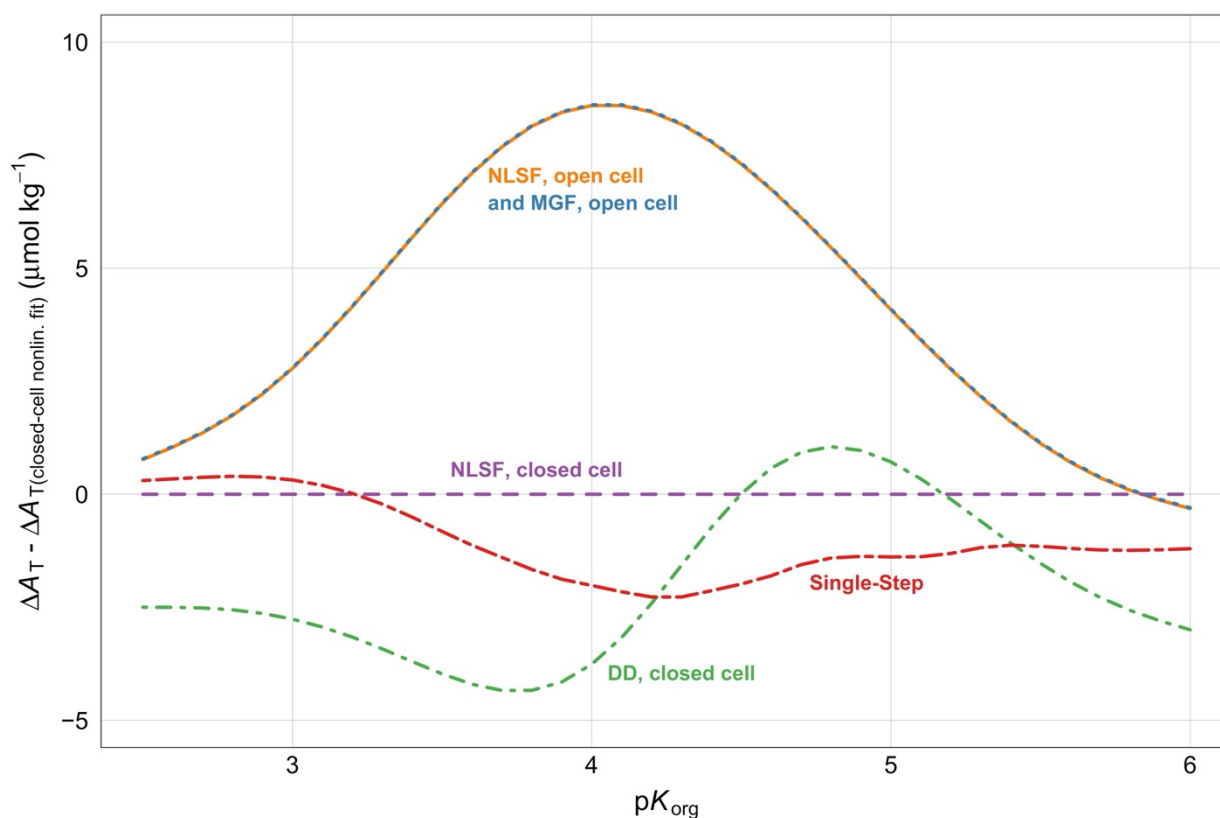


Fig. 4.5. Differences between ΔA_T for the closed-cell NLSF method versus ΔA_T for the other four methods, as a function of $\text{p}K_{\text{org}}$ (2.5 to 6.0). The composition of the sample solution is identical to that used for Fig. 4.4. Note that the scales of the x- and y-axes differ from those of Fig. 4.4.

Aside from the systematic offset of the DD method (Fig. 4.3), the ΔA_T values are relatively consistent among the different data analysis methods for high $\text{p}K_{\text{org}}$ values (6.0–9.5). However,

the ΔA_T values begin to diverge more significantly for $pK_{\text{org}} < 6.0$. To emphasize the divergence among methodologies at low pK_{org} (i.e., < 6.0), Fig. 4.5 shows ΔA_T values within this range relative to ΔA_T obtained from the closed-cell NLSF approach, which tends to provide values intermediate to the other approaches.

The largest ΔA_T values at low pK_{org} are associated with the two multi-step open-cell titration methods, which show nearly identical results. For these two methods, low- pK organic acids exert a relatively strong influence across the low pH range over which the titration data are analyzed.

The NLSF of the full titration curve using closed-cell titration data shows slightly greater ΔA_T values than the other methods at pK_{org} values from about 6 to 8 and lower values than the multi-step open-cell methods at pK_{org} values less than 6 (Fig. 4.4). The inclusion of titration data spanning a wide range of pH for the closed-cell NLSF minimizes the effect of low- pK organics on $A_{T(\text{meas})}$ compared to the open-cell NLSF.

The DD method produces ΔA_T values in the low pK_{org} range that are offset from the closed-cell NLSF ΔA_T values by an average of about $-2.5 \mu\text{mol kg}^{-1}$ (Fig. 4.5). This offset varies in magnitude, however, near $pK_{\text{org}} = 4.3$. This variation is due to the approximate location of the second titration equivalence point near $\text{pH} = 4.3$, which is therefore where the DD function peaks. The offset itself is due largely to the systematic offset that is observed between $A_{T(\text{meas})}$ obtained via the DD method versus $A_{T(\text{meas})}$ obtained via the other measurement approaches (Fig. 4.3).

The single-step method produces ΔA_T values in the low- pK_{org} range that are mostly smaller than the closed-cell NLSF method (Fig. 4.5). This result is likely due to the relatively high pH (~ 4.20) at which the titration is terminated. This early termination limits the amount of low- pK organic matter that is titrated, thus limiting the amount detected in the calculation of $A_{T(\text{meas})}$.

4.6.2.2 Effect of dissolved organic content

Values of ΔA_T scale proportionally with dissolved organic content. This linear scaling has been described in previous studies using measurements of dissolved organic carbon concentration ([DOC]) (Kim and Lee, 2009; Koeve and Oschlies, 2012; Kuliński et al., 2014) and is confirmed by our modeling work using a range of ORG_T .

Fig. 4.6 shows ΔA_T values that increase linearly as a function of ORG_T (0 to 100 $\mu\text{mol kg}^{-1}$). The slope of each line is a function of measurement approach and pK_{org} . For example, with a pK_{org} of 6.0 (Fig 4.6b), each measurement approach produces a line with a slope very near to one. However, with a pK_{org} of 4.5 (Fig. 4.6a), the slopes vary widely by measurement approach and in some cases are much smaller than one.

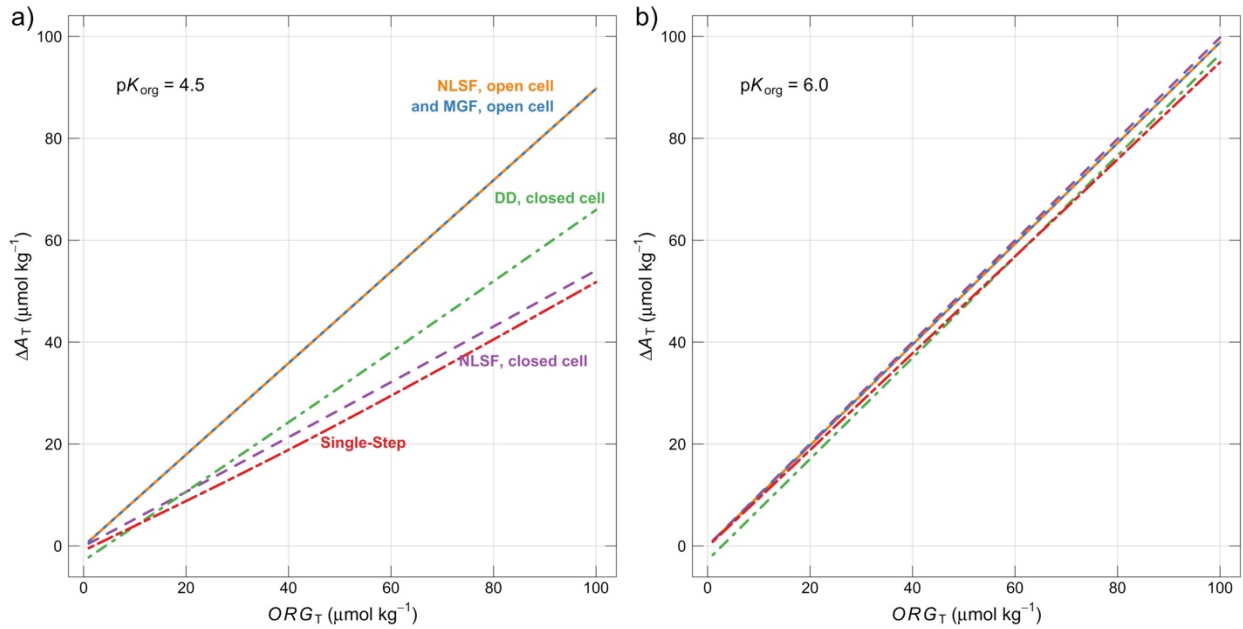


Fig. 4.6. Modeled differences between $A_{T(\text{meas})}$ and A_{inorg} as a function of total organic content ($ORG_T = 0$ to $100 \mu\text{mol kg}^{-1}$). The sample solutions are oxygenated seawater with $\text{pH}_T = 8.1$, $C_T = 2000 \mu\text{mol kg}^{-1}$, $P_T = 1.0 \mu\text{mol kg}^{-1}$, $Si_T = 15.0 \mu\text{mol kg}^{-1}$, $t = 25 \text{ }^\circ\text{C}$, $S = 35$, and $p = 1 \text{ atm}$. The results for two pK_{org} values are shown here: (a) $pK_{\text{org}} = 4.5$ and (b) $pK_{\text{org}} = 6.0$.

4.6.3 Implications of differing $A_{T(\text{meas})}$ results

Differences in the values of ΔA_T among various measurement approaches are significant because, as discussed in section 4.3.2, different approaches are used by different investigators across the oceanographic community to produce $A_{T(\text{meas})}$ values. However, in the presence of titratable organic molecules, the different approaches don't all generate identical values. Nevertheless, $A_{T(\text{meas})}$ values are treated identically once reported as A_T , and little consideration is given to the potential systematic uncertainties that might vary in magnitude as a function of measurement approach. Going a step further, small variations in how each measurement approach is applied (e.g., fitting an open-cell titration curve across the pH range of 3.7–3.2 rather than 3.5–3.0) can also produce differences in ΔA_T , and thus, differences in reported $A_{T(\text{meas})}$.

In the presence of low- pK organic acids (i.e., $pK_{\text{org}} < 6.0$), the difference between $A_{T(\text{meas})}$ and A_{inorg} is relatively small for the closed-cell titration and single-step methods compared to the multi-step open-cell titration methods (Figs. 4.4 and 4.5). This pK_{org} range is notable because low- pK carboxyl groups represent a significant portion of dissolved organic matter in natural waters (Hertkorn et al., 2006; Milne et al., 2001; Ritchie and Perdue, 2003; Tipping, 1998). Therefore, a good option for limiting systematic overestimates of A_{inorg} in organic-rich environments may be to employ either the closed-cell NLSF method or the single-step method. Alternatively, multi-step open-cell methods might benefit from evaluations at somewhat higher pH, which can obviate the unwanted influence of low- pK organics while maintaining a relatively simple chemical system. Overall, the potential benefits of modifying specific aspects of commonly employed titration methods or experimenting with new methods must be balanced against the advantages of current best practices.

For many applications, such as using A_T to detect the effects of ocean acidification on marine calcification (Ilyina et al., 2009; Carter et al., 2016), consistency in A_T measurements is most critical. Studies like these that rely on detecting small changes in A_T over time have been made possible by the distribution of CRMs (Dickson, 2010a) and the development of best practices (Dickson et al., 2007). For other applications, such as calculating air–sea CO_2 flux using A_T (e.g., Williams et al., 2017), accuracy in determining carbonate alkalinity from total alkalinity is most critical. In this case, carefully obviating or accounting for organic alkalinity may be more important than obtaining historically consistent results.

Finally, the ΔA_T values discussed in this paper assume perfect execution of an alkalinity titration with respect to sample preparation, measurement procedure, and data analysis. However, additional influences on measurement precision and accuracy outside of organic alkalinity should also be considered. For example, closed-cell titrations can suffer uncertainties related to volume calibration (which can introduce major errors in reported alkalinity) and the presence of bicarbonate (which makes equivalence point determinations less reliable) (Dickson et al., 2003). Though certain open-cell titration methods leave the door open for potential systematic errors introduced by titratable organics, they benefit from removal of bicarbonate and, sometimes, gravimetric sample measurement (Dickson et al., 2003).

4.6.4 Calculated carbonate system parameters in the presence of titratable organics

One of the more impactful consequences of titratable organic matter is its effect on carbonate system calculations performed using measured alkalinity as an input parameter (Hoppe et al., 2012; Ko et al., 2016; Koeve and Oschlies, 2012). Titratable organics have been shown to cause misinterpretations of alkalinity titrations when attempting to estimate A_{inorg} (see section

4.6.2). These misinterpretations propagate to carbonate system parameters calculated from erroneous A_{inorg} values, thus distorting subsequent calculations of air–sea CO_2 flux, degrees of CaCO_3 saturation, budgets and fluxes of inorganic carbon, and more. In other words, titratable organic matter can adversely influence interpretations of a wide array of biogeochemical data.

In the following sections, $\Delta X_{(A_T, Y)}$ refers to the difference between (a) parameter X calculated from $A_{\text{T(meas)}}$ and parameter Y (i.e., $X_{(A_T, Y)}$) versus (b) parameter X as defined by the model (i.e., $X_{(\text{model})}$), which can be thought of as a perfectly measured or perfectly calculated parameter X : $\Delta X_{(A_T, Y)} = X_{(A_T, Y)} - X_{(\text{model})}$.

Tables D1.4 and D1.5 provide comprehensive sets of errors (due exclusively to organic alkalinity) in carbonate system parameters calculated using different A_{T} -containing input pairs, measurement approaches, and ranges of $\text{p}K_{\text{org}}$ values (Table D1.4) and initial carbonate chemistries (Table D1.5). Subsections 4.6.4.1–4.6.4.3 provide illustrative figures and interpretations of these calculation errors.

Results are shown for calculations made at 25 °C and atmospheric pressure, but the interpretations generally hold true for calculations made at conditions relevant to in situ marine and estuarine environments. However, it is important to note that calculations of in situ parameters will still be in error without knowledge of the proton-exchange properties of all acid–base species in a sample, even if the input parameters are perfectly measured at laboratory conditions and even if neither of those measured parameters is A_{T} . This is because A_{T} is an intermediary step for all laboratory to in situ conversions. This subtlety, which can be easily overlooked, highlights the importance of developing accurate in situ measurement technologies (Byrne, 2014).

4.6.4.1 Calculated $p\text{CO}_2$

Fig. 4.7 shows $\Delta p\text{CO}_2(A_T, \text{pH}_T)$ and $\Delta p\text{CO}_2(A_T, C_T)$ (at 25 °C) as a function of $\text{p}K_{\text{org}}$ (2.5 to 9.5) for an ORG_T of $20 \mu\text{mol kg}^{-1}$ and the inorganic chemical conditions given in Table 4.4. Additional results for $\Delta p\text{CO}_2(A_T, Y)$ are given in Tables D1.4 and D1.5.

The results demonstrate patterns similar to those of the ΔA_T results (Fig. 4.4), with maximum $\Delta p\text{CO}_2(A_T, Y)$ values near the center of the $\text{p}K_{\text{org}}$ range and higher variability among measurement approaches in the low- $\text{p}K_{\text{org}}$ range. Differences in $\Delta p\text{CO}_2(A_T, C_T)$ between approaches can be as much as $15 \mu\text{atm}$ with an input of $ORG_T = 20 \mu\text{mol kg}^{-1}$.

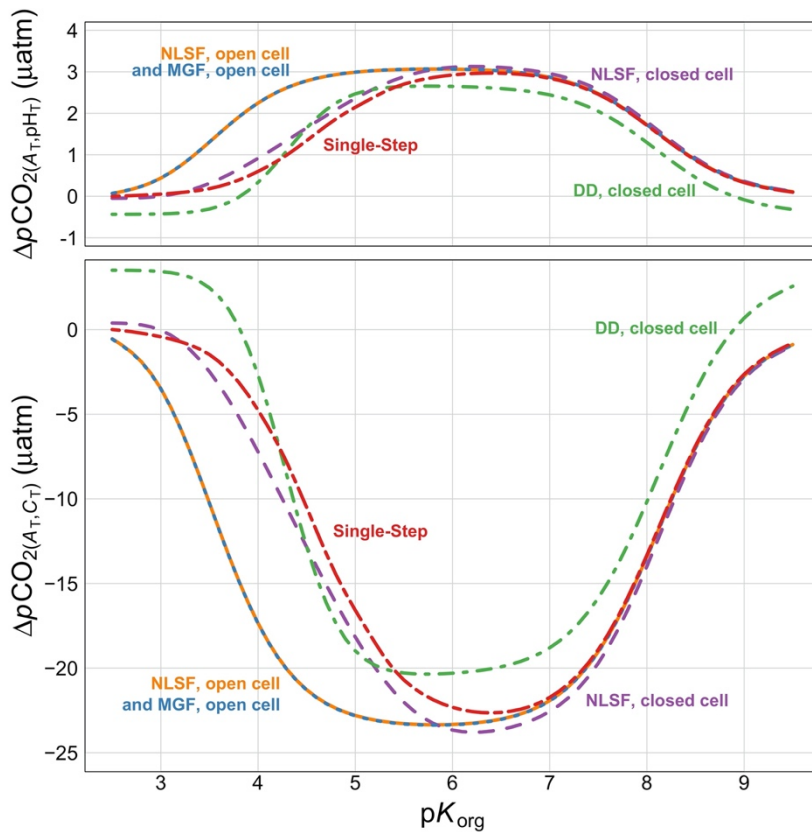


Fig. 4.7. Modeled difference between $p\text{CO}_2$ calculated from $A_{T(\text{meas})}$ paired with another parameter (pH_T or C_T) versus true $p\text{CO}_2(\text{model})$, as a function of $\text{p}K_{\text{org}}$ (2.5 to 9.5). The composition of the sample solution is identical to that used for Figs. 4.4 and 4.5. The scale of top panel is expanded by a factor of about 2.5 relative to the bottom panel.

Values of $\Delta p\text{CO}_2(A_T, \text{pH})$ are positive and relatively small, whereas values of $\Delta p\text{CO}_2(A_T, C_T)$ are negative and of greater magnitude. This difference is the result of the input-error sensitivity of the iterative process that uses A_T and C_T to determine pH, which is then used to calculate $p\text{CO}_2$ (Koeve and Oschlies, 2012). This difference in the magnitude of $p\text{CO}_2$ calculation errors arising from different input parameters in high-organic environments has been highlighted before (Kim and Lee, 2009; Hoppe et al., 2012; Koeve and Oschlies, 2012; Yang et al., 2015), and it has implications for the design of certain investigations — e.g., phytoplankton culture experiments or coastal/estuarine examinations of CO_2 flux.

Errors in $p\text{CO}_2$ consistent with those that can arise from calculations based on $A_{T(\text{meas})}$ in organic-influenced environments can predictably lead to CO_2 flux estimates that are significantly in error. However, the results displayed in Fig. 4.7 demonstrate that those errors can be partially mitigated by choosing to pair $A_{T(\text{meas})}$ with measured pH_T rather than C_T , and can be even further reduced in the presence of low- pK organics by choosing closed-cell titration approaches or the single-step approach rather than multi-step open-cell titrations.

4.6.4.2 Calculated pH_T

Values of $\Delta \text{pH}_T(A_T, Y)$ were calculated in a similar manner as $\Delta p\text{CO}_2(A_T, Y)$. To illustrate the effect of initial carbonate chemistry on the propagation of nonzero ΔA_T values to calculations of pH_T , Fig. 4.8 shows $\Delta \text{pH}_T(A_T, C_T)$ and $\Delta \text{pH}_T(A_T, p\text{CO}_2)$ (at 25 °C) as a function of initial pH_T ($\text{pH}_{T(\text{model})} = 7.2$ to 8.2) and corresponding C_T ($C_{T(\text{model})} = 2341$ to 1895 $\mu\text{mol kg}^{-1}$) with three fixed pK_{org} values. Inorganic chemical conditions besides pH_T and C_T are given in Table 4.4. The C_T range was determined by calculation with input pH_T values and a constant A_{inorg} of 2300 $\mu\text{mol kg}^{-1}$. Additional results for $\Delta \text{pH}_T(A_T, Y)$ are given in Tables D1.4 and D1.5.

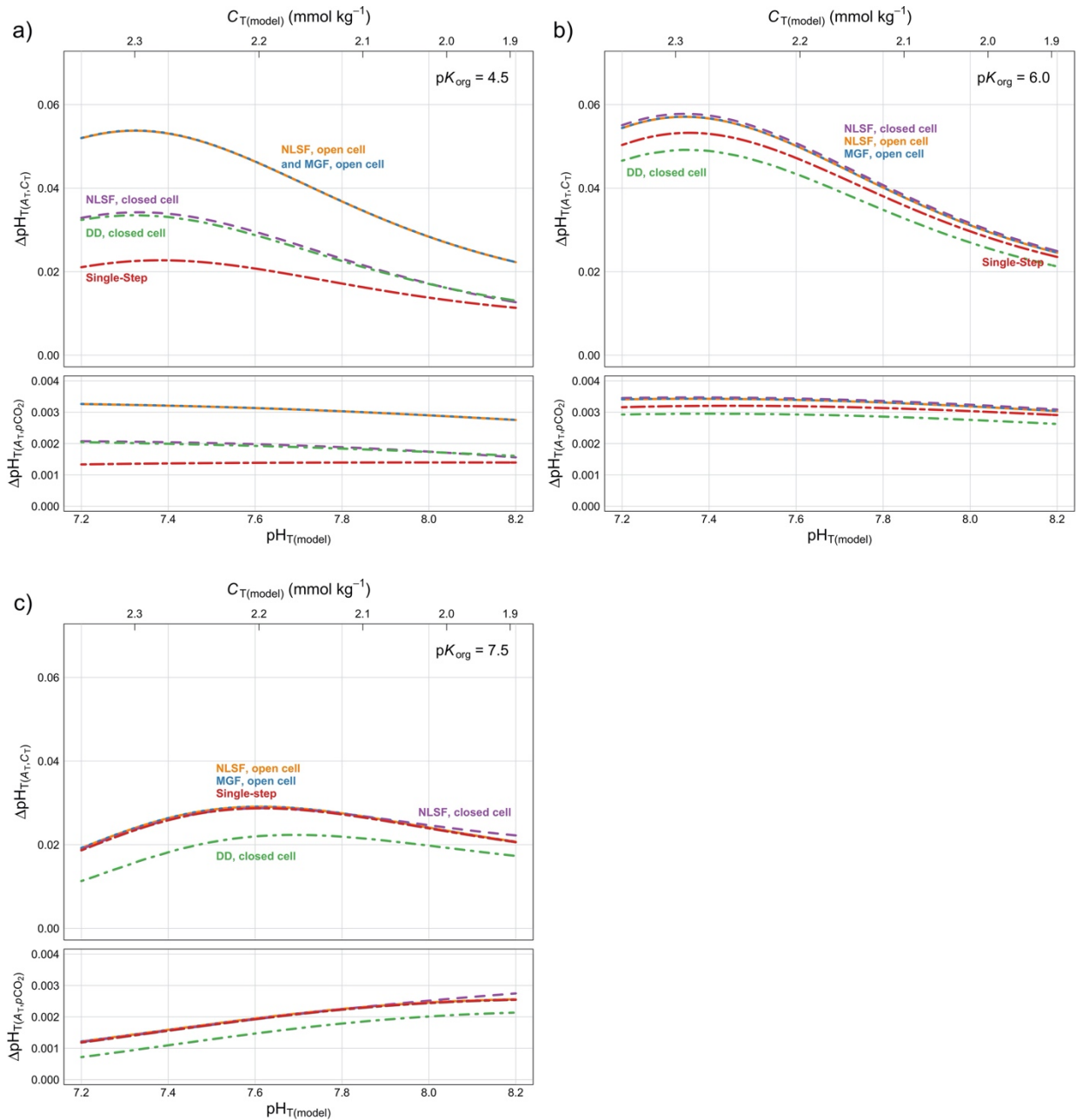


Fig. 4.8. Modeled differences between pH_T calculated from $A_T(\text{meas})$ and another parameter (C_T or $p\text{CO}_2$) versus true $\text{pH}_T(\text{model})$, as a function of $\text{pH}_T(\text{model})$ and $C_{T(\text{model})}$. The $C_{T(\text{model})}$ range was determined by calculation with $\text{pH}_T(\text{model})$ values and a constant A_{inorg} of $2300 \mu\text{mol kg}^{-1}$. The sample solutions are oxygenated seawater with $P_T = 1.0 \mu\text{mol kg}^{-1}$, $Si_T = 15.0 \mu\text{mol kg}^{-1}$, $t = 25^\circ\text{C}$, $S = 35$, $p = 1 \text{ atm}$, and $ORG_T = 20 \mu\text{mol kg}^{-1}$. The results for three $\text{p}K_{\text{org}}$ values are shown here: (a) $\text{p}K_{\text{org}} = 4.5$, (b) $\text{p}K_{\text{org}} = 6.0$, and (c) $\text{p}K_{\text{org}} = 7.5$. The scale of the bottom panel in each figure is expanded by a factor of about 7 relative to the top panel.

In this exercise, the effects of organic acids with pK values of 4.5, 6.0, and 7.5 were examined separately. The acid with a pK_{org} of 4.5 (Fig. 4.8a) can be viewed as a traditional carboxyl-type group, the acid with a pK_{org} of 6.0 (Fig. 4.8b) can be viewed as a more basic carboxyl-type group (Ritchie and Perdue, 2003; Tipping, 1998; Tipping and Hurley, 1992), and the acid with a pK_{org} of 7.5 (Fig. 4.8c) represents the bulk organic pK values (discussed more in section 4.6.5.1) determined from Baltic Sea data (Kuliński et al., 2014; Ulfsbo et al., 2015). Phenolic-type organics with higher pK values are not included because their high pK values result in minimal contribution to $A_{\text{T(meas)}}$.

Fig. 4.8 shows that $\Delta\text{pH}_{\text{T}(A_{\text{T}},C_{\text{T}})}$ values are consistently much larger than $\Delta\text{pH}_{\text{T}(A_{\text{T}},p\text{CO}_2)}$ values in the presence of titratable organics. This discrepancy between input parameter pairs is due to the aforementioned input-error sensitivity of the iterative procedure to determine pH from A_{T} and C_{T} .

In addition to differences in $\Delta\text{pH}_{\text{T}(A_{\text{T}},Y)}$ based on input parameter pair, different conditions (i.e., pK_{org} value and measurement approach) can produce subtly different patterns in $\Delta\text{pH}_{\text{T}(A_{\text{T}},Y)}$ as a function of $\text{pH}_{\text{T(model)}}$. With pK_{org} values of 4.5 and 6.0, ΔA_{T} values — which essentially amount to errors in input A_{T} for calculations of $\text{pH}_{\text{T}(A_{\text{T}},C_{\text{T}})}$ and $\text{pH}_{\text{T}(A_{\text{T}},p\text{CO}_2)}$ — are nearly constant regardless of $\text{pH}_{\text{T(model)}}$ for a given measurement approach (Table D1.3). However, the calculation to obtain pH_{T} from A_{T} and C_{T} exhibits greater sensitivity to ΔA_{T} at low pH_{T} . So, the slopes in $\Delta\text{pH}_{\text{T}(A_{\text{T}},C_{\text{T}})}$ as functions of $\text{pH}_{\text{T(model)}}$ in the top panels of Figs. 4.8a and 4.8b are mainly due to this calculation sensitivity rather than any pattern in ΔA_{T} as a function of $\text{pH}_{\text{T(model)}}$. The $\text{pH}_{\text{T}(A_{\text{T}},p\text{CO}_2)}$ calculation is more linearly influenced by ΔA_{T} , so the slopes in the bottom panels of Figs. 4.8a and 4.8b are close to zero. With a pK_{org} value of 7.5, ΔA_{T} values change as a function of $\text{pH}_{\text{T(model)}}$ for each measurement approach (Table D1.3); specifically, ΔA_{T} increases with higher initial pH_{T} . However, the $\text{pH}_{\text{T}(A_{\text{T}},C_{\text{T}})}$ calculation exhibits greater sensitivity to ΔA_{T} at low pH_{T} . So, the patterns

in $\Delta\text{pH}_{\text{T}(A_{\text{T}},C_{\text{T}})}$ values as functions of $\text{pH}_{\text{T}(\text{model})}$ in the top panel of Fig. 4.8c are results of these two dueling influences. The $\text{pH}_{\text{T}(A_{\text{T}},p\text{CO}_2)}$ calculation is more linearly influenced by ΔA_{T} , so the slopes in the bottom panel of Fig. 4.8c are modestly positive.

The slopes of $\Delta\text{pH}_{\text{T}(A_{\text{T}},C_{\text{T}})}$ versus $\text{pH}_{\text{T}(\text{model})}$ for all approaches except the single-step titration in Fig. 4.8a ($\text{p}K_{\text{org}} = 4.5$) and for all approaches in Fig. 4.8b ($\text{p}K_{\text{org}} = 6.0$) are between -0.022 and -0.034 . These slopes are similar, in terms of sign and magnitude, to those observed in analogous comparisons of pH_{T} measured spectrophotometrically versus pH_{T} calculated from open-ocean measurements of A_{T} and C_{T} (Carter et al., 2013; 2018; Fong and Dickson, 2019; Williams et al., 2017). This similarity is expected based on the sensitivity of the $\Delta\text{pH}_{\text{T}(A_{\text{T}},C_{\text{T}})}$ calculation, but emphasizes the possibility explored by Fong and Dickson (2019) that “excess alkalinity” (A_{X}) from organic bases could be a real complicating factor in internal consistency analyses of marine carbonate system measurements, even in the open ocean. This potential problem of open-ocean organic alkalinity is discussed in more detail in section 4.6.6.

4.6.4.3 Calculated Ω_{ca}

Calcite saturation state (Ω_{ca}) and aragonite saturation state (Ω_{ar}) are important parameters for modeling ocean geochemistry and for studying the physiology of ocean calcifiers. Here, values of $\Delta\Omega_{\text{ca}(A_{\text{T}},Y)}$ were calculated using the same input conditions as were used to calculate $\Delta\text{pH}_{\text{T}(A_{\text{T}},Y)}$. Fig. 4.9 shows $\Delta\Omega_{\text{ca}(A_{\text{T}},C_{\text{T}})}$, $\Delta\Omega_{\text{ca}(A_{\text{T}},\text{pH}_{\text{T}})}$, and $\Delta\Omega_{\text{ca}(A_{\text{T}},p\text{CO}_2)}$ as a function of $\Omega_{\text{ca}(\text{model})}$. Values of $\Delta\Omega_{\text{ca}(A_{\text{T}},Y)}$ are displayed as relative quantities (i.e., percentages of $\Omega_{\text{ca}(\text{model})}$) due to the large range of Ω_{ca} (~ 1 to 6.5). Additional results for $\Delta\Omega_{\text{ca}(A_{\text{T}},Y)}$ are given in Tables D1.4 and D1.5.

Similar calculations were performed for the case of aragonite. Relative $\Delta\Omega_{\text{ar}(A_T, Y)}$ values (not shown) display similar patterns to $\Delta\Omega_{\text{ca}(A_T, Y)}$. However, because aragonite is more soluble than calcite, the absolute values of $\Delta\Omega_{\text{ar}(A_T, Y)}$ are smaller in magnitude than those of $\Delta\Omega_{\text{ca}(A_T, Y)}$.

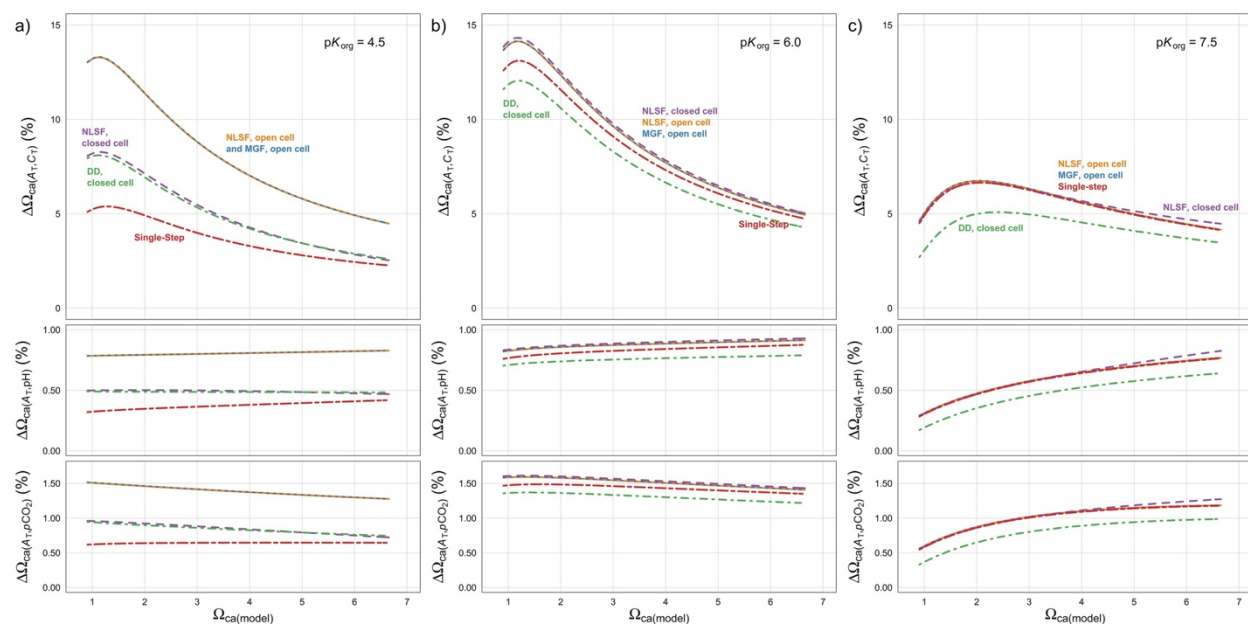


Fig. 4.9. Modeled relative differences between Ω_{ca} calculated from $A_T(\text{meas})$ and another parameter (C_T , pH_T , or $p\text{CO}_2$) versus $\Omega_{\text{ca}(\text{model})}$, as a function of $\Omega_{\text{ca}(\text{model})}$. The compositions of the sample solutions are identical to those used for Fig. 4.8. Three $\text{p}K_{\text{org}}$ values are modeled: (a) $\text{p}K_{\text{org}} = 4.5$, (b) $\text{p}K_{\text{org}} = 6.0$, and (c) $\text{p}K_{\text{org}} = 7.5$. In each figure, the scale of the panels is different.

Fig. 4.9 shows that $\Delta\Omega_{\text{ca}(A_T, C_T)}$ values are about an order of magnitude larger than both $\Delta\Omega_{\text{ca}(A_T, \text{pH})}$ and $\Delta\Omega_{\text{ca}(A_T, p\text{CO}_2)}$. These large differences, as in the case of calculated $p\text{CO}_2$, are a result of the input-error sensitivity of the iterative process that uses A_T and C_T to determine pH , which is used to calculate $[\text{CO}_3^{2-}]$ and, finally, Ω . The differences again highlight the troubling errors that can occur when using the A_T – C_T pair to perform carbonate system calculations for a marine system that contains titratable organics. The relative values of $\Delta\Omega_{\text{ca}(A_T, C_T)}$ can be particularly large at near-

saturation conditions (i.e., $\Omega \approx 1$). Like other calculated parameters, $\Delta\Omega_{\text{ca}(A_T, Y)}$ values are larger for multi-step open-cell methods when $\text{p}K_{\text{org}}$ is near 4.5.

Errors in calculated Ω , especially under near-saturation conditions, can bring about mischaracterizations of conceptually important geochemical benchmarks. Errors in Ω can lead to the misidentification of saturation horizon depths by hundreds of meters (Naviaux et al., 2019a; Patsavas et al., 2015b). Further, such errors can lead to misinterpretations of CaCO_3 dissolution data. These misinterpretations can encourage the proposal of dissolution suppressors or enhancers, such as soluble reactive phosphate (Berner and Morse, 1974; Walter and Burton, 1986), organic coatings (Honjo and Erez, 1978; Keir, 1980; Naviaux et al., 2019a; Subhas et al., 2018), or metabolic processes (Archer, 1991; Emerson and Bender, 1981; Hales, 2003), that may not be active or as significantly active as implied by the misinterpreted data. Accurate description of CaCO_3 dissolution behavior is critical in constructing ocean models to reliably predict changes in carbonate chemistry and carbon cycling that will occur in the future as ocean acidification progresses.

Orr et al. (2018) report similar uncertainties in Ω calculations for all input pairs except $\text{pH}_T\text{-pCO}_2$. These similarities are primarily due to the high degree of influence that solubility product uncertainty exerts on Ω uncertainty. So, most parameter pairs are equally adequate for calculating Ω in low-organic ocean environments. However, when titratable organics are likely present in solution, the $A_T\text{-}C_T$ pair especially should be avoided due to the high degree of Ω uncertainty that can result from that parameter pair (Fig. 4.9).

4.6.5 Practical methods of accounting for organic alkalinity

As the prevalence of organic alkalinity (A_{org}) in marine and estuarine settings has become more apparent, investigators have examined several different ways to parameterize or directly measure A_{org} . The following subsections review those methods, which are summarized in Table 4.5.

Table 4.5. Summary of methods that can be used to account for organic alkalinity.

| Method | Citations | Measurements needed | Pros | Cons |
|----------------------------|---|---|--|---|
| Empirical parameterization | Kuliński et al. (2014), Ulfsbo et al. (2015) | [DOC], two additional carbonate system parameters | Can be applied to a full dataset within a given region | Overdetermination of carbonate system necessary, only applicable when $A_{\text{org}} > \sim 8 \mu\text{mol kg}^{-1}$ |
| Proton-binding model | Koopal et al. (2005), Tipping et al. (2011) | [DOC] | Can be applied to a full dataset within a given region | Proton binding models are available only for freshwater organic matter |
| Secondary titration | Cai et al. (1998), Yang et al. (2015) | Back-titration with NaOH | Provides a direct measurement of excess alkalinity | Potential issues with incomplete removal of dissolved CO_2 and addition of excess CO_2 from NaOH |
| Advanced curve fitting | Asuero and Michałowski (2011), Michałowski and Asuero (2012) | None | No additional measurements needed | Not yet extensively tested or utilized in the marine chemistry community |

4.6.5.1 Parameterization using [DOC]

One way to estimate the effect of dissolved organics on alkalinity titrations is to use measurements of [DOC] paired with empirical characterizations of organic protonation behavior.

Kuliński et al. (2014), working in the organic-rich Baltic Sea, parameterized a bulk dissociation constant for dissolved organics in a given dataset (K_{DOM}), along with the fraction (f) of [DOC] that carries weakly acidic groups that are protonated during an alkalinity titration by using the equation:

$$K_{\text{DOM}} = \frac{[\text{H}^+]A_{\text{org}}}{(f \cdot [\text{DOC}] - A_{\text{org}})} \quad (4.18)$$

A_{org} values were determined by subtracting A_{inorg} calculated from pH_{T} and C_{T} from $A_{\text{T(meas)}}$ obtained by titration (i.e., $A_{\text{org}} = A_{\text{T(meas)}} - A_{\text{inorg}}$). Then, K_{DOM} and f were parameterized by a nonlinear least squares fit using Eq. (4.18) with estimates of A_{org} and measurements of $[\text{H}^+]$ and $[\text{DOC}]$.

It should be noted that, with an approach like this, all uncertainties in equilibrium constants and thermodynamic inconsistencies in carbonate system measurements are incorporated into the A_{org} term. Yang et al. (2015) calculated that A_{org} values determined based on differences between measured and calculated A_{T} could be reasonably attributed to an organic influence only if they were greater than about $8 \mu\text{mol kg}^{-1}$. The authors used this conclusion to advocate for direct measurements of organic alkalinity in coastal environments, with uncertainties much smaller than $8 \mu\text{mol kg}^{-1}$.

Another way to estimate the effect of dissolved organics on alkalinity titrations is to use a humic acid proton-binding model such as the Windermere Humic Aqueous Model (WHAM) (Tipping et al., 2011), which uses a continuous distribution of $\text{p}K$ values to represent the proton-exchange properties of humic substances. This can be useful in coastal waters or inland seas — like the Baltic — that are highly influenced by the input of terrestrial organics. Ulfso et al. (2015) obtained $\text{p}K_{\text{DOM}}$ and f values for a corrected version of the Kuliński et al. (2014) Baltic sea dataset;

they compared their f value ($f=0.12$) to that which would be predicted by WHAM ($f=0.125$), and obtained impressive agreement.

Whether using bulk K_{DOM} values or a humic acid model like WHAM to account for organic alkalinity, the results are necessarily informed by ancillary measurements of [DOC] and overdeterminations of the carbonate system. Though these ancillary measurements add complexity to alkalinity analyses, they also provide more realistic representations of acid–base behavior (by including a term for organics in the A_{T} equation) and can reduce errors in carbonate system calculations (by allowing more accurate estimates of A_{inorg}). Methods like these should be tested more extensively in a wide array of marine and estuarine environments to assess the universality or regionality of certain bulk pK_{DOM} values and organic acid proton-binding models.

4.6.5.2 Secondary titrations

A more rigorous option for assessing organic alkalinity on a sample-by-sample basis is to augment traditional alkalinity titrations with secondary titrations after removal of dissolved CO_2 . Secondary titrations were used by many of the references in Table 4.3 to estimate the pK values of natural organics.

As an example, Yang et al. (2015) described a fast spectrophotometric secondary titration procedure that builds upon the open-cell single-step titration approach of measuring A_{T} . After the initial open-cell alkalinity titration and removal of CO_2 , NaOH is added to raise sample pH. Then a secondary acidimetric titration is performed using bromocresol purple as an indicator (to cover pH 6–4.5). This process is then repeated using cresol red as an indicator for the secondary titration (to cover pH 8–6). These secondary titrations provide an explicit measurement of A_{org} , which can then be subtracted from $A_{\text{T(meas)}}$ (obtained from the initial titration) to determine A_{inorg} . This method

benefits from the precision offered by spectrophotometric pH indicators; it is also relatively fast and does not require a separate [DOC] measurement.

The work of Yang et al. (2015) provides a valuable framework for the continued development of alkalinity titration procedures that explicitly account for organic influence. Consistency in titration procedure and data analysis methodology is important here. The initial acidimetric titration should be terminated at a pH that provides a reliable measurement of A_T (e.g., pH = 4.20) and is able to be repeated with precision so that the same organic functional groups are titrated during each A_{org} measurement.

4.6.5.3 Novel curve-fitting methods

Novel titration curve-fitting methods should also be explored as a way to incorporate organics into A_T determinations. Asuero and Michałowski (2011) and Michałowski and Asuero (2012) have described computational procedures flexible enough to analyze titration curves for complex systems such as natural waters. Unlike traditional alkalinity titration data analysis methods that pre-suppose a particular acid–base model, these curve-fitting methods emphasize the description of constituents with undefined compositions and proton-exchange properties (e.g., fulvic acids).

4.6.6 Organic alkalinity in the open ocean?

It has generally been postulated that titratable dissolved organics have little to no effect on $A_{T(\text{meas})}$ values obtained from open-ocean alkalinity titrations. However, consider typical open ocean surface DOC concentrations (Hansell et al., 2009) of about 70–80 $\mu\text{mol kg}^{-1}$. If, as in Ulfsbo et al. (2015), it is assumed that this DOC is composed entirely of WHAM fulvic acid, then we can

use $f = 0.125$ as an estimate of the fraction of weakly acidic groups of DOC that will be protonated across the pH range of an alkalinity titration. Multiplying $70\text{--}80 \mu\text{mol kg}^{-1}$ of DOC by 0.125 results in about $8.8\text{--}10.0 \mu\text{mol kg}^{-1}$ of titratable organic matter in open ocean surface waters. Assigning this organic matter a functional pK of 7.34 (Ulfsbo et al., 2015) results in up to about $8.5 \mu\text{mol kg}^{-1}$ of measured excess alkalinity.

Admittedly, the assumption that all marine DOC consists of WHAM terrestrial fulvic acid is an oversimplification (Tipping et al., 1991). Additionally, the pH distribution of fulvic acid ionizable sites would be somewhat different for open ocean seawater ($S \approx 35$, $C_T \approx 2000$) than for the Baltic Sea water ($S = 6.15$, $C_T = 1470$) studied by Ulfsbo et al. (2015). Still, many of the fundamental molecular structures in terrestrially-derived organics also occur in marine dissolved organic matter (e.g., Arakawa et al., 2017), and terrestrial organic matter can be transported to the deep ocean by ocean circulation (Medeiros et al., 2016). Further, phytoplankton culture studies have shown that autochthonous marine dissolved organic molecules do contain ionizable sites, some of which participate in proton exchange across the range of a typical alkalinity titration. Kim and Lee (2009), for example, demonstrated a species-specific relationship between ΔA_T and [DOC] in marine phytoplankton cultures; Ko et al. (2016) assigned numerical pK values to DOC produced by marine phytoplankton (see Table 4.3). The slopes reported by these authors for ΔA_T –[DOC] relationships actually suggest much larger f values than predicted by the WHAM model, so it is reasonable to expect dissolved organics to influence alkalinity titrations, even in open ocean waters.

This expectation is supported by evidence from carbonate system internal consistency analyses. Repeatedly observed disagreements between certain measured and calculated parameters can be remedied by the introduction of excess alkalinity terms, and many authors have suggested

organics as a source of this excess. Millero et al. (2002) assumed some amount of excess alkalinity on two WOCE Pacific Ocean cruises to bring measured versus calculated CO_2 fugacity values into agreement. Patsavas et al. (2015b) subtracted 0.18% ($\sim 4 \mu\text{mol kg}^{-1}$) of measured A_T from shelf samples ($S \leq 35$) on two coastal ocean cruises to bring measured versus calculated A_T values into agreement. Fong and Dickson (2019) subtracted between 3.5 and 6.6 $\mu\text{mol kg}^{-1}$ from measured A_T values on four separate GO-SHIP cruises to bring measured versus calculated pH_T values into agreement.

Realistic representations of excess alkalinity from organics would not, however, be wholesale corrections to datasets, but would include protonation characteristics (i.e., $\text{p}K_{\text{org}}$ values) and concentrations that vary with location, depth, and time. Hertkorn et al. (2013) emphasized the change in dissolved organic matter composition as a function of depth in the ocean; specifically, they showed that the fraction of carboxylic acids in the dissolved organic matter pool increases with depth. This or any other change in composition would influence the way the dissolved organics in a sample respond to an alkalinity titration, thus changing the appropriate value of A_X .

To account for likely spatial variations in A_X values, studies can be undertaken to constrain the protonation characteristics of the dissolved organic matter pool in different ocean regions. Perhaps future GO-SHIP cruises could incorporate back-titrations for a subset of A_T measurements to investigate these characteristics. Alternatively, alkalinity anomalies could be paired with [DOC] data to infer organic protonation characteristics. Acquisition of these data would surely be a substantial undertaking, but would allow for future evaluations of marine A_T with realistic representations of organic alkalinity — including geographic- and depth-dependent estimates of $\text{p}K$ values. This more complete thermodynamic model of seawater acid–base behavior should help

to resolve inconsistencies between measured and calculated pH values (see section 4.6.4.2), along with other carbonate system parameters.

4.7 Conclusions

Most modern alkalinity titration data analysis methods that are used throughout the marine chemistry community produce $A_{T(\text{meas})}$ values that accurately describe A_T (and A_{inorg}) when performed on carefully collected titration data from systems where alkalinity is controlled exclusively by inorganic chemical species (i.e., where $A_T = A_{\text{inorg}}$; Fig. 4.3). However, when titratable organics with pK values between about 2.5 and 9.5 are present in solution (Fig. 4.4), potentially significant differences (ΔA_T) between reported $A_{T(\text{meas})}$ and A_{inorg} occur, no matter the data analysis method. Those differences are largest for organic molecules with pK values between about 5 and 7.

When low- pK titratable organics (i.e., $2.5 < pK_{\text{org}} < 6.0$) are present, quantitative differences occur among the ΔA_T values resulting from the five A_T measurement approaches studied in this work (Figs. 4.4 and 4.5). The largest ΔA_T values in this low- pK_{org} range are associated with multi-step open-cell titrations that are analyzed by either MGFs or NLSFs. These low- pK results are especially important because a common class of organic functional groups found in natural waters — carboxyl groups — exhibit pK values in this problematic range. If alkalinity measurements are being made in a system expected to have a high concentration of low- pK organics and accurate A_{inorg} values are critical for a research goal, this outsized influence on multi-step open-cell titrations should be kept in mind. If, however, consistency in alkalinity titration results over time is critical, the current A_T measurement practices should certainly be retained.

Non-zero values of ΔA_T can lead to significant systematic errors in carbonate system parameters calculated from $A_{T(\text{meas})}$ in organic-influenced environments (i.e., when $A_{T(\text{meas})}$ is presumed equal to A_{inorg}). These errors, like values of ΔA_T , exhibit differences among measurement methods, especially in the presence of low- pK titratable organics. Errors in calculated $p\text{CO}_2$ (Fig. 4.7), pH_T (Fig. 4.8), and Ω (Fig 4.9) incurred by incorrectly equating $A_{T(\text{meas})}$ with A_{inorg} are each significantly greater for the A_T - C_T input pair than for any other input pair. Errors in calculated $p\text{CO}_2$ can yield air-sea CO_2 flux estimates with particularly large errors (either too low a CO_2 flux out of the ocean or too great a CO_2 flux in). Errors in calculated pH_T may contribute to the internal inconsistencies often observed in over-determined marine carbonate system datasets. Errors in calculated Ω are often greatest in terms of percentages under conditions of near-saturation and may therefore skew efforts to identify saturation horizon depths and interpret CaCO_3 dissolution data.

An important point to emphasize is that when organic acids with $\text{p}K_{\text{org}}$ values near the *ZLP* ($\text{p}K_A^0 = 4.5$) are present, $A_{T(\text{meas})}$ becomes an ambiguous representation of A_T . Dickson's (1981) cutoff between proton acceptors and donors was designed to describe alkalinity associated with inorganic chemical species that have the following properties in natural waters: (1) all have well-defined and discrete $\text{p}K_A^0$ values and (2) none have a $\text{p}K_A^0$ value close to 4.5. Organic functional groups found in natural waters, however, do not exhibit these properties. Instead, they (1) exhibit a continuous spectrum of $\text{p}K_A^0$ values and (2) appear to be characterized by a major functional class that exhibits dissociation behavior very near $\text{p}K_A^0 = 4.5$ (carboxyl groups). This functional behavior of dissolved organics results in ambiguity as to how to treat them in the context of defining and measuring A_T .

Several characteristics of organics in natural waters suggest that the way total alkalinity is measured, particularly in coastal and estuarine environments, should be re-evaluated: the ubiquity

and heterogeneity of titratable organics, the inability of traditional alkalinity titration methods to obviate the influence of organics on carbonate system calculations, and the ambiguity of $A_{T(\text{meas})}$ values in the presence of low- pK organics. Section 4.6.5 suggests some practices that can be implemented to account for organic alkalinity. In implementing any changes, a major focus should be on optimizing new or revised analytical procedures for precision, accuracy, simplicity, and speed, while keeping in mind the continuous spectrum of pK values displayed by natural dissolved organic matter.

Finally, it must be recognized that the organic alkalinity problem may exist not only in coastal areas but the open ocean as well. Overall, recent indications of significant contributions by organic matter to alkalinity titrations in a wide array of environments should motivate a critical evaluation of how A_T is determined in marine and estuarine waters around the globe.

4.8 Acknowledgements

Support for J.D. Sharp was provided by the National Science Foundation (NSF) Graduate Research Fellowship Program, Award #1144244, and by the William and Elsie Knight Endowed Fellowship for Marine Science from the University of South Florida College of Marine Science. This project was also supported by NSF Award #1658321. We thank Tonya Clayton for her insightful comments and editorial assistance. We are also thankful for the helpful comments of three anonymous reviewers.

CHAPTER FIVE:

EXCESS ALKALINITY IN CARBONATE SYSTEM REFERENCE MATERIALS

Note: This chapter is currently in revision for Marine Chemistry:

Sharp, J.D., Byrne, R.H. Technical note: Excess alkalinity in carbonate system reference materials. In revision for *Marine Chemistry*.

5.1 Abstract

Certified reference materials (CRMs) for oceanic carbonate system measurements are critical for verifying the accuracy of laboratory protocols and the reliability of field sensors. CRMs are certified for total alkalinity and dissolved inorganic carbon, parameters that are (1) stable for a long period of time when a sample is properly stored and (2) not affected by changes in temperature and pressure. In experimentation initially designed to measure the total boron to salinity ratio of seawater, an interesting result has emerged regarding CRMs. A unique acidimetric titration method has shown that three different batches of CRM contain excess alkalinity (i.e., alkalinity that is not attributable to inorganic bases included in the traditional definition of seawater total alkalinity) that is statistically greater than the excess alkalinity measured in open-ocean water from the Gulf of Mexico. Further, the amount of excess alkalinity appears to differ in certain CRM batches. Excess alkalinity in CRMs is likely caused by organic proton acceptors that are not completely oxidized by the ultraviolet sterilization procedure that CRMs undergo. The primary use of CRMs — to maintain the accuracy and consistency of carbonate system measurements — may be

inhibited by excess alkalinity, which can cause differences in total alkalinity values determined by different titration methods. Excess alkalinity also invalidates the assumptions applied to CO₂ system calculations, and so would produce incorrect values of CO₂ system parameters calculated from certified total alkalinity and dissolved inorganic carbon values of CRMs. Finally, excess alkalinity analyses highlight the marine chemistry community's urgent need for a universally agreed upon total boron to salinity ratio.

5.2 Introduction

The changes in ocean chemistry that have been induced by an influx of carbon dioxide (CO₂) to the ocean–atmosphere system from fossil fuel burning and land use change (Friedlingstein et al., 2019) have been well-documented (Caldeira and Wickett, 2003; Feely et al., 2004; Orr et al., 2005). The total amount of dissolved inorganic carbon in the ocean is increasing, causing an increase in hydrogen ion concentration (i.e., ocean acidification), a decrease in carbonate ion concentration, and myriad associated effects on marine organisms.

Chemical changes to the ocean are monitored in part by measuring parameters of the marine carbonate system. These parameters include total alkalinity (A_T), total dissolved inorganic carbon (C_T), the negative logarithm of the hydrogen ion concentration (pH), and the fugacity of CO₂ (f_{CO_2}). Standard operating procedures (SOPs) have been detailed for measurement of each of these parameters (Dickson et al., 2007).

Seawater A_T is defined as the total moles of hydrogen ions equal to the excess of proton acceptors over proton donors in one kilogram of seawater (Dickson, 1981). Proton acceptors are defined as bases formed from weak acids with a pK^0 greater than 4.5, whereas proton donors are

defined as weak acids with a pK^0 less than 4.5. Seawater A_T is typically described by the following equation (Dickson, 1981; Wolf-Gladrow et al., 2007):

$$A_T = [\text{HCO}_3^-] + 2[\text{CO}_3^{2-}] + [\text{B}(\text{OH})_4^-] + [\text{OH}^-] + [\text{HPO}_4^{2-}] + 2[\text{PO}_4^{3-}] + [\text{SiO}(\text{OH})_3^-] + [\text{HS}^-] + 2[\text{S}^{2-}] + [\text{NH}_3^0] + \dots - [\text{H}^+]_f - [\text{HSO}_4^-] - [\text{HF}^0] - [\text{H}_3\text{PO}_4^0] - \dots \quad (5.1)$$

where brackets represent total ion concentrations and subscript f denotes the free H^+ concentration. The ellipses represent additional proton acceptors and donors that are not explicitly included in the equation.

Seawater C_T is simply the total moles of dissolved inorganic carbon in one kilogram of seawater, described by:

$$C_T = [\text{CO}_2^*] + [\text{HCO}_3^-] + [\text{CO}_3^{2-}] \quad (5.2)$$

where brackets again represent total ion concentrations and $[\text{CO}_2^*]$ is equal to the sum of dissolved CO_2 and carbonic acid: $[\text{CO}_2^*] = [\text{CO}_{2(\text{aq})}] + [\text{H}_2\text{CO}_3^0]$.

Those two parameters — A_T and C_T — are invariant with changes in temperature and pressure when defined in terms of moles per kilogram of seawater, and can be preserved in a sample for a long period of time if properly stored. Because of this behavior, certified reference materials (CRMs) with verified values of A_T and C_T have been produced for the last three decades (Dickson, 2010) at Scripps Institution of Oceanography (SIO).

CRMs are prepared from natural seawater collected off the coast of Southern California (Dickson, 2010). That seawater is filtered, sterilized with ultraviolet radiation, poisoned with a saturated solution of mercuric chloride (HgCl_2) to suppress biological activity, collected into clean borosilicate bottles, and certified for A_T and C_T . Each bottle is sealed with a glass stopper, Apiezon® L grease, and a tightly applied rubber band. Along with detailed SOPs, CRMs have

been instrumental in improving consistency in A_T and C_T measurements over time and between different research groups (Bockmon and Dickson, 2015; Dickson, 2010; Olsen et al., 2019).

In an effort to characterize the ratio of total boron to salinity in seawater (r_B), we designed a novel acidimetric titration approach. This work was motivated by the fact that the two values of r_B most commonly used by the marine chemistry community (Uppström, 1974; Lee et al., 2010) — which were both determined using curcumin-based methods (Uppström, 1968; Liu and Lee, 2009) — differ by about 4%. Our goal was to obtain an independent measure of r_B using a method unrelated to the curcumin method.

For this purpose, seawater from the surface Gulf of Mexico (GoM) was collected and three different batches of CRM were acquired (batch 172, 176, and 183). Titrations were performed in near-absence of CO_2 using coulometrically standardized HCl (Dickson et al., 2003). Each titration was initiated from a pH as near as possible to the negative logarithm of the boric acid dissociation constant ($\text{p}K_B$) of the sample. At this condition, borate concentration ($[\text{B}(\text{OH})_4^-]$) is equal to half the total boron concentration (B_T).

As a result of these titrations, excess alkalinity was noted in most samples when employing either the Uppström (1974) or Lee et al. (2010) r_B to account for borate alkalinity. “Excess alkalinity” refers to an alkalinity contribution that is not attributable to inorganic bases included in the traditional definition of seawater total alkalinity (i.e., from Dickson, 1981). Excess alkalinity values were greater for the CRMs than for the GoM seawater, and appeared to differ between certain CRM batches.

We interpret excess alkalinity to be most probably associated with unidentified dissolved organic bases that bind protons during the course of a titration (e.g., Brewer et al., 1986; Bradshaw and Brewer, 1988; Cai et al., 1998; Hernandez-Ayón et al., 1999; 2007; Kim and Lee, 2009; Yang

et al., 2015), and that persist despite the ultraviolet irradiation step of CRM preparation. However, the analyses detailed here provide no definitive connection between excess alkalinity values and any dissolved organic bases, so we maintain the “excess alkalinity” terminology throughout this note.

Excess alkalinity (A_X) invalidates typically assumed relationships between A_T and other carbonate system parameters, potentially contributing to thermodynamic inconsistency in marine carbonate system datasets (e.g., Fong and Dickson 2019). The prevalence of A_X in CRMs has been suspected (Andrew Dickson, personal communication), but not robustly demonstrated until now. A_X in CRMs has the potential to cause errors in both CRM-based quality control of A_T measurements and CRM-based derivations of CO₂ system parameters (e.g., pH, f_{CO_2} , etc.).

5.3 Methods

5.3.1 Pre-treatment of samples

Seawater from an SIO CRM or the surface GoM was collected into a 1 L bottle, then acidified with 1 M HCl to a pH between about 3.0 and 3.5. This acidified seawater was purged of CO₂ for ~1 hour using a stream of ultra-high purity N₂ passed through a column of Ascarite II CO₂ absorbent (Thomas Scientific). Ancillary experimentation indicated that this process raises sample salinity by 0.039 ± 0.016 ($n = 9$). This salinity increase was accounted for in calculations and the standard deviation accounted for in the uncertainty analysis (section 2.6). After bubbling with N₂, the bottle was sealed tightly using a cap with integrated valves for gas input and solution output.

Headspace pressure was applied with N₂ to force about 150 mL of seawater into an open-top glass cell that was placed in a cell holder thermostatted to 18 °C and positioned within the light path of an Agilent 8453 UV-visible spectrophotometer. The temperature of 18 °C was chosen as a

practical compromise between stability of temperature control in a room-temperature laboratory and limitation of the uncertainty contribution from the dissociation constant of water (K_w), which is lower at lower temperatures. Submerged in the sample were a custom-built plastic stirrer, a temperature probe, and a glass ROSS™ combination pH electrode (model 8102BN, Orion™) connected to a pH meter (model 720A, Orion™). An atmosphere of high-purity N_2 was maintained over the cell; the atmosphere was confirmed to be CO_2 -free using a LI-7000 CO_2/H_2O Analyzer (LI-COR Biosciences).

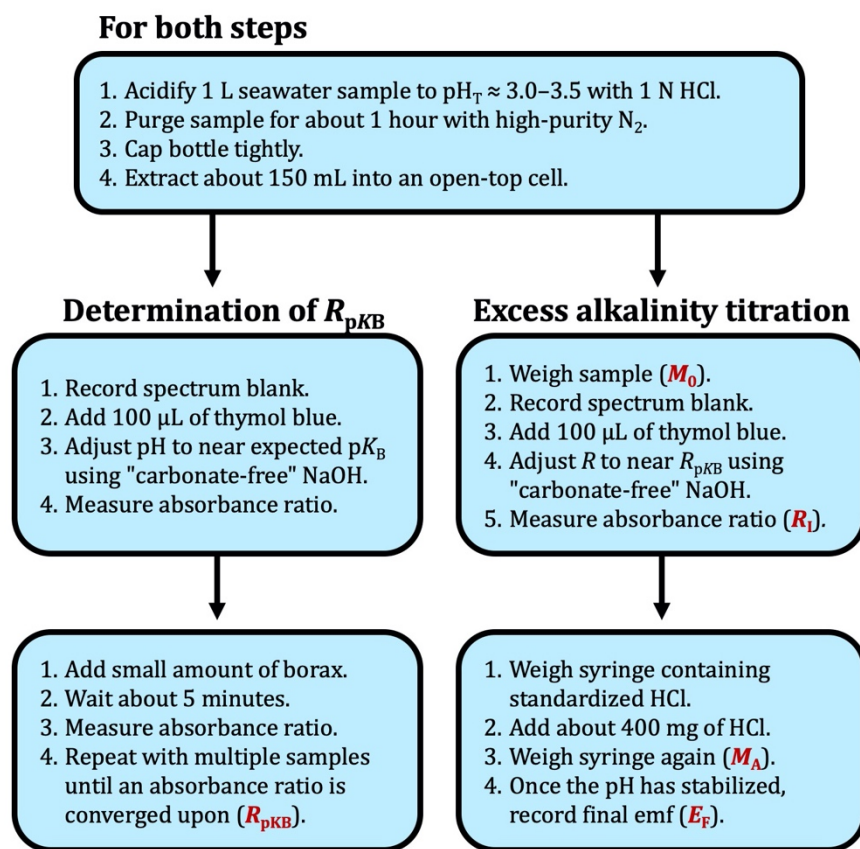


Figure 5.1. The two steps of the experimental procedure are detailed here. Important measured quantities are bold and red in color.

The method then proceeded in two steps, which were repeated a number of times for each seawater sample. Fig. 5.1 provides an overview of the measurement procedure, which is described in detail in the following paragraphs.

5.3.2 Identification of R_{pK_B}

The first step of the experimental procedure involved identifying the absorbance ratio of a pH indicator dye that corresponded to the apparent dissociation constant of boric acid (pK_B) for each sample at 18 °C (Fig. 5.1). We used thymol blue (TB; Zhang and Byrne, 1996) due to its optimal indicating range of approximately $7.5 < pH_T < 8.9$. Absorbance ratios (R) for TB are determined by:

$$R = (A_{596} - A_{750}) / (A_{435} - A_{750}) \quad (5.3)$$

where A_n is absorbance measured at wavelength n . pH_T is calculated via an equation of the form:

$$pH_T = \log\{K_2 e_2\} + \log\{(R - e_1) / (1 - R \cdot e_3 / e_2)\} \quad (5.4)$$

where K_2 is the dissociation constant of the HI^- form of the indicator dye and e_x terms are molar absorption ratios defined as follows (Zhang and Byrne, 1996):

$$e_1 = \frac{596 \epsilon_{HI}}{435 \epsilon_{HI}} \quad (5.5a)$$

$$e_2 = \frac{596 \epsilon_I}{435 \epsilon_{HI}} \quad (5.5b)$$

$$e_3 = \frac{435 \epsilon_I}{435 \epsilon_{HI}} \quad (5.5c)$$

where $\lambda \epsilon_k$ is the molar absorbance coefficient of species k at wavelength λ .

Though a purification process for TB has been developed (Hudson-Heck and Byrne, 2019), we used unpurified dye for this work. The congruence between pK_2 values of TB determined using purified versus unpurified TB (Hudson-Heck and Byrne, 2019) and determined by different investigators using unpurified TB obtained from different vendors (Mosley et al., 2004) indicates

that the effect of impurities on pH_T measured with TB is small. Further, our uncertainty analysis suggests that quantitative inaccuracy in measurements of initial pH_T is not a significant uncertainty contributor to our results (see section 3).

A spectrophotometer blank was taken before adding 100 μL of 10 mM TB to the seawater. Then, “carbonate-free” NaOH (1 M) was added to adjust the seawater pH to near the $\text{p}K_B$ value. “Carbonate-free” NaOH was prepared by treating NaOH with $\text{CaO}_{(s)}$ in a sealed bottle to precipitate calcium carbonate (Sipos et al., 2000), then allowing particles to settle for 48–72 hours. Using a 50 μL gastight syringe (Hamilton Company), NaOH was extracted from the center of the bottle to avoid contamination from particles.

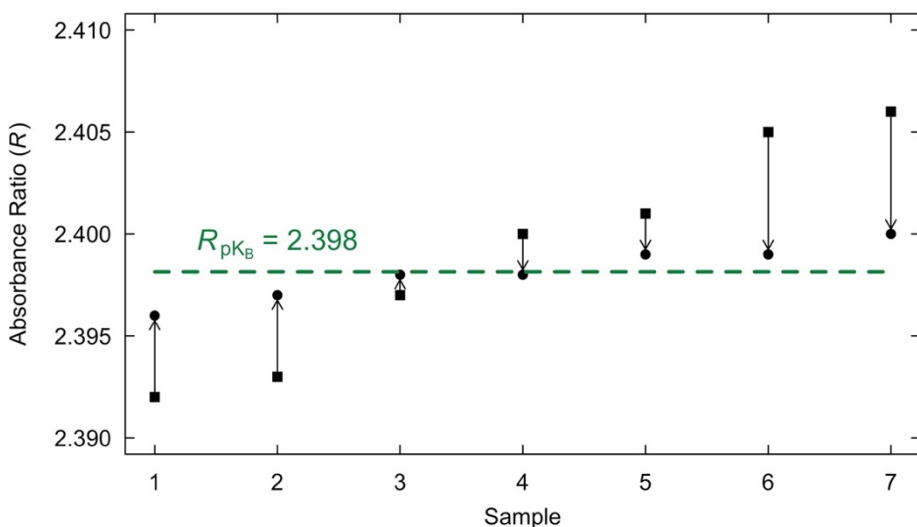


Figure 5.2. Identification of a sample’s absorbance ratio corresponding to its $\text{p}K_B$ value ($R_{\text{p}K_B}$). The squares represent R after an initial pH adjustment with “carbonate-free” NaOH, the arrows ending at the circles represent the changes in R upon addition of borax, and the dotted line represents the $R_{\text{p}K_B}$.

Finally, sodium borate decahydrate ($\text{Na}_2\text{B}_4\text{O}_7 \cdot 10\text{H}_2\text{O}$; borax) was added to the seawater, forming boric acid ($\text{B}(\text{OH})_3^0$) and borate ($\text{B}(\text{OH})_4^-$), thus causing the pH of the seawater to trend

toward the pK_B . Five absorbance spectra were taken before and after addition of borax for calculation of R (Eq. (5.3)). This process was repeated with several subsamples from the 1 L bottle to achieve convergence toward the absorbance ratio at which the pH of the sample was equal to its pK_B (i.e., R_{pK_B}). Fig. 5.2 demonstrates the logic behind this first step.

5.3.3 Excess alkalinity titration

The second step of the experimental procedure involved acidimetric titration starting from $pH = pK_B$ (Fig. 5.1). This step was designed to measure borate alkalinity for easy calculation of B_T . However, early results indicated persistent excess alkalinity, suggesting that isolation of borate alkalinity alone would be impossible. So, the titration starting point (i.e., $pH = pK_B$) instead allowed measurement of the magnitude of borate alkalinity plus any other excess alkalinity source.

Seawater was weighed upon addition to the open-top cell. Again, a spectrophotometer blank was taken before adding 100 μL of 10mM TB to the seawater. Then, “carbonate-free” NaOH (1 M) was added to adjust the seawater absorbance ratio as near as possible to R_{pK_B} . An initial absorbance ratio (R_I) was measured, along with the electromotive force (emf) at initial conditions (E_I), both for calculation of initial pH_T (pH_I). Finally, certified HCl titrant (Dickson et al., 2003) with a concentration of 0.100362 mol kg^{-1} (± 0.000009 mol kg^{-1} ; Batch A17) was used to titrate the seawater to a pH between about 4.4 and 5.0. The emf measured via glass pH electrode after titration was recorded (E_F) for calculation of final pH_T (pH_F). This process was repeated with several subsamples from each 1 L bottle.

5.3.4 Calculations of borate alkalinity and excess alkalinity

Combined equilibrium borate alkalinity (A_B) and excess alkalinity (A_X) were calculated by:

$$A_{B+X} = A_B + A_X = A_T - A_C - A_m \quad (5.6)$$

where A_{B+X} is the combination of equilibrium borate alkalinity and excess alkalinity, A_T is the total alkalinity determined from each titration, A_C is the carbonate alkalinity, and A_m is the alkalinity contributed by “minor components” such as nutrients and the hydroxide ion. The distinction of A_B as “equilibrium” borate alkalinity means A_B is equal to $[B(OH)_4^-]$ at $pH = pK_B$. This treatment allows for direct comparison of salinity-normalized A_{B+X} values between different samples, the advantages of which are discussed later. Carbonate alkalinity (A_C) was minimized by purging CO_2 from acidified samples using high-purity N_2 (section 2.1).

The full derivation of Eq. (5.6) is given in Appendix E1; the A_T , A_C , and A_m terms are summarized below. In each of the following equations, total solute concentrations for calculations of individual species were either estimated from salinity (F_T , B_T) or from direct measurements (P_T , Si_T , C_T).

Total alkalinity, A_T , is determined by:

$$A_T = \frac{(M_A C_A - M_T ([H^+]_F + [HF^0]_F - [HCO_3^-]_F - [HPO_4^{2-}]_F - [B(OH)_4^-]_F - [OH^-]_F + [H_3PO_4^0]_F))}{M_0} \quad (5.7)$$

where M_0 is the initial sample mass, M_A is the added acid mass, M_T is equal to M_0 plus M_A , C_A is the acid concentration, and $[x]_F$ represents the final concentration of species x at the titration endpoint. Species with concentrations less than 1 nmol kg^{-1} at the titration endpoint (e.g., $[CO_3^{2-}]$ and $[PO_4^{3-}]$) are treated as negligible.

Values of $[x]_F$ were calculated from pH_F , which was determined using E_F and the equation:

$$pH_T = (E - E_0)/(RT \cdot \ln(10)/F) \quad (5.8)$$

where E is the measured emf, E_0 is the electrode intercept potential, R is the ideal gas constant, T is temperature in Kelvin, and F is the Faraday constant.

Glass electrodes used to measure emf were periodically confirmed to give a Nernstian response by titration of 0.7 M NaCl with HCl. Once the expected response was confirmed, the ideal Nernstian slope ($RT \cdot \ln(10)/F$) was used. One-point calibrations were performed prior to each seawater titration using the pH_T measurement provided by thymol blue, similar to the one-point mCP calibrations discussed by Easley et al. (2012). The electrode intercept potential (E_0) was adjusted slightly so that pH_I measured using Eq. (5.4) with R_I and using Eq. (5.8) with E_I were identical.

Alkalinity contributed by bicarbonate and carbonate, A_C , is determined by:

$$A_C = [\text{HCO}_3^-]_I + 2[\text{CO}_3^{2-}]_I = \frac{C_T K_1 ([\text{H}^+]_I + 2K_2)}{[\text{H}^+]_I^2 + K_1 [\text{H}^+]_I + K_1 K_2} \quad (5.9)$$

where C_T is experimentally estimated (see section 2.5). Alkalinity contributed by minor components, A_m , is determined by:

$$A_m = [\text{OH}^-]_I + 2[\text{PO}_4^{3-}]_I + [\text{HPO}_4^{2-}]_I + [\text{SiO}(\text{OH})_3^-]_I - [\text{H}^+]_I + [\text{B}(\text{OH})_4^-]_{ex} \quad (5.10)$$

In Eqs. (5.9) and (5.10), $[x]_I$ represents the initial concentration of species x at the start of the titration. Species with concentrations less than 1 nmol kg^{-1} at the initial pH (e.g., $[\text{HF}^0]$ and $[\text{H}_3\text{PO}_4^0]$) are treated as negligible. Values of $[x]_I$ were calculated from pH_I , determined via thymol blue absorbance ratios (Eqs. (5.3–5.5)).

$[\text{B}(\text{OH})_4^-]_{ex}$ is a measure of the degree to which the initial borate concentration ($[\text{B}(\text{OH})_4^-]_I$) was greater than (+) or less than (–) the borate equilibrium value ($[\text{B}(\text{OH})_4^-]_{eq}$) at the start of the titration:

$$[\text{B}(\text{OH})_4^-]_{ex} = [\text{B}(\text{OH})_4^-]_I - [\text{B}(\text{OH})_4^-]_{eq} = B_T / (1 + \frac{[\text{H}^+]_I}{K_B}) - B_T / 2 \quad (5.11)$$

$[\text{B}(\text{OH})_4^-]_{ex}$ was calculated using an average of B_T estimated from Uppström (1974) and from Lee et al. (2010) and was generally between -2.0 and $+2.0 \mu\text{mol kg}^{-1}$. Including $[\text{B}(\text{OH})_4^-]_{ex}$ in the A_m term allows for A_{B+X} values to be directly compared between samples with identical salinity, and salinity-normalized A_{B+X} values to be directly compared between any two samples.

Because $\text{pH} = \text{p}K_B$ was independently determined, uncertainty in the salinity- and temperature-based characterization of $\text{p}K_B$ (Dickson, 1990) was circumvented. Further, any minor changes to $\text{p}K_B$ induced by interactions between boric acid and bicarbonate (McElligott and Byrne, 1998; Mojica-Prieto and Millero, 2002) or boric acid and dissolved organics (Mackin, 1986) would also be accounted for by this method.

To obtain excess alkalinity (A_X), the A_B component had to be subtracted from A_{B+X} (Eq. (5.6)). The A_B component was determined using both the r_B ratio of Uppström (1974) and of Lee et al. (2010).

5.3.5 C_T measurements

To account for residual dissolved CO_2 , a custom-built gas extraction system coupled to a Picarro G5131-*I* cavity ringdown spectrometer for CO_2 quantification was used to measure the C_T of the N_2 -purged seawater samples ($C_{T(\text{samp.})}$) and the NaOH titrant solution ($C_{T(\text{NaOH})}$). The system has demonstrated good precision for seawater C_T measurements made in our laboratory, comparable to that of a coulometer ($\pm 0.1\%$; X. Liu, unpublished data). For the purposes of this study (i.e., C_T measurements of nearly CO_2 -free samples), the standard deviations between duplicate samples given in Table E2.3 can provide some idea of the system's precision ($\pm 0.15 \mu\text{mol kg}^{-1}$).

For measurements of the seawater samples, N₂ headspace pressure was applied after purging to force ~230 mL of solution into a glass BOD bottle under an N₂ atmosphere. For measurements of the NaOH solution, Milli-Q water was heated and bubbled with high-purity N₂ as it cooled to remove dissolved CO₂. Then, N₂ headspace pressure was applied to force ~230 mL of Milli-Q water into a glass BOD bottle under an N₂ atmosphere. To half of the Milli-Q-filled flasks, 150 µL of “carbonate-free” NaOH was added, whereas half consisted of CO₂-purged Milli-Q water only. All bottles were rapidly sealed with greased glass stoppers.

Each sample was acidified and the evolved CO₂ run through a Picarro G5131-*I* cavity ringdown spectrometer to measure C_T. The average C_{T(samp.)} was used as an estimate for residual C_T in each sample after purging. The difference between the C_T of NaOH-spiked Milli-Q and pure Milli-Q was used to determine the added C_{T(NaOH)} per µL of “carbonate-free” NaOH. The repeatability of these C_T measurements was accounted for in the uncertainty analysis.

5.3.6 Uncertainty analysis

A detailed uncertainty analysis was performed to assign a standard uncertainty to the A_X results. This was done by propagating standard uncertainties in measured values ($u(x_n)$) using a Gaussian approach (Ellison and Williams, 2012):

$$u_c^2(A_X) = \left(\frac{\delta(A_X)}{\delta x_1}\right)^2 u^2(x_1) + \dots + \left(\frac{\delta(A_X)}{\delta x_n}\right)^2 u^2(x_n) \quad (5.12)$$

Uncertainty in r_B was not included in this analysis, and is instead addressed by directly comparing A_X values determined via the Uppström (1974) r_B versus the Lee et al. (2010) r_B .

Non-parametric pairwise analysis of variance (ANOVA) tests were used to assess differences between the mean A_X values of sample types. The FATHOM toolbox for MATLAB® was used for these analyses (Jones, 2017). To test significance, p values were determined by a

permutation test ($n = 10,000$) and corrected for multiple comparisons using Holm's correction (Holm, 1979).

The statistical test was first run directly on measured A_X values. Then, in a Monte Carlo error analysis, simulated uncertainty was added to each measurement of A_X using a normal distribution centered around zero with a standard deviation equal to $u_c(A_X)$. The non-parametric pairwise ANOVA was run 10,000 times with this added uncertainty, and resulting p values were interpreted.

5.4 Results

Table 5.1 shows the properties of each measured sample, including the R_{pK_B} values determined by the methodological step described in section 2.2. Full titration data are given in Table E2.1 of Appendix E2, and a summary of results is given in Table E2.2.

Table 5.1. Properties of different measured seawater samples. Salinity before purging with N_2 (S), total phosphate concentration (P_T), total silicate concentration (Si_T), and absorbance ratio at $pH = pK_B$ (R_{pK_B}) are provided for each.

| Sample Type | S | P_T | Si_T | R_{pK_B} |
|-------------|--------|-------|--------|------------|
| Surface GoM | 36.286 | 0.21 | 1.7 | 2.311 |
| CRM 172 | 33.450 | 0.42 | 2.8 | 2.386 |
| CRM 176 | 33.532 | 0.29 | 1.7 | 2.365 |
| CRM 183 | 33.420 | 0.35 | 2.1 | 2.372 |

Fig 5.3. shows $C_{T(\text{samp.})}$ measurements that were made on purged seawater samples (Table E2.3), most of which were below $4.0 \mu\text{mol kg}^{-1}$ ($1.7 \pm 1.9 \mu\text{mol kg}^{-1}$, $n = 12$). For the NaOH titrant, pairs of NaOH-spiked Milli-Q water and pure Milli-Q water gave a carbonate content of

5.7 ± 1.7 nanomoles C_T per μL titrant ($n = 6$, Table E2.4). This value was used with the amount of NaOH added to each sample in μL to estimate the added $C_{T(\text{NaOH})}$ in $\mu\text{mol kg}^{-1}$ (e.g., 100 μL NaOH added to 150 grams of seawater adds $3.8 \pm 1.3 \mu\text{mol kg}^{-1} C_T$).

Added $C_{T(\text{NaOH})}$ was used with the average $C_{T(\text{samp.})}$ to represent the total C_T present in titrated samples during calculations of A_X . This resulted in about 5.0–7.0 $\mu\text{mol kg}^{-1} C_T$ per sample. The standard deviations of both $C_{T(\text{samp.})}$ and $C_{T(\text{NaOH})}$ measurements were used to represent standard input uncertainties for the uncertainty analysis.

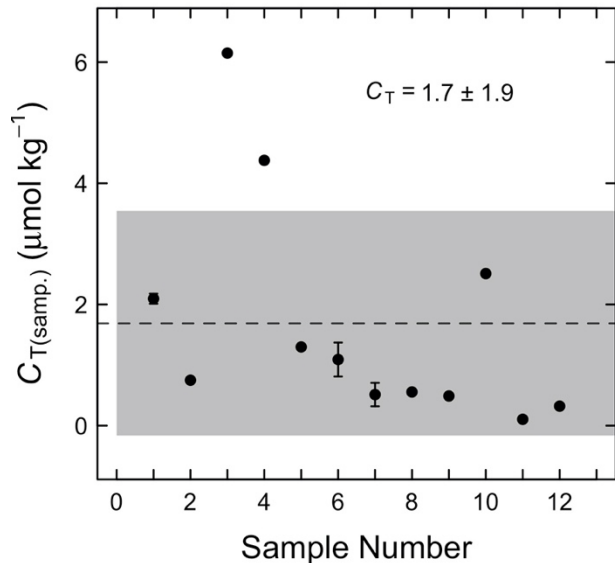


Figure 5.3. Dissolved inorganic carbon ($C_{T(\text{samp.})}$) in seawater samples that had been purged for ~ 1 hour with high-purity N_2 gas. Measurements are displayed in the order of analysis. The dashed line and grey rectangle represent the mean and standard deviation of the measurements, respectively. Data points that represent duplicate measurements include error bars representing the standard deviation of the two measurements.

Salinity-normalized values of A_{B+X} (nA_{B+X}) are shown in Fig. 5.4. These were determined according to Eq. (5.6), and normalized to $S = 35$ to account for salinity-dependent differences in total boron concentrations between the samples. This normalization allows nA_{B+X} to be directly compared between samples. However, normalizing the entire A_{B+X} quantity misleadingly implies

that A_X , like A_B , is proportional to salinity. Also, because nA_{B+X} values are representative of $\text{pH} = \text{p}K_B$, the A_B component is much larger than it would be for a sample at its natural pH .

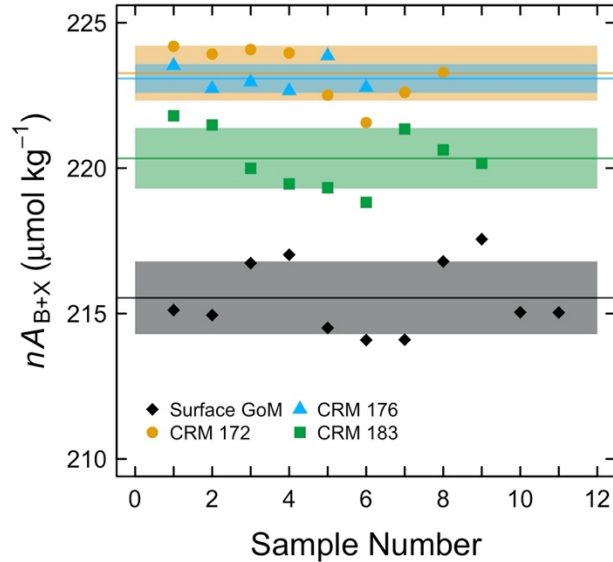


Figure 5.4. Salinity-normalized values of A_{B+X} (nA_{B+X}) for surface GoM seawater, CRM 172, CRM 176, and CRM 183. The colored lines and rectangles represent the means and standard deviations for each sample type.

To isolate A_X , two different total boron to salinity ratios were applied to account for A_B . Fig. 5.5 shows A_X determined using the r_B of both Uppström (1974) and Lee et al. (2010). Because the Lee et al. ratio ($0.1336 \text{ mg kg}^{-1} \text{ ‰}^{-1}$; $B_T = 432.6 \text{ } \mu\text{mol kg}^{-1}$ at $S = 35$) is larger than the Uppström ratio ($0.1284 \text{ mg kg}^{-1} \text{ ‰}^{-1}$; $B_T = 415.8 \text{ } \mu\text{mol kg}^{-1}$ at $S = 35$), A_B makes up a greater proportion of A_{B+X} when calculated using the Lee et al. ratio. For this reason, A_X values calculated using Lee et al. ratio are smaller than those calculated using the Uppström ratio.

Combined standard uncertainty in A_X ($u_c(A_X)$) was estimated by propagating input uncertainties for a model sample titration. Table 5.2 shows the main input parameters that contribute to A_X uncertainty. Uncertainty in r_B was not considered because we explicitly discuss differences caused by using either the Uppström (1974) or Lee et al. (2010) ratio.

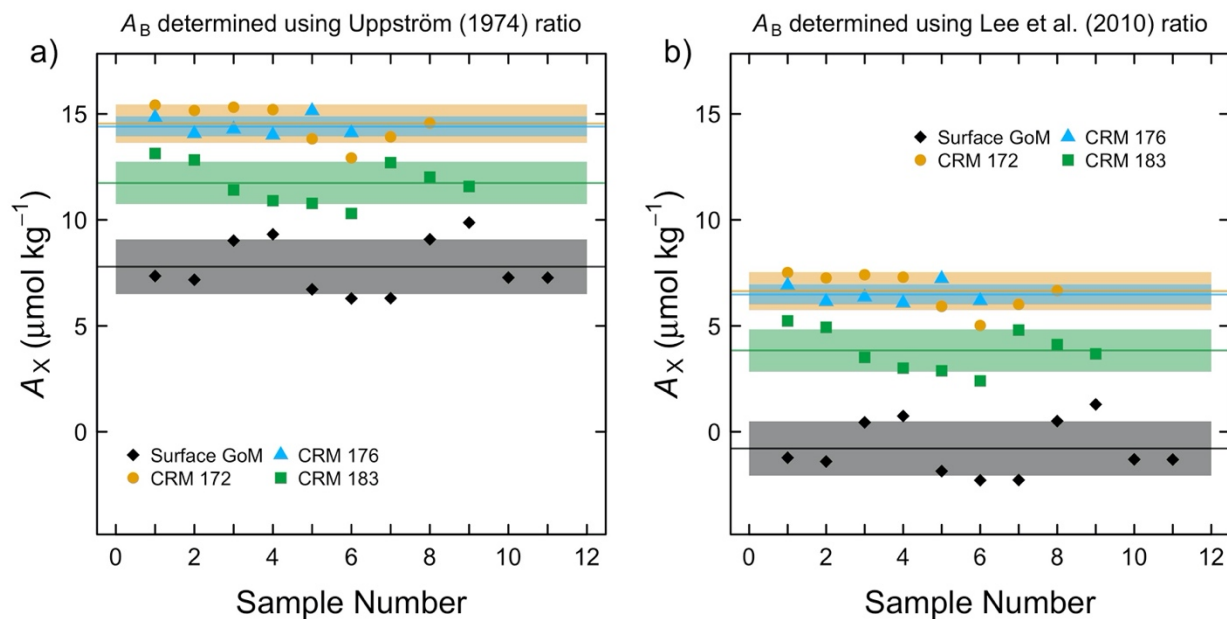


Figure 5.5. Values of A_X determined by applying (a) the total boron to salinity ratio of Uppström (1974) and (b) Lee et al. (2010). The colored lines and rectangles represent the means and standard deviations for each sample type.

The most important input uncertainties are associated with residual C_T after purging ($C_{T(\text{samp.})}$) and carbonate added with the NaOH titrant ($C_{T(\text{NaOH})}$). These uncertainties were estimated as the standard deviations of repeated C_T measurements (Tables E2.3 and E2.4).

Uncertainty in final pH_T was estimated at 0.01 based on the rather conservative estimate of “total uncertainty” in pH given by Orr et al. (2018). This is a somewhat important contributor; however, its influence is lessened by the high pH at which the titration is terminated. The relatively high pH ($\text{pH}_T \approx 4.4\text{--}5.0$) limits the excess acid term to about $10\text{--}40 \mu\text{mol kg}^{-1}$.

Uncertainty in R_{pKB} was estimated from repetitions of the process for identifying R_{pKB} , which is detailed in section 2.2. Uncertainty in R_{pKB} influences estimates of excess borate ($[\text{B}(\text{OH})_4^-]_{\text{ex}}$) at the titration starting point.

The uncertainty contribution from pK_W was taken from the estimate of Orr et al. (2018).

This uncertainty is influenced by the temperature at which the titration is completed; for example,

$(\delta(A_X)/\delta x)^2 \cdot u^2(x)$ changes from $0.12 \mu\text{mol}^2 \text{kg}^{-2}$ at $18 \text{ }^\circ\text{C}$ to $0.30 \mu\text{mol}^2 \text{kg}^{-2}$ at $25 \text{ }^\circ\text{C}$.

Table 5.2. Uncertainties in input parameters for the calculation of A_X and their propagation to combined standard uncertainty in A_X in $\mu\text{mol kg}^{-1}$; calculated using Eq. (5.12). These were determined using a model titration of seawater with $S = 35$, $t = 18 \text{ }^\circ\text{C}$, $M_0 = 150 \text{ g}$, and $M_A = 400 \text{ mg}$.

| Parameter (x) | x (approx.) | $u(x)$ | $\delta(A_X)/\delta x$ | $(\delta(A_X)/\delta x)^2 \cdot u^2(x)$ | $u(A_X)$ ($\mu\text{mol kg}^{-1}$) |
|--|---------------|--------|------------------------|---|--------------------------------------|
| $C_{T(\text{samp.})}$ (μmol) | 1.7 | 1.9 | 1.2 | 5.2 | 1.8 |
| $C_{T(\text{NaOH})}$ (nmol) | 5.7 | 1.7 | 0.8 | 1.9 | 0.7 |
| pH_F | 4.622 | 0.010 | -56.8 | 0.3 | 0.1 |
| R_{pK_B} | 2.410 | 0.010 | -51.7 | 0.3 | 0.1 |
| $\text{p}K_{W(18 \text{ }^\circ\text{C})}$ | 13.50 | 0.01 | -34.4 | 0.1 | 0.0 |
| M_A (g) | 0.4000 | 0.0005 | -668.0 | 0.1 | 0.0 |
| $u_c(A_X)$ ($\mu\text{mol kg}^{-1}$) | | | | | 2.8 |

Uncertainties in other input parameters were considered and used in the calculation of $u_c(A_X)$, but are not listed here as their contributions were quite small. A comprehensive accounting of uncertainties as well as rationale for input uncertainty estimates is given in Table E2.5.

Uncertainty in M_A was estimated as 5 times the resolution of the balance used for M_A measurements. Uncertainty in M_A is the smallest contributor listed here, partly due to the relative precision with which M_A can be measured.

Pairwise ANOVA tests conducted on directly measured A_X values for each sample type indicated a significant difference between each group ($p = .001$), except for CRM 172 versus CRM 176 (Table 5.3). (To account for multiple comparisons, p values were corrected using Holm's correction (Holm, 1979).)

Table 5.3. Results of non-parametric pairwise ANOVA tests. Tests were performed on A_X values calculated using both the Uppström (1974) and Lee et al. (2010) r_B . All comparisons besides CRM 172 versus CRM 176 showed significant differences ($p = .001$) in measured A_X . With 10,000 simulations of uncertainty on A_X measurements, only comparisons of GoM versus CRM samples showed significant differences ($p < .05$) in more than 55% of simulations.

| Comparison | A_X from Uppström (1974) | | A_X from Lee et al. (2010) | |
|-----------------|----------------------------|-------------------------------------|------------------------------|-------------------------------------|
| | p value (no uncert.) | Percent $p < .05$ (with uncert.) | p value (no uncert.) | Percent $p < .05$ (with uncert.) |
| GoM vs. CRM 172 | .001 | 96.2% | .001 | 98.6% |
| GoM vs. CRM 176 | .001 | 90.5% | .001 | 95.8% |
| GoM vs. CRM 183 | .001 | 56.8% | .001 | 74.9% |
| CRM 172 vs. CRM | .745 | 1.5% | .709 | 1.6% |
| CRM 172 vs. CRM | .001 | 22.9% | .001 | 24.0% |
| CRM 176 vs. CRM | .001 | 17.7% | .001 | 18.5% |

When simulated uncertainty based on the $u_c(A_X)$ estimate ($2.8 \mu\text{mol kg}^{-1}$; Table 5.2) was added to measured A_X values for the Monte Carlo error analysis, pairwise ANOVA tests indicated significant p values (i.e., $p < .05$) for more than 55% of simulations for all comparisons of CRMs to GoM seawater, and for more than 90% of simulations for comparisons of CRM 172 and CRM 176 to GoM seawater (Table 5.3). However, comparisons among CRM groups were not consistently significant at a level of $\alpha = .05$ when simulated uncertainty was considered.

5.5 Discussion

5.5.1 Excess alkalinity in CRMs

Our results indicate a small alkalinity excess in CRMs that is greater than the alkalinity excess found in GoM seawater ($p = .001$) by between 3.9 and $7.4 \mu\text{mol kg}^{-1}$ (Fig. 5.5; Table E2.2). This alkalinity excess may vary to a small degree between CRM batches, despite the fact that the

p values are not consistently significant (at a level of $\alpha = .05$) when uncertainty is simulated (Table 5.3).

Though the absolute values of A_X in each sample type are somewhat uncertain due to factors like the residual C_T estimate and the choice of r_B , the difference between A_X in the CRMs versus the GoM seawater is repeatable and robust. This demonstrates that, even if A_X in the GoM seawater is not detectable (Fig. 5.5b), A_X is present at detectable concentrations ($\sim 4\text{--}7 \mu\text{mol kg}^{-1}$) in the CRMs. Further, if A_X in the GoM seawater is greater than zero (Fig. 5.5a), A_X is present at even greater concentrations ($\sim 12\text{--}15 \mu\text{mol kg}^{-1}$) in the CRMs.

The excess alkalinity values presented here are not exactly equivalent to those that would appear in standard alkalinity titrations. That is because our titrations were initiated from $\text{pH} = \text{p}K_B$ ($\text{pH}_T \approx 8.6\text{--}8.7$) and terminated at $\text{pH}_T \approx 4.4\text{--}5.0$; typical alkalinity titrations are initiated from natural seawater pH ($\text{pH}_T \approx 7.2\text{--}8.2$) and terminated at $\text{pH}_T \approx 3.0\text{--}4.2$, depending on the method of titration. Knowledge of the dissociation behavior of the organic acids contributing to excess alkalinity would be necessary to translate A_X values obtained using the method detailed here to those that would be detected in a standard alkalinity titration.

5.5.2 Effect of A_X on CRM-based quality control of TA

The primary purpose of CRMs is to ensure historical and inter-laboratory consistency in A_T measurements. To achieve this goal, an A_T value that matches the certified value must be attainable for repeat measurements of a given CRM batch within an acceptable uncertainty range (e.g., $\pm 2 \mu\text{mol kg}^{-1}$). As long as any A_X component remains fairly constant over time (as it should in HgCl_2 -poisoned samples) there should be little to no differences between A_T values obtained

during the CRM certification process and A_T values obtained during a given laboratory's quality control measures.

However, an assumption of the previous paragraph is that A_T must be determined exactly according to (or very similarly to) the titration protocol employed during the certification of A_T . This procedural similarity will ensure that the same amount of any excess proton acceptor is titrated during both A_T determinations. Potential differences in A_T values obtained via different titration methods in the presence of excess proton acceptors are explored by Sharp and Byrne (2020). Fig. 5.6 shows an example of how those methodology-based differences might manifest for A_T measurements of a CRM with an excess alkalinity contributor ($X_T = 8 \mu\text{mol kg}^{-1}$) across a range of dissociation constant values ($\text{p}K_X$).

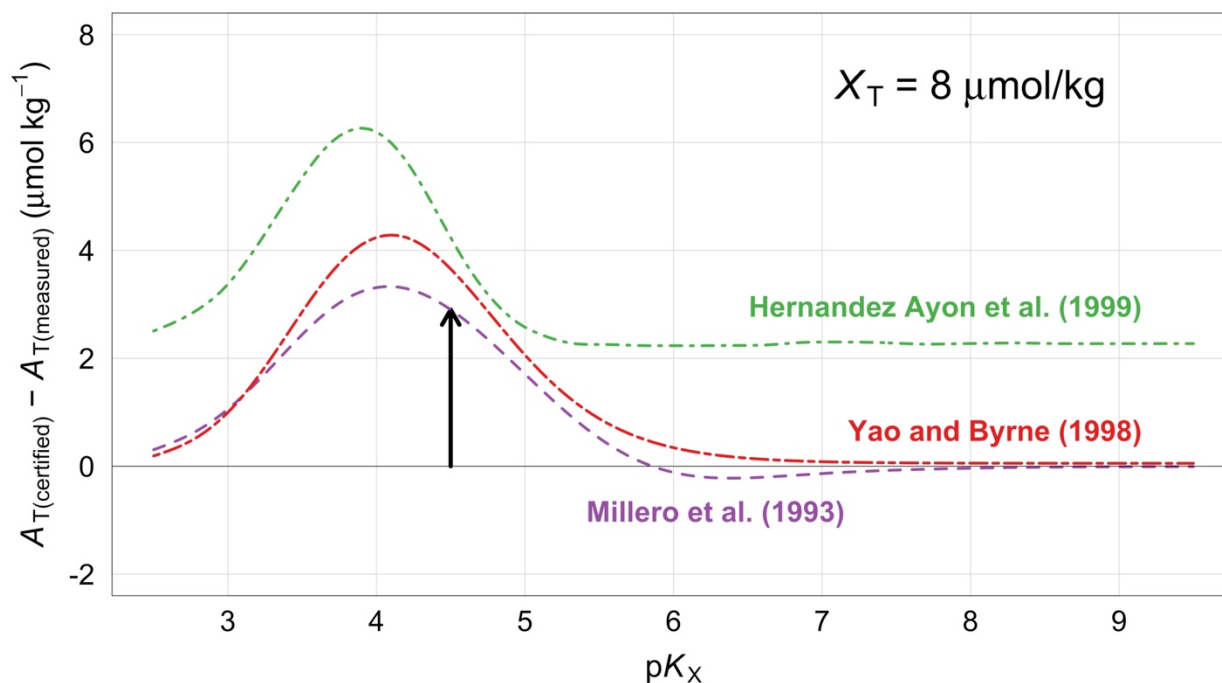


Figure 5.6. Hypothetical differences between certified A_T values versus A_T values measured by closed-cell titrations (e.g., Millero et al., 1993), a fixed endpoint method (e.g., Yao and Byrne, 1998), and a difference derivative approach (e.g., Hernandez-Ayón et al., 1999). Values are determined using the model of Sharp and Byrne (2020), and solution characteristics are as follows: $S = 33.5$, $C_T = 2050.0$, $\text{pH}_T = 7.82$, $t = 20.0 \text{ }^\circ\text{C}$, $P_T = 0.5$, $S_{i_T} = 2.0$.

As an example, consider a CRM with a certified A_T of $2199.0 \mu\text{mol kg}^{-1}$ ($S = 33.5$, $C_T = 2050.0$, $\text{pH}_T = 7.82$, $t = 20.0 \text{ }^\circ\text{C}$, $P_T = 0.5$, $Si_T = 2.0$), and imagine that CRM contains a dissolved organic acid with a total concentration of $8 \mu\text{mol kg}^{-1}$ and a $\text{p}K = 4.5$. Because CRMs are certified using an open-cell titration with data analysis performed via nonlinear fit (Dickson et al., 2003), the organic acid contributes $7.2 \mu\text{mol kg}^{-1}$ to the measured $2199.0 \mu\text{mol kg}^{-1}$ (determined via the ‘TITRATE.m’ model from Sharp and Byrne, 2020). If a laboratory used this CRM to verify its own closed-cell nonlinear fit procedure (e.g., Millero et al., 1993), they would obtain an A_T equal to $2196.1 \mu\text{mol kg}^{-1}$, assuming both titrations were performed perfectly. This may cause that laboratory to presume they have a systematic bias of $-2.9 \mu\text{mol kg}^{-1}$ in their A_T determinations (represented by the arrow in Fig. 5.6) when, in fact, the discrepancy was caused only by a difference in titration procedure.

Importantly, even if that $-2.9 \mu\text{mol kg}^{-1}$ bias were corrected for using a certified A_T value from a CRM — a practice that is common but not necessarily recommended (see Bockmon and Dickson, 2015) — seawater samples from the marine environment are not expected to contain the same amount of organic proton acceptors with the same characteristics as a given CRM. So, unexpected differences in A_T from that which would be measured by the open-cell titration certification of a CRM can still occur.

5.5.3 Effect of A_X on CRM-based derivations of CO_2 system parameters

Occasionally, investigators use CO_2 system parameters (e.g., pH , f_{CO_2} , Ω_A) derived from certified values of CRMs for quality checks of measurements and calculations. This is an appealing practice because CRMs, at least theoretically, offer an out-of-the-box standard for the entirety of the CO_2 system. However, excess alkalinity invalidates the assumptions necessary for quality

checks of this nature to be valid. Especially relevant to this point are the outsized sensitivities of pH , f_{CO_2} , and Ω_{A} to uncertainty in A_{T} when the $A_{\text{T}}-C_{\text{T}}$ pair is used for calculations (see Table 5d of Orr et al., 2018).

Table 5.4. Hypothetical differences ($\Delta\text{pH}_{\text{T}}$) between calculated pH values ($\text{pH}_{\text{calc.}}$) and actual pH values (pH_{true}) of a CRM with a certified alkalinity of $2227.7 \mu\text{mol kg}^{-1}$ and a certified total dissolved inorganic carbon of $2040.0 \mu\text{mol kg}^{-1}$. The CRM includes a generic excess alkalinity contributor (X_{T}) with a given dissociation constant ($\text{p}K_{\text{X}}$), which produces a measured excess alkalinity (A_{X}) determined using the ‘TITRATE.m’ model (Sharp and Byrne, 2020). Calculations of $\text{pH}_{\text{calc.}}$ are made using CO2SYSv3.1 for MATLAB (Sharp et al., 2020), and calculations of pH_{true} are made using a modified version of CO2SYS v3.1 that allows for input of an additional protolyte (i.e., excess alkalinity contributor). Ancillary solution conditions are: $S = 33.5$, $t = 20 \text{ }^{\circ}\text{C}$, $P_{\text{T}} = 0.5 \mu\text{mol kg}^{-1}$, and $S_{i\text{T}} = 2.0 \mu\text{mol kg}^{-1}$.

| A_{T} ($\mu\text{mol kg}^{-1}$) | C_{T} ($\mu\text{mol kg}^{-1}$) | X_{T} ($\mu\text{mol kg}^{-1}$) | $\text{p}K_{\text{X}}$ | A_{X} ($\mu\text{mol kg}^{-1}$) | $\text{pH}_{\text{calc.}}$ | pH_{true} | $\Delta\text{pH}_{\text{T}}$ |
|---|---|---|------------------------|---|----------------------------|---------------------------|------------------------------|
| 2227.7 | 2040.0 | 10.0 | 4.0 | 7.3 | 7.926 | 7.910 | 0.016 |
| | | | 5.0 | 9.6 | 7.926 | 7.905 | 0.021 |
| | | | 6.0 | 9.8 | 7.926 | 7.904 | 0.021 |
| | | | 7.0 | 8.9 | 7.926 | 7.907 | 0.019 |
| | | | 8.0 | 4.5 | 7.926 | 7.916 | 0.010 |
| | | | 9.0 | 0.8 | 7.926 | 7.924 | 0.002 |

As an example, Table 5.4 shows errors in calculations of pH_{T} from certified A_{T} and C_{T} values that would result when an excess alkalinity contributor ($X_{\text{T}} = 10 \mu\text{mol kg}^{-1}$) is present but not properly accounted for in calculations. When the $\text{p}K$ of this excess contributor is between 4.0 and 7.0, pH calculation errors of around 0.02 units will occur. These errors will scale with the magnitude of X_{T} (and therefore A_{X}). Given these levels of error, we do not recommend using derived parameters from CRMs as a quality control check for oceanic CO_2 system measurements that must be known with a high degree of accuracy.

5.5.4 Excess alkalinity in the marine environment

Our results suggest that A_X varies spatially (difference between CRMs and GoM) and temporally (apparent difference between certain CRM batches) in ocean waters. Given the spatial and temporal heterogeneity of dissolved organics that likely contribute to A_X (e.g., Hertkorn et al., 2013; Broek et al., 2020), this is not an unexpected result. This concept has been indirectly implied by investigators who have sought to enhance thermodynamic consistency in carbonate system datasets by applying corrections to A_T measurements (i.e., A_X) that differ between — but not within — datasets (Millero et al., 2002; Patsavas et al., 2015; Fong and Dickson, 2019).

The presence of excess alkalinity in ocean waters is supported by thermodynamic consistency analyses of over-determined carbonate system datasets. Incongruence between calculated and measured carbonate system parameters is a recurring issue, as has been pointed out, for example, with regard to calculated versus measured pH (e.g., McElligott et al., 1998; Carter et al., 2013; 2018; Williams et al., 2017) and calculated versus measured f_{CO_2} at high f_{CO_2} (e.g., Lee et al., 2000; Lueker et al., 2000; Millero et al., 2002). Certain investigators have successfully remedied thermodynamic consistency issues by applying excess alkalinity corrections to measured alkalinity values (Millero et al., 2002; Patsavas et al., 2015; Fong and Dickson, 2019).

This notion that A_X values are non-negligible in seawater and vary spatially and temporally supports the application of measurement techniques like the titration procedure described here to full ocean profiles in order to account for and interpret A_X . Even more beneficial than the procedure described here may be some form of multi-step titration that not only measures A_X but provides an estimate of the charge groups that accept protons within a given pH range (e.g., Muller and Bleie, 2008; Yang et al., 2015; Ko et al., 2016). Uncertainty related to the amount of $C_{T(\text{samp.})}$ and $C_{T(\text{NaOH})}$ does limit quantitative interpretations of excess alkalinity. Still, reasonable estimates of A_X can be

obtained when complicating factors are properly accounted for and interpretations are appropriately caveated in the context of measurement uncertainties (as is done here). Further, with consistent measurement conditions, comparisons between A_X values within a given dataset should be quite valuable.

5.5.5 Implications for the total boron to salinity ratio (r_B)

Values of A_X in GoM surface water are not statistically different from zero (within 1σ) when the r_B of Lee et al. (2010) is used to account for A_B (Fig. 5.5b). This result implies either (1) no excess alkalinity was present in the surface GoM seawater and the Lee et al. (2010) r_B is close to its true value, (2) the true value of r_B is smaller than the Lee et al. (2010) value and the surface GoM seawater contained some excess alkalinity, (3) some complicating factor in our experimentation was improperly accounted for (e.g., an overestimation of $C_{T(\text{samp.})}$), or (4) some combination of explanations (1), (2), and (3). The ambiguity related to this interpretation highlights the difficulty of excess alkalinity analyses. However, to the extent that uncertainties were properly accounted for, this result does set the r_B of Lee et al. (2010) as an upper bound for estimating the total boron concentration in seawater from salinity (i.e., the true value of r_B is equal to or less than r_B from Lee et al. (2010)).

Our results highlight the degree to which the choice of r_B influences interpretations of alkalinity titrations and calculations of carbonate system parameters. The discrepancy between two commonly-employed ratios is magnified in our A_X results ($8\text{--}9 \mu\text{mol kg}^{-1}$), because our titrations start from $\text{pH} = \text{p}K_B$ — where A_B is 50% of B_T — rather than natural seawater pH_T — where A_B is about 10–25% of B_T . However, using one ratio over the other still produces significant differences in interpretations of A_T titrations and in calculations of carbonate system parameters using A_T . For

example, using the B_T/Cl ratio of Uppström (1974) rather than that of Lee et al. (2010) for evaluation of an A_T titration of typical surface seawater ($S = 35.0$, $t = 20.0$ °C, $A_T = 2350.0$ $\mu\text{mol kg}^{-1}$, $C_T = 2100.0$ $\mu\text{mol kg}^{-1}$, $P_T = 1.0$ $\mu\text{mol kg}^{-1}$, $Si_T = 15$ $\mu\text{mol kg}^{-1}$) results in a difference in calculated carbonate alkalinity of about $+4.0$ $\mu\text{mol kg}^{-1}$.

This difference between ratios also has implications for techniques to estimate excess (i.e., organic) alkalinity from back-titrations after removal of dissolved CO_2 (e.g., Cai et al., 1998; Hernández-Ayón et al., 2007; Muller and Bleie, 2008; Yang et al., 2015). These techniques, like the one detailed here, must account for A_B in order to estimate excess alkalinity. A 4 $\mu\text{mol kg}^{-1}$ difference in A_B — though small compared to seawater A_T values, which are typically in excess of 2000 $\mu\text{mol kg}^{-1}$ — is remarkably significant when trying to detect excess alkalinity, which may be present in open-ocean seawater at values on the order of 4 to 8 $\mu\text{mol kg}^{-1}$ (Fong and Dickson, 2019).

In general, our results highlight the need for the establishment of a “best practices” total boron to salinity ratio. The ratio of boron to chlorinity ($Cl = S/1.80655$) of 0.232 determined by Uppström (1974) is still widely used, despite the limitations in the method (Uppström, 1968) that was used to obtain it — pointed out by Liu and Lee (2009). The ratio of 0.2414 determined by Lee et al. (2010) has received recent support from measurements by Lee et al. (2019), both utilizing the same measurement technique (Liu and Lee, 2009). Ko et al. (2016) measured a ratio of 0.2365 off the southern coast of South Korea, also using the Liu and Lee (2009) technique. Fong and Dickson (2019) suggested a ratio of 0.2354 based on the goal of increasing consistency between measured and calculated pH values in open-ocean datasets. A most likely universal r_B value should be established by the oceanographic community to ensure consistency and coherence in carbonate system measurements and calculations moving forward.

5.6 Conclusions

These results indicate a hitherto undescribed excess alkalinity component of A_T in Certified Reference Materials for oceanic CO_2 measurements. This component appears to persist despite filtration and ultraviolet treatment of CRMs, suggesting some dissolved proton acceptors are not fully oxidized by the level of UV light applied to CRMs. Perhaps CRM preparation could benefit from enhanced irradiation, or the sourcing of seawater from a water mass with naturally low concentrations of dissolved organic proton acceptors. Either of these avenues, however, would surely be accompanied by heightened cost and/or other potential drawbacks.

Because CRMs are prepared using natural seawater, the excess alkalinity detected in this study suggests that the thermodynamic model used to describe the seawater acid–base system may be insufficient to relate A_T to other carbonate system parameters at a level of accuracy commensurate with current measurement methods. Further, excess alkalinity in CRMs may have an effect on CRM-based quality control of A_T measurements. Finally, attempts to deconvolve excess alkalinity from borate alkalinity highlight the degree of influence that the total boron to salinity ratio exerts over these investigations.

5.7 Acknowledgements

Support for J.D. Sharp was provided by the National Science Foundation (NSF) Graduate Research Fellowship Program, Award #1144244, and by the William and Elsie Knight Endowed Fellowship for Marine Science from the University of South Florida College of Marine Science. This project was also supported by NSF Award #1658321. We thank Salvatore Caprara for measuring phosphate and silicate concentrations in Gulf of Mexico seawater. We are grateful also for the constructive comments of two anonymous reviewers.

CHAPTER SIX: DISCUSSION AND IMPLICATIONS

6.1 Future Directions in Marine CO₂ System Chemistry

Considering emerging research directions in marine biogeochemistry, this dissertation describes timely scientific contributions. Increasingly, autonomous in situ measurement systems are relied upon to acquire oceanographic observations, including those of the CO₂ system. These observations can inform biogeochemical models with progressively finer resolution, allowing contemporary oceanographic phenomena to be analyzed with greater specificity and future predictions to be made with more confidence.

In situ sensors, when thoughtfully deployed, allow for greater spatial and temporal resolution of observations (Riser et al., 2016; Rudnick, 2016; Bushinsky et al., 2019; Claustre et al., 2019). Still, observational gaps will always exist. To supplement direct observations, regression models and statistical interpolations have been developed as important tools to fill data gaps (e.g., Jones et al., 2015; Bittig et al., 2018; Carter et al., 2018). Both in situ sensors and gap-filling methods require validation by “state-of-the-art” shipboard measurements (Talley et al., 2016). Spectrophotometric measurements of [CO₃²⁻] fit into this framework, as they are well-suited for in situ analysis and can be easily and rapidly performed in a ship’s laboratory.

Direct observations of marine biogeochemistry, including the CO₂ system, inform coupled biogeochemical ocean models, which are instrumental for re-analyzing past phenomena and predicting future responses of the Earth system to anthropogenic forcing (e.g., DeVries et al., 2012;

Gattuso et al., 2015; Long et al., 2016; Kwiatkowski and Orr, 2018; Moore et al., 2018; Fennel et al., 2019). Ocean models necessitate high-quality observations with a high degree of spatial and temporal density. To ensure quality CO₂ system observations, consistency checks are necessarily performed within datasets, between datasets over time, and between datasets collected by different research groups. The work presented here facilitates the identification of mechanisms to explain biases in measurements and/or calculations that might be found during these consistency checks. This information will support CO₂ system thermodynamic consistency analyses and promote better observations of A_T and other CO₂ system variables.

The following sections expand upon the ideas presented here and project toward the future regarding the scientific progress that the work described in this dissertation can foment.

6.2 Direct Measurements of Seawater Carbonate Ion Concentration

The method described and expanded upon in this dissertation for measurements of [CO₃²⁻] in seawater has great potential for implementation in autonomous measurement platforms, though some details must first be considered.

Adapting the [CO₃²⁻] measurement method for in situ implementation can rely on lessons learned from the development of autonomous systems to measure pH, nitrate, and bisulfide. In short, the [CO₃²⁻] method consists of mixing a sample solution with a Pb-based titrant and rapidly measuring the mixture's absorbance properties. This type of procedure has been implemented in autonomous pH measurement systems that rely on absorbance in the visible range (e.g., Martz et al., 2003). Further, reagent-free autonomous systems to measure nitrate and bisulfide are quite mature (Johnson and Coletti, 2002; Johnson et al., 2013; 2017a) and provide reliable data for studies of nutrient cycling (Johnson et al., 2010; Fawcett et al., 2018) and community production

(Plant et al., 2016; Johnson et al., 2017b; Mayot et al., 2018). These nitrate and bisulfide measurements, like the $[\text{CO}_3^{2-}]$ method, rely on absorbance in the ultraviolet range. Thus, the process of developing, testing, and implementing a $[\text{CO}_3^{2-}]$ sensor can be informed by similar sensors. One of the most important ancillary steps will be implementing a system to remove toxic Pb from measured samples (see Appendix C1).

As in the case of automated syringe-pump flow-through $[\text{CO}_3^{2-}]$ analyzers (Shangguan et al., 2019), calibration coefficients would need to be obtained for an in situ $[\text{CO}_3^{2-}]$ system. Further, as in the case of autonomous colorimetric-based pH sensors, validation with shipboard or lab-based measurements will be necessary. Within the measurement cell of a $[\text{CO}_3^{2-}]$ sensor, the biologically toxic Pb titrant may serve to reduce biofouling problems that can occur in many types of autonomous sensors (e.g., DeGrandpre et al., 1995; Liu et al., 2013; Bresnahan et al., 2014).

Autonomous $[\text{CO}_3^{2-}]$ measurement systems, and the measurement technique in general, have the potential to be uniquely beneficial for scientists and stakeholders who are especially interested in $[\text{CO}_3^{2-}]$ and Ω . This may include chemical oceanographers investigating CaCO_3 dissolution kinetics (e.g., Subhas et al., 2015; 2017; 2018; Dong et al., 2018; 2019; Naviaux et al., 2019a; 2019b), biogeochemists studying the effects of changing CO_2 system chemistry on marine calcifiers (e.g., Gimenez et al., 2018; Bednaršek et al., 2019; 2020), and managers of shellfish hatcheries who are concerned about the corrosivity of their source water (Barton et al., 2012; 2015).

6.3 Consistency in Ocean Alkalinity Measurements

Although certified reference materials and improvements in measurement technologies have greatly improved temporal and inter-laboratory consistency in A_T (Dickson, 2010a; Olsen et

al., 2019), issues do remain (Bockmon and Dickson, 2015). The identification and explanation of what *might* go wrong in the measurement of A_T is critical to identifying the source of observed inconsistencies.

To that end, this dissertation analyzes the possible problems in A_T measurements that can be introduced by dissolved organic proton acceptors, considered to be a likely source of CO₂ system inconsistencies (Fong and Dickson, 2019). Mainly, this work shows that different methods of A_T measurement by titration are likely to produce different results when organic proton acceptors are present at significant concentrations.

The adaptable code provided here is a useful tool that can be utilized in future studies that make specific comparisons between A_T values measured by different methods, and the CO₂ system variables that are computed using measured A_T . Preliminary work has already shown that differences in A_T measurement methodologies may be a critical factor explaining the pH-dependent discrepancy between measured and calculated ocean pH (Brendan Carter, unpublished results).

In a related effort, this dissertation identifies an unrecognized component of A_T in marine CO₂ system reference materials, speculates on its potential effect of quality control of A_T measurements, and extends the observation to implications in the marine environment. This novel identification demands further scrutiny into the acid–base chemistry of CO₂ system reference materials. For now, future investigations should not make the assumption that reference material acid–base chemistry is exclusively governed by inorganic species.

One aspect of seawater acid–base chemistry that must be rapidly addressed is the boric acid–borate system. Specifically, a universally applied open-ocean total boron to salinity ratio must be agreed upon. The two most commonly used ratios (Uppström, 1974; Lee et al., 2010)

differ by about 4%, and thus can produce differences of up to $4 \mu\text{mol kg}^{-1}$ in carbonate alkalinity values inferred during CO_2 system calculations. These differences can be significant in assessments of air–sea CO_2 flux that are based on A_T measurements. Borate-related alkalinity uncertainty is even more important in assessments of excess alkalinity, where an uncertainty of $4 \mu\text{mol kg}^{-1}$ can be of the same magnitude as the excess alkalinity signal itself.

6.4 Thermodynamic CO_2 System Consistency

Only with acceptable coherence between measurements and calculations of CO_2 system variables can we be sure that conclusions drawn from observations — and models based on observations — are reliable and robust. Efforts to achieve this coherence are therefore critically important.

Direct $[\text{CO}_3^{2-}]$ measurements can support thermodynamic consistency efforts by providing a fifth master variable with which to perform comparisons between measurements and calculations. A potential next step in the development of the $[\text{CO}_3^{2-}]$ measurement method may be to perform measurements in synthetic seawater (or some modified seawater solution) with direct knowledge of $[\text{CO}_3^{2-}]$; these observations could serve to unmarry the model that converts ultraviolet absorbance ratios to $[\text{CO}_3^{2-}]$ from calculation-based values of $[\text{CO}_3^{2-}]$.

Investigations into the nature of A_T measurements and the reference materials that support them shed light on neglected and misunderstood acid–base interactions that may undermine thermodynamic consistency. Information gleaned from these investigations can be instrumental in assessing inconsistencies in relationships among CO_2 system variables and in making progress toward a quantitatively constrained seawater acid–base system.

6.5 Conclusion

Chemical and mathematical equations associated with the marine CO₂ system describe the behavior of dissolved CO₂ in seawater: its transport across the air–sea interface, its hydration and subsequent dissociation to form bicarbonate and carbonate ions, the buffering effect it exerts to temper changes in seawater pH, its interaction with other seawater acid–base systems that comprise alkalinity, and its effect on (and response to) biological processes. Radiating from the central hub that is marine carbonate chemistry are numerous biogeochemical spokes that represent significant components of the Earth system.

Seawater [CO₃²⁻] is a critical CO₂ system component due to the control it exerts over saturation states, which dictate the tendency for solid CaCO₃ to precipitate or dissolve. CaCO₃ dynamics are important for the strength of the hard-tissue carbon pump (Berelson et al., 2007; Dunne et al., 2012), the survival of ecologically essential marine organisms in the wild (Kleypas et al., 1999; Gattuso and Buddemeier, 2000; Riebesell et al., 2000; Waldbusser et al., 2013; Bednaršek et al., 2014; 2019; 2020), the viability of the economically important shellfish industry (Barton et al., 2012; 2015; Ekstrom et al., 2015; Mathis et al., 2015), the timescale of fossil-fuel CO₂ neutralization (Archer et al., 1997; Sarmiento and Gruber, 2006), and more.

Seawater total alkalinity is uniquely important among the CO₂ system master variables due to the wealth of information it integrates: salinity exerts strong first order control over A_T , CaCO₃ dissolution (precipitation) adds (removes) two moles A_T per mole CaCO₃, nitrogen uptake and remineralization can either increase or decrease A_T depending on the form of dissolved N utilized or produced (Wolf-Gladrow et al., 2007), and phosphate uptake (remineralization) increases (decreases) A_T by one mole per mole P (Wolf-Gladrow et al., 2007). Further, because it mixes

conservatively, A_T is useful as a state variable along with C_T for biogeochemical modelling (e.g., Orr et al., 2005; Hauri et al., 2013; Fiechter et al., 2014; Cossarini et al., 2015).

This work advances a method for measurement of $[\text{CO}_3^{2-}]$ to the point that carbonate ion concentration can be viewed as a fifth measurable “master variable” of the seawater CO_2 system. The method is amenable to in situ analysis and deployment on autonomous sensors. This work facilitates the identification of potential biases in measurements of A_T , which should inform CO_2 system thermodynamic consistency analyses and promote better observations of A_T and other CO_2 system variables. These high-quality observations will be necessary for continued refinement of the CO_2 system dynamics that are incorporated into state-of-the-art biogeochemical models.

CHAPTER SEVEN:

REFERENCES

- Abril, G., Bouillon, S., Darchambeau, F., Teodoru, C.R., Marwick, T.R., Tamoo, F., Ochieng Omengo, F., Geeraert, N., Deirmendjian, L., Polsenaere, P., Borges, A.V., 2015. Technical note: Large overestimation of $p\text{CO}_2$ calculated from pH and alkalinity in acidic, organic-rich freshwaters. *Biogeosciences* 12, 67–78.
- Alin, S.R., Feely, R.A., Hales, B., Byrne, R.H., Cochlan, W.P., Liu, X., Greeley, D., 2017. Dissolved inorganic carbon, total alkalinity, pH, dissolved oxygen, nutrients, and other variables collected from profile and discrete sample observations using CTD, Niskin bottle, and other instruments from Ronald H. Brown in the West Coast of North America from Canada to Mexico from 2016-05-08 to 2016-06-06 (NCEI Accession 0169412). Version 1.1. NOAA National Centers for Environmental Information. Gov.noaa.nodc:0169412.
- Almgren, T., Dyrssen, D., Strandberg, M., 1977. Computerized high-precision titrations of some major constituents of seawater on board the R.V. *Dmitry Mendeleev*. *Deep-Sea Res.* 24, 345–364.
- Altmann, R.S., Buffle, J., 1988. The use of differential equilibrium functions for interpretation of metal binding in complex ligand systems: Its relation to site occupation and site affinity distributions. *Geochim. Cosmochim. Acta* 52, 1505–1519.
- Álvarez, M., Sanleón-Bartolomé, H., Tanhua, T., Mintrop, L., Luchetta, A., Cantoni, C., Schroeder, K., Civitarese, G., 2014. The CO_2 system in the Mediterranean Sea: a basin wide perspective. *Ocean Sci.* 10, 69–92.
- Arakawa, N., Aluwihare, L.I., Simpson, A.J., Soong, R., Stephens, B.M., Lane-Coplen, D., 2017. Carotenoids are the likely precursor of a significant fraction of marine dissolved organic matter. *Sci. Adv.* 3, 1–12.
- Archer, D., 1991. Modeling the calcite lysocline. *J. Geophys. Res.* 96, 17,037–17,050.
- Archer, D., 2005. Fate of fossil fuel CO_2 in geologic time. *J. Geophys. Res.* 110, C09S05.
- Archer, D., Kheshgi, H., Maier-Reimer, E., 1997. Multiple timescales for neutralization of fossil fuel CO_2 . *Geophys. Res. Lett.* 24, 405–408.
- Asuero, A.G., Michałowski, T., 2011. Comprehensive formulation of titration curves for complex acid-base systems and its analytical implications. *Crit. Rev. Anal. Chem.* 41, 151–187.
- Bakker, D.C.E., Pfeil, B., Landa, C.S., Metzl, N., O'Brien, K.M., Olsen, A., et al., 2016. A multi-decade record of high quality $f\text{CO}_2$ data in version 3 of the Surface Ocean CO_2 Atlas (SOCAT). *Earth Syst. Sci. Data* 8, 383–413.
- Baringer, M.O., Bullister, J.L., Feely, R.A., Wanninkhof, R., Millero, F.J., Hansell, D.A., Zhang, J.-Z., Mordy, C., Langdon, C., Schlosser, P., Jenkins, W.J., McNichol, A., Key, R.M., 2016. Dissolved inorganic carbon (DIC), total alkalinity, pH on seawater scale, partial pressure of

- carbon dioxide ($p\text{CO}_2$), dissolved organic carbon (DOC), chlorofluorocarbons (CFC-11, CFC-12), temperature, salinity and other hydrographic and chemical variables collected from discrete samples and profile observations during the R/V Ronald H. Brown cruise CLIVAR_A16N_2013 (EXPOCODE 33RO20130803) in the Atlantic Ocean from 2013-08-03 to 2013-10-01 (NCEI Accession 0157363). NOAA National Centers for Environmental Information.
- Barron, J.L., Dyrssen, D., Jones, E.P., Wedborg, M., 1983. A comparison of computer methods for seawater alkalinity titrations. *Deep-Sea Res. Part A, Oceanogr. Res. Pap.* 30, 441–448.
- Barton, A., Hales, B., Waldbusser, G.G., Langdon, C., Feely, R.A., 2012. The Pacific oyster, *Crassostrea gigas*, shows negative correlation to naturally elevated carbon dioxide levels: Implications for near-term ocean acidification effects. *Limnol. Oceanogr.* 57, 698–710.
- Barton, A., Waldbusser, G.G., Feely, R.A., Weisberg, S.B., Newton, J.A., Hales, B., Cudd, S., Eudeline, B., Langdon, C.J., Jefferds, I., King, T., 2015. Impacts of coastal acidification on the Pacific Northwest shellfish industry and adaptation strategies implemented in response. *Oceanography* 28, 146–159.
- Bates, N.R., 2007. Interannual variability of the oceanic CO_2 sink in the subtropical gyre of the North Atlantic Ocean over the last 2 decades. *J. Geophys. Res.* 112, C09013.
- Bates, N.R., Astor, Y.M., Church, M.J., Currie, K., Dore, J.E., González-Dávila, M., Lorenzoni, L., Muller-Karger, F., Olafsson, J., Magdalena Santana-Casiano, J., 2014. A time-series view of changing surface ocean chemistry due to ocean uptake of anthropogenic CO_2 and ocean acidification. *Oceanography* 27, 126–141.
- Bednaršek, N., Feely, R.A., Beck, M.W., Alin, S.R., Siedlecki, S.A., Calosi, P., Norton, E.L., Saenger, C., Štrus, J., Greeley, D., Nezlin, N.P., 2020. Exoskeleton dissolution with mechanoreceptor damage in larval Dungeness crab related to severity of present-day ocean acidification vertical gradients. *Sci. Tot. Environ.* 716, 136610.
- Bednaršek, N., Feely, R.A., Howes, E.L., Hunt, B.P., Kessouri, F., León, P., Lischka, S., Maas, A.E., McLaughlin, K., Nezlin, N.P., Sutula, M., 2019. Systematic Review and Meta-Analysis Toward Synthesis of Thresholds of Ocean Acidification Impacts on Calcifying Pteropods and Interactions With Warming. *Frontiers Mar. Sci.* 6, 227.
- Bednaršek, N., Feely, R.A., Reum, J.C.P., Peterson, B., Menkel, J., Alin, S.R., Hales, B., 2014. *Limacina helicina* shell dissolution as an indicator of declining habitat suitability owing to ocean acidification in the California Current Ecosystem. *Proc. R. Soc. B* 281, 20140123.
- Bednaršek, N., Feely, R.A., Tolimieri, N., Hermann, A.J., Siedlecki, S.A., Waldbusser, G.G., McElhany, P., Alin, S.R., Klinger, T., Moore-Maley, B., Pörtner, H.O., 2017. Exposure history determines pteropod vulnerability to ocean acidification along the US West Coast. *Sci. Rep.* 7, 4526.
- Bednaršek, N., Tarling, G.A., Bakker, D.C.E., Fielding, S., Jones, E.M., Venables, H.J., Ward, P., Kuzirian, A., Lézé, B., Feely, R.A., Murphy, E.J., 2012. Extensive dissolution of live pteropods in the Southern Ocean. *Nat. Geosci.* 5, 881–885.
- Bednaršek, N., Harvey, C.J., Kaplan, I.C., Feely, R.A., Možina, J., 2016. Pteropods on the edge: Cumulative effects of ocean acidification, warming, and deoxygenation. *Prog. Oceanogr.* 145, 1–24.
- Ben Ali Daoud, A., Tremblay, L., 2019. HPLC-SEC-FTIR characterization of the dissolved organic matter produced by the microbial carbon pump. *Mar. Chem.* 215, 103668.
- Berelson, W.M., Balch, W.M., Najjar, R., Feely, R.A., Sabine, C., Lee, K., 2007. Relating estimates of CaCO_3 production, export, and dissolution in the water column to

- measurements of CaCO₃ rain into sediment traps and dissolution on the sea floor: A revised global carbonate budget. *Global Biogeochem. Cycles* 21, GB1024.
- Berner, R.A., Morse, J.W., 1974. Dissolution kinetics of calcium carbonate in sea water IV. Theory of calcite dissolution. *Am. J. Sci.* 274, 108–134.
- Birk, M.A., Mclean, E.L., Seibel, B.A., 2018. Ocean acidification does not limit squid metabolism via blood oxygen supply. *J. Exp. Biol.* 221, jeb187443.
- Bittig, H.C., Steinhoff, T., Claustre, H., Fiedler, B., Williams, N.L., Sauzède, R., Körtzinger, A., Gattuso, J.P., 2018. An alternative to static climatologies: robust estimation of open ocean CO₂ variables and nutrient concentrations from T, S, and O₂ data using Bayesian neural networks. *Frontiers Mar. Sci.* 5, 328.
- Bockmon, E.E., Dickson, A.G., 2015. An inter-laboratory comparison assessing the quality of seawater carbon dioxide measurements. *Mar. Chem.* 171, 36–43.
- Bopp, L., Resplandy, L., Orr, J.C., Doney, S.C., Dunne, J.P., Gehlen, M., Halloran, P., Heinze, C., Ilyina, T., Seferian, R., Tjiputra, J., Vichi, M., 2013. Multiple stressors of ocean ecosystems in the 21st century: projections with CMIP5 models. *Biogeosciences* 10, 6225–6245.
- Borges, A.V. Gypens, N., 2010. Carbonate chemistry in the coastal zone responds more strongly to eutrophication than ocean acidification. *Limnol. Oceanogr.* 55, 346–353.
- Boyd, P.W., Claustre, H., Levy, M., Siegel, D.A., Weber, T., 2019. Multi-faceted particle pumps drive carbon sequestration in the ocean. *Nature* 568, 327–335.
- Bradshaw, A.L., Brewer, P.G., 1980. The titration of sea-water with strong acid. Tech. Report, Woods Hole Oceanographic Institution.
- Bradshaw, A.L., Brewer, P.G., Shafer, D.K., Williams, R.T., 1981. Measurements of total carbon dioxide and alkalinity by potentiometric titration in the GEOSECS Program. *Earth Planet. Sci. Lett.* 55, 99–115.
- Bradshaw, A.L., Brewer, P.G., 1988. High precision measurements of alkalinity and total carbon dioxide in seawater by potentiometric titration - 1. Presence of unknown protolyte(s)? *Mar. Chem.* 23, 69–86.
- Breland, J.A., Byrne, R.H., 1993. Spectrophotometric procedures for determination of sea water alkalinity using bromocresol green. *Deep-Sea Res. Part I* 40, 629–641.
- Bresnahan Jr., P.J., Martz, T.R., Takeshita, Y., Johnson, K.S., LaShomb, M., 2014. Best practices for autonomous measurement of seawater pH with the Honeywell Durafet. *Methods Oceanogr.* 9, 44–60.
- Brewer, P.G., Bradshaw, A.L., Williams, R.T., 1986. Measurements of total carbon dioxide and alkalinity in the North Atlantic Ocean in 1981. In *The changing carbon cycle* (pp. 348–370). Springer, New York, NY.
- Brewer, P.G., Goldman, J.C., 1976. Alkalinity changes generated by phytoplankton growth. *Limnol. Oceanogr.* 21, 108–117.
- Brewer, P.G., Wong, G.T.F., Bacon, M.P., Spencer, D.W., 1975. An oceanic calcium problem? *Earth Planet. Sci. Lett.* 26, 81–87.
- Broecker, W., Clark, E., 2001. A dramatic Atlantic dissolution event at the onset of the last glaciation. *Geochemistry, Geophysics, Geosystems* 2, 2001GC000185.
- Broecker, W.S., Peng, T.-H., 1982. Tracers in the Sea. Lamont-Doherty Geological Observatory, Palisades, NY.
- Broecker, W.S., Takahashi, T., Andersen, N.R., Malahoff, A., 1978. Neutralization of fossil fuel CO₂ by marine calcium carbonate. in: Andersen, N.R., Malahoff, A. (Eds.), *The Fate of*

- Fossil Fuel CO₂ in the Oceans*. Plenum Press, New York, NY, pp. 213–241.
- Broek, T.A.B., Walker, B.D., Guilderson, T.P., Vaughn, J.S., Mason, H.E., McCarthy, M.D., 2020. Low molecular weight dissolved organic carbon: Aging, compositional changes, and selective utilization during global ocean circulation. *Global Biogeochem. Cycles* 34, 1–20.
- Bushinsky, S.M., Takeshita, Y., Williams, N.L., 2019. Observing changes in ocean carbonate chemistry: our autonomous future. *Current Clim. Change Rep.* 5, 207–220.
- Byrne, R. H., 1981. Inorganic lead complexation in natural seawater determined by UV spectroscopy. *Nature* 290, 487–489.
- Byrne, R.H., 2014. Measuring ocean acidification: New technology for a new era of ocean chemistry. *Environ. Sci. Technol.* 48, 5352–5360.
- Byrne, R.H., Breland, J.A., 1989. High precision multiwavelength pH determinations in seawater using cresol red. *Deep-Sea Res. Part A, Oceanogr. Res. Pap.* 36, 803–810.
- Byrne, R.H., Kester, D.R., 1978. Ultraviolet Spectroscopic Study of Ferric Hydroxide Complexation. *J. Sol. Chem.* 7, 373–383.
- Byrne, R.H., Kester, D.R., 1981. Ultraviolet Spectroscopic Study of Ferric Equilibria at High Chloride Concentrations. *J. Sol. Chem.* 10, 51–67.
- Byrne, R.H., Robert-Baldo, G., Thompson, S.W., Chen, C.T.A., 1988. Seawater pH measurements: an at-sea comparison of spectrophotometric and potentiometric methods. *Deep-Sea Res. Part A. Oceanogr. Res. Papers* 35, 1405–1410.
- Byrne, R. H., Yao, W., 2008. Procedures for measurement of carbonate ion concentrations in seawater by direct spectrophotometric observations of Pb(II) complexation. *Mar. Chem.* 112, 128–135.
- Byrne, R.H., Young, R.W., Miller, W.L., 1981. Lead Chloride Complexation Using Ultraviolet Molar Absorptivity Characteristics. *J. Sol. Chem.* 10, 243–251.
- Cai, W.-J., Wang, Y., Hodson, R.E., 1998. Acid-Base Properties of Dissolved Organic Matter in the Estuarine Waters of Georgia, USA. *Geochim. Cosmochim. Acta* 62, 473–483.
- Caldeira, K., Wickett, M.E., 2003. Anthropogenic carbon and ocean pH. *Nature* 425, 365–365.
- Cantoni, C., Luchetta, A., Celio, M., Cozzi, S., Raicich, F., Catalano, G., 2012. Carbonate system variability in the Gulf of Trieste (North Adriatic Sea). *Estuar. Coast. Shelf Sci.* 115, 51–62.
- Cantrell, K.J., Serkiz, S.M., Perdue, E.M., 1990. Evaluation of acid neutralizing capacity data for solutions containing natural organic acids. *Geochim. Cosmochim. Acta* 54, 1247–1254.
- Carlson, C.A., Hansell, D.A., 2015. DOM sources, sinks, reactivity, and budgets, in: Hansell, D.A., Carlson, C.A. (Eds.), *Biogeochemistry of Marine Dissolved Organic Matter*. Academic Press, pp. 65–126.
- Carpenter, J.H., 1957. The determination of calcium in natural waters. *Limnol. Oceanogr.* 2, 271–278.
- Carter, B.R., Feely, R.A., Mecking, S., Cross, J.N., Macdonald, A.M., Siedlecki, S.A., Talley, L.D., Sabine, C.L., Millero, F.J., Swift, J.H., Dickson, A.G., Rodgers, K.B., 2017. Two decades of Pacific anthropogenic carbon storage and ocean acidification along Global Ocean Ship-based Hydrographic Investigations Program sections P16 and P02. *Global Biogeochem. Cycles* 31, 306–327.
- Carter, B.R., Feely, R.A., Wanninkhof, R., Kouketsu, S., Sonnerup, R.E., Pardo, P.C., Sabine, C.L., Johnson, G.C., Sloyan, B.M., Murata, A., Mecking, S., Tilbrook, B., Speer, K., Talley, L.D., Millero, F.J., Wijffels, S.E., Macdonald, A.M., Gruber, N., Bullister, J.L., 2019. Pacific anthropogenic carbon between 1991 and 2017. *Global Biogeochem. Cycles* 33, 597–

617.

- Carter, B.R., Feely, R.A., Williams, N.L., Dickson, A.G., Fong, M.B., Takeshita, Y., 2018. Updated methods for global locally interpolated estimation of alkalinity, pH, and nitrate. *Limnol. Oceanogr. Methods* 16, 119–131.
- Carter, B.R., Frölicher, T.L., Dunne, J.P., Rodgers, K.B., Slater, R.D., Sarmiento, J.L., 2016. When can ocean acidification impacts be detected from decadal alkalinity measurements? *Global Biogeochem. Cycles* 30, 595–612.
- Carter, B.R., Radich, J.A., Doyle, H.L., Dickson, A.G., 2013. An automated system for spectrophotometric seawater pH measurements. *Limnol. Oceanogr. Methods* 11, 16–27.
- Chen, B., Cai, W.-J., Chen, L., 2015. The marine carbonate system of the Arctic Ocean: assessment of internal consistency and sampling considerations, summer 2010. *Mar. Chem.* 176, 174–188.
- Cheng, L., Abraham, J., Zhu, J., Trenberth, K.E., Fasullo, J., Boyer, T., Locarnini, R., Zhang, B., Yu, F., Wan, L., Chen, X., 2020. Record-setting ocean warmth continued in 2019. *Advances Atmos. Sci.* 37, 137–142.
- Chivers, D.P., McCormick, M.I., Nilsson, G.E., Munday, P.L., Watson, S.-A., Meekan, M.G., Mitchell, M.D., Corkill, K.C., Ferrari, M.C.O., 2014. Impaired learning of predators and lower prey survival under elevated CO₂: a consequence of neurotransmitter interference. *Global Change Biol.* 20, 515–522.
- Claustre, H., Johnson, K.S., Takeshita, Y., 2020. Observing the global ocean with biogeochemical-Argo. *Annu. Rev. Mar. Sci.* 12, 23–48.
- Clayton, T.D., Byrne, R.H., 1993. Spectrophotometric seawater pH measurements: total hydrogen ion concentration scale calibration of m-cresol purple and at-sea results. *Deep-Sea Res. I, Oceanogr. Res. Pap.* 40, 2115–2129.
- Cooley, S.R., Doney, S.C., 2009. Anticipating ocean acidification's economic consequences for commercial fisheries. *Environ. Res. Lett.* 4, 024007.
- Cooley, S.R., Kite-Powell, H.L., Doney, S.C., 2009. Ocean acidification's potential to alter global marine ecosystem services. *Oceanography* 22, 172–181.
- Cossarini, G., Lazzari, P., Solidoro, C., 2015. Spatiotemporal variability of alkalinity in the Mediterranean Sea. *Biogeosciences* 12, 1647–1658.
- Cox, R., Culkin, F., 1966. Sodium, potassium, magnesium, calcium and strontium in sea water. *Deep-Sea Res.* 13, 789–804.
- Cross, J.N., Macdonald, A.M., Alin, S.R., Wanninkhof, R., Dickson, A.G., Carlson, C.A., Johnson, G.C., Baringer, M.O., Mordy, C., Langdon, C., Key, R.M., McNichol, A., Bullister, J.L., Jenkins, W.J., Nelson, N., 2017. Dissolved inorganic carbon (DIC), total alkalinity, pH on total scale, dissolved organic carbon (DOC), chlorofluorocarbons (CFC-11, CFC-12), temperature, salinity and other hydrographic and chemical variables collected from discrete samples and profile observations during the R/V Ronald H. Brown cruise along the GO-SHIP Section P16_2015, Legs 1 and 2 (EXPCODEs 33RO20150410 and 33RO20150525) in the Pacific Ocean, from 2015-04-10 to 2015-06-27 (NCEI Accession 0163182). NOAA National Centers for Environmental Information.
- Culberson, C.H., Pytkowicz, R.M., Hawley, J.E., 1970. Seawater alkalinity determination by the pH method. *J. Mar. Res.* 28, 15–21.
- de Souza Sierra, M.M., Arend, K., Fernandes, A.N., Giovanela, M., Szpoganicz, B., 2001. Application of potentiometry to characterize acid and basic sites in humic substances Testing the BEST7 program with a weak-acid mixture. *Anal. Chim. Acta* 445, 89–98.

- DeGrandpre, M.D., Hammar, T.R., Smith, S.P., Sayles, F.L., 1995. In situ measurements of seawater $p\text{CO}_2$. *Limnol. Oceanogr.* 40, 969–975.
- DeVries, T., Primeau, F., Deutsch, C., 2012. The sequestration efficiency of the biological pump. *Geophys. Res. Lett.* 39, L13601.
- Diaz-Pulido, G., Gouezo, M., Tilbrook, B., Dove, S., Anthony, K.R.N., 2011. High CO_2 enhances the competitive strength of seaweeds over corals. *Ecol. Lett.* 14, 156–162.
- Dickson, A.G., 1981. An exact definition of total alkalinity and a procedure for the estimation of alkalinity and total inorganic carbon from titration data. *Deep-Sea Res. Part A, Oceanogr. Res. Pap.* 28, 609–623.
- Dickson, A.G., 1990a. Thermodynamics of the dissociation of boric acid in synthetic seawater from 273.15 to 318.15 K. *Deep-Sea Res. Part A, Oceanogr. Res. Pap.* 37, 755–766.
- Dickson, A.G., 1990b. Standard potential of the reaction: $\text{AgCl}_{(s)} + 12\text{H}_2_{(g)} = \text{Ag}_{(s)} + \text{HCl}_{(aq)}$, and the standard acidity constant of the ion HSO_4^- in synthetic sea water from 273.15 to 318.15 K. *J. Chem. Thermodyn.* 22, 113–127.
- Dickson, A.G., 2010a. Standards for ocean measurements. *Oceanography* 23, 34–47.
- Dickson, A.G., 2010b. The carbon dioxide system in seawater: Equilibrium chemistry and measurements, in: Riebesell, U., Fabry, V.J., Hansson, I., Gattuso, J.P., eds., *Guide to Best Practices for Ocean Acidification Research and Data Reporting*. European Commission: Brussels, Belgium, 17–40.
- Dickson, A.G., Afghan, J.D., Anderson, G.C., 2003. Reference materials for oceanic CO_2 analysis: A method for the certification of total alkalinity. *Mar. Chem.* 80, 185–197.
- Dickson, A.G., Riley, J.P., 1978. The effect of analytical error on the evaluation of the components of the aquatic carbon-dioxide system. *Mar. Chem.* 6, 77–85.
- Dickson, A.G., Riley, J.P., 1979. The estimation of acid dissociation constants in sea-water media from potentiometric titrations with strong base. I. The ionic product of water — K_w . *Mar. Chem.* 7, 89–99.
- Dickson, A.G., Sabine, C.L., Christian, J.R. (Eds.), 2007. *Guide to Best Practices for Ocean CO_2 Measurements*. North Pacific Marine Science Organization, PICES Special Publication 3, Sidney, B.C., Canada.
- Doney, S.C., Fabry, V.J., Feely, R.A., Kleypas, J.A., 2009. Ocean acidification: The other CO_2 problem. *Annu. Rev. Mar. Sci.* 1, 169–192.
- Dong, S., Subhas, A.V., Rollins, N.E., Naviaux, J.D., Adkins, J.F., Berelson, W.M., 2018. A kinetic pressure effect on calcite dissolution in seawater. *Geochim. Cosmochim. Acta* 238, 411–423.
- Dong, S., Berelson, W.M., Rollins, N.E., Subhas, A.V., Naviaux, J.D., Celestian, A.J., Liu, X., Turaga, N., Kemnitz, N.J., Byrne, R.H., Adkins, J.F., 2019. Aragonite dissolution kinetics and calcite/aragonite ratios in sinking and suspended particles in the North Pacific. *Earth Planet. Sci. Lett.* 515, 1–12.
- Dore, J.E., Lukas, R., Sadler, D.W., Church, M.J., Karl, D.M., 2009. Physical and biogeochemical modulation of ocean acidification in the central North Pacific. *Proc. Natl. Acad. Sci.* 106, 12235–12240.
- Dunne, J.P., Hales, B., Toggweiler, J.R., 2012. Global calcite cycling constrained by sediment preservation controls. *Global Biogeochem. Cycles* 26, GB3023.
- Dunne, J.P., John, J.G., Shevliakova, E., Stouffer, R.J., Krasting, J.P., Malyshev, S.L., Milly, P.C.D., Sentman, L.T., Adcroft, A.J., Cooke, W., Dunne, K.A., Griffies, S.M., Hallberg, R.W., Harrison, M.J., Levy, H., Wittenberg, A.T., Phillips, P.J., Zadeh, N., 2013. GFDL's

- ESM2 global coupled climate–carbon earth system models. Part II: carbon system formulation and baseline simulation characteristics. *J. Clim.* 26, 2247–2267.
- Dyrssen, D., 1965. A Gran titration of sea water on board *Sagitta*. *Acta Chem. Scand.* 19, 1265.
- Dyrssen, D., Sillén, L.G., 1967. Alkalinity and total carbonate in sea water. A plea for p-T-independent data. *Tellus* 19, 113–121.
- Easley, R.A., Byrne, R.H., 2012. Spectrophotometric calibration of pH electrodes in seawater using purified m-cresol purple. *Environ. Sci. Tech.* 46, 5018–5024.
- Easley, R. A., Patsavas, M. C., Byrne, R. H., Liu, X., Feely, R. A., Mathis, J. T., 2013. Spectrophotometric measurement of calcium carbonate saturation states in seawater. *Environ. Sci. Technol.* 47, 1468–1477.
- Ekstrom, J.A., Suatoni, L., Cooley, S.R., Pendleton, L.H., Waldbusser, G.G., Cinner, J.E., Ritter, J., Langdon, C., van Hooidonk, R., Gledhill, D., Wellman, K., Beck, M.W., Brander, L.M., Rittschof, D., Doherty, C., Edwards, P.E.T., Portela, R., 2015. Vulnerability and adaptation of US shellfisheries to ocean acidification. *Nat. Clim. Change* 5, 207–214.
- Ellison, S.L.R., Williams, A. *Eurachem/CITAC guide: Quantifying Uncertainty in Analytical Measurement*, 3rd ed., 2012.
- Emerson, S., Bender, M., 1981. Carbon fluxes at the sediment-water interface of the deep-sea. Calcium carbonate preservation. *J. Mar. Res.* 39, 139–162.
- Fabricius, K.E., Langdon, C., Uthicke, S., Humphrey, C., Noonan, S., De'ath, G., Okazaki, R., Muehllehner, N., Glas, M.S., Lough, J.M., 2011. Losers and winners in coral reefs acclimatized to elevated carbon dioxide concentrations. *Nat. Clim. Chang.* 1, 165–169.
- Fabry, V.J., Seibel, B.A., Feely, R.A., Orr, J.C., 2008. Impacts of ocean acidification on marine fauna and ecosystem processes. *ICES J. Mar. Sci.* 65, 414–432.
- Fajar, N. M., García-Ibáñez, M. I., SanLeón-Bartolomé, H., Álvarez, M., Pérez, F. F., 2015. Spectrophotometric measurements of the carbonate ion concentration: aragonite saturation states in the Mediterranean Sea and Atlantic Ocean. *Environ. Sci. Technol.* 49, 11679–11687.
- Fassbender, A.J., Alin, S.R., Feely, R.A., Sutton, A.J., Newton, J.A., Byrne, R.H., 2017. Estimating total alkalinity in the Washington State coastal zone: Complexities and surprising utility for ocean acidification research. *Estuar. Coasts* 40, 404–418.
- Fawcett, S.E., Johnson, K.S., Riser, S.C., Van Oostende, N., Sigman, D.M., 2018. Low-nutrient organic matter in the Sargasso Sea thermocline: a hypothesis for its role, identity, and carbon cycle implications. *Mar. Chem.* 207, 108–123.
- Feely, R.A., Alin, S.R., Carter, B., Bednaršek, N., Hales, B., Chan, F., Hill, T.M., Gaylord, B., Sanford, E., Byrne, R.H., Sabine, C.L., Greeley, D., Juraneck, L., 2016. Chemical and biological impacts of ocean acidification along the west coast of North America. *Estuar. Coast. Shelf Sci.* 183, 260–270.
- Feely, R.A., Doney, S.C., Cooley, S.R., 2009. Ocean acidification present conditions and future changes in a high-CO₂ world. *Oceanography* 22, 36–47.
- Feely, R.A., Okazaki, R.R., Cai, W.J., Bednaršek, N., Alin, S.R., Byrne, R.H., Fassbender, A., 2018. The combined effects of acidification and hypoxia on pH and aragonite saturation in the coastal waters of the California current ecosystem and the northern Gulf of Mexico. *Continental Shelf Research*, 152, 50–60.
- Feely, R.A., Sabine, C.L., Byrne, R.H., Millero, F.J., Dickson, A.G., Wanninkhof, R., Murata, A., Miller, L.A., Greeley, D., 2012. Decadal changes in the aragonite and calcite saturation state of the Pacific Ocean. *Glob. Biogeochem. Cycles* 26, GB3001.

- Feely, R.A., Sabine, C.L., Hernandez-Ayon, J.M., Ianson, D., Hales, B., 2008. Evidence for upwelling of corrosive “acidified” water onto the continental shelf. *Science* 320, 1490–1492.
- Feely, R.A., Sabine, C.L., Lee, K., Berelson, W., Kleypas, J., Fabry, V.J., Millero, F.J., 2004. Impact of anthropogenic CO₂ on the CaCO₃ system in the oceans. *Science* 305, 362–366.
- Fein, J.B., Daughney, C.J., Yee, N., Davis, T.A., 1997. A chemical equilibrium model for metal adsorption onto bacterial surfaces. *Geochim. Cosmochim. Acta* 61, 3319–3328.
- Fennel K., Gehlen M., Brasseur P., Brown C.W., Ciavatta S., Cossarini G., Crise A., Edwards C.A., Ford D., Friedrichs M.A.M., Gregoire M., Jones E., Kim H.-C., Lamouroux J., Murtugudde R., Perruche C., and the GODAE OceanView Marine Ecosystem Analysis and Prediction Task Team, 2019. Advancing Marine Biogeochemical and Ecosystem Reanalyses and Forecasts as Tools for Monitoring and Managing Ecosystem Health. *Frontiers Mar. Sci.* 6, 89.
- Fernández, N., Beiras, R., 2000. Combined Toxicity of Dissolved Mercury with Copper, Lead and Cadmium on Embryogenesis and Early Larval Growth of the *Paracentrotus lividus* Sea-Urchin. *Ecotoxicology* 10, 263–271.
- Fiechter, J., Curchitser, E.N., Edwards, C.A., Chai, F., Goebel, N.L., Chavez, F.P., 2014. Air-sea CO₂ fluxes in the California Current: Impacts of model resolution and coastal topography. *Global Biogeochem. Cycles* 28, 371–385.
- Fong, M.B., Dickson, A.G., 2019. Insights from GO-SHIP hydrography data into the thermodynamic consistency of CO₂ system measurements in seawater. *Mar. Chem.* 211, 52–63.
- Friedlingstein, P., Jones, M.W., O’Sullivan, M., Andrew, R.M., Hauck, J., Peters, G.P., Peters, W., Pongratz, J., Sitch, S., Le Quéré, C., Bakker, D.C.E., Canadell, J.G., Ciais, P., Jackson, R.B., Anthoni, P., Barbero, L., Bastos, A., Bastrikov, V., Becker, M., Bopp, L., Buitenhuis, E., Chandra, N., Chevallier, F., Chini, L.P., Currie, K.I., Feely, R.A., Gehlen, M., Gilfillan, D., Gkritzalis, T., Goll, D.S., Gruber, N., Gutekunst, S., Harris, I., Haverd, V., Houghton, R.A., Hurtt, G., Ilyina, T., Jain, A.K., Joetjzer, E., Kaplan, J.O., Kato, E., Goldewijk, K.K., Korsbakken, J.I., Landschützer, P., Lauvset, S.K., Lefèvre, N., Lenton, A., Lienert, S., Lombardozzi, D., Marland, G., McGuire, P.C., Melton, J.R., Metzl, N., Munro, D.R., Nabel, J.E.M.S., Nakaoka, S.-I., Neill, C., Omar, A.M., Ono, T., Peregón, A., Pierrot, D., Poulter, B., Rehder, G., Resplandy, L., Robertson, E., Rödenbeck, C., Séférian, R., Schwinger, J., Smith, N., Tans, P.P., Tian, H., Tilbrook, B., Tubiello, F.N., van der Werf, G.R., Wiltshire, A.J., Zaehle, S., 2019. Global Carbon Budget 2019. *Earth Syst. Sci. Data* 11, 1783–1838.
- Fukushima, M., Tanaka, S., Hasebe, K., Taga, M., Nakamura, H., 1995. Interpretation of the acid–base equilibrium of humic acid by a continuous p*K* distribution and electrostatic model. *Anal. Chim. Acta* 302, 365–373.
- Gattuso, J.-P., Buddemeier, R.W., 2000. Calcification and CO₂. *Nature* 407, 311–313.
- Gattuso, J.P., Magnan, A., Billé, R., Cheung, W.W., Howes, E.L., Joos, F., Allemand, D., Bopp, L., Cooley, S.R., Eakin, C.M., Hoegh-Guldberg, O., Kelly, R.P., Pörtner, H.-O., Rogers, A.D., Baxter, J.M., Laffoley, D., Osborn, D., Rankovic, A., Rochette, J., Sumaila, U.R., Treyer, S., Turley, C., 2015. Contrasting futures for ocean and society from different anthropogenic CO₂ emissions scenarios. *Science* 349, aac4722.
- Gieskes, J.M., 1973. Interstitial water studies, Leg 15 – Alkalinity, pH, Mg, Ca, Si, PO₄, and NH₄. Initial Reports Deep Sea Drill. Proj. 20, 813–829.
- Gimenez, I., Waldbusser, G.G., Hales, B., 2018. Ocean acidification stress index for shellfish

- (OASIS): Linking Pacific oyster larval survival and exposure to variable carbonate chemistry regimes. *Elem. Sci. Anth.* 6, 51.
- Goldman, J.C., Brewer, P.G., 1980. Effect of nitrogen source and growth rate on phytoplankton-mediated changes in alkalinity. *Limnol. Oceanogr.* 25, 352–357.
- Gran, G., 1950. Determination of the equivalent point in potentiometric titrations. *Acta Chem. Scand.* 4, 559–577.
- Gran, G., 1952. Determination of the Equivalent Point in Potentiometric Titrations. Part II. *Analyst* 77, 661–671.
- Gruber, N., Clement, D., Carter, B.R., Feely, R.A., Van Heuven, S., Hoppema, M., Ishii, M., Key, R.M., Kozyr, A., Lauvset, S.K., Monaco, C.L., 2019. The oceanic sink for anthropogenic CO₂ from 1994 to 2007. *Science* 363, 1193–1199.
- Gruber, N., Hauri, C., Lachkar, Z., Loher, D., Frölicher, T.L., Plattner, G.-K., 2012. Rapid Progression of Ocean Acidification in the California Current System. *Nature* 337, 220–223.
- Hales, B., 2003. Respiration, dissolution, and the lysocline. *Paleoceanography* 18, 1099.
- Hansell, D.A., Carlson, C.A., Repeta, D.J., Schlitzer, R., 2009. Dissolved organic matter in the ocean. *Oceanography* 22, 202–211.
- Hansson, I., Jagner, D., 1973. Evaluation of the accuracy of Gran plots by means of computer calculations: Application to the potentiometric titration of the total alkalinity and carbonate content in sea water. *Anal. Chim. Acta* 65, 363–373.
- Hernández-Ayón, J.M., Belli, S.L., Zirino, A., 1999. pH, alkalinity and total CO₂ in coastal seawater by potentiometric titration with a difference derivative readout. *Anal. Chim. Acta* 394, 101–108.
- Hernández-Ayón, J.M., Zirino, A., Dickson, A.G., Camiro-Vargas, T., Valenzuela-Espinoza, E., 2007. Estimating the contribution of organic bases from microalgae to the titration alkalinity in coastal seawaters. *Limnol. Oceanogr. Methods* 5, 225–232.
- Hertkorn, N., Benner, R., Frommberger, M., Schmitt-Kopplin, P., Witt, M., Kaiser, K., Ketrup, A., Hedges, J.I., 2006. Characterization of a major refractory component of marine dissolved organic matter. *Geochim. Cosmochim. Acta* 70, 2990–3010.
- Hertkorn, N., Harir, M., Koch, B.P., Michalke, B., Schmitt-Kopplin, P., 2013. High-field NMR spectroscopy and FTICR mass spectrometry: powerful discovery tools for the molecular level characterization of marine dissolved organic matter. *Biogeosciences* 10, 1583–1624.
- Heuer, R.M., Grosell, M., 2014. Physiological impacts of elevated carbon dioxide and ocean acidification on fish. *Am. J. Physiol. Integr. Comp. Physiol.* 307, R1061–R1084.
- Holm, S., 1979. A simple sequentially rejective multiple test procedure. *Scand. J. Stat.* 6, 65–70.
- Honjo, S., Erez, J., 1978. Dissolution rates of calcium carbonate in the deep ocean; an in-situ experiment in the North Atlantic Ocean. *Earth Planet. Sci. Lett.* 40, 287–300.
- Hoppe, C.J.M., Langer, G., Rokitta, S.D., Wolf-Gladrow, D.A., Rost, B., 2012. Implications of observed inconsistencies in carbonate chemistry measurements for ocean acidification studies. *Biogeosciences* 9, 2401–2405.
- Hruška, J., Köhler, S., Laudon, H., Bishop, K., 2003. Is a universal model of organic acidity possible: Comparison of the acid/base properties of dissolved organic carbon in the boreal and temperate zones. *Environ. Sci. Technol.* 37, 1726–1730.
- Hu, Y.-B., Liu, C.-Y., Yang, G.-P., Zhang, H.-H., 2015. The response of the carbonate system to a green algal bloom during the post-bloom period in the southern Yellow Sea. *Cont. Shelf Res.* 94, 1–7.
- Hudson-Heck, E.E., Byrne, R.H., 2019. Purification and characterization of thymol blue for

- spectrophotometric pH measurements in rivers, estuaries, and oceans. *Anal. Chim. Acta* 1090, 91–99.
- Humphreys, M.P., Daniels, C.J., Wolf-Gladrow, D.A., Tyrrell, T., Achterberg, E.P., 2018. On the influence of marine biogeochemical processes over CO₂ exchange between the atmosphere and ocean. *Mar. Chem.* 199, 1–11.
- Ilyina, T., Zeebe, R.E., Maier-Reimer, E., Heinze, C., 2009. Early detection of ocean acidification effects on marine calcification. *Global Biogeochem. Cycles* 23, GB1008.
- IPCC, 2013. *Climate Change 2013: The Physical Science Basis. Contribution of Working Group I to the Fifth Assessment Report of the Intergovernmental Panel on Climate Change.* Cambridge University Press, Cambridge, U.K. and New York, NY, U.S.A.
- IPCC, 2014. *Climate Change 2014: Impacts, adaptation, and vulnerability. Part A: global and sectoral aspects. Contribution of Working Group II to the fifth assessment report of the Intergovernmental Panel on Climate Change.* Cambridge University Press, Cambridge, U.K. and New York, NY, U.S.A.
- Ito, T., Minobe, S., Long, M.C., Deutsch, C., 2017. Upper ocean O₂ trends: 1958–2015. *Geophys. Res. Lett.* 44, 4214–4223.
- Jiang, L.Q., Carter, B.R., Feely, R.A., Lauvset, S.K., Olsen, A., 2019. Surface ocean pH and buffer capacity: past, present and future. *Sci. Rep.* 9, 1–11.
- Johansson, O., Wedborg, M., 1982. On the evaluation of potentiometric titrations of seawater with hydrochloric acid. *Oceanol. Acta* 5, 209–218.
- Johnson, K.M., King, A.E., Sieburth, J.M., 1985. Coulometric TCO₂ analyses for marine studies; an introduction. *Mar. Chem.* 16, 61–82.
- Johnson, K.M., Sieburth, J.McN., Williams, P.J.leB., Brändström, L., 1987. Coulometric total carbon dioxide analysis for marine studies: automation and calibration. *Mar. Chem.* 21, 117–133.
- Johnson, K.M., Wills, K.D., Butler, D.B., Johnson, W.K., Wong, C.S., 1993. Coulometric total carbon dioxide analysis for marine studies: maximizing the performance of an automated gas extraction system and coulometric detector. *Mar. Chem.* 44, 167–187.
- Johnson, K.S., Claustre, H., 2016. Bringing biogeochemistry into the Argo age. *Eos*, 97.
- Johnson, K.S., Coletti, L.J., 2002. In situ ultraviolet spectrophotometry for high resolution and long-term monitoring of nitrate, bromide and bisulfide in the ocean. *Deep-Sea Res. Part I: Oceanogr. Res. Pap.* 49, 1291–1305.
- Johnson, K.S., Coletti, L.J., Jannasch, H.W., Sakamoto, C.M., Swift, D.D., Riser, S.C., 2013. Long-term nitrate measurements in the ocean using the In Situ Ultraviolet Spectrophotometer: sensor integration into the Apex profiling float. *J. Atmos. Oceanic Technol.* 30, 1854–1866.
- Johnson, K.S., Plant, J.N., Coletti, L.J., Jannasch, H.W., Sakamoto, C.M., Riser, S.C., Swift, D.D., Williams, N.L., Boss, E., Haëntjens, N., Talley, L.D., Sarmiento, J.L., 2017a. Biogeochemical sensor performance in the SOCCOM profiling float array. *J. Geophys. Res.: Oceans* 122, 6416–6436.
- Johnson, K.S., Plant, J.N., Dunne, J.P., Talley, L.D., Sarmiento, J.L., 2017b. Annual nitrate drawdown observed by SOCCOM profiling floats and the relationship to annual net community production. *J. Geophys. Res.: Oceans* 122, 6668–6683.
- Johnson, K.S., Riser, S.C., Karl, D.M., 2010. Nitrate supply from deep to near-surface waters of the North Pacific subtropical gyre. *Nature* 465, 1062–1065.
- Jones, D. L. 2017 *Fathom Toolbox for MATLAB: software for multivariate ecological and*

- oceanographic data analysis. College of Marine Science, University of South Florida, St. Petersburg, FL, USA. Available from: <https://www.usf.edu/marine-science/research/matlab-resources/index.aspx/>
- Jones, S.D., Le Quéré, C., Rödenbeck, C., Manning, A.C., Olsen, A., 2015. A statistical gap-filling method to interpolate global monthly surface ocean carbon dioxide data, *J. Adv. Model. Earth Syst.* 7, 1554–1575.
- Keir, R.S., 1980. The dissolution kinetics of biogenic calcium carbonates in seawater. *Geochim. Cosmochim. Acta* 44, 241–252.
- Key, R.M., Kozyr, A., Sabine, C.L., Lee, K., Wanninkhof, R., Bullister, J.L., Feely, R.A., Millero, F.J., Mordy, C., Peng, T.-H., 2004. A global ocean carbon climatology: Results from Global Data Analysis Project (GLODAP), *Global Biogeochem. Cycles* 18, GB4031.
- Kim, H.C., Lee, K., 2009. Significant contribution of dissolved organic matter to seawater alkalinity. *Geophys. Res. Lett.* 36, 1–5.
- Kleypas, J.A., Buddemeier, R.W., Archer, D., Gattuso, J.-P., Langdon, C., Opdyke, B.N., 1999. Geochemical consequences of increased atmospheric carbon dioxide on coral reefs. *Science* 284, 118–120.
- Ko, Y.H., Lee, K., Eom, K.H., Han, I.S., 2016. Organic alkalinity produced by phytoplankton and its effect on the computation of ocean carbon parameters. *Limnol. Oceanogr.* 61, 1462–1471.
- Koeve, W., Oschlies, A., 2012. Potential impact of DOM accumulation on $f\text{CO}_2$ and carbonate ion computations in ocean acidification experiments. *Biogeosciences* 9, 3787–3798.
- Koopal, L.K., Saito, T., Pinheiro, J.P., van Riemsdijk, W.H., 2005. Ion binding to natural organic matter: general considerations and the NICA-Donnan model. *Colloids Surf. A: Physicochem. Eng. Asp.* 265, 40–54.
- Kuliński, K., Schneider, B., Hammer, K., Machulik, U., Schulz-Bull, D., 2014. The influence of dissolved organic matter on the acid-base system of the Baltic Sea. *J. Mar. Syst.* 132, 106–115.
- Kwiatkowski, L., Orr, J.C., 2018. Diverging seasonal extremes for ocean acidification during the twenty-first century. *Nat. Clim. Change* 8, 141–145.
- Langdon, C., Atkinson, M.J., 2005. Effect of elevated $p\text{CO}_2$ on photosynthesis and calcification of corals and interactions with seasonal change in temperature/irradiance and nutrient enrichment. *J. Geophys. Res.* 110, C9.
- Langdon, C., Takahashi, T., Sweeney, C., Chipman, D., Goddard, J., 2000. Effect of calcium carbonate saturation state on the calcification rate of an experimental coral reef. *Global Biogeochem. Cycles* 14, 639–654.
- Lauvset, S.K., Gruber, N., Landschützer, P., Olsen, A., Tjiputra, J., 2015. Trends and drivers in global surface ocean pH over the past 3 decades. *Biogeosciences* 12, 1285–1298.
- Le Quéré, C., Andrew, R.M., Friedlingstein, P., Sitch, S., Pongratz, J., Manning, A.C., Korsbakken, J.I., Peters, G.P., Canadell, J.G., Jackson, R.B., Boden, T.A., Tans, P.P., Andrews, O.D., Arora, V.K., Bakker, D.C.E., Barbero, L., Becker, M., Betts, R.A., Bopp, L., Chevallier, F., Chini, L.P., Ciais, P., Cosca, C.E., Cross, J., Currie, K., Gasser, T., Harris, I., Hauck, J., Haverd, V., Houghton, R.A., Hunt, C.W., Hurtt, G., Ilyina, T., Jain, A.K., Kato, E., Kautz, M., Keeling, R.F., Goldewijk, K.K., Körtzinger, A., Landschützer, P., Lefèvre, N., Lenton, A., Lienert, S., Lima, I., Lombardozi, D., Metzl, N., Millero, F., Monteiro, P.M.S., Munro, D.R., Nabel, J.E.M.S., Nakaoka, S., Nojiri, Y., Padin, X.A., Peregón, A., Pfeil, B., Pierrot, D., Poulter, B., Rehder, G., Reimer, J., Rödenbeck, C.,

- Schwinger, J., Séférian, R., Skjelvan, I., Stocker, B.D., Tian, H., Tilbrook, B., Tubiello, F.N., van der Laan-Luijckx, I.T., van der Werf, G.R., van Heuven, S., Viovy, N., Vuichard, N., Walker, A.P., Watson, A.J., Wiltshire, A.J., Zaehle, S., Zhu, D., 2018. Global carbon budget 2017. *Earth Syst. Sci. Data* 10, 405–448.
- Lee, K., Kim, T.W., Byrne, R.H., Millero, F.J., Feely, R.A., Liu, Y.M., 2010. The universal ratio of boron to chlorinity for the North Pacific and North Atlantic oceans. *Geochim. Cosmochim. Acta* 74, 1801–1811.
- Lee, K., Lee, C.-H., Lee, J.-H., Han, I.-S., & Kim, M., 2019. Deviation of boron concentration from predictions using salinity in coastal environments. *Geophys. Res. Lett.* 46, 4809–4815.
- Lee, K., Millero, F.J., Byrne, R.H., Feely, R.A., Wanninkhof, R., 2000. The recommended dissociation constants for carbonic acid in seawater. *Geophys. Res. Lett.* 27, 229–232.
- Lee, K., Tong, L.T., Millero, F.J., Sabine, C.L., Dickson, A.G., Goyet, C., Park, G.H., Wanninkhof, R., Feely, R.A. Key, R.M., 2006. Global relationships of total alkalinity with salinity and temperature in surface waters of the world's oceans. *Geophys. Res. Lett.* 33, L19605.
- Lewis, E., Wallace, D.W.R., 1998. CO2SYS-Program developed for the CO₂ system calculations. ORNL/CDIAC-105, Carbon Dioxide Information Analysis Center, Oak Ridge National Laboratory. US DoE, Oak Ridge, TN.
- Liu, X., Byrne, R.H., Adornato, L., Yates, K.K., Kaltenbacher, E., Ding, X., Yang, B., 2013. In situ spectrophotometric measurement of dissolved inorganic carbon in seawater. *Environ. Sci. Technol.* 47, 11106–11114.
- Liu, X., Byrne, R.H., Lindemuth, M., Easley, R., Mathis, J.T., 2015. An automated procedure for laboratory and shipboard spectrophotometric measurements of seawater alkalinity: Continuously monitored single-step acid additions. *Mar. Chem.* 174, 141–146.
- Liu, X., Patsavas, M.C., Byrne, R.H., 2011. Purification and characterization of meta-cresol purple for spectrophotometric seawater pH measurements. *Environ. Sci. Technol.* 45, 4862–4868.
- Liu, Y.-M., Lee, K., 2009. Modifications of the curcumin method enabling precise and accurate measurement of seawater boron concentration. *Mar. Chem.* 115, 110–117.
- Long, M.C., Deutsch, C., Ito, T., 2016. Finding forced trends in oceanic oxygen. *Global Biogeochem. Cycles* 30, 381–397.
- Longnecker, K., Kujawinski, E.B., 2017. Mining mass spectrometry data: Using new computational tools to find novel organic compounds in complex environmental mixtures. *Org. Geochem.* 110, 92–99.
- Lueker, T.J., Dickson, A.G., Keeling, C.D., 2000. Ocean *p*CO₂ calculated from dissolved inorganic carbon, alkalinity, and equations for *K*₁ and *K*₂: validation based on laboratory measurements of CO₂ in gas and seawater at equilibrium. *Mar. Chem.* 70, 105–119.
- Martz, T.R., Carr, J.J., French, C.R. DeGrandpre, M.D., 2003. A submersible autonomous sensor for spectrophotometric pH measurements of natural waters. *Anal. Chem.* 75, 1844–1850.
- Mathis, J.T., Cooley, S.R., Lucey, N., Colt, S., Ekstrom, J., Hurst, T., Hauri, C., Evans, W., Cross, J.N., Feely, R.A., 2015. Ocean acidification risk assessment for Alaska's fishery sector. *Prog. Oceanogr.* 136, 71–91.
- Mackin, J.E., 1986. The free-solution diffusion coefficient of boron: Influence of dissolved organic matter. *Mar. Chem.* 20, 131–140.
- Matthews, H.D., Gillett, N.P., Stott, P.A., Zickfeld, K., 2009. The proportionality of global warming to cumulative carbon emissions. *Nature* 459, 829–832.

- Mayot, N., Matrai, P., Ellingsen, I.H., Steele, M., Johnson, K., Riser, S.C., Swift, D., 2018. Assessing phytoplankton activities in the seasonal ice zone of the Greenland Sea over an annual cycle. *J. Geophys. Res.: Oceans* 123, 8004–8025.
- McElligott, S., Byrne, R.H., 1998. Interaction of $B(OH)_3^0$ and HCO_3^- in seawater: formation of $B(OH)_2CO_3^-$. *Aquat. Geochem.* 3, 345–356.
- McElligott, S., Byrne, R.H., Lee, K., Wanninkhof, R., Millero, F.J., Feely, R.A., 1998. Discrete water column measurements of CO_2 fugacity and pH_T in seawater: A comparison of direct measurements and thermodynamic calculations. *Mar. Chem.* 60, 63–73.
- Medeiros, P.M., Seidel, M., Niggemann, J., Spencer, R.G.M., Hernes, P.J., Yager, P.L., Miller, W.L., Dittmar, T., Hansell, D.A., 2016. A novel molecular approach for tracing terrigenous dissolved organic matter into the deep ocean, *Global Biogeochem. Cycles* 30, 689–699.
- Meinig, C., Burger, E.F., Cohen, N., Coker, E.D., Cronin, M.F., Cross, J.N., De Halleux, S., Jenkins, R., Jessup, A.T., Lawrence-Slavas, N., Sutton, A.J., 2019. Public Private Partnerships to Advance Regional Ocean Observing Capabilities: A Saildrone and NOAA-PMEL Case Study and Future Considerations to Expand to Global Scale Observing. *Frontiers Mar. Sci.* 6, 448.
- Michałowski, T., Asuero, A.G., 2012. New approaches in modeling carbonate alkalinity and total alkalinity. *Crit. Rev. Anal. Chem.* 42, 220–244.
- Millero, F., 1979. The thermodynamics of the carbonate system in seawater. *Geochim. Cosmochim. Acta* 43, 1651–1661.
- Millero, F.J., 1995. Thermodynamics of the carbon dioxide system in the oceans. *Geochim. Cosmochim. Acta* 59, 661–677.
- Millero, F.J., 2010. Carbonate constants for estuarine waters. *Mar. Freshw. Res.* 61, 139–142.
- Millero, F.J., Feistel, R., Wright, D.G., McDougall, T.J., 2008. The composition of Standard Seawater and the definition of the Reference-Composition Salinity Scale. *Deep Sea Res.* 55, 50–72.
- Millero, F.J., Lee, K., Roche, M., 1998. Distribution of alkalinity in the surface waters of the major oceans. *Mar. Chem.* 60, 111–130.
- Millero, F.J., Pierrot, D., Lee, K., Wanninkhof, R., Feely, R., Sabine, C.L., Key, R.M., Takahashi, T., 2002. Dissociation constants for carbonic acid determined from field measurements. *Deep-Sea Res. I* 49, 1705–1723.
- Millero, F.J., Plese, T., Fernandez, M., 1988. The dissociation of hydrogen sulfide in seawater. *Limnol. Oceanogr.* 33, 269–274.
- Millero, F.J., Zhang, J.Z., Lee, K., Campbell, D.M., 1993. Titration alkalinity of seawater. *Mar. Chem.* 44, 153–165.
- Milne, C.J., Kinniburgh, D.G., Tipping, E., 2001. Generic NICA-Donnan model parameters for proton binding by humic substances. *Environ. Sci. Technol.* 35, 2049–2059.
- Mojica Prieto, F.J., Millero, F.J., 2002. The values of $pK_1 + pK_2$ for the dissociation of carbonic acid in seawater. *Geochim. Cosmochim. Acta* 66, 2529–2540.
- Moore, J.K., Fu, W., Primeau, F., Britten, G.L., Lindsay, K., Long, M., Doney, S.C., Mahowald, N., Hoffman, F., Randerson, J.T., 2018. Sustained climate warming drives declining marine biological productivity. *Science* 359, 1139–1143.
- Morris, A.W., Riley, J.P., 1966. The bromide/chlorinity and sulphate/chlorinity ratio in sea water. *Deep-Sea Res.* 13, 699–705.

- Morse, J.W., 1978. Dissolution kinetics of calcium carbonate in sea water; VI, The near-equilibrium dissolution kinetics of calcium carbonate-rich deep sea sediments. *Am. J. Sci.* 278, 344–355.
- Morse, J.W., Arvidson, R.S., 2002. The dissolution kinetics of major sedimentary carbonate minerals. *Earth-Sci. Rev.* 58, 51–84.
- Mosley, L.M., Husheer, S.L.G., Hunter, K.A., 2004. Spectrophotometric pH measurement in estuaries using thymol blue and m-cresol purple. *Mar. Chem.* 91, 175–186.
- Mucci, A., 1983. The solubility of calcite and aragonite in seawater at various salinities, temperatures, and one atmosphere total pressure. *Am. J. Sci.* 283, 780–799.
- Muller, F.L.L., Bleie, B., 2008. Estimating the organic acid contribution to coastal seawater alkalinity by potentiometric titrations in a closed cell. *Anal. Chim. Acta* 619, 183–191.
- Munday, P.L., Cheal, A.J., Dixon, D.L., Rummer, J.L., Fabricius, K.E., 2014. Behavioural impairment in reef fishes caused by ocean acidification at CO₂ seeps. *Nat. Clim. Chang.* 4, 487–492.
- Munday, P.L., Dixon, D.L., Donelson, J.M., Jones, G.P., Pratchett, M.S., Devitsina, G. V., Døving, K.B., 2009. Ocean acidification impairs olfactory discrimination and homing ability of a marine fish. *Proc. Natl. Acad. Sci. U.S.A.* 106, 1848–52.
- Nadella, S.R., Tellis, M., Diamond, R., Smith, S., Bianchini, A., Wood, C.M., 2013. Toxicity of lead and zinc to developing mussel and sea urchin embryos: Critical tissue residues and effects of dissolved organic matter and salinity. *Comp. Biochem. Physiol. C* 158, 72–83.
- Naviaux, J.D., Subhas, A.V., Dong, S., Rollins, N.E., Liu, X., Byrne, R.H., Berelson, W.M., Adkins, J.F., 2019a. Calcite dissolution rates in seawater: Lab vs. *in-situ* measurements and inhibition by organic matter. *Mar. Chem.* 215, 103684.
- Naviaux, J.D., Subhas, A.V., Rollins, N.E., Dong, S., Berelson, W.M., Adkins, J.F., 2019b. Temperature dependence of calcite dissolution kinetics in seawater. *Geochim. Cosmochim. Acta* 246, 363–384.
- Newton, J.A., Feely, R.A., Jewett, E.B., Williamson, P., Mathis, J., 2014. Global ocean acidification observing network: Requirements and governance plan. GOA-ON. http://www.goa-on.org/docs/GOA-ON_plan_print.pdf.
- Oliver, B.G., Thurman, E.M., Malcolm, R.L., 1983. The contribution of humic substances to the acidity of colored natural waters. *Geochim. Cosmochim. Acta* 47, 2031–2035.
- Olsen, A., Lange, N., Key, R.M., Tanhua, T., Álvarez, M., Becker, S., Bittig, H., Carter, B., Da Cunha, L.C., Feely, R., Van Heuven, S., Hoppema, M., Ishii, M., Jeansson, E., Jones, S.D., Jutterström, S., Karlsen, M.K., Kozyr, A., Lauvset, S.K., Lo Monaco, C., Murata, A., Pérez, F.F., Pfeil, B., Schirnack, C., Steinfeldt, R., Suzuki, T., Telszewski, M., Tilbrook, B., Velo, A., Wanninkhof, R., 2019. GLODAPv2.2019: An update of GLODAPv2. *Earth Syst. Sci. Data* 11, 1437–1461.
- Olsen, A., Lange, N., Key, R.M., Tanhua, T., Bittig, H.C., Kozyr, A., Álvarez, M., Azetsu-Scott, K., Becker, S., Brown, P.J., Carter, B.R., Cotrim da Cunha, L., Feely, R.A., van Heuven, S., Hoppema, M., Ishii, M., Jeansson, E., Jutterström, S., Landa, C.S., Lauvset, S.K., Michaelis, P.M., Murata, A., Pérez, F.F., Pfeil, B., Schirnack, C., Steinfeldt, R., Suzuki, T., Tilbrook, B., Velo, A., Wanninkhof, R., Woosley, R.J., 2020. GLODAPv2. 2020 – the second update of GLODAPv2. *Earth Syst. Sci. Data Discuss.* 1–41.
- Orr, J.C., Epitalon, J., Dickson, A.G., Gattuso, J., 2018. Routine uncertainty propagation for the marine carbon dioxide system. *Mar. Chem.* 207, 84–107.
- Orr, J.C., Fabry, V.J., Aumont, O., Bopp, L., Doney, S.C., Feely, R.A., Gnanadesikan, A.,

- Gruber, N., Ishida, A., Joos, F., Key, R.M., Lindsay, K., Maier-Reimer, E., Matear, R., Monfray, P., Mouchet, A., Najjar, R.G., Plattner, G.K., Rodgers, K.B., Sabine, C.L., Sarmiento, J.L., Schlitzer, R., Slater, R.D., Totterdell, I.J., Weirig, M.F., Yamanaka, Y., Yool, A., 2005. Anthropogenic ocean acidification over the twenty-first century and its impact on calcifying organisms. *Nature* 437, 681–686.
- Park, P.K., 1969. Oceanic CO₂ system: An evaluation of ten methods of investigation. *Limnol. Oceanogr.* 14 (2), 179–186.
- Patsavas, M.C., Byrne, R.H., Yang, B., Easley, R.A., Wanninkhof, R., Liu, X., 2015a. Procedures for direct spectrophotometric determination of carbonate ion concentrations: Measurements in US Gulf of Mexico and East Coast waters. *Mar. Chem.* 168, 80–85.
- Patsavas, M.C., Byrne, R.H., Wanninkhof, R., Feely, R.A., Cai, W.J., 2015b. Internal consistency of marine carbonate system measurements and assessments of aragonite saturation state: insights from two U.S. coastal cruises. *Mar. Chem.* 176, 9–20.
- Paxeus, N., Wedborg, M., 1985. Acid–base properties of aquatic fulvic acid. *Anal. Chim. Acta* 169, 87–98.
- Perdue, E.M., Lytle, C.R., 1983. Distribution model for binding of protons and metal ions by humic substances. *Environ. Sci. Technol.* 17, 654–660.
- Perdue, E.M., Reuter, J.H., Parrish, R.S., 1984. A statistical model of proton binding by humus. *Geochim. Cosmochim. Acta* 48, 1257–1263.
- Pfeil, B., Olsen, A., Bakker, D.C., Hankin, S., Koyuk, H., Kozyr, A., Malczyk, J., Manke, A., Metzl, N., Sabine, C.L., Akl, J., et al., 2013. A uniform, quality controlled Surface Ocean CO₂ Atlas (SOCAT). *Earth Syst. Sci. Data* 5, 125–143.
- Pierrot, D., Lewis, E., Wallace, D.W.R. MS Excel program developed for CO₂ System Calculations. ORNL/CDIAC-105. Carbon Dioxide Information Analysis Center, Oak Ridge National Laboratory, U.S. Department of Energy: Oak Ridge, TN, 2006.
- Plant, J.N., Johnson, K.S., Sakamoto, C.M., Jannasch, H.W., Coletti, L.J., Riser, S.C., Swift, D.D., 2016. Net community production at Ocean Station Papa observed with nitrate and oxygen sensors on profiling floats. *Global Biogeochem. Cycles* 30, 859–879.
- Porzio, L., Buia, M.C., Hall-Spencer, J.M., 2011. Effects of ocean acidification on macroalgal communities. *J. Exp. Mar. Bio. Ecol.* 400, 278–287.
- Raimondi, L., Matthews, J.B.R., Atamanchuk, D., Azetsu-Scott, K., Wallace, D.W.R., 2019. The internal consistency of the marine carbon dioxide system for high latitude shipboard and *in situ* monitoring. *Mar. Chem.* 213, 49–70.
- Ramanathan, V., 1988. The greenhouse theory of climate change: A test by an inadvertent global experiment. *Science* 240, 293–299.
- Repeta, D.J., 2015. Chemical characterization and cycling of dissolved organic matter, in: Hansell, D.A., Carlson, C.A. (Eds.), *Biogeochemistry of Marine Dissolved Organic Matter*. Academic Press, pp. 21–63.
- Ridgwell, A., Zondervan, I., Hargreaves, J.C., Bijma, J., Lenton, T.M., 2007. Assessing the potential long-term increase of oceanic fossil fuel CO₂ uptake due to CO₂-calcification feedback. *Biogeosciences* 4, 481–492.
- Riebesell, U., Zondervan, I., Rost, B., Tortell, P.D., Zeebe, R.E., Morel, F.M.M., 2000. Reduced calcification of marine plankton in response to increased atmospheric CO₂. *Nature* 407, 2–5.
- Rigobello-Masini, M., Masini, J.C., 2001. Application of modified Gran functions and derivative methods to potentiometric acid titration studies of the distribution of inorganic carbon species in cultivation medium of marine microalgae. *Anal. Chim. Acta* 448, 239–250.

- Riley, J.P., 1965. The occurrence of anomalously high fluoride concentrations in the North Atlantic, in: *Deep Sea Research and Oceanographic Abstracts.*: pp. 219–220.
- Riley, J.P., Tongudai, M., 1967. The major cation/chlorinity ratios in seawater. *Chem. Geol.* 2, 263–269.
- Riser, S.C., Freeland, H.J., Roemmich, D., Wijffels, S., Troisi, A., Belbéoch, M., Gilbert, D., Xu, J., Pouliquen, S., Thresher, A., Le Traon, P.Y., 2016. Fifteen years of ocean observations with the global Argo array. *Nat. Clim. Change* 6, 145–153.
- Ritchie, J.D., Perdue, E.M., 2003. Proton-binding study of standard and reference fulvic acids, humic acids, and natural organic matter. *Geochim. Cosmochim. Acta* 67, 85–93.
- Robert-Baldo, G.L., Morris, M.J., Byrne, R.H., 1985. Spectrophotometric determination of seawater pH using phenol red. *Anal. Chem.* 57, 2564–2567.
- Roemmich D., Alford, M.H., Claustre, H., Johnson, K., King, B., Moum, J., Oke, P., Owens, W.B., Pouliquen, S., Purkey, S., Scanderbeg, M., Suga, T., Wijffels, S., Zilberman, N., Bakker, D., Baringer, M., Belbeoch, M., Bittig, H.C., Boss, E., Calil, P., Carse, F., Carval, T., Chai, F., Conchubhair, D.Ó., d’Ortenzio, F., Dall’Olmo, G., Desbruyeres, D., Fennel, K., Fer, I., Ferrari, R., Forget, G., Freeland, H., Fujiki, T., Gehlen, M., Greenan, B., Hallberg, R., Hibiya, T., Hosoda, S., Jayne, S., Jochum, M., Johnson, G.C., Kang, K., Kolodziejczyk, N., Körtzinger, A., Le Traon, P.-Y., Lenn, Y.-D., Maze, G., Mork, K.A., Morris, T., Nagai, T., Nash, J., Naveira Garabato, A., Olsen, A., Pattabhi, R.R., Prakash, S., Riser, S., Schmechtig, C., Schmid, C., Shroyer, E., Sterl, A., Sutton, P., Talley, L., Tanhua, T., Thierry, V., Thomalla, S., Toole, J., Troisi, A., Trull, T.W., Turton, J., Velez-Belchi, P.J., Walczowski, W., Wang, H., Wanninkhof, R., Waterhouse, A.F., Waterman, S., Watson, A., Wilson, C., Wong, A.P.S., Xu, J., Yasuda, I., 2019. On the Future of Argo: A Global, Full-Depth, Multi-Disciplinary Array. *Front. Mar. Sci.* 6, 439.
- Roleda, M.Y., Hurd, C.L., 2012. Seaweed responses to ocean acidification. *Seaweed Biol.* 407–431.
- Rudnick, D.L., 2016. Ocean research enabled by underwater gliders. *Annu. Rev. Mar. Sci.* 8, 519–541.
- Sabine, C.L., Feely, R.A., Gruber, N., Key, R.M., Lee, K., Bullister, J.L., Wanninkhof, R., Wong, C.S., Wallace, D.W.R., Tilbrook, B., Millero, F.J., Peng, T.-H., Kozyr, A., Ono, T., Rios, A.F., 2004. The oceanic sink for anthropogenic CO₂. *Science*, 305, 367–371.
- Sabine, C.L., Feely, R.A., Millero, F.J., Dickson, A.G., Langdon, C., Mecking, S., Greeley, D., 2008. Decadal changes in Pacific carbon. *J. Geophys. Res.* 113, C07021.
- Sabine, C., Key, R.M., Kozyr, A., Feely, R.A., Wanninkhof, R., Millero, F.J., Peng, T.-H., Bullister, J.L., Lee, K., 2005. Global Ocean Data Analysis Project (GLODAP): Results and Data, ORNL/CDIAC-145, NDP-083, Carbon Dioxide Information Analysis Center, Oak Ridge National Laboratory, U.S. Department of Energy, Oak Ridge, TN, U.S.A.
- Salt, L.A., Thomas, H., Bozec, Y., Borges, A.V., de Baar, H.J.W., 2016. The internal consistency of the North Sea carbonate system. *J. Mar. Syst.* 157, 52–64.
- Sarmiento, J.L., Gruber, N., 2006. *Ocean Biogeochemical Dynamics*. Princeton University Press, Princeton, NJ.
- Sauzède, R., Bittig, H.C., Claustre, H., Pasqueron de Fommervault, O., Gattuso, J.P., Legendre, L., Johnson, K.S., 2017. Estimates of water-column nutrient concentrations and carbonate system parameters in the global ocean: a novel approach based on neural networks. *Frontiers Mar. Sci.* 4, 128.
- Schmidtko, S., Stramma, L., Visbeck, M., 2017. Decline in global oceanic oxygen content during

- the past five decades. *Nature* 542, 335–339.
- Shangguan, Q., Shu, H., Li, P., Lin, K., Byrne, R.H., Li, Q., Yuan, D., Ma, J., 2019. Automated spectrophotometric determination of carbonate ion concentration in seawater using a portable syringe pump based analyzer. *Mar. Chem.* 209, 120–127.
- Sharp, J.D., Byrne, R.H., 2020. Interpreting measurements of total alkalinity in marine and estuarine waters in the presence of proton-binding organic matter. *Deep Sea Res. Part I: Oceanogr. Res. Pap.*, 103338.
- Sharp, J.D., Pierrot, D., Humphreys, M.P., Epitalon, J.-M., Orr, J.C., Lewis, E.R., Wallace, D.W.R., 2020 (September 10). CO2SYSv3 for MATLAB (Version 3.1). Zenodo. <http://doi.org/10.5281/zenodo.4023039>
- Sharp, J.D., Byrne, R.H., 2019. Carbonate ion concentrations in seawater: Spectrophotometric determination at ambient temperatures and evaluation of propagated calculation uncertainties. *Mar. Chem.* 209, 70–80.
- Sharp, J.D., Byrne, R.H. Technical note: Excess alkalinity in carbonate system reference materials. In revision for *Mar. Chem.*
- Sharp, J.D., Byrne, R.H., Liu, X., Feely, R.A., Cuyler, E.E., Wanninkhof, R., Alin, S.R., 2017. Spectrophotometric determination of carbonate ion concentrations: Elimination of instrument-dependent offsets and calculation of in situ saturation states. *Environ. Sci. Technol.* 51, 9127–9136.
- Sipos, P., May, P.M., Hefter, G.T., 2000. Carbonate removal from concentrated hydroxide solutions. *Analyst* 125, 955–958.
- Soli, A. L., Stewart, Z. I., Byrne, R. H., 2008. The influence of temperature on PbCO_3^0 formation in seawater. *Mar. Chem.* 110, 1–6.
- Solomon, S., Plattner, G.-K., Knutti, R., Friedlingstein, P., 2009. Irreversible climate change due to carbon dioxide emissions. *Proceedings of the National Academy of Sciences* 106, 1704–1709.
- Speer, K.G., Schulze, L.M., Swift, J.H., Wanninkhof, R., Feely, R.A., Millero, F.J., Rodriguez, C., Carlson, C.A., Key, R.M., McNichol, A., Fine, R.A., Boss, E., Riser, S.C., 2018. Carbon dioxide, hydrographic, and chemical discrete profile data obtained during the R/V N.B. Palmer cruise in the South Pacific Ocean on GO-SHIP/CLIVAR/SOCCOM Repeat Hydrography Section P06E (EXPCODE 320620170820) from 2017-08-20 to 2017-09-30 (NCEI Accession 0175744). NOAA National Centers for Environmental Information.
- Steller, D.L., Hernández-Ayón, J.M., Riosmena-Rodríguez, R., Cabello-Pasini, A., 2007. Effect of temperature on photosynthesis, growth and calcification rates of the free-living coralline alga *Lithophyllum margaritae*. *Ciencias Mar.* 33, 441–456.
- Subhas, A.V., Adkins, J.F., Rollins, N.E., Naviaux, J., Erez, J., Berelson, W.M., 2017. Catalysis and chemical mechanisms of calcite dissolution in seawater. *Proc. Natl. Acad. Sci.* 114, 8175–8180.
- Subhas, A.V., Rollins, N.E., Berelson, W.M., Dong, S., Erez, J., Adkins, J.F., 2015. A novel determination of calcite dissolution kinetics in seawater. *Geochim. Cosmochim. Acta* 170, 51–68.
- Subhas, A.V., Rollins, N.E., Berelson, W.M., Erez, J., Ziveri, P., Langer, G., Adkins, J.F., 2018. The dissolution behavior of biogenic calcites in seawater and a possible role for magnesium and organic carbon. *Mar. Chem.* 205, 100–112.
- Sunda, W.G., Cai, W.J., 2012. Eutrophication induced CO_2 -acidification of subsurface coastal waters: interactive effects of temperature, salinity, and atmospheric pCO_2 . *Environ. Sci.*

- Technol. 46, 10651–10659.
- Sutton, A.J., Sabine, C.L., Feely, R.A., Cai, W.-J., Cronin, M.F., McPhaden, M.J., Morell, J.M., Newton, J.A., Noh, J.-H., Ólafsdóttir, S.R., Salisbury, J.E., Send, U., Vandemark, D.C., Weller, R.A., 2016. Using present-day observations to detect when anthropogenic change forces surface ocean carbonate chemistry outside preindustrial bounds. *Biogeosciences* 13, 5065–5083.
- Sutton, A.J., Feely, R.A., Maenner-Jones, S., Musielwicz, S., Osborne, J., Dietrich, C., Monacci, N., Cross, J., Bott, R., Kozyr, A., Andersson, A.J., Bates, N.R., Cai, W., Cronin, M.F., De Carlo, E.H., Hales, B., Howden, S.D., Lee, C.M., Manzello, D.P., McPhaden, M.J., Meléndez, M., Mickett, J.B., Newton, J.A., Noakes, S.E., Noh, J.H., Ólafsdóttir, S.R., Salisbury, J.E., Send, U., Trull, T.W., Vandemark, D.C., Weller, R.A., 2019. Autonomous Seawater $p\text{CO}_2$ and pH Time Series From 40 Surface Buoys and the Emergence of Anthropogenic Trends. *Earth Syst. Sci. Data* 11, 421–439.
- Sutton, A.J., Sabine, C.L., Maenner-Jones, S., Lawrence-Slavas, N., Meinig, C., Feely, R.A., Mathis, J.T., Musielewicz, S., Bott, R., McLain, P.D., Fought, H.J., Kozyr, A., 2014. A high-frequency atmospheric and seawater $p\text{CO}_2$ data set from 14 open-ocean sites using a moored autonomous system. *Earth Syst. Sci. Data* 6, 353–366.
- Sutton, A.J., Wanninkhof, R., Sabine, C.L., Feely, R.A., Cronin, M.F., Weller, R.A., 2017. Variability and trends in surface seawater $p\text{CO}_2$ and CO_2 flux in the Pacific Ocean. *Geophys. Res. Lett.* 44, 5627–5636.
- Swift, J.H., 2008. A Guide to Submitting CTD/Hydrographic/Tracer Data and Associated Documentation to the CLIVAR and Carbon Hydrographic Data Office. Scripps Institution of Oceanography, University of California: San Diego, CA.
- Takahashi, T., Sutherland, S.C., Sweeney, C., Poisson, A., Metzl, N., Tilbrook, B., Bates, N., Wanninkhof, R., Feely, R.A., Sabine, C., Ólafsson, J., Nojiri, Y., 2002. Global sea-air CO_2 flux based on climatological surface ocean $p\text{CO}_2$, and seasonal biological and temperature effects. *Deep-Sea Res. Part II* 49, 1601–1622.
- Takahashi, T., Sutherland, S.C., Wanninkhof, R., Sweeney, C., Feely, R.A., Chipman, D.W., Hales, B., Friederich, G., Chavez, F., Sabine, C., Watson, A., Bakker, D.C.E., Schuster, U., Metzl, N., Yoshikawa-Inoue, H., Ishii, M., Midorikawa, T., Nojiri, Y., Körtzinger, A., Steinhoff, T., Hoppema, M., Ólafsson, J., Arnarson, T.S., Tilbrook, B., Johannessen, T., Olsen, A., Bellerby, R., Wong, C.S., Delille, B., Bates, N.R., de Baar, H., 2009. Climatological mean and decadal change in surface ocean $p\text{CO}_2$, and net sea-air CO_2 flux over the global oceans. *Deep-Sea Res. Part II* 56, 554–577.
- Talley, L.D., Feely, R.A., Sloyan, B.M., Wanninkhof, R., Baringer, M.O., Bullister, J.L., Carlson, C.A., Doney, S.C., Fine, R.A., Firing, E., Gruber, N., Hansell, D.A., Ishii, M., Johnson, G.C., Katsumata, K., Key, R.M., Kramp, M., Langdon, C., Macdonald, A.M., Mathis, J.T., McDonagh, E.L., Mecking, S., Millero, F.J., Mordy, C.W., Nakano, T., Sabine, C.L., Smethie, W.M., Swift, J.H., Tanhua, T., Thurnherr, A.M., Warner, M.J., Zhang, J.-Z., 2016. Changes in Ocean Heat, Carbon Content, and Ventilation: A Review of the First Decade of GO-SHIP Global Repeat Hydrography. *Annu. Rev. Mar. Sci.* 8, 185–215.
- Tipping, E., 1998. Humic ion-binding model VI: An improved description of the interactions of protons and metal ions with humic substances. *Aquat. Geochem.* 4, 3–48.
- Tipping, E., Hurley, M.A., 1992. A unifying model of cation binding by humic substances. *Geochim. Cosmochim. Acta* 56, 3627–3641.

- Tipping, E., Lofts, C.S., Sonke, J.E., 2011. Humic ion-binding model VII: a revised parameterisation of cation-binding by humic substances. *Environ. Chem.* 8, 225–235.
- Tipping, E., Woof, C., Hurley, M.A., 1991. Humic substances in acid surface waters; modelling aluminium binding, contribution to ionic charge-balance, and control of pH. *Water Res.* 25, 425–435.
- Tishchenko, P.Y., Wallmann, K., Vasilevskaya, N.A., Volkova, T.I., Zvalinskii, V.I., Khodorenko, N.D., Shkirnikova, E.M., 2006. The contribution of organic matter to the alkaline reserve of natural waters. *Oceanology* 46, 192–199.
- Travis, J.C., Acosta, J.C., Andor, G., Bastie, J., Blattner, P., Chunnillall, C.J., Crosson, S.C., Duewer, D.L., Early, E.A., Hengstberger, F., Kim, C.-S., Liedquist, L., Manoocheri, F., Mercader, F., Monard, L.A.G., Nevas, S., Mito, A., Nilsson, M., Noël, M., Rodriguez, A.C., Ruíz, A., Schirmacher, A., Smith, M.V., Valencia, G., van Tonder, N., Zwinkels, J., 2005. Intrinsic Wavelength Standard Absorption Bands in Holmium Oxide Solution for UV/visible Molecular Absorption Spectrophotometry. *J. Phys. Chem. Ref. Data* 34, 41–56.
- Uppström, L.R., 1968. A modified method for determination of boron with curcumin and a simplified water elimination procedure. *Anal. Chim. Acta* 43, 475–486.
- Uppström, L.R., 1974. The boron/chlorinity ratio of deep-sea water from the Pacific Ocean. *Deep-Sea Res.* 21, 161–162.
- Ulfso, A., Kuliński, K., Anderson, L.G., Turner, D.R., 2015. Modelling organic alkalinity in the Baltic Sea using a Humic-Pitzer approach. *Mar. Chem.* 168, 18–26.
- Van Heuven, S., Pierrot, D., Rae, J.W.B., Lewis, E., Wallace, D.W.R., 2011. CO2SYS v 1.1, MATLAB program developed for CO₂ system calculations. ORNL/CDIAC-105b, Carbon Dioxide Information Analysis Center, Oak Ridge National Laboratory. US DoE, Oak Ridge, TN.
- Venable, W.H., Jr., Eckerle, K.L., 1979. Didymium Glass Filters for Calibrating the Wavelength Scale of Spectrophotometers – SRM 2009, 2010, 2013, and 2014. NBS Special Publication 260–266, U.S. Department of Commerce, U.S. Government Printing Office: Washington DC.
- Volk, T., Hoffert, M.I., 1985. Ocean carbon pumps: analysis of relative strengths and efficiencies in ocean-driven atmospheric CO₂ changes. The carbon cycle and atmospheric CO₂: natural variations Archean to present 32, 99–110.
- Volkov, D.L., Wanninkhof, R., Feely, R.A., Millero, F.J., Hansell, D.A., Key, R.M., Bullister, J.L., McNichol, A., Baringer, M.O., Johnson, G.C., Langdon, C., Mordy, C., Zhang, J.-Z., 2019. Dissolved inorganic carbon (DIC), total alkalinity, pH on sea water scale and other hydrographic and chemical variables collected from discrete samples and profile observations during the NOAA Ship Ronald H. Brown cruise along the Global Ocean Ship-Based Hydrographic Investigation Program (GO-SHIP) Section I07N (EXPOCODE 33RO20180423) in the Indian Ocean from 2018-04-23 to 2018-06-06 (NCEI Accession 0189249). NOAA National Centers for Environmental Information.
- Waldbusser, G.G., Brunner, E.L., Haley, B.A., Hales, B., Langdon, C.J., Prahl, F.G., 2013. A developmental and energetic basis linking larval oyster shell formation to acidification sensitivity. *Geophys. Res. Lett.* 40, 2171–2176.
- Waldbusser, G.G., Hales, B., Haley, B.A., 2016. Calcium carbonate saturation state: on myths and this or that stories. *ICES J. Mar. Sci.* 73, 563–568.

- Waldbusser, G.G., Hales, B., Langdon, C.J., Haley, B.A., Schrader, P., Brunner, E.L., Gray, M.W., Miller, C.A., Gimenez, I., 2015. Saturation-state sensitivity of marine bivalve larvae to ocean acidification. *Nat. Clim. Change* 5, 273–280.
- Walter, L.M., Burton, E.A., 1986. The effect of orthophosphate on carbonate mineral dissolution rates in seawater. *Chem. Geol.* 56, 313–323.
- Wanninkhof, R., 1992. Relationship between wind speed and gas exchange over the ocean. *J. Geophys. Res.* 97, 7373–7382.
- Wanninkhof, R., Barbero, L., Byrne, R., Cai, W.-J., Huang, W.-J., Zhang, J.-Z., Baringer, M., Langdon, C., 2015. Ocean acidification along the Gulf Coast and East Coast of the USA. *Cont. Shelf. Res.* 98, 54–71.
- Wanninkhof, R., Doney, S.C., Bullister, J.L., Levine, N.M., Warner, M., Gruber, N., 2010. Detecting anthropogenic CO₂ changes in the interior Atlantic Ocean between 1989 and 2005. *J. Geophys. Res. Ocean.* 115, 1–25.
- Wanninkhof, R., Pierrot, D., Sullivan, K., Barbero, L., Triñanes, J., 2020. A 17-year dataset of surface water fugacity of CO₂ along with calculated pH, aragonite saturation state and air-sea CO₂ fluxes in the northern Caribbean Sea. *Earth Syst. Sci. Data* 12, 1489–1509.
- Wanninkhof, R., Zhang, J.-Z., Baringer, M., Langdon, C., Cai, W.-J., Salisbury, J., Byrne, R.H., 2012. Carbon dioxide and hydrographic measurements during the R/V Ronald H. Brown GOMECC-2 Cruise (July 21 – August 13, 2012). Carbon Dioxide Information Analysis Center, Oak Ridge National Laboratory, US Department of Energy: Oak Ridge, TN. doi: 10.3334/CDIAC/OTG.COASTAL_GOMECC2
- Wanninkhof, R., Zhang, J.-Z., Baringer, M., Langdon, C., Cai, W.J., Salisbury, J., Byrne, R., 2016. Partial pressure (or fugacity) of carbon dioxide, dissolved inorganic carbon, pH, alkalinity, temperature, salinity and other variables collected from discrete sample and profile observations using CTD, bottle and other instruments from NOAA Ship RONALD H. BROWN in the Gray’s Reef National Marine Sanctuary, Gulf of Mexico and North Atlantic Ocean from 2012-07-21 to 2012-08-13 (NCEI Accession 0157619). Version 1.1. NOAA National Centers for Environmental Information. gov.noaa.nodc:0157619.
- Warnau, M., Pagano, G., 1994. Developmental Toxicity of PbCl₂ in the Echinoid *Paracentrotus lividus* (Echinodermata). *Bull. Environ. Contam. Toxicol.* 53, 434–441.
- Waters, J., Millero, F.J., Woosley, R.J., 2014. Corrigendum to “The free proton concentration scale for seawater pH” (MARCHE: 149 (2013) 8–22). *Mar. Chem.* 165, 66–67.
- Wei, G., McCulloch, M.T., Mortimer, G., Deng, W., Xie, L., 2009. Evidence for ocean acidification in the Great Barrier Reef of Australia. *Geochim. Cosmochim. Acta* 73, 2332–2346.
- Weiss, R.F., 1974. Carbon dioxide in water and seawater: the solubility of a non-ideal gas. *Mar. Chem.* 2, 203–215.
- Weiss, R.F., Jahnke, R.A., Keeling, C.D., 1982. Seasonal effects of temperature and salinity on the partial pressure of CO₂ in seawater. *Nature* 300, 511–513.
- Wijffels, S., Roemmich, D., Monselesan, D., Church, J., Gilson, J., 2016. Ocean temperatures chronicle the ongoing warming of Earth. *Nat. Clim. Change* 6, 116–118.
- Williams, N.L., Juranek, L.W., Feely, R.A., Johnson, K.S., Sarmiento, J.L., Talley, L.D., Dickson, A.G., Gray, A.R., Wanninkhof, R., Russell, J.L., Riser, S.C., Takeshita, Y., 2017. Calculating surface ocean pCO₂ from biogeochemical Argo floats equipped with pH: An uncertainty analysis. *Global Biogeochem. Cycles* 31, 591–604.
- Winn, C., Lukas, R., Karl, D., Firing, E., 1991. Hawaii Ocean Time-series Data Report 3.

- University of Hawaii School of Ocean and Earth Science and Technology.
- Winn, C.D., Li, Y.-H., Mackenzie, F.T., Karl, D.M., 1998. Rising surface ocean dissolved inorganic carbon at the Hawaii Ocean Time-series site. *Mar. Chem.* 60, 33–47.
- Wolf-Gladrow, D.A., Zeebe, R.E., Klaas, C., Körtzinger, A., Dickson, A.G., 2007. Total alkalinity: The explicit conservative expression and its application to biogeochemical processes. *Mar. Chem.* 106, 287–300.
- Woosley, R.J., Millero, F.J., Wanninkhof, R., 2016. Rapid anthropogenic changes in CO₂ and pH in the Atlantic Ocean: 2003–2014. *Global Biogeochem. Cycles* 30, 70–90.
- Yang, B., Byrne, R.H., Lindemuth, M., 2015. Contributions of organic alkalinity to total alkalinity in coastal waters: a spectrophotometric approach. *Mar. Chem.* 176, 199–207.
- Yao, W., Byrne, R.H., 1998. Simplified seawater alkalinity analysis: Use of linear array spectrometers. *Deep-Sea Res. Part I* 45, 1383–1392.
- Yao, W., Millero, F.J., 1995. The chemistry of the anoxic waters in the Framvaren Fjord, Norway. *Aquat. Geochem.* 1, 53–88.
- Zeebe, R.E., Wolf-Gladrow, D., 2001. CO₂ in Seawater: Equilibrium, Kinetics, Isotopes. Gulf Professional Publishing.
- Zeebe, R.E., Zachos, J.C., Caldeira, K., Tyrrell, T., 2008. Carbon emissions and acidification. *Science* 321, 51–52.
- Zhang, H., Byrne, R.H., 1996. Spectrophotometric pH measurements of surface seawater at in-situ conditions: Absorbance and protonation behavior of thymol blue. *Mar. Chem.* 52, 17–25.

APPENDIX A: COPYRIGHT PERMISSIONS

Appendix A1. Copyright permission for chapter two



Home Help Email Support Sign in Create Account



Spectrophotometric Determination of Carbonate Ion Concentrations: Elimination of Instrument-Dependent Offsets and Calculation of In Situ Saturation States
Author: Jonathan D. Sharp, Robert H. Byrne, Xuewu Liu, et al
Publication: Environmental Science & Technology
Publisher: American Chemical Society
Date: Aug 1, 2017
Copyright © 2017, American Chemical Society

PERMISSION/LICENSE IS GRANTED FOR YOUR ORDER AT NO CHARGE



This type of permission/license, instead of the standard Terms & Conditions, is sent to you because no fee is being charged for your order. Please note the following:


- Permission is granted for your request in both print and electronic formats, and translations.
- If figures and/or tables were requested, they may be adapted or used in part.
- Please print this page for your records and send a copy of it to your publisher/graduate school.
- Appropriate credit for the requested material should be given as follows: "Reprinted (adapted) with permission from (COMPLETE REFERENCE CITATION). Copyright (YEAR) American Chemical Society." Insert appropriate information in place of the capitalized words.
- One-time permission is granted only for the use specified in your request. No additional uses are granted (such as derivative works or other editions). For any other uses, please submit a new request.

BACK CLOSE WINDOW

© 2020 Copyright - All Rights Reserved | [Copyright Clearance Center, Inc.](#) | [Privacy statement](#) | [Terms and Conditions](#)
Comments? We would like to hear from you. E-mail us at customer@copyright.com

Appendix A2. Copyright permission for chapter three

HomeHelpEmail SupportSign inCreate Account



Carbonate ion concentrations in seawater: Spectrophotometric determination at ambient temperatures and evaluation of propagated calculation uncertainties

Author: Jonathan D. Sharp, Robert H. Byrne

Publication: Marine Chemistry

Publisher: Elsevier

Date: 20 February 2019

© 2018 Elsevier B.V. All rights reserved.

Please note that, as the author of this Elsevier article, you retain the right to include it in a thesis or dissertation, provided it is not published commercially. Permission is not required, but please ensure that you reference the journal as the original source. For more information on this and on your other retained rights, please visit: <https://www.elsevier.com/about/our-business/policies/copyright#Author-rights>

BACK

CLOSE WINDOW

© 2020 Copyright - All Rights Reserved | Copyright Clearance Center, Inc. | [Privacy statement](#) | [Terms and Conditions](#)
Comments? We would like to hear from you. E-mail us at customer@copyright.com

Appendix A3. Copyright permission for chapter four

Home Help Email Support Sign in Create Account



Interpreting measurements of total alkalinity in marine and estuarine waters in the presence of proton-binding organic matter

Author: Jonathan D. Sharp, Robert H. Byrne

Publication: Deep Sea Research Part I: Oceanographic Research Papers

Publisher: Elsevier

Date: Available online 29 July 2020

© 2020 Elsevier Ltd. All rights reserved.

Please note that, as the author of this Elsevier article, you retain the right to include it in a thesis or dissertation, provided it is not published commercially. Permission is not required, but please ensure that you reference the journal as the original source. For more information on this and on your other retained rights, please visit: <https://www.elsevier.com/about/our-business/policies/copyright#Author-rights>

BACK

CLOSE WINDOW

© 2020 Copyright - All Rights Reserved | Copyright Clearance Center, Inc. | [Privacy statement](#) | [Terms and Conditions](#)
Comments? We would like to hear from you. E-mail us at customer@copyright.com

APPENDIX B:

SUPPLEMENTAL INFORMATION FOR CHAPTER TWO

Appendix B1. Supplemental figure for chapter two

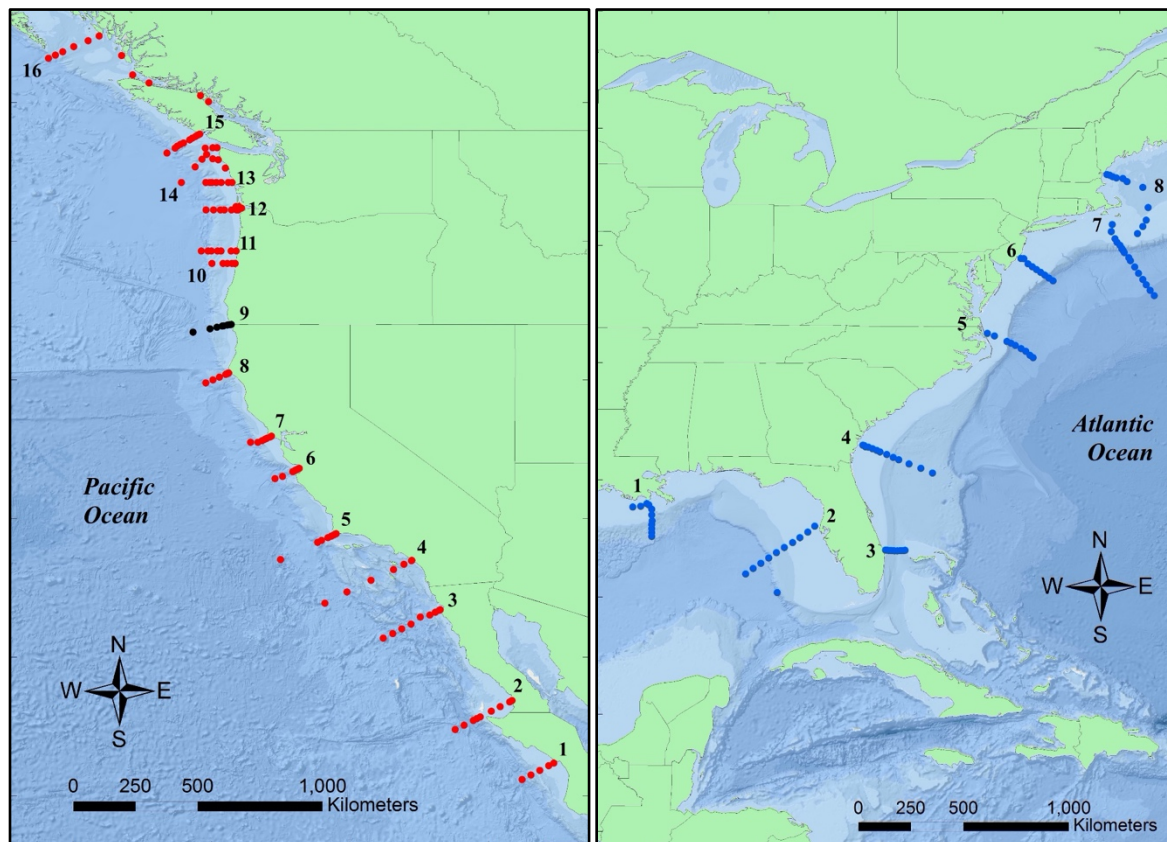


Figure B1.1. Left panel: Station locations for the 2016 West Coast Ocean Acidification Cruise (WCOA 2016). Cross-sections from line 9 (black dots for station locations) are shown in Figure 2.6. Right panel: Station locations for the 2012 Gulf of Mexico and East Coast Carbon Cruise (GOMECC-2). Figure generated using ArcMap 10.2.

APPENDIX C:

SUPPLEMENTAL INFORMATION FOR CHAPTER THREE

Appendix C1. Removal of Pb(II) from analytical samples

The effectiveness of a commercially available cation exchange resin at removing Pb(II) from seawater samples spiked with Pb(ClO₄)₂ was examined closely. A column of Chelex® 100 (Bio-Rad Laboratories) was prepared in a 50 mL glass burette (600 cm in length). A stock solution of seawater with Pb(ClO₄)₂ added to achieve a concentration of 14.7 μmol/kg (equivalent to the Pb concentration in the post-measurement [CO₃²⁻]_{spec} samples) was also prepared. Because the documentation for Chelex 100 (Bio-Rad Laboratories, LIT200 Rev. B) indicates that its selectivity for Pb(II) is highest at a pH of ~4, a phthalate buffer (0.05 M C₈H₅KO₄) was added to the stock solution to achieve this pH (Hetzer et al., 1977; Partanen et al., 1997).

About 1 L of Pb(II)-enriched stock was pumped through the resin column at a flow rate of ~5 mL/min. Throughout the process, samples of effluent were collected, spiked with Bi (for use as an internal standard during ICP-MS analysis), and diluted with concentrated nitric acid to 2% HNO₃. The samples were analyzed with an Agilent 7500cx inductively coupled plasma mass spectrometer (ICP-MS) to assess how effectively the cation exchange resin removed Pb(II) at the given flow rate and column geometry.

The ICP-MS analyses showed that passing the Pb(II)-enriched seawater (representative of [CO₃²⁻]_{spec} samples) through the column of Chelex 100 resin achieved nearly 100% Pb(II) removal. The initial concentration in the sample solution was 14.7 μmol/kg (approximately 3000 ppb). The final concentrations in the effluent from the Chelex column were close to the ICP-MS detection limit (approximately 0.1 ppb).

This experiment exemplifies how Pb(II) should be removed from Pb(II)-spiked [CO₃²⁻]_{spec} samples, either for discrete samples or within an inline or in situ sensor. Though Chelex 100 was utilized in this work, other commercially available cation exchange resins are likely to be similarly effective (e.g., Amberlite® IR120, Dowex® 50WX4, Lewatit® TP 207). A Pb(II) concentration of 0.1 ppb corresponds to a molal concentration of ~500 pM, meaning that effluent from the Chelex column contained at most an order of magnitude more Pb(II) than Atlantic Ocean background levels, which rarely exceed 60 pM (Noble et al., 2015).

After publication of Sharp and Byrne (2019), it was indicated that other resins should be considered (e.g., Nobias-chelate PA1, Toyopearl AF-Chelate 650M®). These work at closer to

natural seawater pH, and so would not require addition of phthalate buffer to adjust the pH of Pb(II)-enriched seawater.

A strong acid can be used to elute metals from the used cation exchange resins, and NaOH can subsequently regenerate the resins to their “clean” sodium forms (Bio-Rad Laboratories, LIT200 Rev. B). For an in situ $[\text{CO}_3^{2-}]_{\text{spec}}$ sensor, repetition of this elution process (while collecting and sequestering the Pb(II)-concentrated waste for future disposal) would allow for extended deployments without unnecessary release of Pb(II) to the environment.

Appendix C2. Modified MATLAB routines

The MATLAB routines that were modified to include $[\text{CO}_3^{2-}]$ and $u([\text{CO}_3^{2-}])$ as input variables are available for download at <https://github.com/jonathansharp>. If you use these routines for $[\text{CO}_3^{2-}]$ -based CO_2 system calculations or uncertainty analyses, please cite the manuscript that this appendix accompanies.

The ‘CO2SYS.m’ routine has been modified from that of Orr et al. (2018), who added a few elements to the routine of van Heuven et al. (2011) to allow for uncertainty propagation. The original CO2SYS code was written for DOS by Lewis and Wallace (1998). The ‘CO2SYS.m’ routine is called, as it typically is, with parameters ‘PAR1TYPE’ and ‘PAR2TYPE’ denoting the input variable types (1 = A_T , 2 = C_T , 3 = pH_T , 4 = $p\text{CO}_2$, 5 = $f\text{CO}_2$). In our modified version, $[\text{CO}_3^{2-}]$ is available as an input variable along with its own parameter type value (6 = $[\text{CO}_3^{2-}]$). Tests have been performed to verify that answers obtained using $[\text{CO}_3^{2-}]$ as an input variable to this routine are internally consistent.

The ‘errors.m’ and ‘derivnum.m’ routines of Orr et al. (2018) have been slightly modified. Both are called as described in Orr et al. (2018). However, $[\text{CO}_3^{2-}]$ is again available as an input parameter with a parameter type value equal to 6. In the case of the ‘errors.m’ routine, the uncertainty for $[\text{CO}_3^{2-}]$ (‘ePAR1’ or ‘ePAR2’) is to be input as a percentage rather than an absolute value. The reason for the percentage input is the wide range of $[\text{CO}_3^{2-}]$ in the marine environment (~ 50 to $250 \mu\text{mol/kg}$) and the observed scaling of uncertainties in measured $[\text{CO}_3^{2-}]$ relative to absolute value.

Appendix C3. Laboratory measurements used to develop the new $[\text{CO}_3^{2-}]_{\text{spec}}$ model

Table C3.1. Data from laboratory measurements made in altered Gulf of Mexico seawater to develop the $[\text{CO}_3^{2-}]_{\text{spec}}$ model of Table 3.2 in the main text. Salinity (S) and total alkalinity (A_T) were deliberately manipulated to provide a range of seawater characteristics. For the measurements of pH on the total hydrogen ion concentration scale (pH_T), measured temperatures (T) and sulfonephthalein absorbance ratios (R) are given, along with the calculated pH_T (Liu et al., 2011). For the measurements of Pb(II) absorbance ratios, measured temperatures (T) and spectrophotometer-specific wavelength offsets at 241.10 nm ($\Delta\lambda_{241.1}$) are given, along with wavelength-corrected absorbance values (R^0) (as in Sharp et al., 2017).

| S | A_T | pH_T Measurements | | | Pb(II) Absorbance Measurements | | |
|-------|---------|----------------------------|-------|---------------|--------------------------------|-------|-------------------------|
| | | T ($^{\circ}\text{C}$) | R | pH_T | T ($^{\circ}\text{C}$) | R^0 | $\Delta\lambda_{241.1}$ |
| 36.92 | 2389.59 | 2.50 | 2.073 | 8.3219 | 3.03 | 0.415 | -0.04 |
| 32.44 | 1936.51 | 2.51 | 1.112 | 8.0253 | 2.74 | 0.462 | -0.04 |
| 32.43 | 2185.10 | 2.53 | 3.001 | 8.5084 | 3.04 | 0.358 | -0.04 |
| 32.44 | 2023.35 | 2.59 | 1.750 | 8.2392 | 2.83 | 0.409 | -0.04 |
| 36.92 | 2143.92 | 2.91 | 0.655 | 7.7742 | 3.10 | 0.573 | -0.04 |
| 36.92 | 2237.90 | 2.96 | 1.163 | 8.0388 | 3.13 | 0.496 | -0.04 |
| 36.92 | 2305.44 | 2.97 | 1.526 | 8.1667 | 2.99 | 0.451 | -0.04 |
| 36.91 | 2440.99 | 3.02 | 2.383 | 8.3835 | 3.09 | 0.398 | -0.04 |
| 29.69 | 1959.66 | 4.93 | 1.662 | 8.1840 | 5.26 | 0.390 | -0.05 |
| 25.01 | 1522.16 | 5.05 | 0.797 | 7.8454 | 5.29 | 0.438 | -0.05 |
| 25.01 | 1752.22 | 5.14 | 2.420 | 8.3723 | 5.81 | 0.332 | -0.05 |
| 20.78 | 1276.01 | 5.20 | 1.106 | 8.0054 | 5.27 | 0.365 | -0.05 |
| 29.69 | 1793.23 | 5.22 | 0.744 | 7.8044 | 5.13 | 0.486 | -0.05 |
| 35.39 | 2243.28 | 5.31 | 1.020 | 7.9431 | 5.70 | 0.494 | -0.26 |
| 29.69 | 2029.42 | 5.34 | 2.220 | 8.3193 | 5.02 | 0.369 | -0.05 |
| 35.39 | 2388.93 | 5.36 | 1.971 | 8.2544 | 5.51 | 0.418 | -0.26 |
| 20.78 | 1201.85 | 5.41 | 0.642 | 7.7516 | 5.37 | 0.421 | -0.05 |
| 35.39 | 2119.31 | 5.97 | 0.534 | 7.6376 | 5.60 | 0.592 | -0.26 |
| 36.92 | 2237.90 | 7.63 | 1.142 | 7.9639 | 7.84 | 0.501 | -0.04 |
| 40.52 | 2338.24 | 7.66 | 0.839 | 7.8200 | 8.52 | 0.579 | -0.03 |
| 40.50 | 2520.44 | 7.84 | 1.493 | 8.0866 | 8.01 | 0.489 | -0.03 |
| 36.92 | 2143.92 | 7.87 | 0.653 | 7.7022 | 8.12 | 0.580 | -0.04 |
| 36.92 | 2389.59 | 7.90 | 2.014 | 8.2315 | 7.93 | 0.427 | -0.04 |

Table C3.1. (Continued)

| | | | | | | | |
|-------|---------|-------|-------|--------|-------|-------|-------|
| 36.92 | 2305.44 | 7.95 | 1.515 | 8.0929 | 7.89 | 0.461 | -0.04 |
| 40.50 | 2590.32 | 8.28 | 1.862 | 8.1867 | 7.75 | 0.456 | -0.03 |
| 35.39 | 2243.28 | 10.23 | 1.004 | 7.8672 | 10.31 | 0.503 | -0.26 |
| 35.39 | 2388.93 | 10.41 | 1.915 | 8.1709 | 10.26 | 0.429 | -0.26 |
| 35.39 | 2182.38 | 10.49 | 0.755 | 7.7320 | 10.54 | 0.543 | -0.26 |
| 35.39 | 2513.33 | 10.55 | 2.629 | 8.3268 | 10.38 | 0.395 | -0.26 |
| 40.52 | 2338.24 | 11.35 | 0.830 | 7.7634 | 11.22 | 0.582 | -0.03 |
| 40.49 | 2675.94 | 11.55 | 2.291 | 8.2438 | 11.22 | 0.440 | -0.03 |
| 32.44 | 2093.75 | 12.76 | 2.156 | 8.2018 | 12.91 | 0.402 | -0.04 |
| 25.01 | 1522.16 | 12.85 | 0.725 | 7.6985 | 13.00 | 0.463 | -0.05 |
| 32.44 | 1936.51 | 12.91 | 1.074 | 7.8655 | 12.92 | 0.484 | -0.04 |
| 20.14 | 1327.05 | 12.92 | 2.122 | 8.2171 | 13.24 | 0.323 | -0.05 |
| 20.23 | 1243.29 | 12.95 | 1.100 | 7.9029 | 13.22 | 0.382 | -0.05 |
| 20.19 | 1151.55 | 12.95 | 0.433 | 7.4768 | 13.18 | 0.453 | -0.05 |
| 25.01 | 1601.11 | 12.98 | 1.215 | 7.9360 | 13.05 | 0.406 | -0.05 |
| 36.91 | 2440.99 | 12.99 | 2.271 | 8.2217 | 13.31 | 0.424 | -0.04 |
| 25.01 | 1424.02 | 12.99 | 0.391 | 7.4147 | 12.99 | 0.519 | -0.05 |
| 32.43 | 2185.10 | 13.00 | 2.815 | 8.3336 | 12.94 | 0.375 | -0.04 |
| 32.44 | 2023.35 | 13.00 | 1.636 | 8.0639 | 12.99 | 0.431 | -0.04 |
| 19.86 | 1396.72 | 13.00 | 3.554 | 8.4813 | 13.45 | 0.291 | -0.05 |
| 36.92 | 2305.44 | 13.01 | 1.486 | 8.0141 | 13.28 | 0.474 | -0.04 |
| 36.92 | 2389.59 | 13.05 | 1.970 | 8.1503 | 13.18 | 0.439 | -0.04 |
| 36.92 | 2143.92 | 13.08 | 0.644 | 7.6240 | 13.22 | 0.590 | -0.04 |
| 36.92 | 2237.90 | 13.10 | 1.117 | 7.8782 | 13.12 | 0.507 | -0.04 |
| 35.39 | 2182.38 | 15.31 | 0.764 | 7.6726 | 15.50 | 0.549 | -0.26 |
| 35.36 | 2367.01 | 15.38 | 2.111 | 8.1524 | 15.58 | 0.429 | -0.26 |
| 35.39 | 2388.93 | 15.45 | 1.853 | 8.0875 | 15.44 | 0.437 | -0.26 |
| 35.39 | 2513.33 | 15.47 | 2.559 | 8.2477 | 15.61 | 0.404 | -0.26 |
| 35.39 | 2243.28 | 15.50 | 1.012 | 7.7995 | 15.49 | 0.512 | -0.26 |
| 35.39 | 2119.31 | 15.66 | 0.534 | 7.5043 | 15.60 | 0.600 | -0.26 |
| 28.99 | 1910.34 | 16.19 | 2.667 | 8.2676 | 16.40 | 0.368 | -0.03 |
| 29.00 | 1820.33 | 16.31 | 1.942 | 8.1075 | 16.48 | 0.397 | -0.03 |

Table C3.1. (Continued)

| | | | | | | | |
|-------|---------|-------|-------|--------|-------|-------|-------|
| 29.01 | 1651.42 | 16.46 | 0.889 | 7.7359 | 16.25 | 0.485 | -0.03 |
| 40.52 | 2338.24 | 16.56 | 0.792 | 7.6702 | 16.67 | 0.593 | -0.03 |
| 40.50 | 2520.44 | 16.57 | 1.452 | 7.9536 | 16.67 | 0.509 | -0.03 |
| 40.50 | 2590.32 | 16.66 | 1.805 | 8.0573 | 16.26 | 0.479 | -0.03 |
| 40.49 | 2675.94 | 16.68 | 2.210 | 8.1568 | 16.61 | 0.454 | -0.03 |
| 32.44 | 2093.75 | 18.67 | 2.074 | 8.1056 | 18.83 | 0.418 | -0.04 |
| 32.45 | 1812.72 | 18.67 | 0.526 | 7.4605 | 18.76 | 0.587 | -0.04 |
| 32.44 | 2023.35 | 18.68 | 1.584 | 7.9737 | 18.95 | 0.446 | -0.04 |
| 32.43 | 2185.10 | 18.77 | 2.742 | 8.2454 | 18.81 | 0.391 | -0.04 |
| 32.44 | 1936.51 | 18.81 | 1.047 | 7.7759 | 18.87 | 0.497 | -0.04 |
| 36.91 | 2440.99 | 18.83 | 2.191 | 8.1264 | 19.02 | 0.438 | -0.04 |
| 36.92 | 2143.92 | 18.83 | 0.644 | 7.5461 | 19.05 | 0.603 | -0.04 |
| 36.92 | 2305.44 | 18.84 | 1.441 | 7.9218 | 19.09 | 0.489 | -0.04 |
| 36.92 | 2237.90 | 18.84 | 1.098 | 7.7929 | 19.05 | 0.520 | -0.04 |
| 36.92 | 2389.59 | 19.02 | 1.910 | 8.0559 | 19.01 | 0.455 | -0.04 |
| 19.86 | 1396.72 | 19.05 | 3.414 | 8.3872 | 19.22 | 0.302 | -0.05 |
| 20.14 | 1327.05 | 19.08 | 2.047 | 8.1240 | 19.25 | 0.336 | -0.05 |
| 20.23 | 1243.29 | 19.17 | 1.002 | 7.7825 | 19.23 | 0.391 | -0.05 |
| 20.07 | 1468.30 | 19.24 | 4.165 | 8.4933 | 19.21 | 0.294 | -0.05 |
| 25.01 | 1522.16 | 20.05 | 0.667 | 7.5678 | 20.16 | 0.482 | -0.05 |
| 25.01 | 1424.02 | 20.11 | 0.322 | 7.2363 | 20.19 | 0.541 | -0.05 |
| 25.01 | 1601.11 | 20.17 | 1.168 | 7.8263 | 20.19 | 0.426 | -0.05 |
| 25.01 | 1752.22 | 20.20 | 2.542 | 8.2044 | 20.16 | 0.356 | -0.05 |
| 25.01 | 1685.42 | 20.22 | 1.896 | 8.0579 | 20.16 | 0.377 | -0.05 |
| 35.39 | 2182.38 | 20.42 | 0.739 | 7.5894 | 20.48 | 0.561 | -0.26 |
| 35.36 | 2367.01 | 20.51 | 2.051 | 8.0713 | 20.61 | 0.440 | -0.26 |
| 35.39 | 2513.33 | 20.54 | 2.479 | 8.1658 | 20.56 | 0.420 | -0.26 |
| 35.39 | 2243.28 | 20.56 | 1.016 | 7.7348 | 20.57 | 0.525 | -0.26 |
| 35.39 | 2119.31 | 20.57 | 0.527 | 7.4333 | 20.48 | 0.615 | -0.26 |
| 35.39 | 2388.93 | 20.58 | 1.838 | 8.0164 | 20.56 | 0.453 | -0.26 |
| 40.52 | 2338.24 | 22.42 | 0.809 | 7.6018 | 22.62 | 0.607 | -0.03 |
| 40.49 | 2675.94 | 22.53 | 2.145 | 8.0648 | 22.64 | 0.472 | -0.03 |

Table C3.1. (Continued)

| | | | | | | | |
|-------|---------|-------|-------|--------|-------|-------|-------|
| 40.50 | 2590.32 | 22.56 | 1.758 | 7.9663 | 22.56 | 0.496 | -0.03 |
| 40.50 | 2520.44 | 22.59 | 1.402 | 7.8570 | 22.60 | 0.525 | -0.03 |
| 29.02 | 1536.85 | 22.73 | 0.449 | 7.3432 | 22.78 | 0.574 | -0.03 |
| 29.00 | 1820.33 | 22.78 | 1.877 | 8.0093 | 22.88 | 0.415 | -0.03 |
| 29.01 | 1651.42 | 22.79 | 0.859 | 7.6390 | 22.80 | 0.501 | -0.03 |
| 28.99 | 1910.34 | 23.80 | 2.547 | 8.1490 | 22.85 | 0.386 | -0.03 |
| 32.43 | 2185.10 | 24.82 | 2.695 | 8.1602 | 24.80 | 0.408 | -0.04 |
| 32.44 | 2023.35 | 24.84 | 1.542 | 7.8820 | 24.80 | 0.465 | -0.04 |
| 32.45 | 1812.72 | 24.84 | 0.478 | 7.3375 | 24.86 | 0.613 | -0.04 |
| 32.44 | 1936.51 | 24.86 | 1.016 | 7.6840 | 24.86 | 0.518 | -0.04 |
| 32.44 | 2093.75 | 24.87 | 2.047 | 8.0203 | 24.80 | 0.435 | -0.04 |
| 20.23 | 1243.29 | 24.93 | 1.010 | 7.7166 | 24.96 | 0.406 | -0.05 |
| 20.19 | 1151.55 | 24.94 | 0.416 | 7.3102 | 25.02 | 0.478 | -0.05 |
| 19.86 | 1396.72 | 24.95 | 3.456 | 8.3250 | 24.87 | 0.316 | -0.05 |
| 20.14 | 1327.05 | 24.96 | 2.049 | 8.0546 | 24.92 | 0.346 | -0.05 |
| 36.91 | 2440.99 | 25.04 | 2.079 | 8.0198 | 25.06 | 0.460 | -0.04 |
| 36.92 | 2389.59 | 25.05 | 1.837 | 7.9585 | 25.09 | 0.475 | -0.04 |
| 36.92 | 2305.44 | 25.07 | 1.407 | 7.8291 | 25.06 | 0.506 | -0.04 |
| 35.39 | 2388.93 | 25.08 | 1.794 | 7.9469 | 25.08 | 0.464 | -0.26 |
| 36.92 | 2237.90 | 25.09 | 1.094 | 7.7097 | 25.06 | 0.540 | -0.04 |
| 36.92 | 2143.92 | 25.09 | 0.682 | 7.4902 | 25.06 | 0.608 | -0.04 |
| 35.39 | 2513.33 | 25.10 | 2.416 | 8.0948 | 25.08 | 0.432 | -0.26 |
| 35.36 | 2367.01 | 25.10 | 1.999 | 7.9999 | 25.12 | 0.454 | -0.26 |
| 35.39 | 2119.31 | 25.12 | 0.525 | 7.3721 | 25.14 | 0.621 | -0.26 |
| 35.39 | 2243.28 | 25.14 | 0.983 | 7.6601 | 25.12 | 0.537 | -0.26 |
| 35.39 | 2182.38 | 25.14 | 0.737 | 7.5271 | 25.13 | 0.573 | -0.26 |
| 40.50 | 2590.32 | 27.90 | 1.695 | 7.8793 | 27.89 | 0.513 | -0.03 |
| 40.50 | 2520.44 | 27.90 | 1.395 | 7.7853 | 27.90 | 0.542 | -0.03 |
| 40.52 | 2338.24 | 27.92 | 0.803 | 7.5263 | 27.94 | 0.627 | -0.03 |
| 40.49 | 2675.94 | 27.95 | 2.077 | 7.9787 | 27.91 | 0.489 | -0.03 |
| 28.99 | 1910.34 | 28.12 | 2.464 | 8.0794 | 28.00 | 0.403 | -0.03 |
| 29.00 | 1820.33 | 28.12 | 1.817 | 7.9274 | 28.07 | 0.430 | -0.03 |

Table C3.1. (Continued)

| | | | | | | | |
|-------|---------|-------|-------|--------|-------|-------|-------|
| 29.01 | 1651.42 | 28.12 | 0.855 | 7.5701 | 28.07 | 0.512 | -0.03 |
| 29.02 | 1536.85 | 28.12 | 0.481 | 7.3065 | 27.98 | 0.585 | -0.03 |
| 35.39 | 2119.31 | 29.48 | 0.528 | 7.3186 | 29.58 | 0.633 | -0.26 |
| 35.39 | 2182.38 | 29.52 | 0.741 | 7.4734 | 29.58 | 0.583 | -0.26 |
| 35.39 | 2513.33 | 29.53 | 2.352 | 8.0255 | 29.48 | 0.445 | -0.26 |
| 35.39 | 2388.93 | 29.57 | 1.752 | 7.8785 | 29.62 | 0.478 | -0.26 |
| 35.36 | 2367.01 | 29.65 | 1.967 | 7.9346 | 29.57 | 0.466 | -0.26 |
| 35.39 | 2243.28 | 29.70 | 0.972 | 7.5969 | 29.68 | 0.549 | -0.26 |
| 25.01 | 1601.11 | 30.57 | 1.125 | 7.6813 | 30.70 | 0.451 | -0.05 |
| 25.01 | 1685.42 | 30.65 | 1.823 | 7.9119 | 30.65 | 0.405 | -0.05 |
| 25.01 | 1752.22 | 30.71 | 2.444 | 8.0578 | 30.42 | 0.382 | -0.05 |
| 32.44 | 2093.75 | 32.14 | 1.963 | 7.9089 | 32.14 | 0.458 | -0.04 |
| 36.91 | 2440.99 | 32.21 | 1.998 | 7.9092 | 32.07 | 0.482 | -0.04 |
| 32.43 | 2185.10 | 32.22 | 2.589 | 8.0482 | 32.00 | 0.431 | -0.04 |
| 32.44 | 2023.35 | 32.22 | 1.530 | 7.7859 | 32.01 | 0.486 | -0.04 |
| 36.92 | 2305.44 | 32.24 | 1.362 | 7.7221 | 32.17 | 0.530 | -0.04 |
| 36.92 | 2237.90 | 32.28 | 1.067 | 7.6057 | 32.14 | 0.563 | -0.04 |
| 19.86 | 1396.72 | 32.28 | 3.248 | 8.2081 | 32.28 | 0.338 | -0.05 |
| 36.92 | 2143.92 | 32.29 | 0.678 | 7.3948 | 32.20 | 0.627 | -0.04 |
| 32.45 | 1812.72 | 32.31 | 0.495 | 7.2584 | 32.17 | 0.631 | -0.04 |
| 32.44 | 1936.51 | 32.32 | 0.960 | 7.5637 | 32.11 | 0.538 | -0.04 |
| 36.92 | 2389.59 | 32.34 | 1.773 | 7.8486 | 32.18 | 0.499 | -0.04 |
| 20.19 | 1151.55 | 32.44 | 0.431 | 7.2382 | 32.25 | 0.493 | -0.05 |
| 20.14 | 1327.05 | 32.46 | 1.963 | 7.9464 | 32.17 | 0.368 | -0.05 |
| 20.23 | 1243.29 | 32.47 | 1.013 | 7.6297 | 32.29 | 0.424 | -0.05 |
| 40.52 | 2338.24 | 33.30 | 0.789 | 7.4490 | 33.10 | 0.642 | -0.03 |
| 40.50 | 2520.44 | 33.47 | 1.351 | 7.6987 | 33.05 | 0.560 | -0.03 |
| 40.50 | 2590.32 | 33.62 | 1.651 | 7.7935 | 33.14 | 0.530 | -0.03 |
| 40.49 | 2675.94 | 33.90 | 1.983 | 7.8799 | 33.19 | 0.507 | -0.03 |
| 28.99 | 1910.34 | 34.18 | 2.368 | 7.9863 | 34.09 | 0.424 | -0.03 |
| 35.39 | 2388.93 | 34.20 | 1.707 | 7.8082 | 34.14 | 0.491 | -0.26 |
| 29.02 | 1536.85 | 34.23 | 0.455 | 7.2065 | 34.14 | 0.600 | -0.03 |

Table C3.1. (Continued)

| | | | | | | | |
|-------|---------|-------|-------|--------|-------|-------|-------|
| 35.39 | 2119.31 | 34.23 | 0.533 | 7.2631 | 34.23 | 0.643 | -0.26 |
| 29.00 | 1820.33 | 34.28 | 1.764 | 7.8384 | 34.12 | 0.450 | -0.03 |
| 35.39 | 2243.28 | 34.31 | 0.955 | 7.5304 | 34.15 | 0.563 | -0.26 |
| 35.39 | 2513.33 | 34.32 | 2.255 | 7.9448 | 34.25 | 0.461 | -0.26 |
| 35.36 | 2367.01 | 34.39 | 1.907 | 7.8603 | 34.20 | 0.482 | -0.26 |
| 35.39 | 2182.38 | 34.40 | 0.736 | 7.4085 | 34.22 | 0.597 | -0.26 |
| 40.50 | 2520.44 | 37.82 | 1.327 | 7.6346 | 37.74 | 0.578 | -0.03 |
| 40.52 | 2338.24 | 37.89 | 0.780 | 7.3846 | 37.70 | 0.660 | -0.03 |
| 40.49 | 2675.94 | 37.92 | 1.974 | 7.8269 | 37.73 | 0.525 | -0.03 |
| 40.50 | 2590.32 | 38.06 | 1.615 | 7.7263 | 37.78 | 0.548 | -0.03 |
| 28.99 | 1910.34 | 38.47 | 2.305 | 7.9213 | 38.38 | 0.438 | -0.03 |
| 29.01 | 1651.42 | 38.55 | 0.827 | 7.4274 | 38.40 | 0.546 | -0.03 |
| 29.00 | 1820.33 | 38.76 | 1.698 | 7.7660 | 38.34 | 0.465 | -0.03 |
| 36.91 | 2440.99 | 39.11 | 1.920 | 7.8033 | 39.09 | 0.509 | -0.04 |
| 20.19 | 1151.55 | 39.36 | 0.468 | 7.1950 | 39.40 | 0.506 | -0.05 |
| 20.23 | 1243.29 | 39.38 | 0.989 | 7.5384 | 39.30 | 0.444 | -0.05 |
| 36.92 | 2305.44 | 39.51 | 1.318 | 7.6149 | 39.28 | 0.556 | -0.04 |
| 20.14 | 1327.05 | 39.54 | 1.862 | 7.8397 | 39.29 | 0.391 | -0.05 |
| 36.92 | 2143.92 | 39.58 | 0.673 | 7.2995 | 39.39 | 0.649 | -0.04 |
| 32.43 | 2185.10 | 39.61 | 2.452 | 7.9305 | 39.41 | 0.458 | -0.04 |
| 36.92 | 2389.59 | 39.63 | 1.694 | 7.7350 | 39.28 | 0.523 | -0.04 |
| 32.45 | 1812.72 | 39.66 | 0.493 | 7.1652 | 39.61 | 0.648 | -0.04 |
| 36.92 | 2237.90 | 39.67 | 1.039 | 7.5000 | 39.26 | 0.587 | -0.04 |
| 32.44 | 2023.35 | 39.70 | 1.465 | 7.6731 | 39.70 | 0.513 | -0.04 |
| 32.44 | 2093.75 | 39.84 | 1.866 | 7.7896 | 39.54 | 0.484 | -0.04 |
| 32.44 | 1936.51 | 39.91 | 0.948 | 7.4641 | 39.61 | 0.561 | -0.04 |
| 25.01 | 1752.22 | 40.26 | 2.276 | 7.9098 | 40.38 | 0.414 | -0.05 |
| 25.01 | 1685.42 | 40.41 | 1.716 | 7.7673 | 40.69 | 0.438 | -0.05 |
| 25.01 | 1424.02 | 40.53 | 0.345 | 7.0171 | 40.42 | 0.589 | -0.05 |
| 25.01 | 1601.11 | 40.54 | 1.091 | 7.5484 | 40.59 | 0.476 | -0.05 |
| 25.01 | 1522.16 | 40.54 | 0.634 | 7.2962 | 40.38 | 0.530 | -0.05 |

Appendix C4. Duplicate $[\text{CO}_3^{2-}]$ measurements from the GOMECC-3 cruise.

Table C4.1. Measurements of $[\text{CO}_3^{2-}]$ using ultraviolet spectrophotometry and the equation from Sharp et al. (2017) for duplicate samples collected on the GOMECC-3 cruise in 2017. Samples were collected in succession from Niskin bottles, each into a ~30 mL quartz cell. Relative and absolute standard deviations between measurements are shown for each pair. At the bottom of the table, average $[\text{CO}_3^{2-}]$, relative standard deviation, and absolute standard deviation are given.

| Sample ID | $[\text{CO}_3^{2-}]_1$ ($\mu\text{mol kg}^{-1}$) | $[\text{CO}_3^{2-}]_2$ ($\mu\text{mol kg}^{-1}$) | StDev (%) | StDev ($\mu\text{mol kg}^{-1}$) |
|-----------|---|---|--------------|--------------------------------------|
| 1109 | 240.82 | 244.15 | 0.97 | 2.35 |
| 2202 | 114.02 | 112.93 | 0.68 | 0.77 |
| 2211 | 94.84 | 93.28 | 1.18 | 1.11 |
| 3105 | 114.18 | 111.25 | 1.84 | 2.08 |
| 4108 | 112.56 | 108.10 | 2.86 | 3.15 |
| 5113 | 91.39 | 89.35 | 1.60 | 1.45 |
| 6105 | 150.48 | 146.24 | 2.02 | 3.00 |
| 6112 | 247.12 | 251.71 | 1.30 | 3.24 |
| 7102 | 127.69 | 129.65 | 1.08 | 1.39 |
| 7114 | 242.21 | 242.80 | 0.17 | 0.42 |
| 8106 | 239.60 | 235.61 | 1.19 | 2.82 |
| 9105 | 241.90 | 245.51 | 1.05 | 2.55 |
| 11104 | 224.46 | 229.64 | 1.61 | 3.66 |
| 13101 | 200.86 | 198.33 | 0.89 | 1.78 |
| 15104 | 128.40 | 127.39 | 0.56 | 0.71 |
| 15110 | 178.26 | 179.70 | 0.57 | 1.02 |
| 16103 | 117.36 | 119.95 | 1.54 | 1.83 |
| 16106 | 141.53 | 142.84 | 0.66 | 0.93 |
| 17107 | 145.76 | 145.96 | 0.10 | 0.14 |
| 17110 | 237.20 | 243.29 | 1.79 | 4.31 |
| 18103 | 108.50 | 107.56 | 0.62 | 0.67 |
| 18113 | 247.62 | 250.90 | 0.93 | 2.32 |
| 20108 | 115.01 | 118.15 | 1.90 | 2.22 |
| 20110 | 152.05 | 151.06 | 0.46 | 0.70 |
| 21102 | 114.81 | 114.94 | 0.07 | 0.09 |
| 21112 | 92.05 | 92.46 | 0.32 | 0.29 |
| 22107 | 144.72 | 142.79 | 0.95 | 1.37 |

Table C4.1. (Continued)

| | | | | |
|-------|--------|--------|------|------|
| 22112 | 246.58 | 244.31 | 0.66 | 1.61 |
| 23103 | 91.11 | 90.62 | 0.39 | 0.35 |
| 23110 | 230.42 | 228.79 | 0.50 | 1.15 |
| 24105 | 153.37 | 151.91 | 0.68 | 1.03 |
| 25104 | 126.81 | 130.28 | 1.91 | 2.45 |
| 25110 | 250.36 | 252.17 | 0.51 | 1.28 |
| 27102 | 148.77 | 148.17 | 0.29 | 0.42 |
| 28101 | 188.70 | 190.79 | 0.78 | 1.48 |
| 29101 | 227.43 | 225.88 | 0.48 | 1.09 |
| 29103 | 214.54 | 215.26 | 0.24 | 0.51 |
| 32101 | 175.55 | 178.41 | 1.14 | 2.02 |
| 34107 | 258.00 | 260.71 | 0.74 | 1.92 |
| 34203 | 229.92 | 228.80 | 0.35 | 0.79 |
| 34208 | 247.70 | 246.53 | 0.33 | 0.83 |
| 34305 | 235.77 | 235.58 | 0.06 | 0.13 |
| 34401 | 178.98 | 178.78 | 0.08 | 0.14 |
| 34404 | 221.79 | 218.31 | 1.12 | 2.46 |
| 34503 | 191.02 | 189.03 | 0.74 | 1.41 |
| 34508 | 230.10 | 232.21 | 0.65 | 1.49 |
| 34708 | 241.47 | 243.43 | 0.57 | 1.38 |
| 34805 | 233.64 | 238.69 | 1.51 | 3.57 |
| 35102 | 120.63 | 120.95 | 0.19 | 0.23 |
| 36102 | 95.72 | 96.41 | 0.50 | 0.48 |
| 36111 | 209.30 | 209.10 | 0.07 | 0.15 |
| 37103 | 100.43 | 96.28 | 2.98 | 2.93 |
| 37116 | 261.25 | 265.56 | 1.16 | 3.05 |
| 38109 | 165.47 | 164.03 | 0.62 | 1.02 |
| 38114 | 260.42 | 258.36 | 0.56 | 1.46 |
| 40102 | 134.69 | 136.47 | 0.93 | 1.26 |
| 41105 | 253.09 | 248.63 | 1.26 | 3.15 |
| 45106 | 241.88 | 242.40 | 0.15 | 0.36 |
| 45108 | 244.56 | 243.28 | 0.37 | 0.90 |
| 47105 | 232.95 | 225.75 | 2.22 | 5.09 |
| 48101 | 198.52 | 200.18 | 0.59 | 1.17 |

Table C4.1. (Continued)

| | | | | |
|-------|--------|--------|------|------|
| 48107 | 240.67 | 240.30 | 0.11 | 0.26 |
| 49108 | 247.41 | 246.82 | 0.17 | 0.42 |
| 49110 | 254.08 | 255.72 | 0.46 | 1.16 |
| 50103 | 91.22 | 90.45 | 0.60 | 0.54 |
| 50112 | 245.86 | 247.84 | 0.57 | 1.40 |
| 51102 | 92.69 | 93.62 | 0.71 | 0.66 |
| 51109 | 165.98 | 166.03 | 0.02 | 0.03 |
| 52106 | 91.75 | 93.20 | 1.11 | 1.02 |
| 52114 | 233.51 | 233.52 | 0.00 | 0.00 |
| 53111 | 120.89 | 120.75 | 0.08 | 0.10 |
| 53117 | 244.68 | 246.36 | 0.48 | 1.18 |
| 54105 | 113.78 | 112.93 | 0.53 | 0.60 |
| 54116 | 134.05 | 134.00 | 0.03 | 0.04 |
| 56102 | 221.54 | 220.92 | 0.20 | 0.43 |
| 57105 | 249.83 | 246.23 | 1.03 | 2.55 |
| 58105 | 245.60 | 244.19 | 0.41 | 1.00 |
| 59105 | 156.27 | 157.48 | 0.55 | 0.86 |
| 60107 | 97.26 | 97.02 | 0.18 | 0.17 |
| 61110 | 92.04 | 91.96 | 0.06 | 0.06 |
| 61116 | 225.64 | 225.93 | 0.09 | 0.20 |
| 62107 | 112.60 | 113.76 | 0.73 | 0.82 |
| 62115 | 105.58 | 104.54 | 0.70 | 0.74 |
| 63108 | 112.28 | 112.78 | 0.31 | 0.35 |
| 63120 | 242.34 | 240.78 | 0.46 | 1.10 |
| 64105 | 115.05 | 114.41 | 0.39 | 0.45 |
| 64116 | 171.36 | 171.62 | 0.11 | 0.18 |
| 65103 | 111.33 | 110.82 | 0.32 | 0.36 |
| 65107 | 217.00 | 215.23 | 0.58 | 1.25 |
| 66103 | 186.11 | 181.61 | 1.73 | 3.19 |
| 66108 | 235.28 | 235.86 | 0.17 | 0.41 |
| 67105 | 242.97 | 237.25 | 1.68 | 4.04 |
| 69106 | 210.43 | 212.63 | 0.74 | 1.55 |
| 71103 | 241.72 | 236.05 | 1.68 | 4.01 |
| 73112 | 90.72 | 91.16 | 0.34 | 0.31 |

Table C4.1. (Continued)

| | | | | |
|-------|--------|--------|------|------|
| 73122 | 249.53 | 250.10 | 0.16 | 0.41 |
| 74117 | 155.49 | 155.95 | 0.21 | 0.32 |
| 74121 | 244.32 | 244.86 | 0.16 | 0.39 |
| 75105 | 100.93 | 101.25 | 0.22 | 0.22 |
| 76104 | 97.39 | 97.10 | 0.21 | 0.20 |
| 76110 | 129.53 | 129.74 | 0.12 | 0.15 |
| 77106 | 113.95 | 114.04 | 0.05 | 0.06 |
| 77112 | 197.28 | 199.75 | 0.88 | 1.74 |
| 78102 | 91.52 | 91.02 | 0.39 | 0.35 |
| 78112 | 228.80 | 230.38 | 0.49 | 1.12 |
| 79103 | 232.39 | 234.40 | 0.61 | 1.42 |
| 79106 | 225.55 | 223.29 | 0.71 | 1.60 |
| 81102 | 200.51 | 196.76 | 1.34 | 2.66 |
| 82103 | 90.79 | 90.90 | 0.08 | 0.08 |
| 82111 | 231.38 | 232.75 | 0.42 | 0.97 |
| 83105 | 104.03 | 105.41 | 0.93 | 0.97 |
| 83113 | 203.69 | 201.78 | 0.67 | 1.35 |
| 84111 | 139.06 | 138.80 | 0.14 | 0.19 |
| 84122 | 244.53 | 245.64 | 0.32 | 0.79 |
| 85103 | 111.96 | 112.10 | 0.09 | 0.10 |
| 85113 | 241.11 | 239.23 | 0.55 | 1.33 |
| 86104 | 109.82 | 109.75 | 0.04 | 0.05 |
| 86117 | 248.25 | 249.45 | 0.34 | 0.85 |
| 87107 | 224.07 | 225.93 | 0.58 | 1.32 |
| 87111 | 246.28 | 244.46 | 0.53 | 1.29 |
| 88105 | 208.17 | 207.14 | 0.35 | 0.73 |
| 88110 | 246.97 | 246.83 | 0.04 | 0.09 |
| 89106 | 171.58 | 170.66 | 0.38 | 0.65 |
| 89116 | 250.02 | 244.79 | 1.50 | 3.70 |
| 90109 | 203.51 | 200.15 | 1.18 | 2.37 |
| 90114 | 246.05 | 251.78 | 1.63 | 4.05 |
| 91105 | 126.00 | 124.44 | 0.88 | 1.10 |
| 92103 | 91.85 | 91.81 | 0.02 | 0.02 |
| 92108 | 226.12 | 219.90 | 1.97 | 4.40 |

Table C4.1. (Continued)

| | | | | |
|------------------|--------|---------------|-------------|-------------|
| 93104 | 172.67 | 173.36 | 0.28 | 0.49 |
| 93107 | 239.14 | 239.74 | 0.18 | 0.42 |
| 94101 | 124.23 | 125.41 | 0.67 | 0.84 |
| 94108 | 240.67 | 241.58 | 0.27 | 0.65 |
| 95104 | 218.35 | 219.82 | 0.47 | 1.04 |
| 97101 | 161.46 | 158.38 | 1.36 | 2.17 |
| 98104 | 140.79 | 142.51 | 0.86 | 1.22 |
| 98110 | 252.34 | 255.14 | 0.78 | 1.98 |
| 99103 | 127.83 | 126.03 | 1.00 | 1.27 |
| 100106 | 184.78 | 185.71 | 0.35 | 0.66 |
| 100110 | 238.30 | 235.92 | 0.71 | 1.68 |
| 101101 | 93.71 | 93.49 | 0.16 | 0.15 |
| 101112 | 245.64 | 247.43 | 0.51 | 1.27 |
| 102105 | 139.50 | 134.69 | 2.48 | 3.40 |
| 103108 | 195.78 | 196.09 | 0.11 | 0.22 |
| 103113 | 240.15 | 239.65 | 0.14 | 0.35 |
| 104104 | 174.55 | 175.29 | 0.30 | 0.52 |
| 106103 | 184.12 | 184.91 | 0.30 | 0.56 |
| 106109 | 248.05 | 252.04 | 1.13 | 2.82 |
| Averages: | | 182.52 | 0.69 | 1.25 |

Appendix C5. Supplementary error-space diagrams

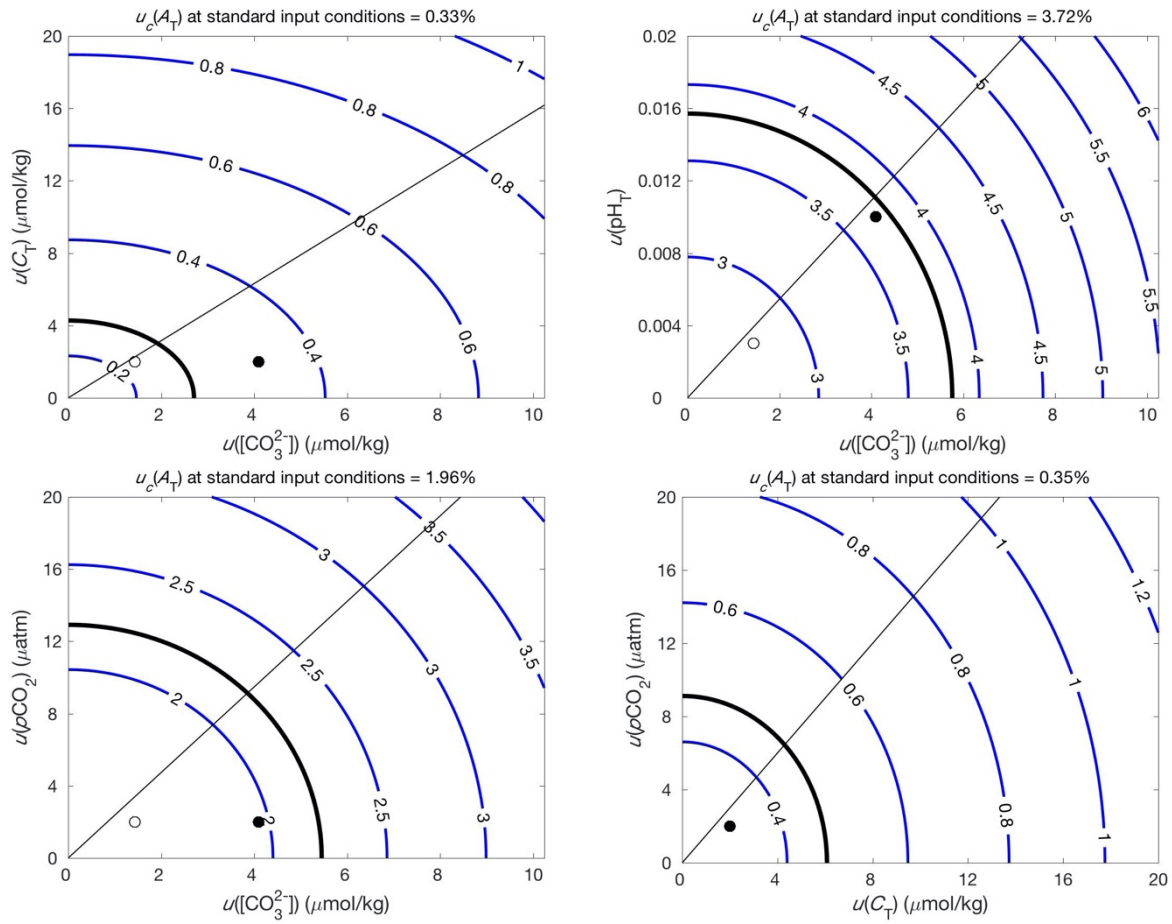


Figure C5.1. Relative combined standard uncertainty (%) in derived A_T as a function of the standard uncertainties in input variables on the x- and y-axes.

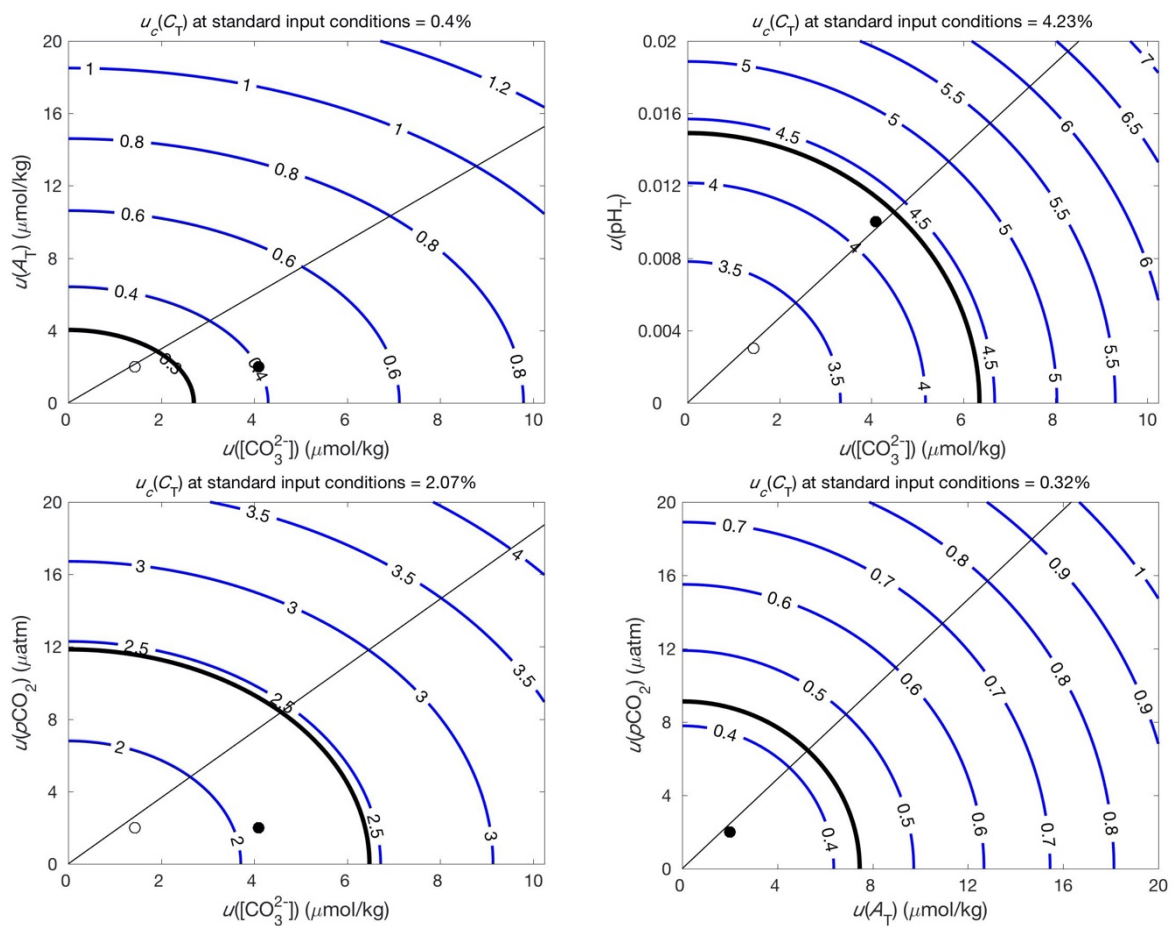


Figure C5.2. Relative combined standard uncertainty (%) in derived C_T as a function of the standard uncertainties in input variables on the x - and y -axes.

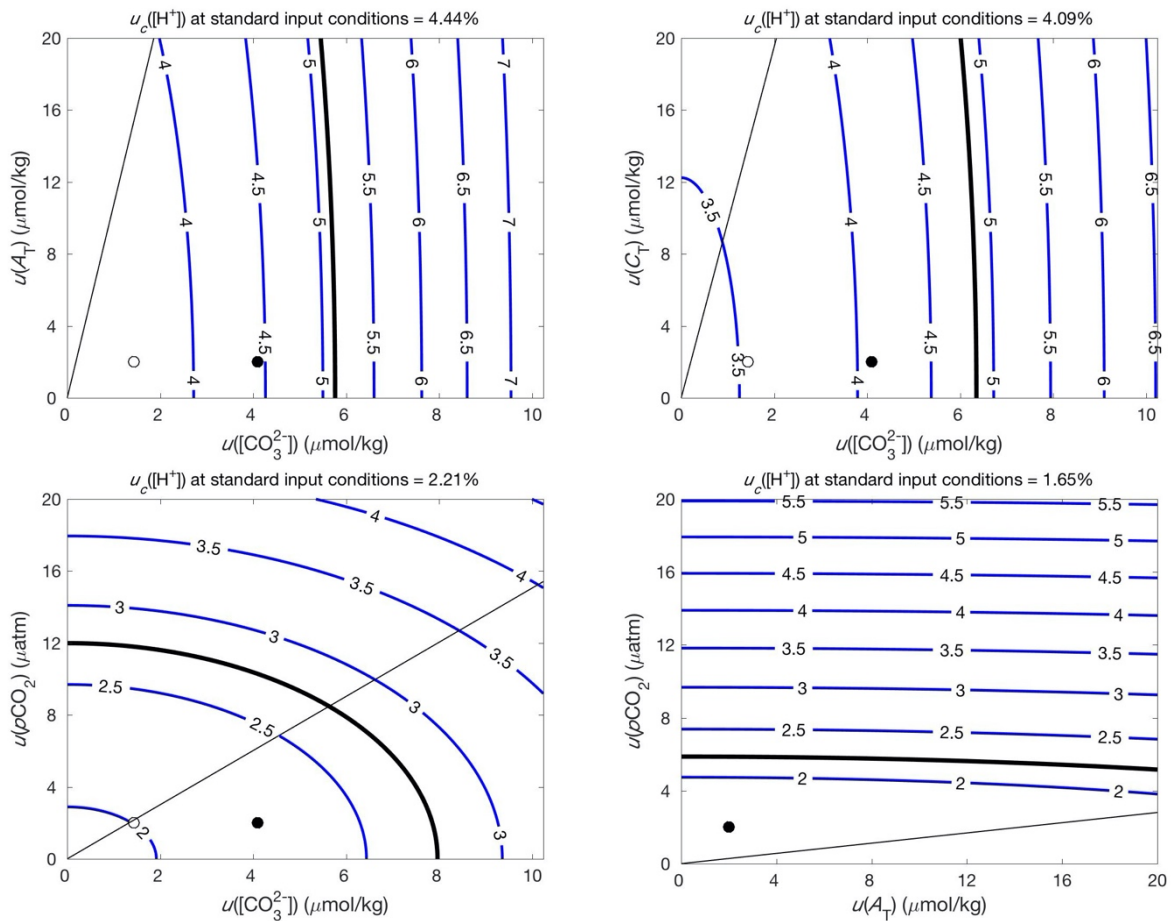


Figure C5.3. Relative combined standard uncertainty (%) in derived $[H^+]$ as a function of the standard uncertainties in input variables on the x - and y -axes.

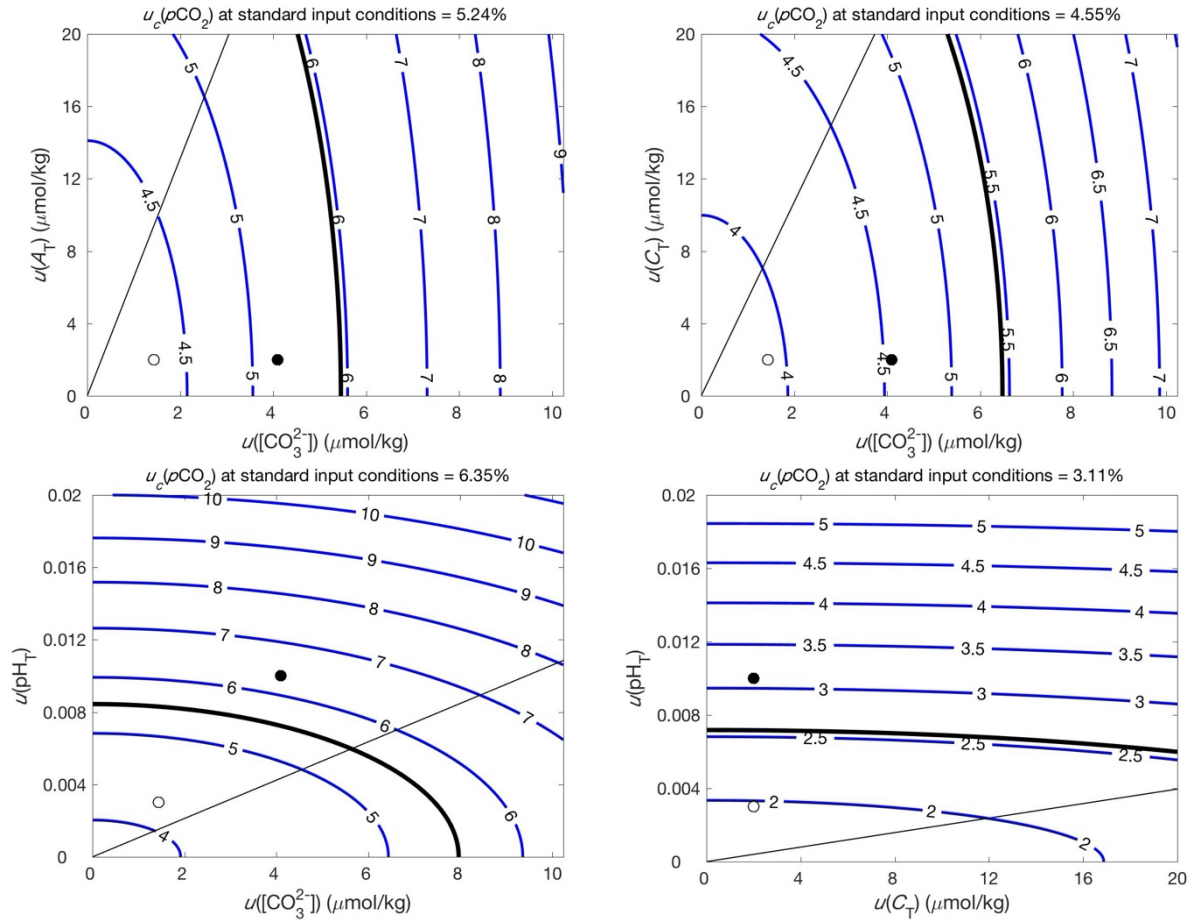


Figure C5.4. Relative combined standard uncertainty (%) in derived $p\text{CO}_2$ as a function of the standard uncertainties in input variables on the x - and y -axes.

Appendix C6. Implications for benchtop and in situ $[\text{CO}_3^{2-}]_{\text{spec}}$ measurements

The ability to measure $[\text{CO}_3^{2-}]_{\text{spec}}$ without the requirement of temperature control is highly advantageous in terms of speed, cost, and simplicity of instrumental setup. With previously proposed models for converting UV absorbance measurements to $[\text{CO}_3^{2-}]_{\text{spec}}$ (Byrne and Yao, 2008; Easley et al., 2013; Patsavas et al., 2015a; Sharp et al., 2017), all samples must be thermostatted to a temperature of 25 °C. The time required for this temperature equilibration, which depends on the initial seawater temperature, can easily approach 30 minutes. Devices necessary for temperature control are also costly: circulating water baths are priced at a few thousand dollars (USD) each and vessels for thermostating optical cells must generally be custom-machined. These components are bulky and can be challenging to transport, especially on small boats.

The time-consuming thermostating process and the need for expensive, cumbersome equipment for temperature control can be circumvented by using the model proposed in the main text (Table 3.2) in conjunction with careful temperature measurements. The temperature of each sample must be measured immediately following the absorbance measurements. Shellfish hatchery managers, marine resource managers, and environmental researchers who need to quickly evaluate CaCO_3 saturation states might especially benefit from this methodological streamlining.

For each 0.1 °C error in temperature measurement, an error of approximately 0.3% in measured carbonate ion concentration is introduced. Therefore, for instances where precision is paramount and thermostating is reasonable, we recommend using a thermostatted water bath and cell-storage vessel in order to carefully maintain a constant temperature of 25 °C. This temperature control will minimize the potential errors introduced by manual temperature measurements.

Extension of the $[\text{CO}_3^{2-}]_{\text{spec}}$ model to a wide range of T makes feasible the prospect of autonomous inline and in situ $[\text{CO}_3^{2-}]_{\text{spec}}$ measurements. Sensors to measure $[\text{CO}_3^{2-}]_{\text{spec}}$ could be constructed, similar to autonomous spectrophotometric pH sensors (Liu et al., 2006; Seidel et al., 2008). Each such instrument would consist of a fiber optic light source, a measurement cell, and a miniature spectrophotometer. A column of cation exchange resin could be included to scrub Pb(II) from slightly acidified wastewater.

Inline $[\text{CO}_3^{2-}]_{\text{spec}}$ sensors could be placed at the ocean intake pipes of shellfish hatcheries to rapidly and autonomously monitor Ω_{arag} . Aragonite saturation state has been identified as a key parameter that impacts bivalve growth and development at the larval stage (Waldbusser et al., 2013, 2015). As such, consistent monitoring of Ω_{arag} would allow hatchery managers to identify ideal spawning times and larval rearing conditions.

Inline or in situ $[\text{CO}_3^{2-}]_{\text{spec}}$ sensors could be paired with pH, $p\text{CO}_2$, or C_T sensors to autonomously characterize the entire CO_2 system. Such $[\text{CO}_3^{2-}]_{\text{spec}}$ sensors could also be paired with periodic titrimetric measurements of $[\text{Ca}^{2+}]$ to provide truly direct calculations of Ω_{arag} . Measurements of this nature would be especially useful in areas where calcium behaves non-conservatively with respect to salinity (Beckwith et al., submitted).

It should be stressed that the current precision of $[\text{CO}_3^{2-}]_{\text{spec}}$ measurements has some potential for improvement. Our experience shows that a practice as simple as taking the average of absorbances measured for multiple cells collected from one seawater batch reduces random uncertainty. The speed and low volume requirement (~ 30 mL per cell) of $[\text{CO}_3^{2-}]_{\text{spec}}$ measurements make this additional step quite reasonable, even for field measurements. Also, an automated apparatus that decreases the amount of manual sample handling between blank and sample measurements would limit the random uncertainty introduced by imperfections in the baseline absorbance correction. In short, there is potential to move the filled dot in Figs. 3.2a–3.5a (representing total $[\text{CO}_3^{2-}]_{\text{spec}}$ measurement uncertainty) closer to the position of the open dot (representing $[\text{CO}_3^{2-}]_{\text{spec}}$ measurement precision, or random uncertainty).

Finally, measured Pb(II) absorbance ratios should always be archived along with $[\text{CO}_3^{2-}]_{\text{spec}}$ concentration values (as is routinely done for sulfonephthalein indicator absorbance ratios used to obtain pH_T (Clayton and Byrne, 1993; Yao et al., 2007)). This practice allows for re-calculation of $[\text{CO}_3^{2-}]_{\text{spec}}$ values should the PbCO_3^0 complexation model be re-evaluated in the future (this concept is elaborated upon in Clayton and Byrne, 1993).

Appendix C7. References for Appendix C

- Beckwith, S., Hallock-Muller, P.M., Byrne, R.H. Saturation state calculations using measured calcium concentrations provide an alternative assessment of regionally-variable calcification potential. Submitted to *Frontiers in Marine Science*.
- Bio-Rad Laboratories. *Chelex® 100 and Chelex 20 Chelating Ion Exchange Resin: Instruction Manual*. 2000 Alfred Nobel Dr., Hercules, CA, LIT200 Rev. B.
- Byrne, R. H., Yao, W., 2008. Procedures for measurement of carbonate ion concentrations in seawater by direct spectrophotometric observations of Pb(II) complexation. *Mar. Chem.* 112 (1), 128–135.
- Clayton, T.D., Byrne, R.H., 1993. Spectrophotometric seawater pH measurements: total hydrogen ion concentration scale calibration of *m*-cresol purple and at-sea results. *Deep-Sea Res.* I 40 (10), 2115–2129.
- Easley, R. A., Patsavas, M. C., Byrne, R. H., Liu, X., Feely, R. A., Mathis, J. T., 2013. Spectrophotometric measurement of calcium carbonate saturation states in seawater. *Environ. Sci. Technol.* 47 (3), 1468–1477.
- Hetzer, H.B., Durst, R.A., Robinson, R.A., Bates, R.G., 1977. Standard pH values for the potassium hydrogen phthalate reference buffer solution from 0 to 60 °C. *J. Res. Natl. Bur. Stand., Sect. A* 81, 21–24.
- Lewis, E., Wallace, D.W.R. Program developed for CO_2 System Calculations. ORNL/CDIAC-105. Carbon Dioxide Information Analysis Center, Oak Ridge National Laboratory, U.S. Department of Energy: Oak Ridge, TN, 1998.
- Liu, X., Wang, Z.A., Byrne, R.H., Kaltenbacher, E.A., Bernstein, R.E., 2006. Spectrophotometric measurements of pH in-situ: Laboratory and field evaluations of instrumental performance. *Environ. Sci. Technol.* 40 (16), 5036–5044.

- Liu, X., Patsavas, M.C., Byrne, R.H., 2011. Purification and characterization of meta-cresol purple for spectrophotometric seawater pH measurements. *Environ. Sci. Technol.* 45 (11), 4862–4868.
- Noble, A.E., Echegoyen-Sanz, Y., Boyle, E.A., Ohnemus, D.C., Lam, P.J., Kayser, R., Reuer, M., Wu, J., Smethie, W., 2015. Dynamic variability of dissolved Pb and Pb isotope composition from the U.S. North Atlantic GEOTRACES transect. *Deep-Sea Res. II* 116, 208–205.
- Orr, J.C., Epitalon, J.-M., Dickson, A.G., Gattuso, J.-P., 2018. Routine uncertainty propagation for the marine carbon dioxide system. *Mar. Chem.* 207, 84–107.
- Partanen, J.I., Minkinen, P.O., 1997. Equations for the calculation of the pH of buffer solutions containing potassium hydrogen phthalate, dipotassium phthalate, and potassium chloride at 298.15 K. *J. Chem. Eng. Data* 42 (4), 805–813.
- Patsavas, M.C., Byrne, R.H., Yang, B., Easley, R.A., Wanninkhof, R., Liu, X., 2015. Procedures for direct spectrophotometric determination of carbonate ion concentrations: Measurements in US Gulf of Mexico and East Coast waters. *Mar. Chem.* 168, 80–85.
- Seidel, M.P., DeGrandpre, M.D., Dickson, A.G., 2008. A sensor for in situ indicator-based measurements of seawater pH. *Mar. Chem.* 109 (1–2), 18–28.
- Sharp, J.D., Byrne, R.H., Liu, X., Feely, R.A., Cuyler, E.E., Wanninkhof, R., Alin, S.R., 2017. Spectrophotometric determination of carbonate ion concentrations: Elimination of instrument-dependent offsets and calculation of in situ saturation states. *Environ. Sci. Technol.* 51 (16), 9127–9136.
- van Heuven, S., Pierrot, D., Rae, J.W.B., Lewis, E., Wallace, D.W.R. MATLAB program developed for CO₂ system calculations. ORNL/CDIAC-105b. Carbon Dioxide Information Analysis Center, Oak Ridge National Laboratory, U.S. Department of Energy: Oak Ridge, TN, 2011.
- Waldbusser, G.G., Brunner, E.L., Haley, B.A., Hales, B., Langdon, C.J., Prahl, F.G., 2013. A developmental and energetic basis linking larval oyster shell formation to acidification sensitivity. *Geophys. Res. Lett.* 40, 2171–2176.
- Waldbusser, G.G., Hales, B., Langdon, C.J., Haley, B.A., Schrader, P., Brunner, E.L., Gray, M.W., Miller, C.A., Gimenez, I., 2015. Saturation-state sensitivity of marine bivalve larvae to ocean acidification. *Nat. Clim. Change* 5 (3), 273.
- Yao, W., Liu, X., Byrne, R.H., 2007. Impurities in indicators used for spectrophotometric seawater pH measurements: Assessment and remedies. *Mar. Chem.* 107 (2), 167–172.

APPENDIX D:

SUPPLEMENTAL INFORMATION FOR CHAPTER FOUR

Appendix D1. Supplemental tables for chapter four*

Table D1.1. Definitions for notation used within chapter four.

| Symbol | Definition |
|-------------------------------|---|
| A_T | Total alkalinity as defined by Dickson (1981) |
| A_{inorg} | Inorganic alkalinity |
| A_{carb} | Carbonate alkalinity |
| $A_{T(\text{meas})}$ | Measured total alkalinity (a result of titration and data analysis methods) |
| $A_{\text{org}(\text{meas})}$ | The contribution of proton-binding organic molecules to $A_{T(\text{meas})}$ |
| C_T | Total dissolved inorganic carbon: $[\text{CO}_2^*] + [\text{HCO}_3^-] + [\text{CO}_3^{2-}]$ |
| B_T | Total boron: $[\text{B}(\text{OH})_4^-] + [\text{H}_3\text{BO}_3^0]$ |
| P_T | Total phosphate: $[\text{H}_3\text{PO}_4^0] + [\text{H}_2\text{PO}_4^-] + [\text{HPO}_4^{2-}] + [\text{PO}_4^{3-}]$ |
| Si_T | Total silicate: $[\text{Si}(\text{OH})_4^0] + [\text{SiO}(\text{OH})_3^-]$ |
| F_T | Total fluoride: $[\text{HF}^0] + [\text{F}^-]$ |
| S_T | Total sulfur: $[\text{HSO}_4^-] + [\text{SO}_4^{2-}]$ |
| NH_3_T | Total ammonia: $[\text{NH}_4^+] + [\text{NH}_3^0]$ |
| K_W | Dissociation constant of water: $[\text{H}^+]_T[\text{OH}^-]$ |
| K_1 | 1 st dissociation constant of carbonic acid: $[\text{H}^+]_T[\text{HCO}_3^-]/[\text{CO}_2^*]$ |
| K_2 | 2 nd dissociation constant of carbonic acid: $[\text{H}^+]_T[\text{CO}_3^{2-}]/[\text{HCO}_3^-]$ |
| K_B | Dissociation constant of boric acid: $[\text{H}^+]_T[\text{B}(\text{OH})_4^-]/[\text{H}_3\text{BO}_3^0]$ |
| K_{P1} | 1 st dissociation constant of phosphoric acid: $[\text{H}^+]_T[\text{H}_2\text{PO}_4^-]/[\text{H}_3\text{PO}_4^0]$ |
| K_{P2} | 2 nd dissociation constant of phosphoric acid: $[\text{H}^+]_T[\text{HPO}_4^{2-}]/[\text{H}_2\text{PO}_4^-]$ |
| K_{P3} | 3 rd dissociation constant of phosphoric acid: $[\text{H}^+]_T[\text{PO}_4^{3-}]/[\text{HPO}_4^{2-}]$ |
| K_{Si} | Dissociation constant of silicic acid: $[\text{H}^+]_T[\text{SiO}(\text{OH})_3^-]/[\text{Si}(\text{OH})_4^0]$ |
| K_F | Dissociation constant of hydrofluoric acid: $[\text{H}^+]_T[\text{F}^-]/[\text{HF}^0]$ |
| K_{HSO_4} | Dissociation constant of bisulphate: $[\text{H}^+]_f[\text{SO}_4^{2-}]/[\text{HSO}_4^-]$ |

Table D1.1. (Continued)

| | |
|-------------------|---|
| K_{NH_4} | Dissociation constant of ammonium: $[\text{H}^+]_{\text{T}}[\text{NH}_3^0]/[\text{NH}_4^+]$ |
| C_{A} | Molality of hydrochloric acid (mol kg^{-1}) |

Table D1.2. Differences between $A_{\text{T}(\text{meas})}$ and A_{inorg} ($\mu\text{mol kg}^{-1}$) obtained using different combinations of titration data analysis methods and organic pK values: $\Delta A_{\text{T}} = A_{\text{T}(\text{meas})} - A_{\text{inorg}}$. For these simulations, $P_{\text{T}} = 1.0 \mu\text{mol kg}^{-1}$, $S_{\text{T}} = 15.0 \mu\text{mol kg}^{-1}$, $t = 25 \text{ }^\circ\text{C}$, $S = 35$, $p = 1 \text{ atm}$, and $ORG_{\text{T}} = 20 \mu\text{mol kg}^{-1}$. The results are displayed graphically in Fig. 4.4. The open-cell modified Gran function (MGF) results and open-cell nonlinear least squares fit (NLSF) results were virtually identical.

| Measurement Approach | Organic pK Value | | | | | | | |
|---|--------------------|------|------|------|------|------|------|------|
| | 2.5 | 3.5 | 4.5 | 5.5 | 6.5 | 7.5 | 8.5 | 9.5 |
| $\text{pH}_{\text{T}} = 8.1, C_{\text{T}} = 2000 \mu\text{mol kg}^{-1}$ | | | | | | | | |
| MGF, open cell / NLSF, open cell | 0.5 | 8.4 | 17.9 | 19.7 | 19.5 | 16.0 | 5.7 | 0.7 |
| NLSF, closed cell | -0.3 | 2.0 | 10.6 | 18.6 | 20.0 | 16.6 | 5.9 | 0.8 |
| Difference derivatives, closed cell | -2.8 | -1.9 | 10.7 | 17.1 | 16.7 | 13.2 | 2.9 | -2.0 |
| Single-step, open cell | 0.0 | 1.2 | 8.7 | 17.3 | 19.1 | 15.8 | 5.6 | 0.7 |
| $\text{pH}_{\text{T}} = 7.7, C_{\text{T}} = 2150 \mu\text{mol kg}^{-1}$ | | | | | | | | |
| MGF, open cell / NLSF, open cell | 0.5 | 8.4 | 17.9 | 19.6 | 18.8 | 12.2 | 2.7 | 0.3 |
| NLSF, closed cell | -0.2 | 2.4 | 11.2 | 18.8 | 19.0 | 12.2 | 2.7 | 0.3 |
| Difference derivatives, closed cell | -2.8 | -1.9 | 10.9 | 17.0 | 16.0 | 9.5 | -0.1 | -2.4 |
| Single-step, open cell | -0.0 | 1.0 | 8.1 | 16.9 | 18.3 | 12.1 | 2.6 | 0.2 |
| $\text{pH}_{\text{T}} = 7.3, C_{\text{T}} = 2300 \mu\text{mol kg}^{-1}$ | | | | | | | | |
| MGF, open cell / NLSF, open cell | 0.5 | 8.4 | 17.9 | 19.5 | 17.2 | 7.7 | 1.2 | 0.1 |
| NLSF, closed cell | -0.2 | 2.5 | 11.4 | 18.7 | 17.3 | 7.6 | 1.2 | 0.1 |

Table D1.2. (Continued)

| | | | | | | | | |
|--|------|------|------|------|------|-----|------|------|
| Difference derivatives, closed cell | -2.7 | -1.8 | 11.1 | 16.8 | 14.5 | 5.0 | -1.6 | -2.6 |
| Single-step, open cell | -0.1 | 0.8 | 7.5 | 16.3 | 16.7 | 7.5 | 1.0 | -0.0 |

Table D1.3. Differences between $A_{T(\text{meas})}$ and A_{inorg} ($\mu\text{mol kg}^{-1}$) obtained using different combinations of titration data analysis methods and initial carbonate chemistries: $\Delta A_T = A_{T(\text{meas})} - A_{\text{inorg}}$. For these simulations, $P_T = 1.0 \mu\text{mol kg}^{-1}$, $Si_T = 15.0 \mu\text{mol kg}^{-1}$, $t = 25 \text{ }^\circ\text{C}$, $S = 35$, $p = 1 \text{ atm}$, and $ORG_T = 20 \mu\text{mol kg}^{-1}$. The open-cell modified Gran function (MGF) results and open-cell nonlinear least squares fit (NLSF) results were virtually identical.

| Measurement Approach | pH _T | | | | | |
|--|-------------------------|------|------|------|------|------|
| | 7.2 | 7.4 | 7.6 | 7.8 | 8.0 | 8.2 |
| | C _T | | | | | |
| | 2341 | 2273 | 2204 | 2123 | 2022 | 1895 |
| | pK _{org} = 4.5 | | | | | |
| MGF, open cell / NLSF, open cell | 17.9 | 17.9 | 17.9 | 17.9 | 17.9 | 17.9 |
| NLSF, closed cell | 11.4 | 11.4 | 11.3 | 11.1 | 10.7 | 10.1 |
| Difference derivatives, closed cell | 11.2 | 11.1 | 11.0 | 10.9 | 10.7 | 10.5 |
| Single-step, open cell | 7.3 | 7.6 | 7.9 | 8.2 | 8.6 | 9.1 |
| | pK _{org} = 6.0 | | | | | |
| MGF, open cell / NLSF, open cell | 18.7 | 19.1 | 19.4 | 19.6 | 19.7 | 19.8 |
| NLSF, closed cell | 19.0 | 19.4 | 19.7 | 19.9 | 20.0 | 20.1 |
| Difference derivatives, closed cell | 16.1 | 16.5 | 16.8 | 16.9 | 17.0 | 17.1 |
| Single-step, open cell | 17.3 | 17.9 | 18.3 | 18.5 | 18.8 | 19.0 |

Table D1.3. (Continued)

| | $pK_{org} = 7.5$ | | | | | |
|--|------------------|-----|------|------|------|------|
| MGF, open cell / NLSF, open cell | 6.7 | 8.8 | 11.1 | 13.3 | 15.2 | 16.7 |
| NLSF, closed cell | 6.6 | 8.7 | 11.0 | 13.3 | 15.5 | 17.9 |
| Difference derivatives, closed cell | 3.9 | 6.1 | 8.3 | 10.5 | 12.4 | 13.9 |
| Single-step, open cell | 6.5 | 8.7 | 11.0 | 13.2 | 15.1 | 16.5 |

Table D1.4. Errors in calculated carbonate system parameters that result from different combinations of measured parameters, titration and data analysis methods, and a range of organic pK values. For these simulations, $pH_T = 8.1$, $C_T = 2000 \mu\text{mol kg}^{-1}$, $P_T = 1.0 \mu\text{mol kg}^{-1}$, $Si_T = 15.0 \mu\text{mol kg}^{-1}$, $S = 35$, $t = 25 \text{ }^\circ\text{C}$, $p = 1 \text{ atm}$, and $ORG_T = 20 \mu\text{mol kg}^{-1}$. The open-cell MGF results and open-cell NLSF results were virtually identical. A subset of these results ($\Delta p\text{CO}_{2(A_T, Y)}$) is displayed graphically in Fig. 4.6.

| Parameter | Measurement approach | pK_{org} | | | | | | | |
|--|-------------------------------------|------------|------|------|------|------|------|-----|------|
| | | 2.5 | 3.5 | 4.5 | 5.5 | 6.5 | 7.5 | 8.5 | 9.5 |
| $\Delta C_{T(A_T, p\text{CO}_2)}$ ($\mu\text{mol kg}^{-1}$) | MGF, open cell / NLSF, open cell | 0.4 | 6.7 | 14.3 | 15.7 | 15.5 | 12.7 | 4.5 | 0.6 |
| | NLSF, closed cell | -0.2 | 1.6 | 8.5 | 14.8 | 16.0 | 13.2 | 4.7 | 0.6 |
| | Difference derivatives, closed cell | -2.2 | -1.6 | 8.5 | 13.6 | 13.3 | 10.5 | 2.3 | -1.6 |
| | Single-step, open cell | 0.0 | 1.0 | 6.9 | 13.8 | 15.2 | 12.6 | 4.5 | 0.5 |
| $\Delta C_{T(A_T, pH)}$ ($\mu\text{mol kg}^{-1}$) | MGF, open cell / NLSF, open cell | 0.5 | 7.6 | 16.1 | 17.7 | 17.5 | 14.3 | 5.1 | 0.7 |
| | NLSF, closed cell | -0.3 | 1.8 | 9.5 | 16.7 | 18.0 | 14.9 | 5.3 | 0.7 |
| | Difference derivatives, closed cell | -2.5 | -1.7 | 9.6 | 15.3 | 15.0 | 11.8 | 2.6 | -1.8 |
| | Single-step, open cell | 0.0 | 1.1 | 7.8 | 15.6 | 17.1 | 14.2 | 5.0 | 0.6 |

Table D1.4. (Continued)

| | | | | | | | | | |
|--|---|------------|------------|-------|-------|-------|-------|-------|------------|
| $\Delta p\text{CO}_2(A_T, C_T)$ (μatm) | MGF, open cell / NLSF, open cell | -0.6 | -10.3 | -21.3 | -23.3 | -23.0 | -19.0 | -7.0 | -0.9 |
| | NLSF, closed cell | 0.4 | -2.5 | -12.8 | -22.0 | -23.6 | -19.7 | -7.3 | -1.0 |
| | Difference derivatives, closed cell | 3.5 | 2.4 | -12.9 | -20.3 | -19.9 | -15.8 | -3.6 | 2.6 |
| | Single-step, open cell | 0.0 | -1.5 | -10.6 | -20.6 | -22.6 | -18.9 | -6.8 | -0.8 |
| $\Delta p\text{CO}_2(A_T, \text{pH})$ (μatm) | MGF, open cell / NLSF, open cell | 0.1 | 1.3 | 2.8 | 3.1 | 3.0 | 2.5 | 0.9 | 0.1 |
| | NLSF, closed cell | 0.0 | 0.3 | 1.6 | 2.9 | 3.1 | 2.6 | 0.9 | 0.1 |
| | Difference derivatives, closed cell | -0.4 | -0.3 | 1.7 | 2.6 | 2.6 | 2.0 | 0.5 | -0.3 |
| | Single-step, open cell | 0.0 | 0.2 | 1.3 | 2.7 | 3.0 | 2.5 | 0.9 | 0.1 |
| $\Delta \text{pH}_T(A_T, C_T)$ | MGF, open cell / NLSF, open cell | 0.001 | 0.012 | 0.025 | 0.027 | 0.027 | 0.022 | 0.008 | 0.001 |
| | NLSF, closed cell | 0.000 | 0.003 | 0.015 | 0.026 | 0.028 | 0.023 | 0.008 | 0.001 |
| | Difference derivatives, closed cell | -0.00 4 | -0.00 3 | 0.015 | 0.024 | 0.023 | 0.018 | 0.004 | -0.00 3 |
| | Single-step, open cell | 0.000 | 0.002 | 0.012 | 0.024 | 0.026 | 0.022 | 0.008 | 0.001 |
| $\Delta \text{pH}_T(A_T, p\text{CO}_2)$ | MGF, open cell / NLSF, open cell | 0.000 | 0.001 | 0.003 | 0.003 | 0.003 | 0.003 | 0.001 | 0.000 |
| | NLSF, closed cell | 0.000 | 0.000 | 0.002 | 0.003 | 0.003 | 0.003 | 0.001 | 0.000 |
| | Difference derivatives, closed cell | -0.00 0 | 0.000 | 0.002 | 0.003 | 0.003 | 0.002 | 0.001 | 0.000 |
| | Single-step, open cell | 0.000 | 0.000 | 0.001 | 0.003 | 0.003 | 0.003 | 0.001 | 0.000 |

Table D1.4. (Continued)

| | | | | | | | | | |
|---------------------------------|---|-------|-------|------|------|------|------|------|-------|
| $\Delta\Omega_{ca(A_T, C_T)}$ | MGF, open cell / NLSF, open cell | 0.01 | 0.14 | 0.30 | 0.32 | 0.32 | 0.26 | 0.09 | 0.01 |
| | NLSF, closed cell | 0.00 | 0.03 | 0.17 | 0.31 | 0.33 | 0.27 | 0.10 | 0.01 |
| | Difference derivatives, closed cell | -0.05 | -0.03 | 0.18 | 0.28 | 0.28 | 0.22 | 0.05 | -0.03 |
| | Single-step, open cell | 0.00 | 0.02 | 0.14 | 0.29 | 0.31 | 0.26 | 0.09 | 0.01 |
| $\Delta\Omega_{ca(A_T, pCO_2)}$ | MGF, open cell / NLSF, open cell | 0.00 | 0.03 | 0.07 | 0.08 | 0.08 | 0.07 | 0.02 | 0.00 |
| | NLSF, closed cell | 0.00 | 0.01 | 0.04 | 0.08 | 0.08 | 0.07 | 0.02 | 0.00 |
| | Difference derivatives, closed cell | -0.01 | -0.01 | 0.04 | 0.07 | 0.07 | 0.05 | 0.01 | -0.01 |
| | Single-step, open cell | 0.00 | 0.01 | 0.04 | 0.07 | 0.08 | 0.07 | 0.02 | 0.00 |
| $\Delta\Omega_{ca(A_T, pH)}$ | MGF, open cell / NLSF, open cell | 0.00 | 0.02 | 0.05 | 0.05 | 0.05 | 0.04 | 0.01 | 0.00 |
| | NLSF, closed cell | 0.00 | 0.01 | 0.03 | 0.05 | 0.05 | 0.04 | 0.02 | 0.00 |
| | Difference derivatives, closed cell | -0.01 | -0.01 | 0.03 | 0.04 | 0.04 | 0.03 | 0.01 | -0.01 |
| | Single-step, open cell | 0.00 | 0.00 | 0.02 | 0.04 | 0.05 | 0.04 | 0.01 | 0.00 |

Table D1.5. Errors in calculated carbonate system parameters that result from different combinations of measured parameters, titration and data analysis methods, and a range of initial carbonate chemistries. For these simulations, $P_T = 1.0 \mu\text{mol kg}^{-1}$, $Si_T = 15.0 \mu\text{mol kg}^{-1}$, $t = 25^\circ\text{C}$, $S = 35$, $p = 1 \text{ atm}$, $ORG_T = 20 \mu\text{mol kg}^{-1}$, and $pK_{org} = 7.5$. The open-cell MGF results and open-cell NLSF results were virtually identical. Subsets of these results ($\Delta\text{pH}_{T(A_T, Y)}$ and $\Delta\Omega_{ca(A_T, Y)}$) are displayed graphically in Figs. 4.7 and 4.8.

| Parameter | Measurement Approach | pH _T | | | | | |
|--|--|--|--------|-------|-------|-------|-------|
| | | 7.2 | 7.4 | 7.6 | 7.8 | 8.0 | 8.2 |
| | | C _T ($\mu\text{mol kg}^{-1}$) | | | | | |
| | | 2341 | 2273 | 2204 | 2123 | 2022 | 1895 |
| $\Delta C_{T(A_T, p\text{CO}_2)}$ ($\mu\text{mol kg}^{-1}$) | MGF, open cell / NLSF, open cell | 6.4 | 8.3 | 10.1 | 11.6 | 12.5 | 12.8 |
| | NLSF, closed cell | 6.3 | 8.2 | 10.0 | 11.6 | 12.8 | 13.7 |
| | Difference derivatives, closed cell | 3.8 | 5.7 | 7.6 | 9.2 | 10.2 | 10.7 |
| | Single-step, open cell | 6.2 | 8.1 | 10.0 | 11.5 | 12.4 | 12.7 |
| $\Delta C_{T(A_T, \text{pH})}$ ($\mu\text{mol kg}^{-1}$) | MGF, open cell / NLSF, open cell | 6.8 | 8.8 | 10.9 | 12.6 | 13.9 | 14.6 |
| | NLSF, closed cell | 6.7 | 8.7 | 10.7 | 12.6 | 14.2 | 15.7 |
| | Difference derivatives, closed cell | 4.0 | 6.1 | 8.2 | 10.0 | 11.4 | 12.2 |
| | Single-step, open cell | 6.6 | 8.7 | 10.7 | 12.5 | 13.8 | 14.5 |
| $\Delta p\text{CO}_2(A_T, C_T)$ (μatm) | MGF, open cell / NLSF, open cell | -146.0 | -125.6 | -86.1 | -50.1 | -26.5 | -13.4 |
| | NLSF, closed cell | -144.1 | -123.7 | -85.0 | -50.0 | -27.1 | -14.4 |
| | Difference derivatives, closed cell | -86.4 | -87.5 | -65.6 | -40.1 | -21.8 | -11.3 |
| | Single-step, open cell | -141.8 | -123.2 | -85.0 | -49.6 | -26.3 | -13.4 |

Table D1.5. (Continued)

| | | | | | | | |
|--|--|-------|-------|-------|-------|-------|-------|
| $\Delta p\text{CO}_2(A_T, \text{pH})$ (μatm) | MGF, open cell / NLSF, open cell | 10.1 | 8.3 | 6.4 | 4.6 | 3.1 | 1.9 |
| | NLSF, closed cell | 10.0 | 8.2 | 6.3 | 4.6 | 3.2 | 2.1 |
| | Difference derivatives, closed cell | 5.9 | 5.7 | 4.8 | 3.7 | 2.5 | 1.6 |
| | Single-step, open cell | 9.8 | 8.1 | 6.3 | 4.6 | 3.1 | 1.9 |
| $\Delta \text{pH}_T(A_T, C_T)$ | MGF, open cell / NLSF, open cell | 0.019 | 0.026 | 0.029 | 0.028 | 0.024 | 0.021 |
| | NLSF, closed cell | 0.019 | 0.026 | 0.029 | 0.027 | 0.025 | 0.022 |
| | Difference derivatives, closed cell | 0.011 | 0.018 | 0.022 | 0.022 | 0.020 | 0.017 |
| | Single-step, open cell | 0.019 | 0.026 | 0.029 | 0.027 | 0.024 | 0.021 |
| $\Delta \text{pH}_T(A_T, p\text{CO}_2)$ | MGF, open cell / NLSF, open cell | 0.001 | 0.002 | 0.002 | 0.002 | 0.002 | 0.003 |
| | NLSF, closed cell | 0.001 | 0.002 | 0.002 | 0.002 | 0.003 | 0.003 |
| | Difference derivatives, closed cell | 0.001 | 0.001 | 0.001 | 0.002 | 0.002 | 0.002 |
| | Single-step, open cell | 0.001 | 0.002 | 0.002 | 0.002 | 0.002 | 0.003 |
| $\Delta \Omega_{ca}(A_T, C_T)$ | MGF, open cell / NLSF, open cell | 0.04 | 0.09 | 0.15 | 0.20 | 0.24 | 0.28 |
| | NLSF, closed cell | 0.04 | 0.09 | 0.14 | 0.20 | 0.25 | 0.30 |
| | Difference derivatives, closed cell | 0.02 | 0.06 | 0.11 | 0.16 | 0.20 | 0.23 |
| | Single-step, open cell | 0.04 | 0.09 | 0.14 | 0.20 | 0.24 | 0.28 |

Table D1.5. (Continued)

| | | | | | | | |
|---------------------------------|--|------|------|------|------|------|------|
| $\Delta\Omega_{ca(A_T, pCO_2)}$ | MGF, open cell / NLSF, open cell | 0.01 | 0.01 | 0.02 | 0.03 | 0.05 | 0.08 |
| | NLSF, closed cell | 0.01 | 0.01 | 0.02 | 0.03 | 0.05 | 0.08 |
| | Difference derivatives, closed cell | 0.00 | 0.01 | 0.01 | 0.03 | 0.04 | 0.07 |
| | Single-step, open cell | 0.00 | 0.01 | 0.02 | 0.03 | 0.05 | 0.08 |
| $\Delta\Omega_{ca(A_T, pH)}$ | MGF, open cell / NLSF, open cell | 0.00 | 0.01 | 0.01 | 0.02 | 0.03 | 0.05 |
| | NLSF, closed cell | 0.00 | 0.01 | 0.01 | 0.02 | 0.03 | 0.05 |
| | Difference derivatives, closed cell | 0.00 | 0.00 | 0.01 | 0.02 | 0.03 | 0.04 |
| | Single-step, open cell | 0.00 | 0.01 | 0.01 | 0.02 | 0.03 | 0.05 |

APPENDIX E:

SUPPLEMENTAL INFORMATION FOR CHAPTER FIVE

Appendix E1: Derivations of terms

Section 5.3.4 states that combined borate alkalinity (A_B) and excess alkalinity (A_X) were calculated by:

$$A_B + A_X = A_T - A_C - A_m \quad (\text{E1.1})$$

This appendix provides detailed derivations of the A_T , A_C , A_m , A_B , and A_X terms.

A_T term

The proton condition defining the equivalence point of natural water titrations (Dickson, 1981; Wolf-Gladrow et al., 2007) is given by:

$$[\text{HCO}_3^-] + 2[\text{CO}_3^{2-}] + [\text{B}(\text{OH})_4^-] + [\text{OH}^-] + [\text{HPO}_4^{2-}] + 2[\text{PO}_4^{3-}] + [\text{SiO}(\text{OH})_3^-] = [\text{H}^+]_f + [\text{HSO}_4^-] + [\text{HF}^0] + [\text{H}_3\text{PO}_4^0] \quad (\text{E1.2})$$

where brackets represent total ion concentrations and subscript f denotes the free H^+ concentration. The form of Eq. (E1.2) allows the analytical hydrogen ion concentration (C_H) to be expressed as:

$$C_H = [\text{H}^+]_f + [\text{HSO}_4^-] + [\text{HF}^0] + [\text{H}_3\text{PO}_4^0] - [\text{HCO}_3^-] - 2[\text{CO}_3^{2-}] - [\text{B}(\text{OH})_4^-] - [\text{OH}^-] - [\text{HPO}_4^{2-}] - 2[\text{PO}_4^{3-}] - [\text{SiO}(\text{OH})_3^-] \quad (\text{E1.3})$$

and the total alkalinity (A_T) to be expressed as the negative of C_H :

$$A_T = -C_H = [\text{HCO}_3^-] + 2[\text{CO}_3^{2-}] + [\text{B}(\text{OH})_4^-] + [\text{OH}^-] + [\text{HPO}_4^{2-}] + 2[\text{PO}_4^{3-}] + [\text{SiO}(\text{OH})_3^-] - [\text{H}^+]_f - [\text{HSO}_4^-] - [\text{HF}^0] - [\text{H}_3\text{PO}_4^0] \quad (\text{E1.4})$$

Throughout the course of an acidimetric titration of M_0 grams of seawater with M_A grams of HCl of concentration C_A , C_H can be expressed as (Dickson, 1981):

$$C_H = (M_A C_A - M_0 A_T) / (M_0 + M_A) \quad (\text{E1.5})$$

This means that, at any point in the titration, A_T can be described by:

$$A_T = (M_A C_A - C_H(M_0 + M_A))/M_0 \quad (\text{E1.6})$$

or:

$$A_T = \frac{(M_A C_A - [\text{H}^+]_f + [\text{HSO}_4^-] + [\text{HF}^0] + [\text{H}_3\text{PO}_4^0] - [\text{HCO}_3^-] - 2[\text{CO}_3^{2-}] - [\text{B}(\text{OH})_4^-] - [\text{OH}^-] - [\text{HPO}_4^{2-}] - 2[\text{PO}_4^{3-}] - [\text{SiO}(\text{OH})_3^-])}{M_0} \quad (\text{E1.7})$$

By combining $[\text{H}^+]_f$ and $[\text{HSO}_4^-]$ into total hydrogen ion concentration ($[\text{H}^+]$, according to the convention stated above that brackets represent total concentrations) and eliminating terms that are vanishingly small at the endpoints of our titrations (i.e., $\text{pH} \approx 4.4$ to 5.0), Eq. (5.7) in the main text can be obtained from Eq. (E1.7). Eq. (5.7) includes “F” subscripts to denote final concentrations after titration with HCl.

A_C term

The goal in this work, however, was not to simply measure A_T , but to identify any imbalance between expected A_T and A_T measured via titration with HCl. Quantifying that imbalance requires contributions from each dissolved acid–base species to be accounted for mathematically or operationally.

Carbonate species that contribute to A_T — $[\text{HCO}_3^-]$ and $[\text{CO}_3^{2-}]$ — were operationally minimized by the procedure detailed in section 2.1 of the main text: initial acidification and bubbling with high-purity N_2 . Acidification shifts carbonate equilibria so that CO_2^* (i.e., $\text{H}_2\text{CO}_3 + \text{CO}_{2(\text{aq})}$) is the dominant species. Bubbling with N_2 liberates CO_2 from solution, promoting the reaction of HCO_3^- with H^+ to replace the lost CO_2^* . This process continues, allowing for sustained removal of dissolved inorganic carbon from solution.

Carbonate species that were not operationally removed by this purging step were mathematically accounted and subtracted from A_T measured by titration. This was done by estimating both the total dissolved inorganic carbon (C_T) in purged samples and the C_T added via NaOH. These measurements were made using a Picarro G5131-*I* cavity ringdown spectrometer and are detailed in section 2.5 of the main text. These two C_T estimations were added to represent sample C_T , and A_C could then be calculated by:

$$A_C = [\text{HCO}_3^-]_I + 2[\text{CO}_3^{2-}]_I = \frac{C_T K_1 ([\text{H}^+]_I + 2K_2)}{[\text{H}^+]_I^2 + K_1 [\text{H}^+]_I + K_1 K_2} \quad (\text{E1.8})$$

where subscript “I” denotes initial concentrations, before acidimetric titration.

A_m term

Minor alkalinity contributors (A_m) were accounted for mathematically by subtracting their initial concentrations from A_T measured via titration. One of those minor contributors was

$[\text{B(OH)}_4^-]_{ex}$, a measure of the degree to which the initial borate concentration ($[\text{B(OH)}_4^-]_I$) was greater than (+) or less than (-) the borate equilibrium value ($[\text{B(OH)}_4^-]_{eq}$) at the start of the titration:

$$[\text{B(OH)}_4^-]_{ex} = [\text{B(OH)}_4^-]_I - [\text{B(OH)}_4^-]_{eq} = B_T / (1 + \frac{[\text{H}^+]_I}{K_B}) - B_T / 2 \quad (\text{E1.9})$$

$[\text{B(OH)}_4^-]_{ex}$ was calculated using an average of B_T estimated from Uppström (1974) and from Lee et al. (2010) and was generally between -2 and $+2 \mu\text{mol kg}^{-1}$. Including $[\text{B(OH)}_4^-]_{ex}$ in the A_m term allows for A_{B+X} values to be directly compared between samples with identical salinity, and salinity-normalized A_{B+X} values to be directly compared between any two samples.

Initial pH_T measured spectrophotometrically using thymol blue indicator dye was used to calculate initial species concentrations ($[x]_I$). Equations to make these calculations are detailed elsewhere (e.g., Dickson et al., 2007) and the sources used for equilibrium constants characterizations were as follows: K_W from Millero (1995), K_1 and K_2 from Lueker et al. (2000), K_P and K_{Si} from Yao and Millero (1995), and K_F from Dickson and Riley (1979).

Considering all this, A_m can be represented by:

$$A_m = [\text{OH}^-]_I + 2[\text{PO}_4^{3-}]_I + [\text{HPO}_4^{2-}]_I + [\text{SiO(OH)}_3^-]_I - [\text{H}^+]_{f,I} - [\text{HSO}_4^-]_I - [\text{HF}^0]_I - [\text{H}_3\text{PO}_4^0]_I + [\text{B(OH)}_4^-]_{ex} \quad (\text{E1.10})$$

As with A_T , combining $[\text{H}^+]_f$ and $[\text{HSO}_4^-]$ into $[\text{H}^+]$ and eliminating terms that are vanishingly small at the starting points of our titrations (i.e., $\text{pH} \approx 8.6$ to 8.7), allows one to obtain Eq. (5.10) in the main text from Eq. (E1.10).

A_B term

When A_C and A_m are subtracted from A_T (Eq. (E1.1)), one is left with the equilibrium concentration of borate (i.e., A_B at $\text{p}K_B$; in this paper referred to simply as A_B) and any “excess alkalinity” component (A_X) that was titrated over the pH range of the titration (i.e., $\text{pH} \approx 8.6$ – 8.7 to $\text{pH} \approx 4.4$ – 5.0).

The equilibrium concentration of borate (A_B in $\mu\text{mol kg}^{-1}$) can be determined using salinity and one of two total boron to salinity ratios (r_B), either from Uppström (1974) or Lee et al. (2010):

$$A_B = \frac{r_B S}{2} / m_B \quad (\text{E1.11})$$

Where r_B is total boron to salinity in $\text{mg kg}^{-1} \text{‰}^{-1}$, S is salinity, and m_B is the molar mass of boron in mg mol^{-1} .

A_X term

Subtracting A_B from A_{B+X} leaves the excess alkalinity (A_X) that was titrated over the pH range of the titration (i.e., pH \approx 8.6–8.7 to pH \approx 4.4–5.0). This quantity differs depending on the value of r_B used to determine A_B , the implications of which are discussed in the main text. This quantity also differs slightly from the A_X that would contribute to a “normal” alkalinity titration, due to the pH range over which these samples were titrated.

Importantly, A_X results presented here are correlated with neither pH_I nor pH_F, implying that differences between sample groups are due to the nature of each sample type rather than any slight differences between the pH ranges of titrations.

Appendix E2: Supplementary tables for chapter five.

Table E2.1. Sample titration data. This table includes pK_B -corresponding absorbance ratio (R_{pK_B}), sample mass (M_0), added mass of HCl titrant (M_A), initial absorbance ratio (R_I), final electromotive force (E_F), estimated dissolved inorganic carbon concentration (C_T), total phosphate concentration (P_T), and total silicate concentration (Si_T) for each titration performed ($n = 34$).

| Date | Sample Type | R_{pK_B} | M_0 (g) | M_A (g) | R_I | E_F (mV) | C_T ($\mu\text{mol kg}^{-1}$) | P_T ($\mu\text{mol kg}^{-1}$) | Si_T ($\mu\text{mol kg}^{-1}$) |
|---------|-------------|------------|-----------|-----------|-------|------------|-----------------------------------|-----------------------------------|------------------------------------|
| 3/11/20 | Surface GoM | 2.308 | 149.41 | 0.4123 | 2.335 | 146.3 | 5.06 | 0.21 | 1.7 |
| 3/11/20 | Surface GoM | 2.308 | 148.91 | 0.4090 | 2.333 | 145.5 | 5.03 | 0.21 | 1.7 |
| 3/11/20 | Surface GoM | 2.308 | 142.44 | 0.3691 | 2.333 | 124.6 | 5.03 | 0.21 | 1.7 |
| 3/11/20 | Surface GoM | 2.308 | 149.57 | 0.3958 | 2.289 | 136.2 | 5.06 | 0.21 | 1.7 |
| 3/12/20 | CRM 172 | 2.308 | 145.55 | 0.4263 | 2.392 | 160.4 | 6.24 | 0.42 | 2.8 |
| 3/12/20 | CRM 172 | 2.308 | 149.78 | 0.3632 | 2.381 | 109.5 | 6.17 | 0.42 | 2.8 |
| 3/16/20 | CRM 183 | 2.308 | 151.66 | 0.3970 | 2.404 | 142.0 | 5.50 | 0.35 | 2.1 |
| 3/16/20 | CRM 183 | 2.308 | 150.12 | 0.3814 | 2.386 | 135.3 | 5.50 | 0.35 | 2.1 |
| 3/16/20 | CRM 183 | 2.308 | 148.03 | 0.3863 | 2.352 | 145.2 | 5.51 | 0.35 | 2.1 |
| 3/18/20 | CRM 172 | 2.308 | 153.38 | 0.4027 | 2.371 | 142.6 | 5.53 | 0.42 | 2.8 |
| 3/18/20 | CRM 172 | 2.308 | 144.64 | 0.4119 | 2.384 | 156.9 | 5.53 | 0.42 | 2.8 |
| 3/18/20 | CRM 172 | 2.386 | 151.12 | 0.3822 | 2.369 | 134.2 | 5.51 | 0.42 | 2.8 |
| 3/20/20 | CRM 183 | 2.386 | 145.71 | 0.3811 | 2.402 | 142.4 | 6.70 | 0.35 | 2.1 |
| 3/20/20 | CRM 183 | 2.386 | 147.03 | 0.4032 | 2.401 | 151.9 | 6.73 | 0.35 | 2.1 |
| 3/20/20 | CRM 183 | 2.386 | 150.66 | 0.4069 | 2.377 | 150.4 | 6.73 | 0.35 | 2.1 |

Table E2.1. (Continued)

| | | | | | | | | | |
|---------|-------------|-------|--------|--------|-------|-------|------|------|-----|
| 5/1/20 | CRM 183 | 2.386 | 140.15 | 0.3764 | 2.355 | 149.1 | 5.89 | 0.35 | 2.1 |
| 5/1/20 | CRM 183 | 2.386 | 151.93 | 0.4092 | 2.368 | 149.6 | 5.94 | 0.35 | 2.1 |
| 5/1/20 | CRM 183 | 2.386 | 149.93 | 0.4000 | 2.374 | 147.8 | 5.92 | 0.35 | 2.1 |
| 5/5/20 | CRM 172 | 2.386 | 146.83 | 0.4756 | 2.398 | 171.1 | 6.55 | 0.42 | 2.8 |
| 5/5/20 | CRM 172 | 2.372 | 151.30 | 0.3918 | 2.404 | 136.8 | 6.59 | 0.42 | 2.8 |
| 5/5/20 | CRM 172 | 2.372 | 151.75 | 0.4054 | 2.399 | 144.2 | 6.58 | 0.42 | 2.8 |
| 5/7/20 | Surface GoM | 2.372 | 148.09 | 0.4016 | 2.283 | 144.1 | 5.68 | 0.21 | 1.7 |
| 5/7/20 | Surface GoM | 2.372 | 150.72 | 0.4159 | 2.288 | 148.0 | 5.60 | 0.21 | 1.7 |
| 5/7/20 | Surface GoM | 2.372 | 150.37 | 0.3879 | 2.309 | 128.0 | 5.57 | 0.21 | 1.7 |
| 5/14/20 | Surface GoM | 2.372 | 150.05 | 0.4154 | 2.302 | 145.5 | 5.69 | 0.21 | 1.7 |
| 5/20/20 | Surface GoM | 2.372 | 146.50 | 0.3917 | 2.255 | 139.3 | 5.32 | 0.21 | 1.7 |
| 5/20/20 | Surface GoM | 2.372 | 154.43 | 0.4044 | 2.322 | 131.7 | 4.92 | 0.21 | 1.7 |
| 5/20/20 | Surface GoM | 2.372 | 153.93 | 0.4076 | 2.332 | 134.6 | 4.93 | 0.21 | 1.7 |
| 7/6/20 | CRM 176 | 2.365 | 155.21 | 0.4155 | 2.430 | 142.2 | 5.74 | 0.29 | 1.7 |
| 7/6/20 | CRM 176 | 2.365 | 151.33 | 0.3854 | 2.397 | 131.2 | 5.69 | 0.29 | 1.7 |
| 7/6/20 | CRM 176 | 2.365 | 152.12 | 0.3839 | 2.368 | 129.8 | 5.78 | 0.29 | 1.7 |
| 7/6/20 | CRM 176 | 2.365 | 157.88 | 0.3820 | 2.378 | 108.8 | 5.63 | 0.29 | 1.7 |
| 7/6/20 | CRM 176 | 2.365 | 152.16 | 0.4034 | 2.367 | 142.7 | 5.78 | 0.29 | 1.7 |
| 7/6/20 | CRM 176 | 2.365 | 152.36 | 0.3751 | 2.324 | 124.6 | 5.67 | 0.29 | 1.7 |

Table E2.2. Average titration results for each sample type. Normalized borate plus excess alkalinity (nA_{B+X}), excess alkalinity determined using total boron from Uppström (1974) ($A_{X,Upp.}$), and excess alkalinity determined using total boron from Lee et al. (2010) ($A_{X,Lee}$) are each given along with standard deviations in units of $\mu\text{mol kg}^{-1}$.

| Sample Type | nA_{B+X} | $A_{X,Upp.}$ | $A_{X,Lee}$ |
|--------------------------|-----------------|----------------|----------------|
| Surface GoM ($n = 11$) | 215.5 ± 1.2 | 7.8 ± 1.3 | -0.8 ± 1.3 |
| CRM 172 ($n = 8$) | 223.3 ± 0.9 | 14.5 ± 0.9 | 6.6 ± 0.9 |
| CRM 176 ($n = 6$) | 223.1 ± 0.5 | 14.4 ± 0.5 | 6.5 ± 0.5 |
| CRM 183 ($n = 9$) | 220.3 ± 1.0 | 11.7 ± 1.0 | 3.8 ± 1.0 |

Table E2.3. Total dissolved inorganic carbon ($C_{T(\text{samp.})}$) measurements of purged seawater samples. When $C_{T(\text{samp.})}$ is an average of duplicate measurements, the standard deviation (StDev) of the two measurements is given.

| Date | Sample No. | $C_{T(\text{samp.})}$ ($\mu\text{mol kg}^{-1}$) | StDev ($\mu\text{mol kg}^{-1}$) |
|---------|------------|--|--------------------------------------|
| 5/12/20 | 1 | 2.09 | 0.08 |
| 5/12/20 | 2 | 0.75 | 0.03 |
| 5/18/20 | 3 | 6.15 | N/A |
| 5/18/20 | 4 | 4.38 | N/A |
| 5/18/20 | 5 | 1.30 | N/A |
| 5/22/20 | 6 | 1.09 | 0.28 |
| 5/22/20 | 7 | 0.51 | 0.19 |
| 7/3/20 | 8 | 0.55 | N/A |
| 7/3/20 | 9 | 0.49 | N/A |
| 7/3/20 | 10 | 2.51 | N/A |
| 7/3/20 | 11 | 0.10 | N/A |
| 7/3/20 | 12 | 0.32 | N/A |

Table E2.4. Total dissolved inorganic carbon ($C_{T(\text{NaOH})}$) measurements of Milli-Q water (230 g) spiked with NaOH titrant (150 μL).

| Date | Sample No. | $C_{T(\text{NaOH})}$ ($\mu\text{mol kg}^{-1}$) |
|-------------|-------------------|---|
| 5/18/20 | 1 | 2.95 |
| 5/18/20 | 2 | 3.01 |
| 5/22/20 | 3 | 5.30 |
| 5/22/20 | 4 | 2.46 |
| 7/3/20 | 5 | 4.61 |
| 7/3/20 | 6 | 3.84 |

Table E2.5. A comprehensive list of uncertainties in input parameters for the calculation of A_X and their propagation to combined standard uncertainty in A_X in $\mu\text{mol kg}^{-1}$; calculated using Eq. (5.12) in the main text. These were determined using a model titration of seawater with $S = 35$, $t = 18\text{ }^\circ\text{C}$, $M_0 = 150\text{ g}$, and $M_A = 400\text{ mg}$. The last column gives rationale for each estimated $u(x)$ value.

| Parameter (x) | x value (approx.) | $u(x)$ | $\delta(A_X)/\delta x$ | $(\delta(A_X)/\delta x)^2 \cdot u^2(x)$ | $u(A_X)$ ($\mu\text{mol kg}^{-1}$) | Rationale for $u(x)$ value |
|--|---------------------|--------|------------------------|---|--------------------------------------|-------------------------------------|
| $C_{T(\text{samp.})}$ ($\mu\text{mol kg}^{-1}$) | 1.69 | 1.85 | 1.23 | 5.21 | 1.84 | Measurements of purged samples |
| $C_{T(\text{NaOH})}$ ($\text{nmol } \mu\text{L}^{-1}$) | 5.66 | 1.68 | 0.82 | 1.91 | 0.67 | Measurements of NaOH in Milli-Q |
| pH_F | 4.622 | 0.010 | -56.76 | 0.32 | 0.11 | Estimated for electrode pH |
| $R_{\text{p}K_B}$ | 2.410 | 0.010 | -51.70 | 0.27 | 0.09 | Based on repeat measurements |
| $\text{p}K_{W(18\text{ }^\circ\text{C})}$ | 13.50 | 0.010 | -34.41 | 0.12 | 0.04 | Orr et al. (2018) |
| M_A (g) | 0.4000 | 0.0005 | -668.03 | 0.11 | 0.04 | 5x instrument resolution |
| pH_I | 8.681 | 0.005 | 38.37 | 0.04 | 0.01 | Estimated for spec. pH |
| S | 35.00 | 0.02 | 6.16 | 0.02 | 0.01 | Std. dev. of salinity after purging |
| $Temp.$ | 18.00 | 0.05 | 1.95 | 0.01 | 0.00 | Conservatively estimated |
| P_T | 0.20 | 0.05 | 1.91 | 0.01 | 0.00 | Conservatively estimated |

Table E2.5. (Continued)

| | | | | | | |
|----------|--------|----------|----------|------|---|-----------------------------|
| M_0 | 150.00 | 0.05 | 1.78 | 0.01 | 0.00 | 5x instrument resolution |
| C_A | 0.10 | 0.000001 | -2663.12 | 0.01 | 0.00 | Documentation for batch A17 |
| S_{iT} | 1.00 | 0.1 | 0.13 | 0.00 | 0.00 | Conservatively estimated |
| | | | | | $u_c(A_x)$ ($\mu\text{mol kg}^{-1}$) | 2.83 |

Appendix E3. References for Appendix E

- Dickson, A.G., Riley, J.P., 1979. The estimation of acid dissociation constants in sea-water media from potentiometric titrations with strong base. I. The ionic product of water — K_w . *Mar. Chem.* 7, 89–99.
- Dickson, A.G., 1981. An exact definition of total alkalinity and a procedure for the estimation of alkalinity and total inorganic carbon from titration data. *Deep-Sea Res. Part A, Oceanogr. Res. Pap.* 28, 609–623.
- Dickson, A.G., Sabine, C.L., Christian, J.R. (Eds.), 2007. Guide to Best Practices for Ocean CO₂ Measurements. North Pacific Marine Science Organization, PICES Special Publication 3, Sidney, B.C., Canada.
- Lueker, T.J., Dickson, A.G., Keeling, C.D., 2000. Ocean $p\text{CO}_2$ calculated from dissolved inorganic carbon, alkalinity, and equations for K_1 and K_2 : validation based on laboratory measurements of CO₂ in gas and seawater at equilibrium. *Mar. Chem.* 70, 105–119.
- Millero, F.J., 1995. Thermodynamics of the carbon dioxide system in the oceans. *Geochim. Cosmochim. Acta* 59, 661–677.
- Orr, J.C., Epitalon, J.-M., Dickson, A.G., Gattuso, J.-P., 2018. Routine uncertainty propagation for the marine carbon dioxide system. *Mar. Chem.* 207, 84–107.
- Wolf-Gladrow, D.A., Zeebe, R.E., Klaas, C., Körtzinger, A., Dickson, A.G., 2007. Total alkalinity: The explicit conservative expression and its application to biogeochemical processes. *Mar. Chem.* 106, 287–300.
- Yao, W., Millero, F.J., 1995. The chemistry of the anoxic waters in the Framvaren Fjord, Norway. *Aquat. Geochem.* 1, 53–88.